

KMS Technologies – KJT Enterprises Inc.

An EMGS/rxt-company

Chapter 1 Introduction

extract from

Strack, K.-M., 1992, reprinted 1999
***Exploration with deep transient
electromagnetic:*** Elsevier, 373 pp.

This material is not longer cover by copyright. The copyright was released by Elsevier to Dr. Strack on November 5th, 2007.

The author explicit authorizes unrestricted use of this material as long as proper reference is given.

Chapter 1

Introduction

A significant amount of research in electromagnetic geophysics has been done around the globe because electromagnetic techniques offer a unique way of determining the resistivity at depth from the surface. The resistivity can be correlated with different pore fluids and porosity and thus aid the geological interpretation.

The intention of this book is to give the novice a comprehensive practical review of the subject as well as bringing him to the present state-of-the-art of the technique as it is used in the exploration environment. The expert should be able to use this book to design his own depth sounding system and carry out field measurements.

To demonstrate the usefulness of deep transient electromagnetics, case histories are included in most chapters. These case histories originate from many different parts of the world as shown in figure 1.1.

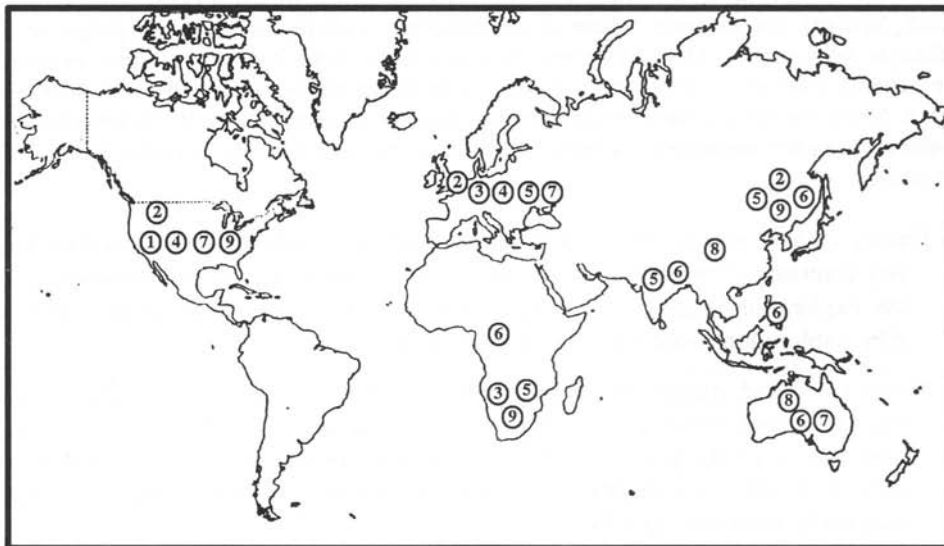


Fig.1.1: Location of the case histories shown in this book. The numbers represent the chapters where the case histories can be found.

The concept of the text follows the general background on how resistivities can be related to real geology and where the uncertainties lie in the resistivity determination.

From the basic physical background which starts with Maxwell's equations, the reader will be guided as to how to convert the field data to apparent resistivities. The latter give a representation of the changes in resistivity with time/depth. When acquiring real field data, one must overcome a significant signal-to-noise problem. This can be achieved using data processing techniques as described in chapter 3. The results of the data processing are smooth apparent resistivity curves as theoretically required. They can be interpreted using a class of inversion methods and in some selected cases even 3-D numerical modeling.

Before describing the deep transient electromagnetic sounding method, the framework in exploration geophysics is given. Further, the interpreter must understand the limitation of electrical resistivity determination.

THE ROLE OF ELECTROMAGNETIC METHODS IN EXPLORATION

In search for new energy resources, exploration methods alternative to reflection seismics have become increasingly important. The increase in *nonseismic methods* on the world scene is mainly due to the fact that new oil fields are now being found in environments where the quality of the seismic data is not adequate. During the years 1983 – 1987 seven giant oil fields have been found. Three of them (Brazil, Colombia, North Yemen) are in areas where electromagnetic techniques have the potential to delineate new targets. Many different techniques are being applied to either improve the seismic data or to solve the exploration problem by tackling it from a different angle. Since the oil industry predominantly uses seismic methods, the techniques are sometimes called *nonseismic methods*. *Nonseismic methods* can be classified into five categories:

- *Gravity* – Land, marine, helicopter, airborne, and borehole gravity respond to density contrasts of the geologic structure. Gravity methods are well established in the exploration industry. They are cost-effective and their general use for specific exploration problems is well understood.
- *Magnetics* – Land, marine, airborne magnetic measurements are a standard tool for the exploration industry, since the methods respond to susceptibility contrasts. Their use is similarly well understood as it is for gravity. In oil exploration magnetic techniques are slightly less used, in mineral exploration they are more frequently used than gravity.
- *Electromagnetics* – Electromagnetic (EM) methods show in general less ambiguity than the above mentioned potential field techniques. However, they are a lot more difficult to understand than most geophysical techniques. This is mainly due to the different behavior of the electromagnetic induced currents for different techniques. Land, airborne and borehole measurements are available to

the explorationist. Borehole measurements are routinely done in most exploration wells. Airborne electromagnetics (AEM) is a routine technique for mineral and groundwater exploration (Palacky, 1983). Oil exploration has not used the technique as much as it could, which is mainly due to the limited depth of investigation. Land techniques, although frequently used around the world, are still exotic and only the past decade has seen some more routine applications of magnetotellurics. There is an increased need for EM techniques, but the instrumentation and integration with other geophysical techniques will take time. Many techniques are presently being evaluated; among them the most promising are the transient EM technique because of its simplicity in operation and similarity in data processing techniques to the seismic method. This method has also the advantage of having the highest coupling of all EM techniques of the measured signal to the resistivity structure of the subsurface. For these reasons we have chosen the transient electromagnetic technique as our research emphasis.

- *DC-resistivity* – In rare instances direct current (DC) resistivity methods are used for hydrocarbon exploration. This is mainly, because the methods integrate over a very large volume using large current electrode spacings when the depth penetration of 3 – 4 km is required. Resulting from this large volume of integration is the lack of detailed resolution. Thus, if DC-resistivity is applied for oil exploration, it is only being used for large scale reconnaissance. The DC-resistivity technique employed is mostly a mapping technique, the dipole-dipole mapping.
- *Induced polarization* – During the past three decades induced polarization methods have been applied for oil exploration. In some cases the technique was successful (Oehler and Sternberg, 1984) and in others not. A serious drawback of the method has been that many different cultural effects (such as pipelines etc.) can produce induced polarization responses similar to subsurface mineralization. The interest in the technique has faded during the past years even though not completely disappeared.

Among the large variety of exploration problems are some which are particularly suited for electromagnetic techniques. In the following, those applications have been selected for which case histories can be found literature. Among them are:

- *permafrost* – velocity and thickness variations in permafrost layers can cause false structural interpretation of anticlines or synclines if based on seismic alone. In order to obtain reliable static corrections, transient electromagnetic techniques have been applied (Rozenberg et al, 1985).
- *oil-water contact* – many hydrocarbon producing fields contain highly saline connate water or brine, which is underneath or at the edge of the hydrocarbon deposit. The seismic velocities do not always change very much between the oil and brine saturated reservoirs, whereas the electrical conduc-

tivity changes greatly. Transient electromagnetic methods have been successfully applied to this type of exploration/production problem in the USSR and USA (Spies, 1983; Earth Technology Corporation, 1985).

- *volcanic cover* – exhibits scattering of the seismic waves, especially at high frequencies. Also, very large impedance contrasts cause reverberation of the seismic waves. Many different *nonseismic techniques* have been applied to the volcanic exploration problem. Among them are gravity, magnetics and electromagnetics (Prieto et al, 1985; Keller et al, 1984).
- *overthrusting, diapirism* – causes scattering in the seismic waves. Many different *nonseismic techniques* have been applied to this problem including surface gravity, borehole gravity, and electromagnetics. The results are encouraging but not conclusive.
- *deeply weathered overburden* – causes in some instances severe problems with the static corrections in reflection seismics. Almost all *nonseismic* geophysical techniques have been applied to this problem which is encountered in many different varieties (Christopherson, 1990).
- *extreme topography in connection with any of the above* – again causes problems with the seismic static corrections. *Nonseismic* methods can be used effectively as reconnaissance tools in this case, since they integrate over a larger volume.
- *mapping of porosity variations* – in areas where good seismic data exist, but porosity variation can not be defined from the seismic, electromagnetic methods can sometimes be very helpful. Even if porosity variations are interpreted from the seismic data (i.e. using shear wave; Robertson, 1987), electromagnetic techniques can give complementary information. For instance, once a well log and seismic data are available, one can fix the structure for the inversion from the seismic interpretation, use the well log for deriving a calibration curve for resistivity and porosity (or sand-to-shale ratio) and then invert the data for resistivities. These can then be converted to porosity maps to help the explorationist interpret the geology (Strack et al, 1989b). This will probably be the most important future application, since approximately 40 % of the world oil reserves are located in carbonates, where seismic methods do not yield enough information to interpret porosities.
- *deep crustal studies* – in order to investigate the earth crust, deep seismic profiles are being measured around the world. In many instances a low velocity zone appears within the upper 10 kilometers of the section. Sometimes this low velocity zone can be correlated with a low resistivity anomaly

(Strack et al, 1990; De Beer et al, 1991). Long Offset Transient ElectroMagnetics (LOTEM) can be effective in that particular depth range in defining the resistivity structure.

- *massive sulphide mineralization* – most base metals occur in nature as sulphide minerals which are electrically conductive, particularly when massive. Direct exploration for base metal sulphide ores has been the main impetus for the development of electromagnetic techniques, including TEM.

HISTORICAL DEVELOPMENT OF LOTEM

Before starting with the main topic, the *deep transient electromagnetic method*, the history of transient EM methods is given and categorized as needed for the context of this book. A detailed description of the theoretical background can be found in a recent monograph by Kaufman and Keller (1983). The beginning of direct current (DC) geoelectric measurement was marked by the early work of Wenner (1912) and Schlumberger (1922), whereas the alternating current applications are documented by a German patent (322040, 1913, assigned to K. Schilowsky) and an American patent (U.S. patent 1211197, assigned to H. Conklin). The first depth soundings were conducted by L. W. Blau (U.S. patent 1911137, 1933) who used an electric dipole as transmitter. Through the grounded wire he injected a pulse into the subsurface and measured the electric field changes.

For mining applications Wait (1951a, b) published the basic theory for a transient prospecting method followed by a patent (Wait, 1956; US patent 2735980) assigned to Newmont Mining Corp. (Nabighian and Macnae, 1991). Newmont subsequently developed and successfully applied several systems (Dolan, 1970). The first airborne TEM system (INPUT) was developed by Barringer in 1958 (Barringer, 1962). In the same year, research started in the Soviet Union at the Moscow Institute of Geological Prospecting where their first transient EM field system MPPO-1 was developed. In 1968 a Soviet patent of the MPPO system appeared in Australia (Australian patent 415022 assigned to Vsesojuzny Nauchno-Issledovatelsky Institut Metodiki Tekhniki Razvedki), which was at that time a promising frontier for transient electromagnetic technique because TEM could penetrate through the Australian conductive overburden. In 1973, Lazenby and Wondergem (US patent 3737768) patented an "Apparatus for remote detection of conducting bodies utilizing electromagnetic waveforms exhibiting abrupt discontinuities." The Canadian transient EM systems were mainly directed towards the search for ore bodies. In Australia, Buselli from the CSIRO developed the first computerized transient EM system and patented in 1981 (US patent 4247821) his SIROTEM development with emphasis on the noise compensation of the system. Most transient EM related patents between 1960 and 1980 were directed towards mineral exploration. Rocroi patented 1985 the Transiel system (US patent 4535293 and related French patents 1979, 7917766 and 1980, 8003159) of CGG which was mainly used for

measurements of the induced polarization. Interpretation was stated in his patent application to be only qualitative. Since the system was adopted to seismic contractor needs, several similarities to seismics can already be seen in their patent application which covers a tremendous range of applications and hardware configuration. Presently, only a new generation of field hardware using new concepts would be patentable.

To date, not much has changed from the original field techniques. The improvements – apart from the hardware and acquisition side – have mainly been made in understanding the physics and how to transform the observation to information which helps the geologist. The problem with the EM methods in early days was the misconception that the signals measured were caused by reflections of the electromagnetic waves. As expected, the method gained a lot of interest in oil exploration. It was not until the theory was fully understood (Yost, 1952; Yost et al, 1952; Orsinger and Van Nostrand, 1954) that everybody realized that the signals measured on the earth surface were not caused by reflections. It happened several times between early days and the present that inexperienced companies offered similar techniques to the oil industry, without properly understanding the physics behind the method. This caused a tremendous distrust by the oil industry of any electrical method. Only today, with the thorough research done on electromagnetics (and magnetotellurics in particular) and the increase in computer power available to the geophysicist, can we see a complete new generation of cost-effective exploration techniques evolving, although the distrust in its practical application still exists.

In the past decades, most electromagnetic methods were understood and applied in academia before the oil industry accepted them. In *magnetotellurics (MT)* only very recently was the large amount of work done around the world reviewed by K. Vozoff (1972; 1991). The MT method is now well established in industry, about 20 years after the initial efforts by Geoscience Inc. applying the technique in the United States. *Transient electromagnetics* has not come that far yet, since for oil exploration neither enough case histories nor a complete understanding of the theory has been, to date, accomplished. There have been several review papers on mining applications where transient electromagnetics has been accepted for many years as the most effective EM technique (see special transient EM issue in *Geophysics* 49(7); Macnae and Spies, 1989). The growing interest in controlled source electromagnetic techniques (Nekut and Spies, 1989) leads to an increase in controlled source EM instruments. Almost every manufacturer of EM instruments has or is preparing a deep TEM system.

The principal difference between a time domain and a frequency domain system lies in the signals for time domain systems which are measured in the absence of the source signal. For frequency domain systems the primary signal is always present. Thus, time domain signals are easier to measure and interpret. Figure 1.2 shows the two basic modes of both domains. In the figure the frequency domain primary field is for practical reasons a square wave. At the receiver site the primary field and the superimposed secondary field is measured. For the time domain setup no secondary field is being generated after the current switching, and the secondary signal is recorded in the absence of the primary field.

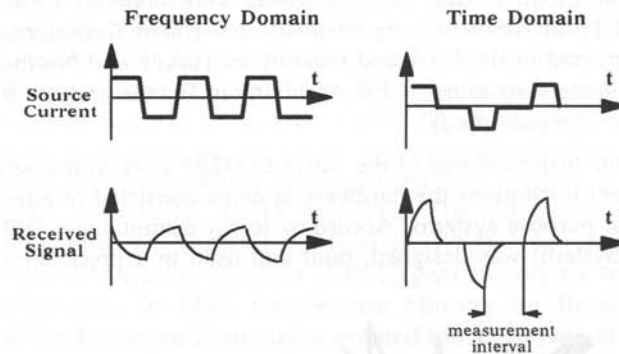


Fig.1.2: Signal and source waveforms in frequency and time domain systems (after Nekut and Spies, 1989)

Among the *transient electromagnetic techniques* are two which have been the most promising during the past years: the UTEM (University of Toronto EM) system and the LOTEM (Long Offset Transient EM) system. The UTEM system is being used primarily by Lamontagne Geophysics Ltd. in Canada and around the world. From the system concept and the interpretation scheme it is probably the most advanced and the most versatile system in the world. Its only drawback for oil exploration as can be seen today, is the limited depth range in conductive environment and that UTEM can only resolve conductive targets due to the use of an inductive source. Thus, the UTEM system is primarily applied to mineral exploration. The LOTEM system is the deeper penetrating system of the two. Because of the different terminologies among *transient EM systems*, the name LOTEM was invented in Australia by Vozoff and Strack to distinguish between the shallow systems like SIROTEM and EM37 (by Geonics) and the deeper ones. *LOTEM means that the distance between transmitter and receiver is approximately equal to or greater than the exploration depth.* LOTEM measurements require also a tradeoff between the practical field aspects and the theory. The theory would like to have the receiver as close as possible to the transmitter to avoid uncertainties due to lateral inhomogeneities, whereas the practical constraints (selection of the optimum time window) such as power line noise restrict the method to a minimum offset in order to obtain signal frequencies undistorted by power line noise or analog filters used in the system.

The roots of *transient electromagnetics* for deep exploration as discussed here are in the Soviet Union (Kraev, 1937; Tikhonov, 1946; Vanyan, 1967). Although Vanyan's monograph (1967) gives the impression that *transient electromagnetics* is a routine exploration tool, not many case histories have reached the western world. Keller did most of the pioneering work with the method at the Colorado School of Mines and his geothermal exploration company Group Seven Inc. (see Keller et al, 1984 for a historic summary of these efforts). Offsprings from CSM were Geopacific Resources Inc., Group Seven Inc. and from Group Seven Inc. and CSM, Integrated Geosciences Inc.. Geopacific Resources Inc. conducted the first transient electromagnetic measure-

ments in Asia (unpublished). Further measurements were done by CSM in Iceland (Tulinius, 1980) and Latin America (unpublished). Integrated Geosciences Inc. has mainly applied the method in the USA and recently in Turkey and Northern Ireland. Mostly unknown are some tests done by Elf Aquitaine in France and the Middle East during the early 1980s (unpublished).

Figure 1.3 shows the historical tree of the active LOTEM work in the western hemisphere. At the different institutions the hardware systems consisted of either modified commercial or special purpose systems. According to my terminology, DEMS I (Digital ElectroMagnetic System) was designed, built and used in a production mode at

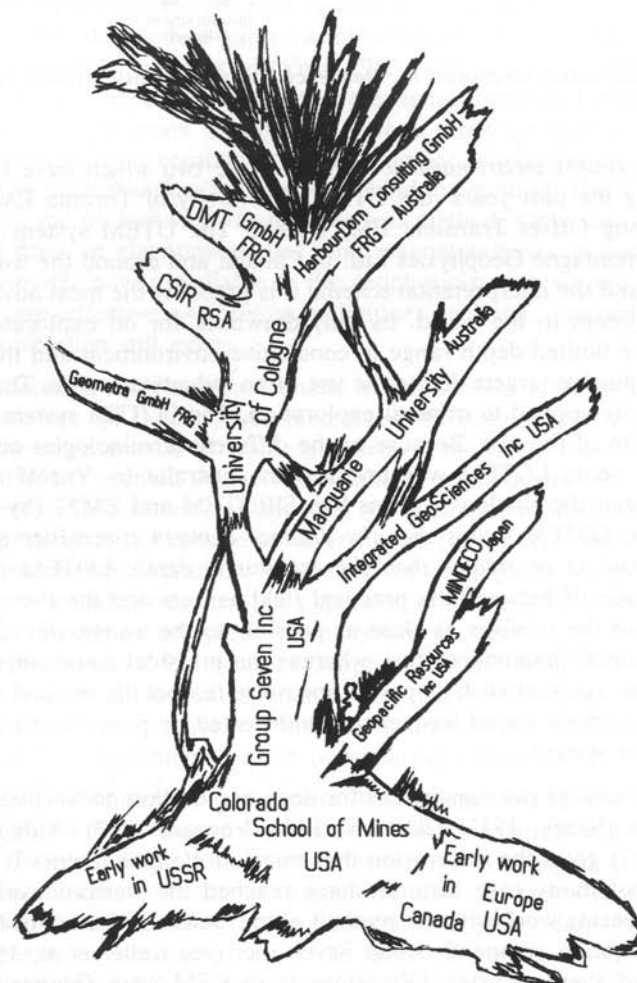


Fig.1.3: Historical tree of the different organizations involved in deep transient electromagnetics.

Group Seven Inc. DEMS I consisted of off-the-shelf components mounted on a truck. The hardware was powered by a 12V DC to 110V AC converter. Integrated GeoSciences Inc. used DEMS II, which was an improved version of the developments at CSM and Geopacific Inc.. DEMS II was a special purpose battery powered portable acquisition system. Subsequently, 1983, DEMS III, an improved combination of DEMS I and II was built in Australia. DEMS III was a modified full scale computer with all standard power supplies replaced by ruggedized field versions such that it completely operated on DC without DC to AC converter. The initial work in Australia (Strack, 1984) was continued by Vozoff (Vozoff et al, 1985), who used for the first time a general purpose EM system (Zonge's GDP 12 general purpose receiver) for *deep transient electromagnetics*. In 1985, the German Ministry for Research and Technology (BMFT) and the European Community granted the University of Cologne the support for the development of the new generation of equipment, called DEMS IV. DEMS IV is a portable system, completely battery powered and containing a computer with more power and a removable hard disk for data transfer. DEMS IV was the first system which acquired and kept all individual ("raw") records for prestack processing. DEMS IV was manufactured by Metronix GmbH under the University of Cologne's supervision for the LOTEM demonstration project in China and India.

During 1988 and 1989 the DEMS IV system was successfully used for six months without major breakdown in China and India. During the same year DEMS IV was successfully combined with a Zonge transmitter for deep crustal research in South Africa. The South African research group at the CSIR is presently developing a special purpose system for ultra deep crustal studies.

The latest generation of deep transient EM equipment follows a new acquisition principle: using remote units which acquire the data independently, thus (in principal) not limiting the number of channels. This generation is called DEMS V. The development is based on the SEAMEX (patent pending) seismic system of WBK (now DMT) of Bochum, Germany. The patent for the new system (called TEAMEX) has been applied for by WBK-DMT. The received data is acquired with instantaneous floating point amplifiers and stored in the remote unit. The data is then sent unmultiplexed in digital form to the central unit via a two wire telemetry. Several new generations of LOTEM hardware are on the drawing board with the most promising coming from seismic industry.

ELECTRICAL CONDUCTIVITY / RESISTIVITY IN EXPLORATION

Exploration geophysicists dealing with electromagnetic data are facing the problem that they must assume the electrical properties of rocks to be given or measured correctly. Already this assumption in itself is very restrictive, since significant uncertainties are associated with the resistivities of rocks. In this section only some of the key problems of electrical resistivity necessary for the interpretation of LOTEM data are addressed. Excellent reviews of the subject can be found in Keller (1988) and Palacky

With these data and the conditions in the target area, it is relatively easy to select an optimum survey layout. This should be done as final step to give input to the logistics operator for the survey design: optimum transmitter–receiver offset, optimum time window, required accuracy for the data. The latter always results in a tradeoff: the longer you stay at one receiver site the better your averaged signal becomes, but also the costs per station increase. The feasibility study can put limits on the required accuracy and therefore help in both, time–planning and in cost estimation.

You may refine the presurvey feasibility study even more, if you have more data available. If noise measurements from the survey area and the system response of your system exists, you may actually want to calculate synthetic, noisy, raw field data and simulate the whole interpretation process. The more time you spend on the feasibility study the more time you will save during the data acquisition and interpretation phase.

In the next section artificial noise is added to the data and the resolution is investigated under production conditions by looking at the inversion results.

RESOLVING A DEEP CARBONATE UNIT

A difficult target for EM techniques is the determination of resistivity and thickness of thick resistive units at a depth of 4 to 6 km. For production and exploration problems this is however very important because accurate porosity predictions can save money spent on dry wells. To simulate this situation we have selected a case history simulating an exploration situation in China (Baxian Depression). The objective of the feasibility study was to find the optimum survey strategy under the following conditions:

- The LOTEM measurements are carried out in a production mode along a profile.
- Two wells at either end of the profile and a good seismic section are available.
- The interpretation is restricted to one–dimensional modeling to maintain production and constrain the effort in interpretation.
- Archie's formula applies to the carbonates embedded in clastic sediments.

The color figures for this feasibility study are given in Appendix 7. Figure A.7.2 (top) shows an electrical section with three layers which has an additional fourth layer embedded between 4 and 6 km depth. The section without the additional layer represents the overall structure of the Baxian Depression according to Chen Leshou et al's (1988) interpretation of magnetotelluric data (table 6.3). The Baxian Depression is part of the Bohai Gulf Basin which has a great variety of different oil and gas pool

The integration of the above concepts starts already in the field. When carrying out field measurements, the observer should notice changes in physical properties or the environment. Production of reliable data can only be increased when effective quality control is done on a continual basis. In particular, the success of a method strongly depends on a field crew and the amount of quality control done in the field. During the interpretation phase, the knowledge of possible combinations of the physical parameters such as possible resistivity variations associated with porosity variations is extremely important. This knowledge is usually the key factor when separating unreasonable subsurface images from the realistic ones. The geophysicist is usually responsible for the integration of theory and model realization. He/she will in most instances provide the interpretation tools such as numerical and analog modeling. These tools can only be effectively applied when the range of possible resistivities and their meaning is understood. During this interaction the geophysicist will in most instances be responsible for the transfer of his knowledge of processing theory and methods to the other members of the interpretation team. This will enable them to come up with the most reasonable interpretation in accordance with the field data. Avoiding this interaction most likely will produce biased interpretation results.

Figure 1.5 shows the resistivity range for consolidated and unconsolidated sediments. Knowing the rock type does not suffice, since the ranges are very large. Additional information about the petrophysical behavior of the rocks and their in situ conditions is needed to narrow down these ranges and to obtain reliable estimates of the resistivities. For example, coal which may vary in resistivity over five and a half decades can puzzle the interpreter. Wet, "dirty" coal is conductive and dry, clean coal resistive. The interpreter must consider all dependencies of assumed resistivity in order to obtain reliable information.

The resistivity of a rock with respect to its components is not easily expressed in terms of a formula. The best review of the subject is given in one of the Schlumberger manuals (Schlumberger, 1987). For clean compacted sand Archie (1942) derived an empirical formula:

$$\rho = \rho_w \frac{a}{\phi^m} \frac{1}{S^n}, \quad (1.1)$$

where ρ is the resistivity of the formation, ρ_w is the resistivity of the pore fluid, a is an empirically determined constant, ϕ is the porosity of the formation, and S is the fraction of the pore volume occupied by formation water, m and n are empirical constants. Unless found different, n is recommended by Schlumberger (1987) as $n = 2$. The exponent m is also called cementation factor. For sands the formation factor $F = a / \phi^m$ is

$$F = \frac{0.62}{\phi^{2.15}} \quad (\text{Humble formation factor}) \quad (1.2)$$

and for compacted formations $F = 1 / \phi^2$ (Archie formation factor). When the forma-

tion becomes shaly, the above relation no longer applies and further corrections need to be applied. An example is given in one of the Schlumberger manuals (Schlumberger, 1987):

$$\rho = \frac{F \rho_w}{S^2 (1 - V_x)} + \frac{C V_x}{\rho_x}, \quad (1.3)$$

where ρ_x is the resistivity of the shale or clay, V_x its volume and C a term related to the water saturation. Table 1.1 shows possible values for the constants for the determination of the formation factor constants for different rock types.

Table 1.1: Different constants to be substituted in Archie's formula when lithology of a rock is known (after Keller, 1988).

DESCRIPTION OF ROCK	a	m
Weakly-cemented detrital rocks, such as sand, sandstone, and some limestones, with a porosity range from 25 to 45 %, usually Tertiary in age	0.88	1.37
Moderately well cemented sedimentary rocks, including sandstones and limestones, with a porosity range from 18 to 35 %, usually Mesozoic age	0.62	1.72
Well-cemented sedimentary rocks with a porosity range from 5% to 25%, usually Paleozoic in age	0.62	1.95
Highly porous volcanic rocks, such as tuff, Aa and Pahoehoe, with porosity in the range from 10% to 80%	3.5	1.44
Rocks with less than 4% porosity, including dense igneous rocks and metamorphosed sedimentary rocks	1.4	1.58

From the above table, even the determination of a simple parameter such as the rock resistivity can be difficult under static conditions due to the composition of rocks. The determination of the rock resistivity becomes even more difficult in situ when the behavior of rocks changes with temperature and depth, salinity and porosity. Figure 1.6 shows the change in resistivity versus temperature for different salt concentrations of the pore fluid. All factors need to be considered when deriving a reliable estimate for a particular formation at a particular depth.

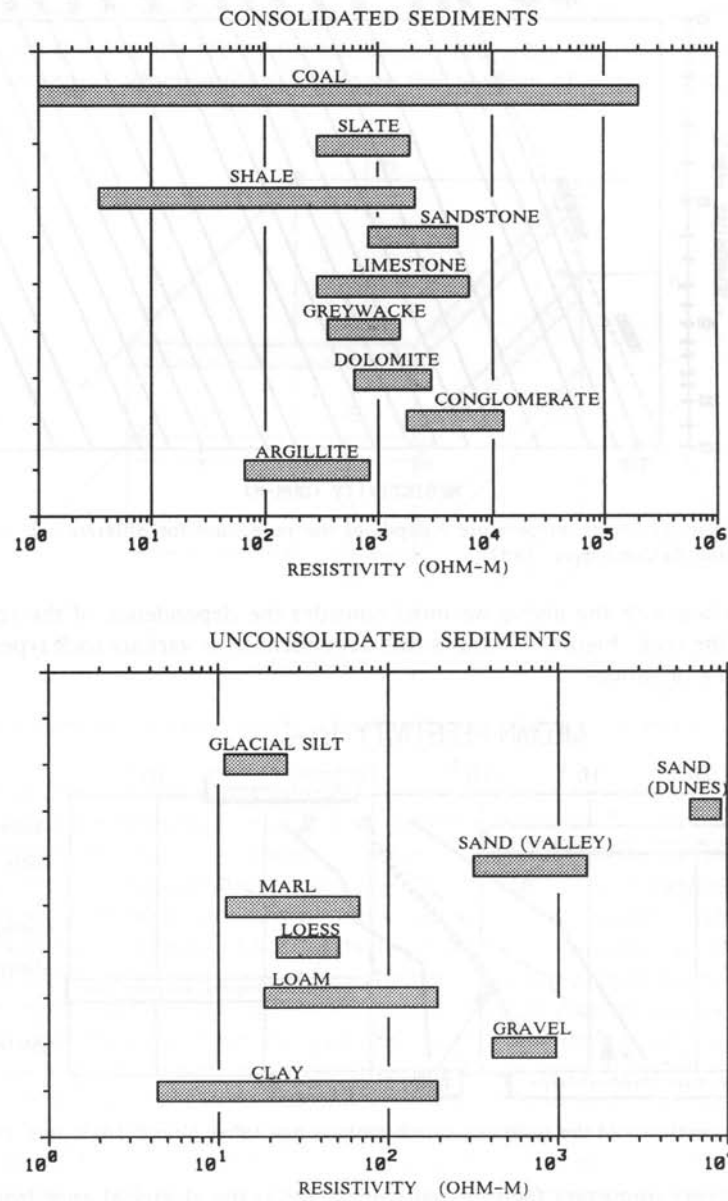


Fig. 1.5: Ranges of resistivity for consolidated and unconsolidated sedimentary rocks (modified after Angenheister, 1982).

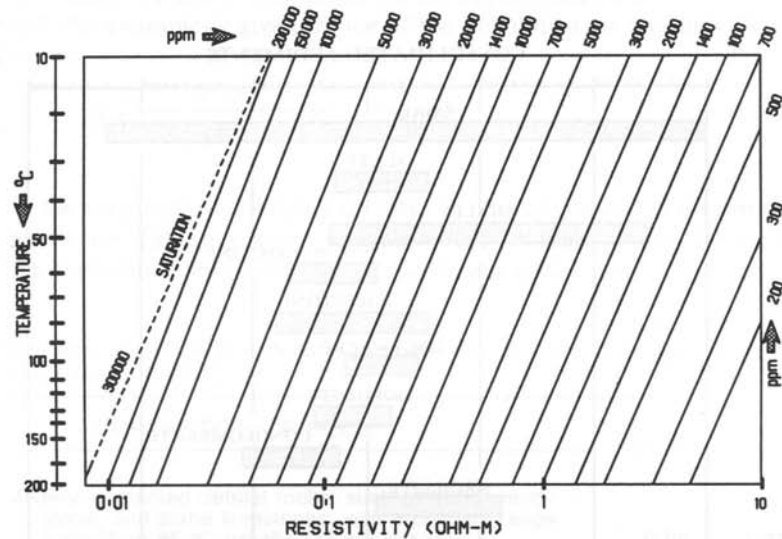


Fig.1.6: Resistivity versus temperature / depth of the pore fluid for different salt concentrations (after Schlumberger, 1987).

In combination with the above we must consider the dependence of the resistivity on the age of the rock. Figure 1.7 shows this dependence for various rock types, based on a statistical evaluation.

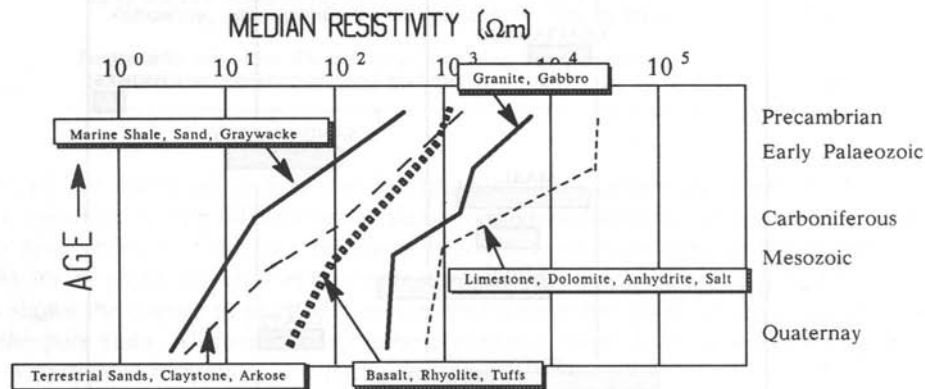


Fig.1.7: Dependency of the resistivity versus geologic age (after Vozoff 1989 pers. comm.).

Another very important factor usually neglected is the electrical anisotropy of rocks. We speak of anisotropy when the resistivity of a rock is different in longitudinal (horizontal) and transverse (vertical) direction. Strictly speaking, we are using anisotropy in a two-dimensional sense, i.e. the difference between resistivity measured in vertical and horizontal direction (assuming no horizontal anisotropy). For most sedimentary

areas this is valid because of the slow sedimentation process which deposits sediments in a layer-cake. Figure 1.8 illustrates this anisotropy with a block model. Here a cyclic deposition process has been assumed which causes a cyclic change in resistivities from ρ_1 to ρ_2 . When deriving the theory for anisotropic cases the scalar resistivity must be replaced by a tensor which quickly increases the number of possible solutions to a problem.

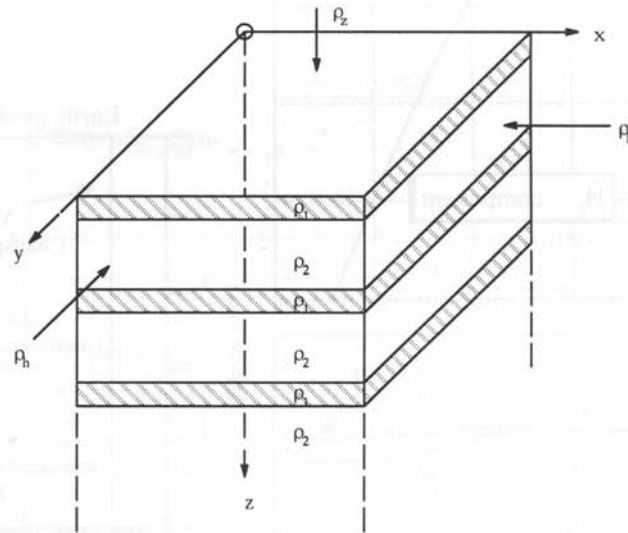


Fig.1.8: Resistivity anisotropy as a result of horizontal bedding during cyclic deposition.

Since the problem of anisotropy is more complex than can be considered here, only simple examples are discussed. How can we observe anisotropy in the data with the LOTEM method? We must find means to measure the vertical current flow and display it. In addition to horizontal induction current flow the LOTEM method generates vertical currents with the grounded wire transmitter (see next chapter). When considering the magnetic component of the receiver, we will predominantly see the effect of horizontal induction or in the sense of this chapter longitudinal resistivities. The electric receiver signal contains also information about vertical current flow or the transverse resistivity of the subsurface. In figure 1.9 this effect is used to demonstrate how electrical anisotropy influences the signal measured with deep transient electromagnetics. The top and bottom graphs compare a half space with an average resistivity of 10 Ohm-m (typical value for sediments) with the same basic geologic model plus two thin (each 50 m thick) resistive layers at great depth (2000 m and 2250 m respectively). It can be shown in figure 1.8 that this model represents an anisotropic situation. For the magnetic field derivative (top), measured with an induction loop magnetometer, the anisotropy can not be seen which is due to the nature of the magnetic field measurements which only sense horizontal current flows. The two curves do not differ from each other. For the electric fields the anisotropy becomes visible which is

expressed by the difference between the half-space response and the anisotropic model response from approximately 0.5 s on.

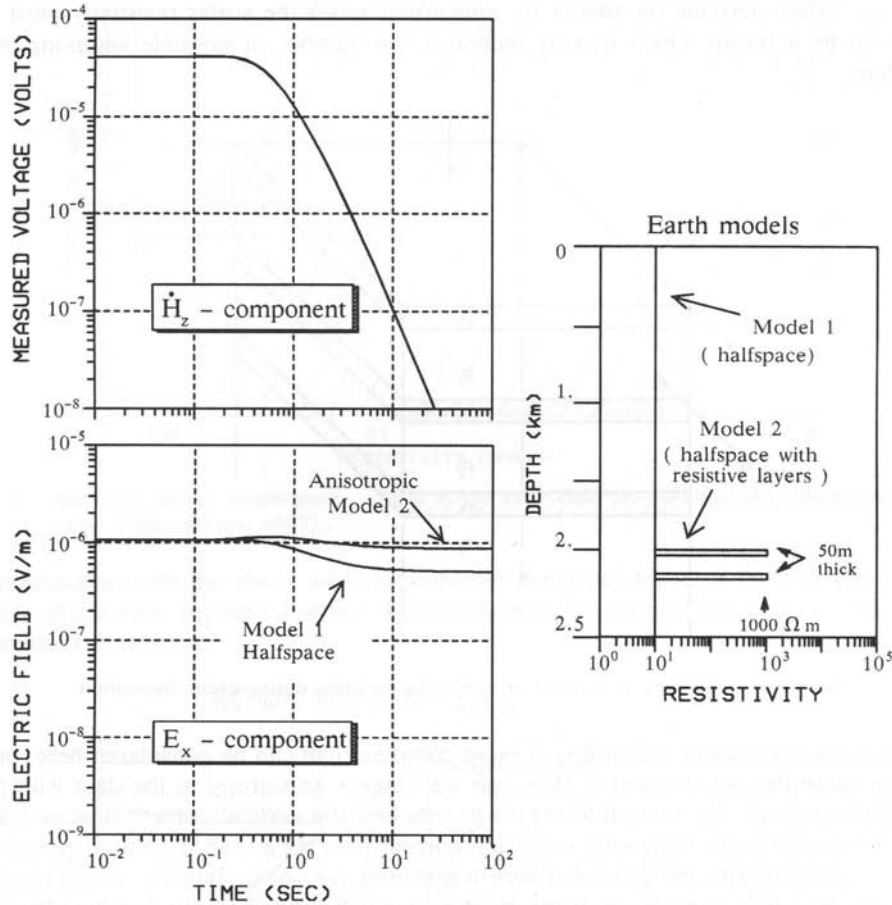


Fig. 1.9: Simulation of an anisotropic model for the LOTEM method for the magnetic field derivative (top) and electric field (bottom) responses. The half space has a resistivity of 10 Ohm-m and all measurements are taken at 7 km offset. The anisotropic model includes two embedded resistive layers (each 50 m thick, 1000 Ohm-m resistivity) at a depth of 2000 m and 2250 m.

So far, we learned that electrical anisotropy manifests itself in LOTEM data only in the electric field components. The next question which arises for the interpreter is: How do we get an idea about the anisotropy in an exploration area? This is usually done using well logs or when the appropriate measurements have been done on core samples. Figure 1.10 shows an example for the longitudinal resistivities of two formations (from the Denver-Julesberg Basin) and the corresponding coefficient of anisotropy along the area (Keller, 1971). The anisotropy coefficient is the square root

of the ratio of vertical and horizontal resistivity. The data was obtained from well log and core analysis. This type of information allows the interpreter to obtain a realistic first interpretation for an area, while at the same time drawing his attention to possible interpretation problems due to anisotropy. In figure 1.10 interpretation problems could be anticipated for data from range 50 to 54 where the coefficient of anisotropy rises. Using reliable interpretation input can save a significant amount of time and avoid problems due to possible misinterpretation.

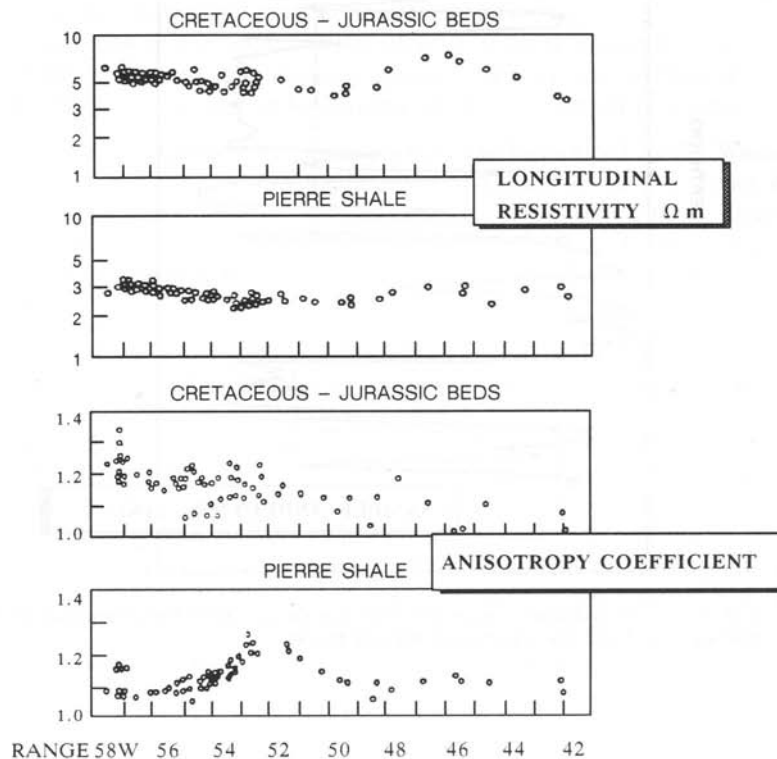


Fig.1.10: Example of longitudinal resistivities (top) and electrical anisotropies (bottom) for two formations across an area in the Denver-Julesburg Basin, USA (after Keller, 1971).

In most cases an excellent resistivity interpretation across a profile (as in figure 1.10) does not exist. Then, one can use a well log to derive a basic electric model for the area. The finely resolved well log can then be reduced to a coarser blocked one as shown in figure 1.11. Here the blocking has been done by visual inspection. Also, the near surface conductor was not considered because the LOTEM system is not designed to resolve this shallow depth range. A description on how a more accurate blocking is done can be found in the chapter on presurvey feasibility studies. If even a

single well log does not exist, the interpreter must rely completely on his/her judgement not forgetting all the inaccuracies and changes with the electrical resistivity.

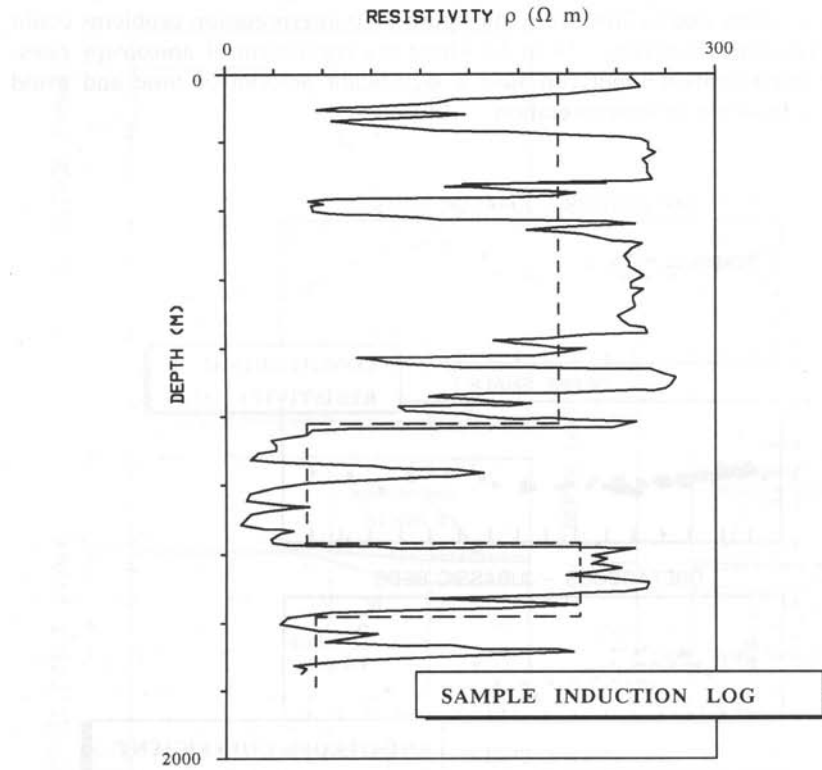


Fig.1.11: Example of an induction log as used for the definition of the interpretation model. The dashed line shows the interpreted starting model.

SUMMARY CHAPTER 1

Among electromagnetic techniques, magnetotellurics has become an acceptable tool for the exploration industry while transient electromagnetics is still in the evaluation phase. Transient electromagnetic methods can give very useful additional information for exploration problems associated with permafrost, oil-water contact, volcanic covers, overthrusting, diapirism, deeply weathered overburden, extreme topography in connection with any of the above, delineation of porosity variation, and deep crustal studies. In all cases transient electromagnetics can provide additional information which helps in clarifying and understanding of the exploration problem.

Historically, deep transient electromagnetics was introduced to the Western world by Keller at the Colorado School of Mines and Group Seven Inc. From there, the research activities spread out to Asia, Australia and subsequently to Germany and South Africa. Nowadays, several different research groups exist worldwide which are working on the advancement and in particular the industrial application of the technique.

When applying electromagnetic techniques to exploration problems, a thorough understanding of the basic assumptions such as resistivity estimates is very important. In particular, the reliability of these resistivity estimates must be evaluated by considering the individual components in the empirical formulae relating them to the rock resistivity. Even then, the range of resistivity variations given to us by the geology is rather large and forces the explorationist to continuously question his/her assumptions. Any additional information which can be obtained is extremely important to derive the best basic model which can then be related to the geophysical measurements. Even after finding the best geophysical model, the question of ambiguity caused by anisotropy must be eliminated by carrying out proper field measurements and evaluating the existence of and corrections for the anisotropy.

PROBLEMS CHAPTER 1

1. What is Archie's law or formula?
2. Which formula would you use to define the bulk resistivity of a sandstone with a sand-to-shale ratio of 50%?
3. How do we observe electrical anisotropy in LOTEM data?
4. Given a new exploration area, what information would you be looking for to evaluate whether you can apply LOTEM? Outline the strategy you would follow if one of the selected pieces of information is missing or non conclusive.
5. Calculate the rock resistivities for well-cemented sediments, highly porous volcanic rocks, and crystalline rocks for porosity values of 5, 10, 20, 30%.
6. Calculate resistivity as a function of depth for sandstones with 25% porosity and a salt concentration of 14 000 ppm. Use the standard geothermal gradient.
7. What are the main differences between a time domain and a frequency domain system?

KMS Technologies – KJT Enterprises Inc.
6420 Richmond Ave., Suite 610
Houston, Texas, 77057, USA
Tel: 713.532.8144

Please visit us
<http://www.kmstechnologies.com>

This material is not longer covered by copyright. The copyright was released by Elsevier to Dr. Strack on November 5th, 2007.

The author explicitly authorizes unrestricted use of this material as long as proper reference is given.

KMS Technologies – KJT Enterprises Inc.

An EMGS/rxt-company

Chapter 2 Basic Theoretical Background

extract from

Strack, K.-M., 1992, reprinted 1999
***Exploration with deep transient
electromagnetic:*** Elsevier, 373 pp.

This material is not longer cover by copyright. The copyright was released by Elsevier to Dr. Strack on November 5th, 2007.

The author explicit authorizes unrestricted use of this material as long as proper reference is given.

Chapter 2

Basic Theoretical Background

The original theory of *transient electromagnetics* can be found in two textbooks (Vanyan, 1967; Kaufman and Keller, 1983). Here, only the key equations will be given. The derivations of the equations are slightly different from the concepts in the above mentioned books, but give a more consistent picture suitable for today's numerical implementations. One exemplary derivation is given in appendix 1. We mainly follow the concepts by Weidelt (1985), and Ward and Hohmann (1988). A well described summary of all equations and the derivations can be found in Petry (1987) and Boerner (1992), and of the entire LOTEM system in Strack (1985). The general framework how to relate the derivations to controlled source electromagnetic techniques for petroleum exploration can be found in Nekut and Spies (1989).

After explaining the physical and of deep transient electromagnetics, emphasis is given to the different ways of presentation of the field data. The goal is to provide the reader with ways of relating the material in this chapter to standard geoelectric data presentation (apparent resistivities) and a more direct of the resistivity structure.

PHYSICAL PRINCIPLES

The deep transient electromagnetic method described in this book uses a grounded wire transmitter and receivers for the electric field and the time derivative of the magnetic field (figure 2.1). The transmitter dipole is usually several hundred meters to several kilometers long. The distance between transmitter and receiver site, called *offset*, varies between 2 and 20 km. Shorter or longer offsets are possible but are less often used. When the offset is approximately equal or larger than the exploration depth, the method is also called Long Offset Transient Electromagnetics (LOTEM).

A square wave current is injected into the ground through the transmitter bipole (following called dipole). The current switching induces electromagnetic induction currents in the subsurface. The diffusion process of the transient electromagnetic fields can be visualized using the *smoke ring concept* (Nabighian, 1979; Oristaglio and Hohmann, 1984; Gunderson et al, 1986). For a grounded wire transmitter which consists of a small bipole, one can calculate the electric field within a half-space shown in figure 2.2. The solid contour lines represent lines of equal electrical field strength corresponding to positive current flow, whereas the dashed ones represent negative current flows. The induction currents flow perpendicular to the plane of the drawing. Therefore, one can imagine the current flow extending out of the page at the top and

returning in the lower part of the frame. The individual frames in the figure represent snapshots at different times after current turn off, denoted on the lower right of the frames. At early times the currents are predominantly located near the transmitter wire. With increasing time the induction currents diffuse downwards.

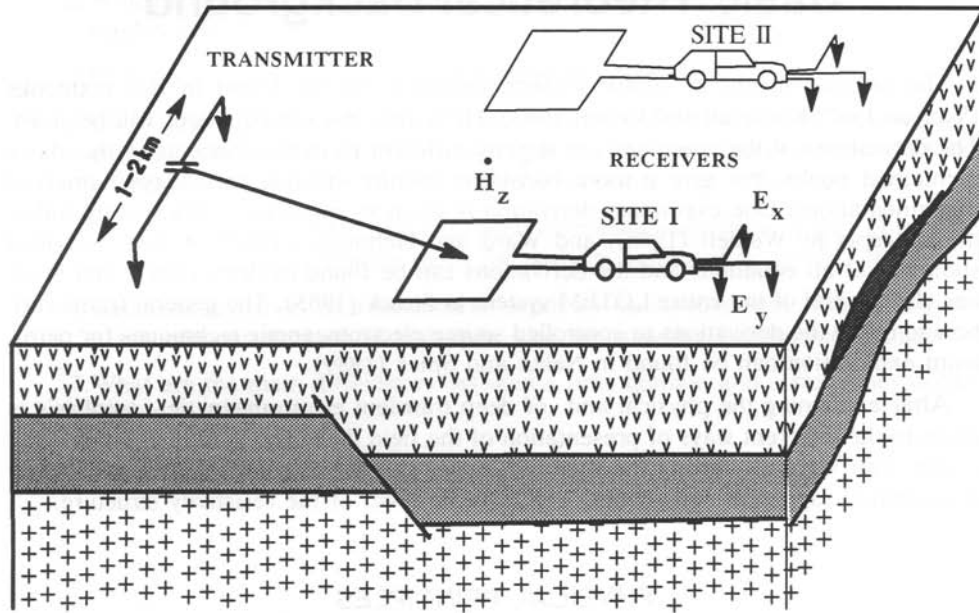


Fig. 2.1: Typical LOTEM transmitter and receiver setup (single site system).

If we now introduce an intermediate layer in the earth model, the diffusion patterns change. In figure 2.3 an additional layer of 2000 Ohm-m resistivity has been introduced at a depth of 3 kilometers. When the induced currents, which are flowing perpendicular to the plane of the drawing, reach the layer boundary, they start to diffuse outwards with increasing time. This causes the signal information at the receiver to come from an area of integration somewhere between the transmitter and receiver. Figure 2.4 gives a comparison of the diffusion process for a half-space and two-layer models for the 10 msec snapshot. The diffusion speed depends strongly on the resistivity of the subsurface. In the two-layer case a typical resistivity contrast for German crustal applications has been selected. The sharp corners in some of the contour lines are solely due to the resolution of the contouring.

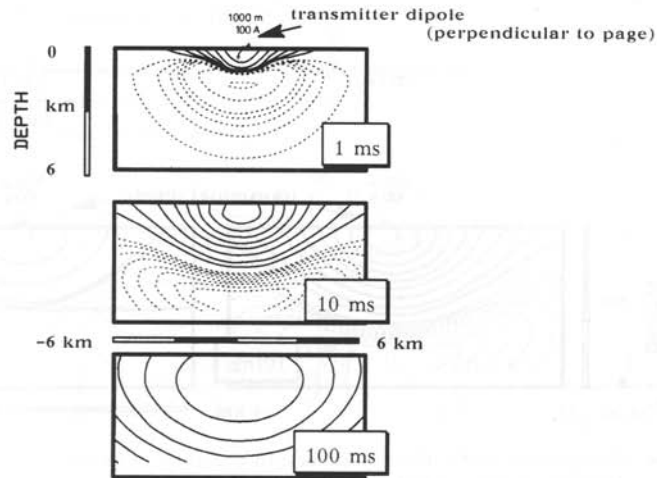


Fig. 2.2: *Smoke rings* for a grounded dipole in a half-space with $200 \Omega\text{m}$ resistivity. The different frames mark different times after current turn off. The contours represent lines of equal electric field strength. The dashed lines mark opposite polarity.

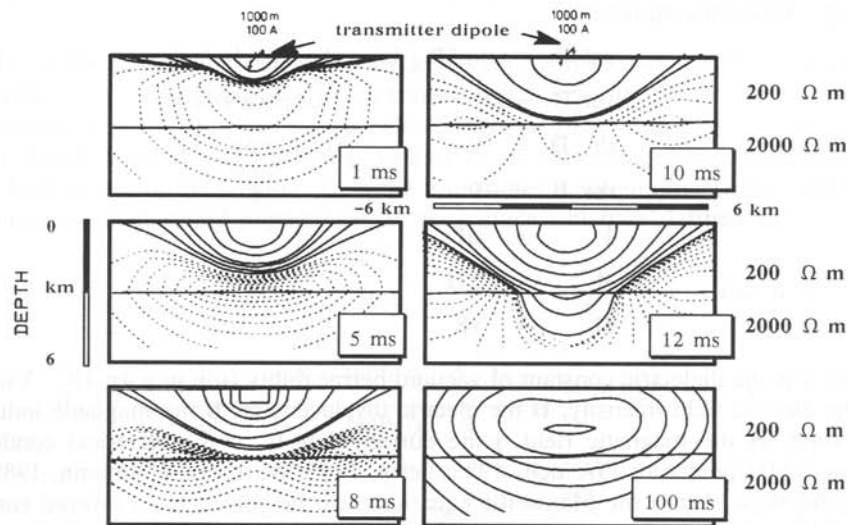


Fig. 2.3: System of *smoke rings* for a grounded wire dipole on a two-layer earth model. The contours represent lines of equal electric field strength. The dashed lines mark opposite polarity.

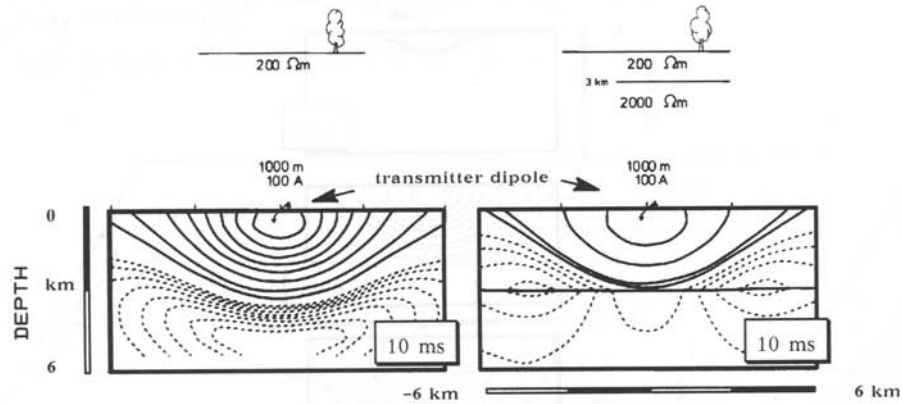


Fig. 2.4: Comparison of the diffusion process of induction currents 10 ms after current turn off for a half-space and a two-layer earth model.

THEORETICAL BACKGROUND

The derivation of the electromagnetic field equations is based upon the quasi-stationary Maxwell's equations:

$$\text{rot } \mathbf{E} = - \delta \mathbf{B} / \delta t \quad (\text{Faraday's law})$$

$$\text{rot } \mathbf{H} = \mathbf{j} \quad (\text{Ampere's law})$$

$$\text{div } \mathbf{D} = 0 \quad (\text{Coulomb's law})$$

$$\text{div } \mathbf{B} = 0$$

$$\mathbf{j} = \sigma \mathbf{E}$$

$$\mathbf{B} = \mu \mathbf{H}$$

$$\mathbf{D} = \epsilon \mathbf{E}$$

(2.1)

where ϵ is the dielectric constant of vacuum permeability ($\mu = \mu_0 = 4\pi \cdot 10^{-7} \text{ Vs/Am}$), \mathbf{E} is the electric field intensity, \mathbf{D} the electric displacement, \mathbf{B} the magnetic induction, t the time, \mathbf{H} the magnetic field, \mathbf{j} the current density, σ the electrical conductivity. Using scalar potentials (Weidelt, 1985; Petry, 1987; Ward and Hohmann, 1988; Boerner and West, 1989) the Maxwell's equations can be solved for a layered earth. The selected scalar potentials are commonly denoted ϕ_E and ϕ_M . They satisfy the above equations independently. In potential theory these scalar potentials are sometimes called Debye potentials or poloidal and toroidal potentials. ϕ_E does not generate an electric field component in vertical direction and ϕ_M does not generate a magnetic component in vertical direction. Thus ϕ_E is also called transverse or tangential electric

(TE) mode and ϕ_M is called transverse or tangential magnetic (TM) mode. Often the word polarization is used equivalent to mode.

In the 1-D case the TE mode contains only horizontal and the TM mode vertical currents. The following equations are for the voltages measured by induction loop magnetometers, U, or electric field sensors, V:

$$U_z(\mathbf{r}, t) = \frac{-1}{2\pi} \int_{-\infty}^{\infty} \mu_0 A e^{i\omega t} \frac{D_0 \cos \phi}{4\pi} \int_0^{\infty} \frac{B_{E1}(\kappa, \omega) - \kappa}{B_{E1}(\kappa, \omega) + \kappa} \kappa J_1(\kappa r) d\kappa d\omega \quad (2.2)$$

$$V_x = l E_x(\mathbf{r}, t) = \frac{-l}{2\pi i} \int_{-\infty}^{\infty} \frac{e^{i\omega t}}{\omega} \frac{-i\omega \mu_0 D_0}{4\pi} \int_0^{\infty} \left\{ \left(\frac{B_{H1}(\kappa, \omega) - \kappa}{\alpha^2} - \frac{1}{B_{E1}(\kappa, \omega) + \kappa} \right) \left(\frac{2}{r} J_1(\kappa r) (2 \cos^2 \phi - 1) - 2 \kappa J_0(\kappa r) \cos^2 \phi \right) + \frac{B_{E1}(\kappa, \omega) - \kappa}{B_{E1}(\kappa, \omega) + \kappa} \kappa J_0(\kappa r) \right\} d\kappa d\omega + \frac{\rho_1 D_0}{2\pi r^3} (2 - 3 \sin^2 \phi) \quad (2.3)$$

where U_z is the voltage induced in an induction coil with the area A . ϕ is the angle between the x-coordinate (parallel to the transmitter dipole) and the offset vector \mathbf{r} , y is the coordinate perpendicular to the dipole, ω is the angular frequency, κ is the wave number, J_0 and J_1 are Bessel functions, V_x and V_y are the voltages measured with an electric field sensor of the length l , D_0 is the transmitter dipole moment. B_{E1} and B_{H1} are the reciprocal modified impedances at the surface which are defined as:

$$B_{En, Hn} = \alpha_n \quad \alpha_m^2 = \kappa^2 + i\omega \mu_0 \sigma_m$$

$$B_{Em} = \alpha_m \frac{B_{Em+1} + \alpha_m \tanh(\alpha_m d_m)}{\alpha_m + B_{Em+1} \tanh(\alpha_m d_m)} \quad (2.5)$$

$$B_{Hm} = \alpha_m \frac{B_{Hm+1} + \alpha_m \beta_m \tanh(\alpha_m d_m)}{\alpha_m \beta_m + B_{Hm+1} \tanh(\alpha_m d_m)} \quad (2.6)$$

$$m = M - 1, \dots, 1 \quad d_m = h_{m+1} - h_m \quad \beta_m = \sigma_{m+1} / \sigma_m$$

where n is the number of layers and h_i their respective thicknesses. The recursion is defined such that it starts with the lowest layer, the bottom half-space. There the electromagnetic field disappears at infinity which allows its solution. From this n -th layer one works upwards to the $(n-1)$ -th layer until the surface is reached. With these formulae the voltages for a layered earth model can be calculated and compared with the voltages received in the field.

One of the frequently asked questions is why there are no direct electromagnetic reflections when the equation can be nicely expressed as recursion formula for the individual layers. The cause lies in the neglect of the displacement currents which reduce the wave equation to a diffusion equation. To show that the latter can be neglected, we use the wave equations for the electric and magnetic fields:

$$\nabla^2 \mathbf{E} + (\mu \epsilon \omega^2 - i \mu \sigma \omega) \mathbf{E} = 0 \quad (2.7)$$

and

$$\nabla^2 \mathbf{H} + (\mu \epsilon \omega^2 - i \mu \sigma \omega) \mathbf{H} = 0. \quad (2.8)$$

The bracket can be reduced to $(-i \mu \sigma \omega)$ when the first term is very small or $1 / \epsilon \omega \rho \gg 1$. For most rocks the dielectric constant ϵ is in the order of 10^{-10} As/Vm. For resistivities around 1 to 10000 Ωm and frequency below 1kHz the quantity $1 / \rho \omega \epsilon = 1 / (10^4 \cdot 10^3 \cdot 10^{-10}) = 10^3 \gg 1$. This means the displacement current can be neglected indeed.

The above theory is sufficient for the inversion, but leaves the operator with no feeling for the data and their correspondence to the geology. Thus we need to find a way of presenting the data for the operator in the field. We borrow from other electrical methods the concept of apparent resistivity to do this.

APPARENT RESISTIVITY

One definition of apparent resistivity is given by Sheriff (1984):

"The resistivity of homogeneous isotropic ground which would give the same voltage – current relationship as measured."

With this, apparent resistivities have been defined for all electrical and electromagnetic methods. All of them have as their goal to define the physical change of the

subsurface as a function of a parameter specific to the method. In DC-resistivity soundings, the spacing can be used to obtain an estimate about the exploration depth. For frequency domain methods (magnetotellurics, audio magnetotellurics, controlled source audio magnetotellurics, frequency domain soundings and others), the apparent resistivity and phase curves are related to frequency which is connected directly via the skin depth to the exploration depth. For transient EM methods the time window is directly related to the exploration depth range (Spies, 1989). The distance between transmitter and receiver, called offset, is the governing factor at which time window conductivity features in the subsurface are resolvable by an instrument with a given dynamic range. The resolution of these features strongly depends upon the signal-to-noise ratios obtained in the survey area. In electrical/electromagnetic methods, one standard procedure is used to derive the apparent resistivity formulae. The goal of this procedure is to relate the apparent resistivity to the resistivity of a half-space. The resulting equations are to be manipulated only with the knowledge of the field parameters (voltages, array dimension, current, frequency, time etc.) until an apparent resistivity formula can be found. The general steps are:

- Derive the equation for a half-space voltage as a function of the half-space resistivity.
- Rewrite this equation to show the half-space resistivity as a function of the measured voltage, U_m .
- Normalize the measured voltage and relate it to the half-space voltage, i.e.

$$\frac{\rho_a}{\rho_{HS}} = \frac{U_m}{U_{HS}} \quad (2.9)$$

- Leave the unknown, wanted quantity ρ_a on one side of the equation and adjust the equation such that the unknown resistivity of the half-space will cancel out.

Usually, additional constraints from physics help in carrying out the third and fourth steps. For DC-resistivity methods it means that for very long spacings the apparent resistivity approaches the resistivity of the bottom half-space. Similarly, for frequency domain methods, the high and low frequencies yield the true resistivities of the uppermost and deepest half-space. For time domain methods the very early time apparent resistivity gives the top layer and the late time apparent resistivity the bottom layer.

Following this procedure, the apparent resistivity formula can be used to correlate the earth response with the true resistivity changes in the subsurface. For LOTEM the derivation is slightly more complicated, since the half-space voltage depends in a nonlinear fashion on the half-space resistivity, namely:

$$V(t) = \frac{3 D_0 A \rho y}{2 \pi r^5} \left[\operatorname{erf} \left(\frac{u}{\sqrt{2}} \right) - \sqrt{\frac{2}{\pi}} u \left(1 + \frac{u^2}{3} \right) e^{-u^2/2} \right] \quad (2.10)$$

$$\text{with } u = \frac{2 \pi r}{\tau} \quad \tau^2 = \frac{8 \pi^2 \rho t}{\mu_0}$$

and erf as the error function (Abramowitz and Stegun, 1964), $V(t, \rho)$ is uniquely computable, whereas $\rho(t, V)$ is not. There are times when a solution can be found. We thus need to consider the time limits of the above equation. For $t \rightarrow 0$, $u \rightarrow \infty$ and

$$\lim_{u \rightarrow \infty} \text{erf} \left(\frac{u}{\sqrt{2}} \right) = 1 \quad \text{which yields} \quad (2.11)$$

$$U_{\text{ET}}^{\text{HS}} = \lim_{t \rightarrow 0} U(t) = \frac{3 D_0 A y \rho}{2 \pi r^5} \quad (2.12)$$

For $\tau \rightarrow \infty$ we obtain similarly:

$$U_{\text{LT}}^{\text{HS}} = \lim_{\tau \rightarrow \infty} U(t) = \frac{D_0 A y}{40 \pi \sqrt{\pi}} \frac{\mu_0^{5/2}}{\rho^{3/2} t^{5/2}} \quad (2.13)$$

where the subscript ET and LT indicate the early time ($t \rightarrow 0$) and the late time ($t \rightarrow \infty$), respectively. The early time equation is only valid for $\tau/r \leq 2$ and the late time equation for $\tau/r \gg 16$. Using the above and the rule for deriving the apparent resistivity formula we can define early and late time apparent resistivities as:

$$\frac{\rho_a^{\text{ET}}}{\rho_1} = \frac{U(t)_m}{U(t)_{\text{ET}}^{\text{HS}}} \quad \text{or} \quad \rho_a^{\text{ET}} = \frac{2 \pi r^5}{3 D_0 A y} U(t)_m \quad (2.14)$$

$$\frac{\rho_a^{\text{LT}}}{\rho_1} = \left(\frac{U(t)_{\text{LT}}^{\text{HS}}}{U(t)_m} \right)^{2/3} \quad \text{or} \quad \rho_a^{\text{LT}} = \left(\frac{D_0 A y}{40 \pi \sqrt{\pi} U(t)_m} \right)^{2/3} \left(\frac{\mu_0}{t} \right)^{5/3} \quad (2.15)$$

where ρ_a^{ET} = early time apparent resistivity

ρ_1 = resistivity of the half-space

i.e. $\rho_a \begin{cases} = \rho_1 & \text{for early times } \rho \text{ approaches the 1st layer resistivity} \\ = \rho_n & \text{for very late times } \rho \text{ approaches the last layer resistivity} \end{cases}$

ρ_a^{LT} = late time apparent resistivity

$$U(t)_m = \text{measured voltage}$$

$$U(t)_{\text{ET}}^{\text{HS}} = \text{early time half-space voltage}$$

$$U(t)_{\text{LT}}^{\text{HS}} = \text{late time half-space voltage}$$

An example of half-space early and late time apparent resistivity curves is given in figure 2.5. Immediately after current switching, the early time apparent resistivity of the half-space is identical to the true resistivity of the medium. From the vertical marker when $\tau/r \leq 2$ at 0.6 seconds to approximately 30 seconds the apparent resistivity curve does not reflect the true subsurface resistivity (intermediate times). From

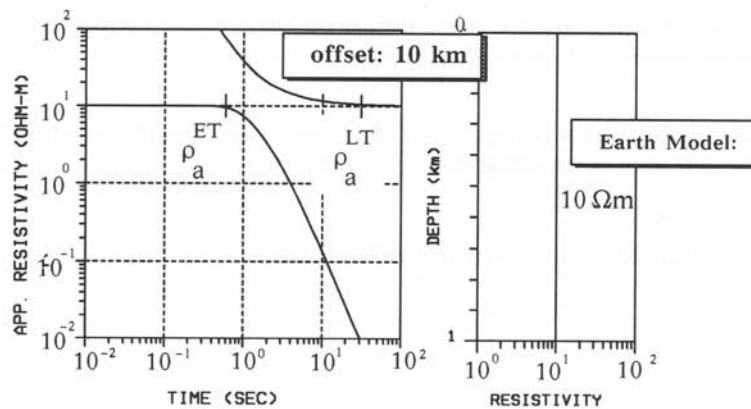


Fig. 2.5: Example of an early and late time apparent resistivity curve for a homogenous half-space with 10 Ωm resistivity.

30 seconds on we reach the so called late times when $\tau/r \gg 16$ and the apparent resistivity curve reflects the true earth resistivity again. Figure 2.6 shows the apparent resistivity curves for a three-layered earth. We can see an increase in the apparent resistivity curve at early times caused by the more resistive second layer. It then decreases again because it loses its validity and only reflects the decay of the physical electromagnetic field. The late time apparent resistivity curve, on the other hand, asymptotes to a value representative of the lowest (semi-infinite) layer.

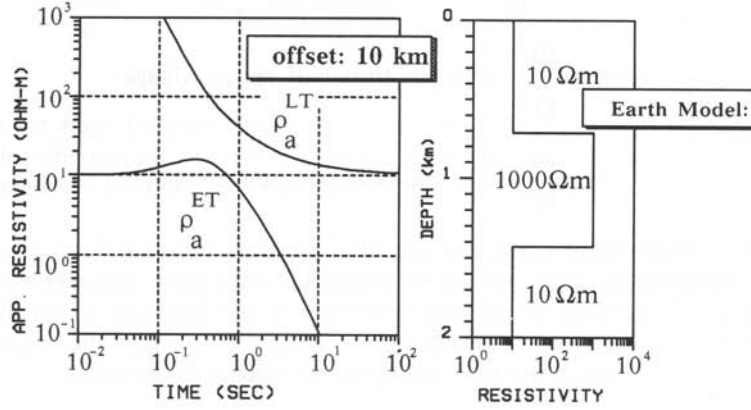


Fig. 2.6: Example of an early and late time apparent resistivity curve for a three-layer earth model with the second layer being highly resistive.

Following this formalism (Petry, 1987) one can derive the apparent resistivity formulae for the different electromagnetic field components which are usually measured in the field:

for the time derivative of the vertical magnetic field:

$$\rho_{a,z}^{ET}(t) = \frac{2\pi r^5}{3AD_0y} U_z(t) \quad (2.16)$$

$$\rho_{a,z}^{LT}(t) = \left(\frac{AD_0y}{40\pi\sqrt{\pi}U_z(t)} \right)^{2/3} \cdot \left(\frac{\mu_0}{t} \right)^{5/3} \quad (2.17)$$

for the electric field parallel to the wire (E_x):

$$\rho_a^{ET}(t) = \frac{4\pi r^3 E_x}{3D_0 \sin^2 \phi} \quad (2.18)$$

$$\rho_a^{LT}(t) = \frac{-2\pi r^3 E_x}{D_0 \left(1 - \frac{3}{2} \sin^2 \phi \right)} \quad (2.19)$$

and for the electric field perpendicular to the wire (E_y):

$$\rho_a^{ET}(t) = \frac{-4\pi r^3 E_y}{3D_0 \cos \phi \sin \phi} \quad (2.20)$$

$$\rho_a^{LT}(t) = \frac{-4\pi r^3 E_y}{3D_0 \cos \phi \sin \phi} \quad (2.21)$$

When carrying out LOTEM measurements, one has to overcome the electromagnetic noise in the survey area. Usually, this means that analog filters are used during the recording of the data. When converting the data to apparent resistivities, the curves look different from the curves in figures 2.5 and 2.6. The curves usually have a steep slope at early times. This slope is caused by the system response, which will be explained in the next chapter. Because the data contains the system response, these curves are called *resistivity transforms* rather than apparent resistivities. Figure 2.7 shows an example of the *resistivity transforms* for the earth models from figure 2.5 and 2.6.

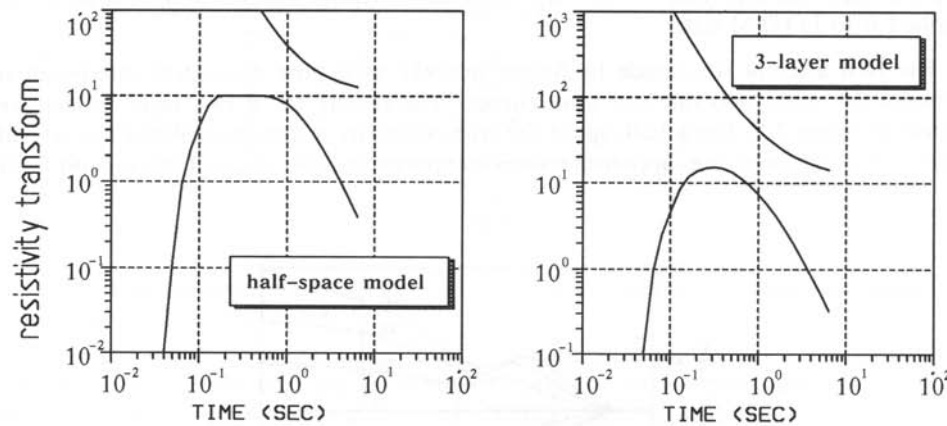


Fig. 2.7: Resistivity transforms for the models from figure 2.5 (left) and 2.6 (right).

At this point, a warning about the use of apparent resistivities for LOTEM seems appropriate. They show only one way of normalizing the data for a first quick look at the field results. Because of the complicated field behaviour and imperfections in the data acquisition (system response and noise) it is difficult to derive a reliable earth model directly from the apparent resistivity curves. Actually, the apparent resistivities have very little meaning for the electric fields and we thus always use the voltages and invert strictly on voltages which are, as already mentioned above, a very good way of

accurately evaluating the data. There have been several attempts without much success to derive an apparent resistivity formula valid for all times for LOTEM (Yang, 1986; Spies and Eggers, 1986; Strack, 1987). They are summarized in the following for completeness.

ALL TIME APPARENT RESISTIVITY

Although the usefulness of apparent resistivity curves for interpretation purposes is debatable, they can help to compare field data from different receiver sites and to obtain some form of normalized data set for contouring and imaging.

Because the increasing number of data sets requires a fast way of data presentation, the quest for an all time apparent resistivity is becoming more important. In the literature only one paper for LOTEM *all time apparent resistivity* (Yang, 1986) is readily available. Yang extended the *all time resistivity* concept and derived a formulation for some specific cases. Similar earlier semi-successful attempts were carried out by Stoyer and Strack (Strack, 1985). All of them have in common that they use the voltage curve as basis for all time apparent resistivity formulation. Spies and Eggers (1986) mention a more promising route using the magnetic field values as basis. They applied their concept only to in-loop TEM data. Karlik (Karlik and Strack, 1990) applied it to LOTEM data.

The first attempt was made by Stoyer in 1981 as a time dependent interpolation between the early and the late time curves. The results for a two-layer model are shown in figure 2.8. For a half-space the true resistivity is obtained. When the second layer is less resistive, the apparent resistivity approaches the value of the second layer

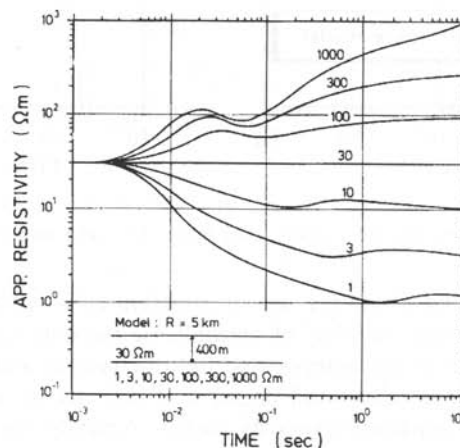


Fig. 2.8: All time apparent resistivity curves by Stoyer for a two-layer model (after Strack, 1985).

and then undershoots before reapproaching it again. For a more resistive second layer it first undershoots and then approaches the resistivity of the second layer. Since the undershoots do not always appear at the same time window, it is very difficult for the interpreter to recognize them without attributing them to an additional layer.

Strack (1985) used a least squares technique to avoid some of the additional flexures. When an additional flexure was automatically recognized as such, a flat part in the apparent resistivity curve resulted. However, even for a four-layer model, additional flexure in the curve could not be completely avoided. In figure 2.9 the curve for a 1500 m thick third conductive layer exhibits the part where no solution could be found between 0.6 to approximately 2 seconds. If this layer is only 1000 m thick the *all time apparent resistivity* curve is smooth but reflects a typical five-layer apparent resistivity curve.

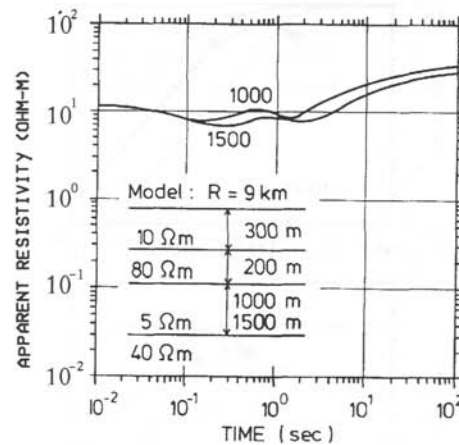


Fig. 2.9: *All time apparent resistivity* curves for a four-layer model using Strack's least square formulation (after Strack, 1985).

Yang (1986) conditioned the least squares process further and obtained a larger class of all time apparent resistivity curves without significant flexures. However, he could not obtain curves for all classes of models, in particular, not for realistic long offsets. Only slight additional flexure is visible in his three-layer curves. It is difficult to decide which one of these flexures is due to real geology or due to the algorithm. Since Yang used mainly offsets smaller than four times the dipole length, the applicability of his approach for LOTEM data is limited.

Karlik (Karlik and Strack, 1990) used the idea described by Spies and Eggers (1986) which uses the magnetic field instead of its derivative. This is achieved by integrating the voltage response. The measured data set (as a function of transmitter to receiver offset) is compared with the magnetic field of a homogenous half-space for which the conductivity is to be found such that:

$$H_z^m = H_z^{HS} \quad \text{or} \quad H_z^m - H_z^{HS} = 0$$

or in general terms:

$$g - f(\rho) = 0 \quad (2.22)$$

From this equation, one can obtain ρ using

$$\rho = f^{-1}(g) \quad (2.23)$$

Equation 2.23 can only be solved numerically using a technique such as the Newton-Raphson method. The initial resistivity of the homogenous half-space is varied until equation 2.22 is satisfied. Using this procedure and the magnetic field rather than the voltage response avoids the problem of the non-single valued function described in

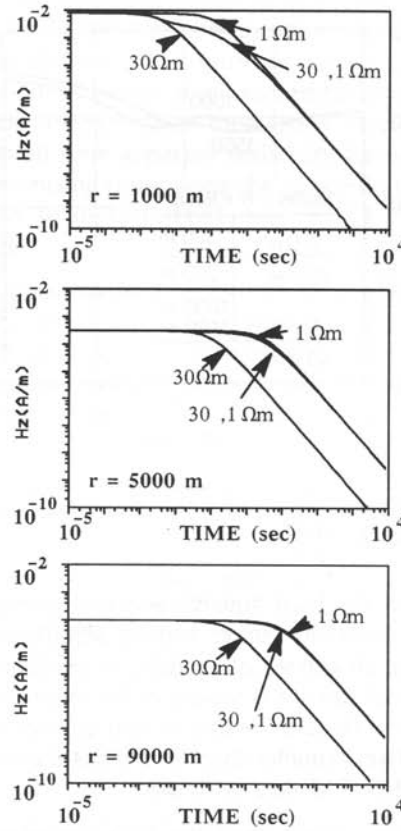


Fig. 2.10: Magnetic fields for two half-spaces with the resistivities of $30 \Omega m$ and $1 \Omega m$ and for a two-layer model with the same resistivities ($30 \Omega m$, $1 \Omega m$; first layer thickness = $400 m$) for offsets of $1 km$, $5 km$ and $9 km$.

equation 2.10 for the voltage response. Figure 2.10 shows the magnetic field response for two half-spaces with different resistivities and a two-layer model with the two respective half-spaces resistivities. The magnetic field for the two-layer model follows first the upper layer resistivity and then approaches the curve of the resistivity of the second layer. The magnetic field is a monotonic function which allows the calculation of its inverse. The result is the resistivity ρ as a function of the magnetic field. Only slight deviations from the shape of the half-space magnetic field are obtained for different offsets. These deviations are strongest for the upper layer when close to the transmitter, as can be seen in figure 2.11.

Figure 2.11 shows a suite of three-layer *all time apparent resistivity* curves with varying second layer resistivity. The curves are well behaved and do not show the additional flexure as shown above.

Note that no undershoot or overshoots exist as usually for frequency domain curves (Spies and Eggers, 1986).

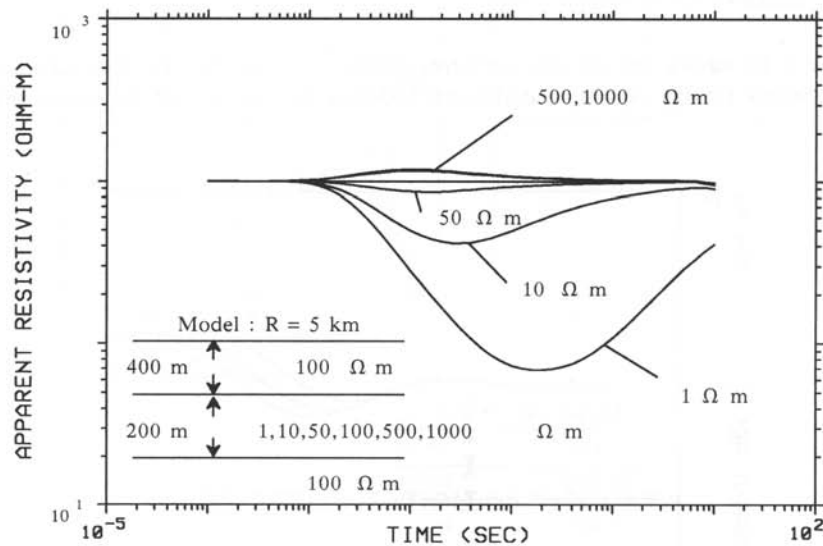


Fig. 2.11: *All time apparent resistivity* curves for a three-layer model with varying second layer resistivity (after Karlik and Strack, 1990).

Figure 2.12 shows the results using the *all time apparent resistivity* formulation for the same model as used by Yang (1986). It is clear that all time apparent resistivity does not show the flexures as exhibited in Yang's approach.

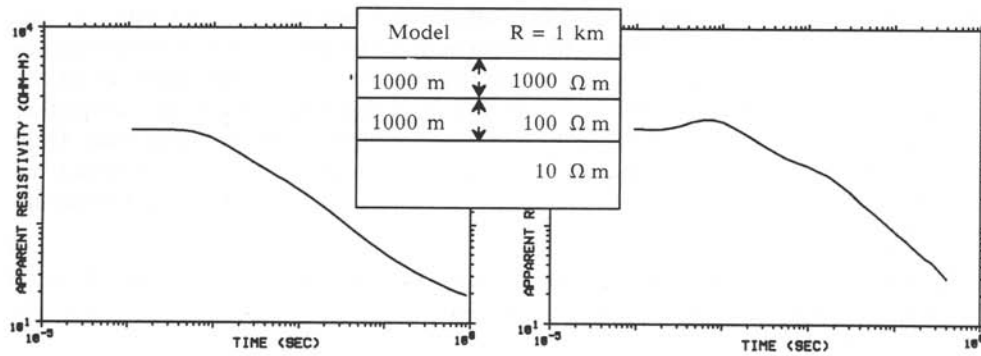


Fig. 2.12: All time apparent resistivity curves for the three-layer model used by Yang (see figure 2.10) (Karlik and Strack, 1990). Left is the all time apparent resistivity curve derived from the magnetic field and on the right the corresponding curve by Yang. Both curves are calculated for an offset of 1 km.

Figure 2.13 shows the all time apparent resistivity curves for the four-layer model used by Strack (1985). Again no additional flexures are visible and the curves are well behaved.

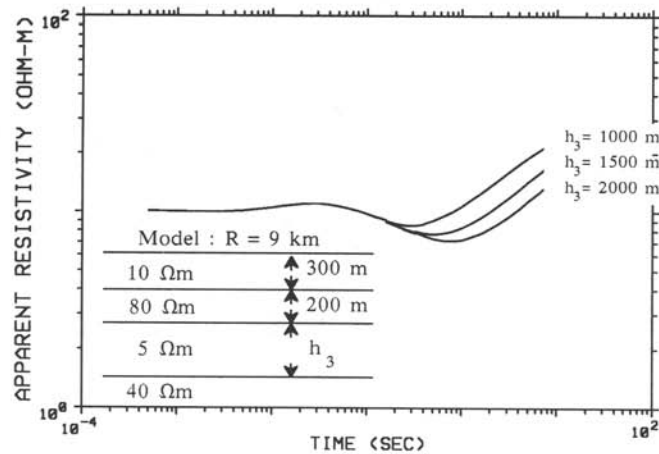


Fig.2.13: All time apparent resistivity curves for a four-layer model used for figure 2.9 (after Karlik and Strack, 1990).

The above calculations were done with synthetic data. Applying this procedure to real data one generally faces two problems:

- The data is influenced at early times by the system response and is thus distorted.

- At later time the noise prevails and causes additional numerical errors.

Therefore, the *all time* algorithm should be only applied to deconvolved data – that is data after removal of the system response. Figure 2.14 shows an example of a field data set. The left side of the figure shows the conventional early and late time apparent resistivity curves with the 95% confidence envelopes. The right graph shows the respective *all time* curve derived from the field data. For better visualization the data has been displayed without error bars. The arrow marks the location where the all time curve is no longer reliable and the error prevails. This is very difficult to recognize from the all time curve alone.

The advantage of having the all time curve lies in the capability of generating less biased pseudo-sections and image sections which were otherwise misrepresented by the early and late time approximation.

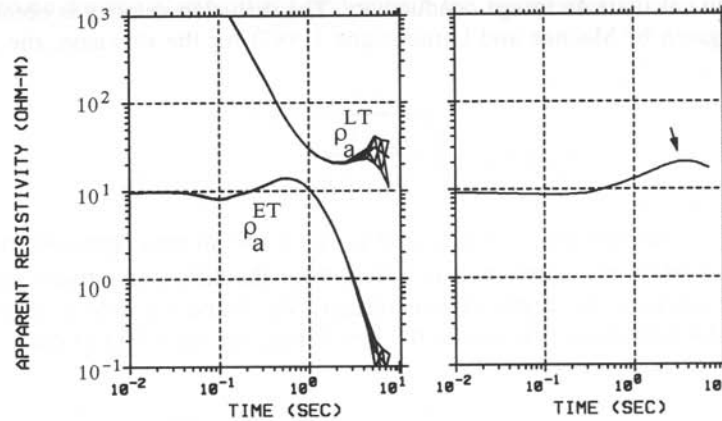


Fig. 2.14: Field data of an early and late time apparent resistivity curves (left) and the respective *all time* apparent resistivity curve (after Karlik and Strack, 1990).

IMAGE PRESENTATION OF THE DATA

The conversion of electromagnetic data to a direct subsurface image has been investigated by many researchers. The goal is the conversion of the measurements to a subsurface image which approximates the geology. Significant work was done in the Soviet Union (i.e. Zhdanov and Matusevich, 1984) with the concept of migrating the EM fields similar to seismics. Some of the early work of interpreting electromagnetic data by transformation to interval resistivities was done by Kamenetsky (Kamenetsky 1985; Kamenetsky and Porstendorfer, 1983). In the western world many papers concerning the direct presentation of transient EM data appeared in the literature (Nabighian, 1979; Barnett, 1984; Raiche and Gallagher, 1985; Spies and Eggers 1986; Polzer, 1986; Nekut 1987; Macnae and Lamontagne 1987; Fullagar, 1989; Eaton and Hohman, 1989; Macnae et al, 1991; Smith and Buselli, 1991). All these techniques

have the advantages and drawbacks. The reason lies in the different field behaviors for different field layouts and also for the large range of resistivity contrasts. For details on the different methods, the reader is referred to the above mentioned articles. Here two different approaches are described. The first approach goes via a simple transformation from the data directly the resistivity/conductivity image. The second approach uses a model assumption and compares the measured data with the model response until a satisfactory fit is obtained.

The first approach is based on the all time apparent resistivity curve. The goal is to find a transformation such that this curve is converted to a resistivity versus depth curve. As all time apparent resistivity curve one should preferably use the all time curve derived through the magnetic field conversion as described above. This curve is used to calculate the diffusion velocity and with the diffusion velocity a diffusion depth. From the diffusion depth and the total conductance of all strata above this depth one can calculate an image conductivity. The diffusion velocity is obtained using the formula given by Macnae and Lamontagne (1987) for the slowness, the inverse of the velocity;

$$v_d(t) = \sqrt{\frac{\rho_a(t)}{\mu_0 2t}} \quad (2.24)$$

where $v_d(t)$ is the diffusion velocity and $\rho_a(t)$ the all time apparent resistivity. The factor 1/2 inside the square root is different for the different authors and depends on how they express the depth of penetration. We found the above expression by Macnae and Lamontagne (1987) to be the best fitting one for LOTEM data. The diffusion depth is then:

$$z(t) = \int_0^t v_d(t) dt \quad (2.25)$$

Knowing the diffusion depth for every time, we assume that the apparent resistivity is :

$$\rho_a(t) = \frac{Z_d(t)}{S_d(Z(t))} \quad (2.26)$$

which $S_d(Z(t))$ is the total conductance of the strata above a specific time and diffusion depth. Subscript d denotes the respective values using the diffusion depth. The image conductivity (inverse resistivity) in a depth interval dz is the change of the conductance with depth or:

$$\sigma_i = \frac{1}{\rho_i} = \frac{dS}{dz_d} = \frac{d(z/\rho_a)}{dz_d} \quad (2.27)$$

Because this conductivity is the conductivity between depth intervals it is termed *interval conductivity* / or *interval resistivity*. Figure 2.17 (below) shows an example of the *interval conductivity* in comparison with the *source image conductivity* and is discussed below.

The second approach follows closely the approach of Eaton and Hohman (1989). The derivation is explained in more detail because it gives fast subsurface images for LOTEM. The technique proposed by Eaton and Hohman uses a single image which varies in position with time while Macnae and Lamontagne (1987) use multiple images. The basis for the imaging technique is the comparison of the magnetic field of the image current with the measured earth response converted to magnetic field values. The image is located underneath the transmitter with identical dipole moment. It is thus called *source image* or *current image*. Its depth as function of time is defined via the maximum of the electric field inside a homogeneous half-space. As for equation 2.10 we obtain for the electric field underneath the transmitter:

$$E_x(z,t) = \frac{D_0 \rho}{\pi z^3} \left[\operatorname{erf} \left(\frac{u}{\sqrt{2}} \right) - \frac{1}{2} + \left(\sqrt{\frac{2}{\pi}} u - \frac{1}{2} \right) \left(1 + \frac{u^2}{2} \right) e^{-u^2/2} \right] \quad (2.28)$$

The time of maximum of E_x for a given depth is obtained by calculating the first derivative of E_x with respect to time

$$\left. \frac{dE_x(z,t)}{dt} \right|_{z=z_{\text{image}}} = 0 \quad (2.29)$$

From this, the image depth is calculated:

$$z^2(t)_{\text{image}} = \frac{4t}{\mu_0 \sigma} \quad (2.30)$$

The magnetic field at the receiver site from a current filament located at this depth is according to Biot-Savart's law:

$$H_z = \frac{I}{4\pi} \frac{y}{y^2 + z^2} \frac{x+l}{((x+l)^2 + y^2 + z^2)^{1/2}} - \frac{x-l}{((x-l)^2 + y^2 + z^2)^{1/2}} \quad (2.31)$$

where l is half of the transmitter dipole length dl ; z is the image depth. From the above equation $z(t)$ is determined by iteratively fitting the image magnetic field to the measured or calculated one.

We now have the magnetic field from a current filament (*source image*) at the receiver site and the image depth as a function of conductivity. From equation 2.30, we

can calculate a slowness:

$$\frac{dt}{dz} = \frac{1}{2} z \mu_0 \sigma \quad (2.32)$$

Building the second derivative with respect to z yields the conductivity of the image:

$$\sigma = \frac{2}{\mu_0} \frac{d^2 t}{dz^2} \quad (2.33)$$

This expression is similar to the ones derived by Eaton and Hohmann (1989) and Macnae and Lamontagne (1987).

The computation of the *source image* can be split in three steps. First, the conversion of the field data (deconvolved) or synthetic data to magnetic field values. Second, the calculation of the image depth by fitting the image magnetic field to the measured one. Third, the calculation of the image conductivity. When calculating the magnetic field no major problems occur except when the field data becomes very noisy. The image depth values are obtained for given time values for a guess half-space resistivity. In practice, the all time apparent resistivity is calculated and its inverse used as input to calculate iteratively the image depth. If the guess half-space resistivity does not represent the average underlying earth model, the fit between the magnetic fields will not be good for all times. In this case, one should select a more appropriate half-space resistivity. Depending on how the procedures implemented, scale factors for the image depth and image conductivity must be derived by comparison with synthetic curves.

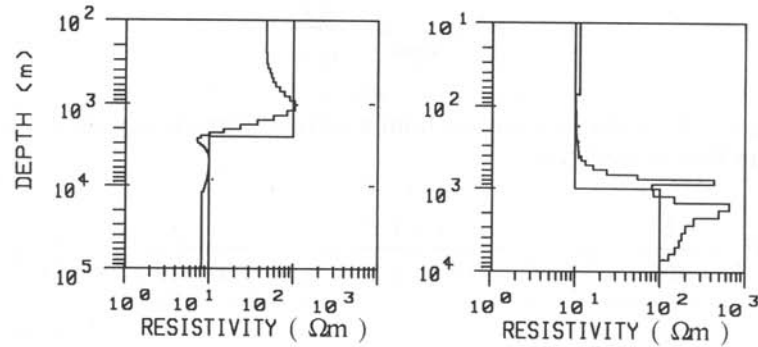


Fig. 2.15: *Source image* for a two-layer model.

The *source image* can be tested using synthetic data for a two-layer model as shown in figure 2.15 and a three-layer model displayed in figure 2.16. When the model

resistivity in figure 2.15 goes from a more resistive to a less resistive medium, only a small undershoot appears. When the resistivity increases sharply a large overshoot occurs. This overshoot has been observed by most authors and was the motivation for Smith et al (1991) to develop the spiked conductivity imaging. For figure 2.16, typical H, K, Q, and A-type three-layer models were selected. The Q-type (decreasing resistivity with depth) and the A-type model (increasing resistivity with depth) are reasonably well represented. For the H-type model (intermediate conductive layer), the conductive layer is well represented, but an overshoot occurs when reaching the boundary to the more resistive layer. For the K-type model (intermediate resistive layer), the *source image* is broadened over a large depth range. When considering that the source image is a fast – almost real time – initial guess, it represents the resistivity structure reasonably well.

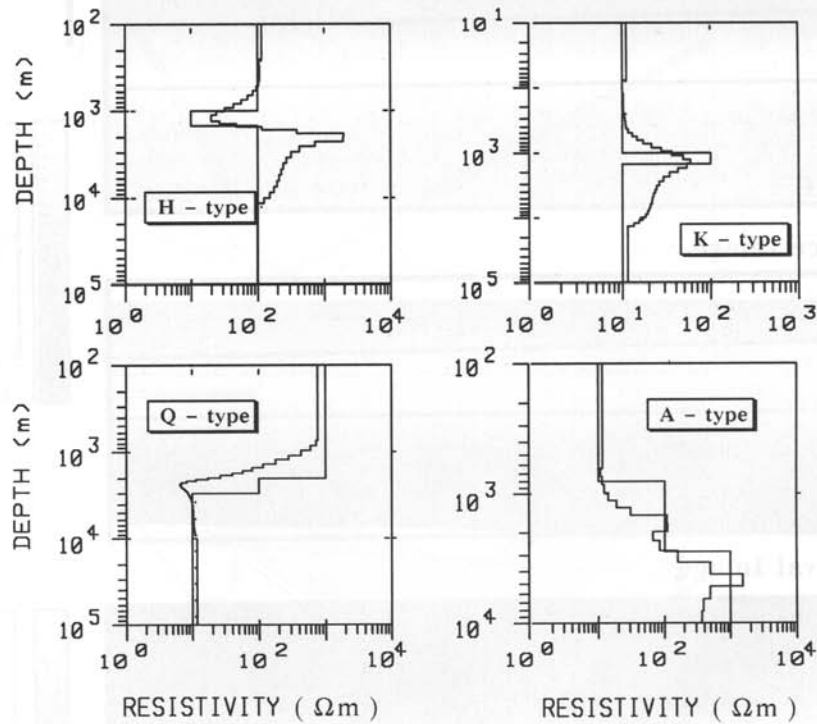


Fig. 2.16: *Source image* for a three-layer model.

For practical applications one needs to know how well the imaging techniques represent structure along a profile. Thus, synthetic data was calculated for a slightly dipping H-type three-layer model simulated with a 1-D layered earth algorithm. This data was then imaged and the results are displayed in figure 2.17. The top of the figure shows the synthetic model in a gray scale representation. The center frame is the

source image and the bottom frame is the *interval resistivity image*. The source image clearly represents the H-type nature of the model and also reflects the dipping of the intermediate layer. The third layer resistivity from the *source image* is higher than the model. This is caused by the typical overshoot in imaging when going to more resistive layers. For the *interval resistivity image*, the gray scale has a smaller range because the *interval resistivity* exhibits less dynamic range. Also, the *interval image* does not clearly reflect the H-type nature of the model. This means that the *source image* preserves more structure of the data than the *interval resistivity image*.

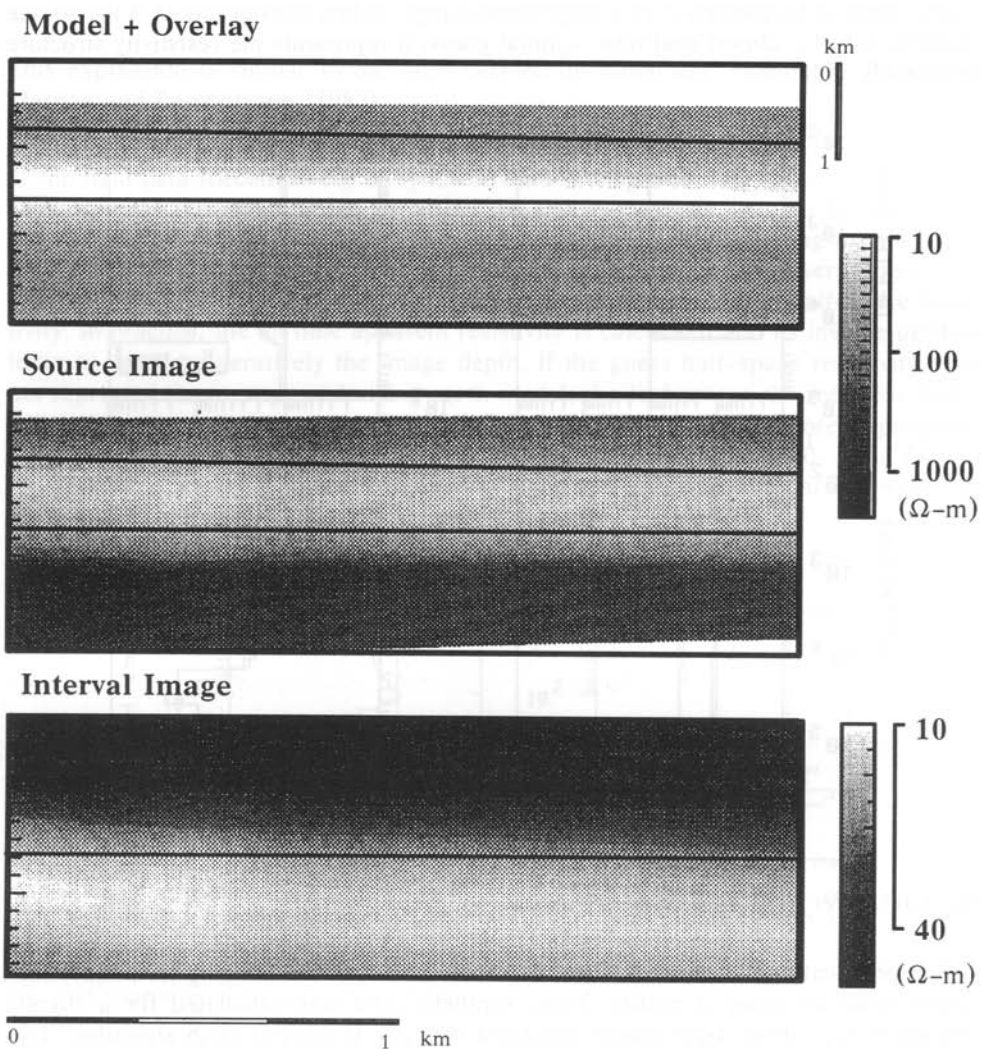


Fig. 2.17: Earth model (top) and the *source imaging* (center) and *interval imaging* (bottom) results.

Since the imaging assumes a 1-D model, namely a layered earth, one must question its applicability to 3-D structures. A typical 3-D effect in LOTEM data are sign reversals (see chapter 4). To illustrate that the source imaging sees a 3-D effect, 3-D synthetic data were calculated for a case history where 1-D and 3-D modeling had to be used to interpret a profile. For this interpretation the reader is referred to chapter 4 and 7 where the respective 1-D and 3-D interpretation is discussed. The 3-D model is shown in figure 2.18. A profile was chosen (A - A') such that it crosses the 3-D anomaly and is close to the station where 3-D effects (sign reversals) were observed.

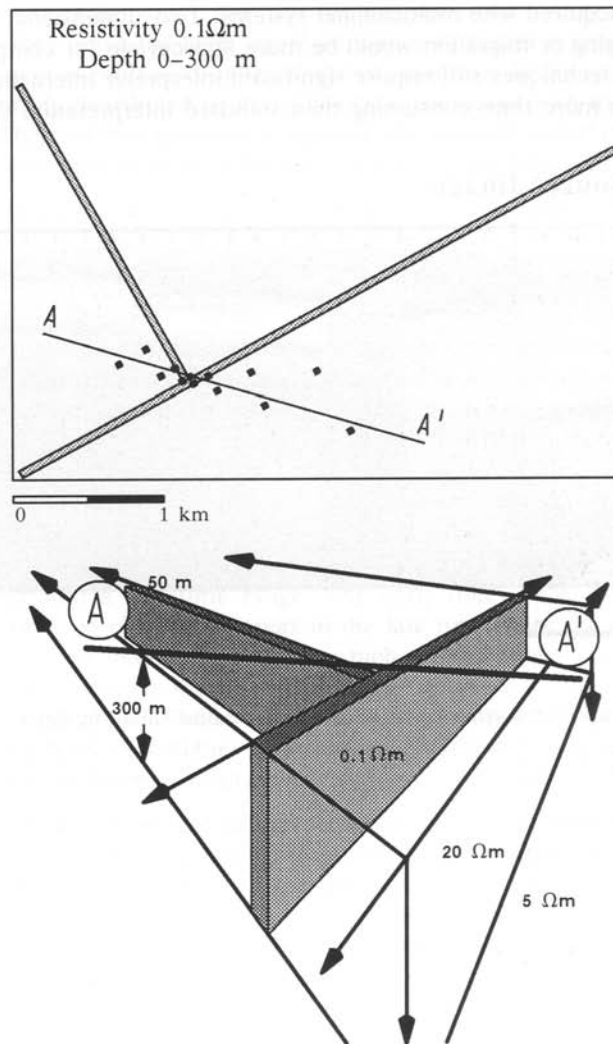


Fig. 2.18: 3-D model and profile location used to calculate the synthetic data for the *source imaging*.

At the same time the profile also contains a part where 1-D interpretation is applicable. The *source image* for this profile is shown in figure 2.19. It clearly exhibits an anomalous area (white part) where the reversals were observed in the field. This means that the source imaging can be used to get a very fast overview where 3-D structures exist.

The above example shows that simple 1-D *source imaging* is a reasonable approach to obtain a fast first interpretation. The computation of the *source image* is so fast, that it can be done in the field within minutes while a full inversion of the same data would take many CPU hours. This is extremely important when considering the increasing amount of data acquired with multichannel systems. Two-dimensional or even three-dimensional imaging or migration would be more appropriate for complex structures, but to date these techniques still require significant interpreter interaction which make the imaging even more time-consuming than standard interpretation (James, 1991).

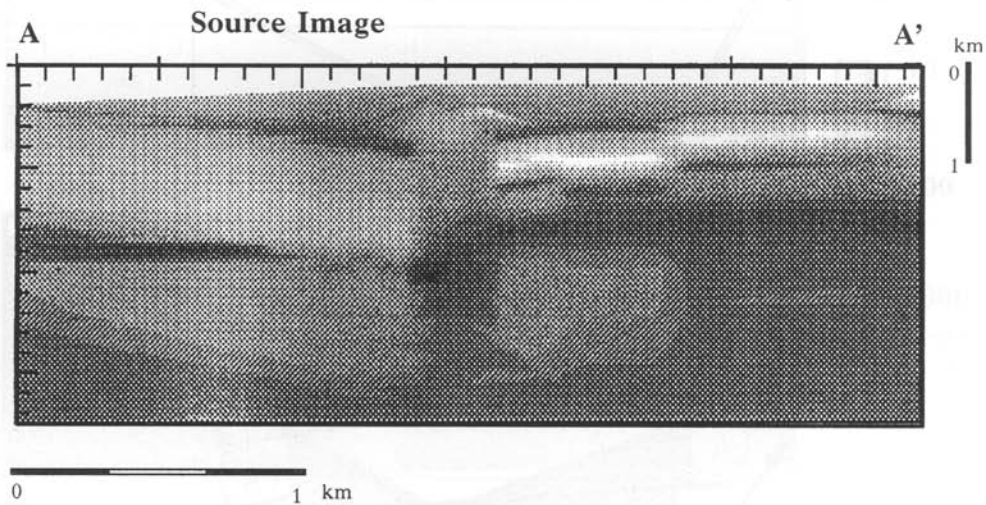


Fig. 2.19: *Source image* of the synthetic data for the 3-D model shown in figure 2.18

KMS Technologies – KJT Enterprises Inc.
6420 Richmond Ave., Suite 610
Houston, Texas, 77057, USA
Tel: 713.532.8144

Please visit us
<http://www.kmstechnologies.com>

This material is not longer covered by copyright. The copyright was released by Elsevier to Dr. Strack on November 5th, 2007.

The author explicitly authorizes unrestricted use of this material as long as proper reference is given.

KMS Technologies – KJT Enterprises Inc.

An EMGS/rxt-company

Chapter 4 Data Interpretation

extract from

Strack, K.-M., 1992, reprinted 1999
***Exploration with deep transient
electromagnetic:*** Elsevier, 373 pp.

This material is not longer cover by copyright. The copyright was released by Elsevier to Dr. Strack on November 5th, 2007.

The author explicit authorizes unrestricted use of this material as long as proper reference is given.

Chapter 4

Data Interpretation

There are several different ways to interpret EM field data. One way is to normalize the data and to generate anomaly maps. When TEM is applied in the mining industry the results are usually displayed on parallel profiles and maps because in most cases multi-dimensional anomalies are being considered. Another way is a quantitative interpretation to obtain an earth model with resistivities and layer thicknesses. This is usually called inversion and is the way most EM sounding data is interpreted. Inversion techniques as used for LOTEM data will be discussed. An excellent review of inversion methods can be found in Lines and Treitel (1984). After the initial review of the theoretical concepts, the inversion statistics and newer applications of the inversion such as *profile inversion* and *Occam inversion* are explained using real data examples in this chapter.

Three-dimensional structures are generally very difficult to interpret. One must first use some characteristic effects in the data, such as reversals, to obtain an estimate on how to approach the interpretation problem. This is essential because 3-D modeling algorithms still take a lot of computer time. Different 3-D algorithms can be used for different effects in the data. This allows the derivation of a first quantitative interpretation of the data. After discussing the interpretation of reversals, some selected 3-D models are shown.

ONE-DIMENSIONAL INVERSION

The overall goal of the inversion is to find the optimum earth model which fits the field data using a minimum of computer time. At the same time, it is important to obtain reliability estimates of the inversion run and the resulting model. These inversion statistics allow us to evaluate the result and find the optimum solution. In other scientific disciplines this procedure is called differently: the statisticians talk about *regression*, the electrical engineers talk about *system identification*. The geophysicists talk about *inversion* for two different reasons:

- We are trying to go from the data to the model parameters. This is the inverse way of forward modeling.
- An ill-conditioned matrix is to be inverted, which is a difficult task.

Figures 4.1a and b show the relationship between forward modeling and inversion for

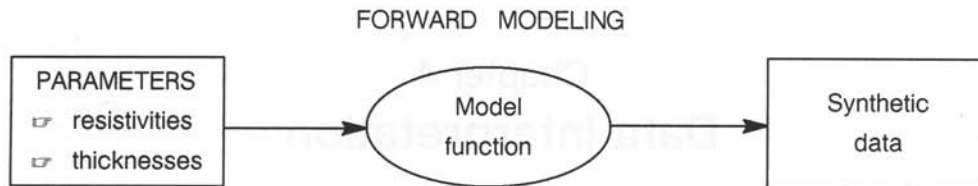


Fig.4.1a: FORWARD modeling functional diagram.

electromagnetic data. In the forward modeling sense we start with the estimated or known geoelectric *model parameters* and calculate the response function or *synthetic data* of our method using a predefined *model function*. The better we can get an idea about our earth model using well logs, other geophysical results and geology, the better our synthetic data will be. In the inverse modeling sense, we use an initial guess to compare our field data with our preconceived model. The more information we can get about our model, the faster we will obtain a reliable result. This additional information is called *a priori* information and can either be incorporated in the initial model or in adjustments of the iteration model. Latter is done in such a way that the known information is maintained and the unknown information is varied to find the optimum solution. In one sentence one could say:

The objective of inversion is to aid the interpreter in such a way that his subjective guess is quantified and thus might appear more objective.

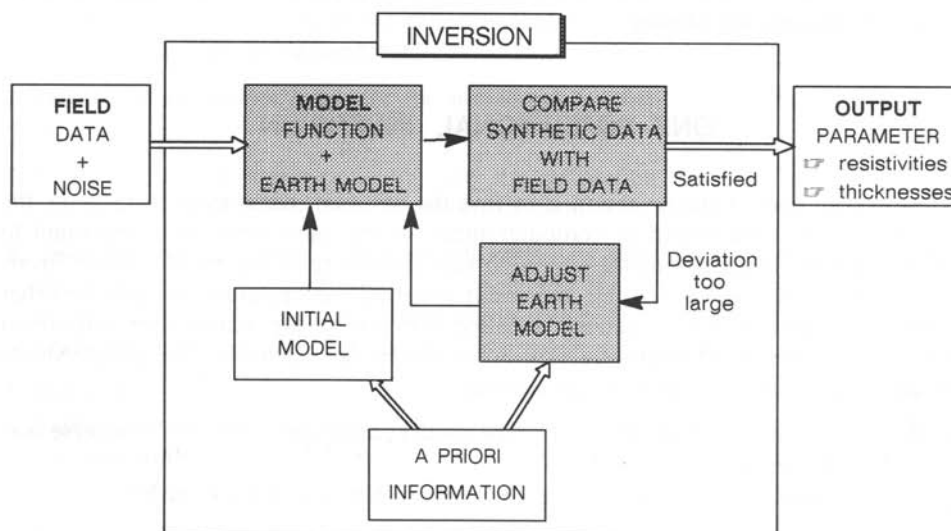


Fig. 4.1b: INVERSE modeling functional diagram.

If we want to calculate the response of an earth model, we must first have all the necessary model parameters available. For electromagnetic methods these are the resistivities ρ_j ($j = 1 \dots M$) and the thicknesses h_j of the layers ($j = 1, \dots, M-1$). These parameters describe the model sketched in figure 4.2. We also have a model function telling us how to calculate synthetic data from the model parameters. Let this model function be f or f_i , if evaluated for the i -th synthetic data point ($i = 1, \dots, n$):

ρ_j are m parameters, $\rho_1, \dots, \rho_M, h_1, \dots, h_{M-1}$, $m = 2M - 1$

$f_i = f_i(\mathbf{p})$ are n model functions,

y_i are the data points measured in the field, or

$y_i = f_i(\mathbf{p})$ are the synthetic data forward modeling case, and

σ_i are the standard deviations of the data points derived from the measurements.

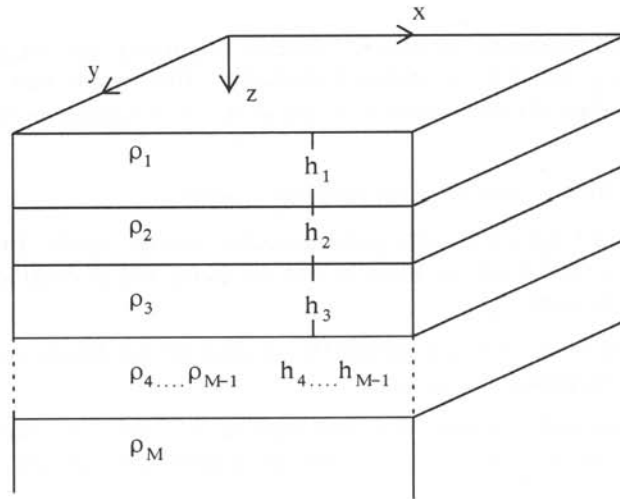


Fig.4.2: Model of a horizontally layered earth made up of M layers with respective resistivities and thicknesses.

All of the above are components of the respective vectors \mathbf{p} , \mathbf{f} , \mathbf{y} , and σ . The forward model curve or synthetic curve is a set of all function values f_i . If you go from the forward modeling to the inverse modeling or inversion, y_i becomes the observed data and f_i the modeled data. This leads us to two main goals of inversion:

- Minimize the difference \mathbf{q} between the *observed* and *modeled* data:

$$\mathbf{q} = |\mathbf{y} - \mathbf{f}|^2. \quad (4.1)$$

- Estimate the reliability of your model by calculating confidence bounds.

In this chapter, we shall focus on answering the question on how to reach the above two goals for the LOTEM method. More detailed information can be found in Jupp and Vozoff (1975), Vozoff and Jupp (1975), Lines and Treitel (1984), Petry (1987) and Hördt (1989).

Since all parameters are physical parameters and cannot become negative, the inversion is done with logarithmic data and logarithmic parameters. This is also more reasonable from the physical point of view, since electromagnetic waves are damped exponentially in the subsurface (skin effect). It also allows the use of a larger dynamic range in the signal and stabilizes the inversion process.

In a least squares sense, a measure of the error between real data and modeled data is defined by Jackson (1972):

$$\chi^2 = \frac{1}{n} \sum_{i=1}^n \frac{(f_i - y_i)^2}{\sigma_i^2}, \quad (4.2)$$

which is the average quadratic deviation between calculated and measured data weighting every data point with its standard deviation. This means that ideally this value is equal to 1, when the the obtained deviation $(f_i - y_i)$ is equal to the expected deviation σ_i .

Deviations larger than 1 from this can have two causes:

- The earth model does not sufficiently describe the real earth. This means a layer-cake description of the earth is not adequate and a multi-dimensional models must be used.
- The calculation of σ_i does not adequately consider all possible sources of error or the error propagation is incorrect.

The latter is the more likely cause (in sedimentary areas), since the standard deviation is derived from the stacking and processing or system errors before stacking do not get considered.

When χ^2 becomes smaller than 1, it means that the problem is underdetermined, i.e. there are more model parameters used than necessary. In this case, it is easily noticed that the data is being overinterpreted and that one is interpreting the noise.

The most common way to minimize the least squares sum is the Gauss-Newton method. This method always works when the problem is linear. For non-linear problems, one first has to linearize the problem by expanding it into a Taylor series:

$$f_i = f_i(\mathbf{p}) \approx f_i(\mathbf{p}_0) + \sum_{j=1}^m \left. \frac{\delta f_i(\mathbf{p})}{\delta p_j} \right|_{\mathbf{p}=\mathbf{p}_0} \underbrace{(p_j - p_{j,0})}_{\Delta p_j} \quad (4.3)$$

or

$$f(\mathbf{p}) \approx f(\mathbf{p}_0) + \mathbf{J} \Delta \mathbf{p} = \begin{pmatrix} \frac{\delta f_1}{\delta p_1} & \dots & \frac{\delta f_1}{\delta p_m} \\ \vdots & & \vdots \\ \frac{\delta f_n}{\delta p_1} & \dots & \frac{\delta f_n}{\delta p_m} \end{pmatrix} \Delta \mathbf{p} + f(\mathbf{p}_0)$$

or

$$J_{ij} = \left. \frac{\delta f_i}{\delta p_j} \right|_{\mathbf{p}=\mathbf{p}_0} \quad i=1, \dots, n; j=1, \dots, m$$

$$f(\mathbf{p}) \approx f(\mathbf{p}_0) + \mathbf{J} \Delta \mathbf{p} \quad (4.4)$$

\mathbf{J} is the Jacobian matrix containing for each data point the derivative of the model functions with respect to the parameters. $\Delta \mathbf{p}$ is the parameter difference vector also sometimes called $\Delta \mathbf{p}$, and \mathbf{p}_0 contains the initial guess model parameters. The Jacobian shows how the model function reacts to small changes in the model parameters and can thus be used for sensitivity analysis.

We recall the goal to find the parameter vector \mathbf{p} such that

$$q = \left| \mathbf{y} - \mathbf{f} \right|^2 = \mathbf{e}^T \mathbf{e} = \text{minimum} \quad (4.5)$$

where

$$\mathbf{e} = \mathbf{y} - \mathbf{f}(\mathbf{p}_0) - \mathbf{J} \Delta \mathbf{p} \quad \text{is the difference or error vector.}$$

This error vector can be directly related to the standard deviations of the data and the χ^2 error measure. The inverse standard deviations are written on the main diagonal of the weighting matrix \mathbf{W} (Jackson, 1972):

$$W_{ij} = \delta_{ij} \frac{1}{\sigma_i},$$

where $\delta_{ij} = \begin{cases} 1 & \text{for } i=j \\ 0 & \text{otherwise} \end{cases}$ is the Kronecker symbol. Then χ^2 can be written as

$$\chi^2 = \frac{1}{n} \mathbf{e}^T \mathbf{W}^2 \mathbf{e} \quad (4.6)$$

If we define a discrepancy vector

$$\mathbf{g} = \mathbf{y} - \mathbf{f}(\mathbf{p}_0) \quad \text{then} \quad \mathbf{e} = \mathbf{g} - \mathbf{J} \Delta \mathbf{p} \quad \text{and} \quad (4.7)$$

$$\chi^2 = \frac{1}{n} (\mathbf{g} - \mathbf{J} \Delta \mathbf{p})^T \mathbf{W}^2 (\mathbf{g} - \mathbf{J} \Delta \mathbf{p}) \quad (4.8)$$

we must find the minimum of χ^2 which means

$$\frac{\delta \chi^2}{\delta p_j} = 0 \quad \text{for } j = 1, \dots, m. \quad (4.9)$$

Doing this yields the linear system (Lines and Treitel, 1984):

$$\mathbf{J}^T \mathbf{W}^2 \mathbf{J} \Delta \mathbf{p} = \mathbf{J}^T \mathbf{W}^2 \mathbf{g} \quad \text{with the solution} \quad (4.10)$$

$$\Delta \mathbf{p} = (\mathbf{J}^T \mathbf{W}^2 \mathbf{J})^{-1} \mathbf{J}^T \mathbf{W}^2 \mathbf{g}. \quad (4.11)$$

If the model function $\mathbf{f}(\mathbf{p})$ is linear, equation 4.4 gives an exact equality. The required parameter vector can be obtained from $\mathbf{p}_1 = \mathbf{p}_0 + \Delta \mathbf{p}$, which is already the solution in a linear case. χ^2 will exhibit a minimum at \mathbf{p}_1 . For linear cases only, one iteration will yield the solution. For non-linear cases the new obtained parameter vector, \mathbf{p}_1 , is substituted in the above equation instead of \mathbf{p}_0 and the procedure is repeated until convergence is reached.

Figure 4.3 illustrates the above situation. The dashed line represents the error due to the linearization at the parameter $\mathbf{p}_n^{\text{est}}$. It is a hyperbola parallel to E at the point $\mathbf{p}_n^{\text{est}}$. The next iteration will go to the \mathbf{p}_{n+1} position. There the error is calculated and a similar procedure done until the global minimum has been reached. In doing so, there arise three new questions:

- How do we make sure we always reach the best minimum (which in most cases is the global minimum but sometimes also a local minimum)?
- How can we reduce the number of iterations and thus computation time and cost?
- How can we stabilize the above procedure, that it works even with poorly conditioned field data?

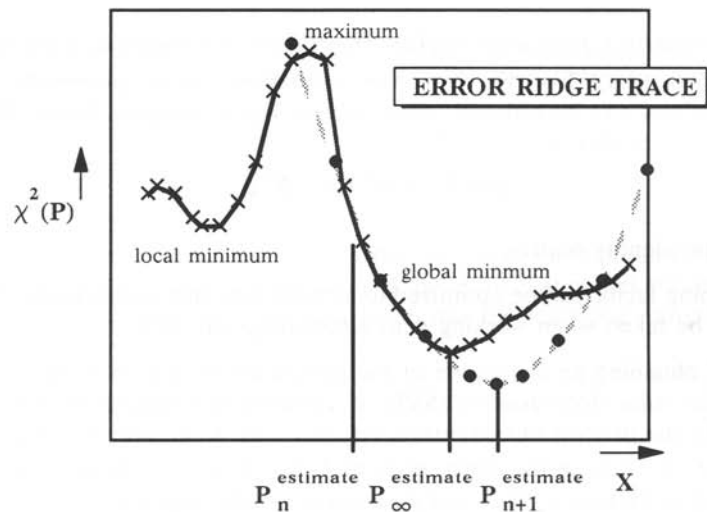


Fig. 4.3: Error ridge trace as function of the estimated model parameters (after Menke, 1984).

The answer to the first question is quite simple: **We don't**. There are two different ways of inverting geophysical data. One way is the mathematically correct way, yielding the best fit model and the other the physically reasonable (which does **not** mean mathematical incorrect!). Since we are, however, dealing with real geology and real noise superimposed on the data, we need to distinguish between mathematically correct and physically reasonable. This is done by using inversion statistics which provides us with error bounds for our results, which can then be used to correlate adjacent stations. As example, if we consider two receiver stations next to each other (500 m apart), both of them have quite noisy signals. One of them yields a conductor at 2 kilometers depth, whereas the other yields a conductor at 4 kilometers depth. Interpretation was done in both ways: The first way – the mathematically correct one – yields a best fit model which is not a consistent model for both stations. The curve fitting error for both stations is below 1%. The other possible solution is a conductor at three kilometers depth at both stations, but the error lies around 10%. The geology, however, tells us that we have a sedimentary basin and the layering is almost horizontal. From this knowledge, a geophysicist would probably justify using the poorer fitting results as the more probable ones. Fortunately, we always have more than just 2 stations and ambiguity is greatly reduced.

The second question can be readily answered with a large variety of techniques. We will in this chapter only consider the *Marquardt-Levenberg method* with the *singular value decomposition*, since most inversion programs use this technique. This leads us directly to the answer of the third question about the inversion stability. In the above mentioned technique a damping factor is introduced to increase the stability of the

inverse. For the following the weighting matrix is dropped which causes no loss of generality.

When the matrix $\mathbf{J}^T \mathbf{J}$ becomes singular ($\det \mathbf{J}^T \mathbf{J} = 0$) we obtain no solution. If $\mathbf{J}^T \mathbf{J}$ is almost singular ($\det \mathbf{J}^T \mathbf{J} \ll 1$) we obtain oscillations (large parameter variations). These oscillations can be reduced when introducing a damping factor, K , such that equation 4.10 is modified:

$$\Delta \mathbf{p} (\mathbf{J}^T \mathbf{J} + K^2 \mathbf{I}) = \mathbf{J}^T \mathbf{g} \quad (4.12)$$

where \mathbf{I} is the identity matrix.

The damping factor can be optimized to achieve very fast convergence, but extreme care should be taken when working with electromagnetic data.

A way of obtaining an evaluation of the parameter resolution is the additional use of the *singular value decomposition* (SVD) or spectral decomposition. The Jacobian is substituted by the product of two orthogonal matrices, \mathbf{V} , \mathbf{U} , and one diagonal matrix, \mathbf{S} , containing the roots or the eigenvalues of \mathbf{J} , \mathbf{S}_i . A detailed description of the SVD can be found in Jackson (1972) and a summary in the appendix.

Let
$$\mathbf{J} = \mathbf{U} \mathbf{S} \mathbf{V}^T \quad (4.13)$$

From equation 4.10 this yields:

$$\Delta \mathbf{p} = (\mathbf{J}^T \mathbf{J})^{-1} \mathbf{J}^T \mathbf{g} = (\mathbf{V} \mathbf{S} \mathbf{U}^T \mathbf{U} \mathbf{S} \mathbf{V}^T)^{-1} \mathbf{V} \mathbf{S} \mathbf{U}^T \mathbf{g} = \mathbf{V} \mathbf{S}^{-1} \mathbf{U}^T \mathbf{g} \quad (4.14)$$

where
$$\mathbf{U}^T \mathbf{U} = \mathbf{V}^T \mathbf{V} = \mathbf{V} \mathbf{V}^T = \mathbf{I}_n \quad (4.15)$$

Equation 4.14 is not defined if one of the singular values equals zero. We therefore introduce the damping factor K for stabilization:

$$\Delta \mathbf{p} = (\mathbf{V} \mathbf{S}^2 \mathbf{V}^T + K^2 \mathbf{I}_n)^{-1} \mathbf{V} \mathbf{S} \mathbf{U}^T \mathbf{g} \quad (4.16)$$

or

$$\Delta \mathbf{p} = \mathbf{V} (\mathbf{S}^2 + K^2 \mathbf{I}_n)^{-1} \mathbf{V}^T \mathbf{V} \mathbf{S} \mathbf{U}^T \mathbf{g} \quad (4.17)$$

or

$$\Delta \mathbf{p} = \mathbf{V} \text{diag} \left(\frac{\mathbf{S}_i}{\mathbf{S}_i^2 + K^2} \right) \mathbf{U}^T \mathbf{g} = \mathbf{V} \mathbf{T} \mathbf{S}^* \mathbf{U}^T \mathbf{g} \quad (4.18)$$

where \mathbf{S}^* is defined as

$$S_{ii}^* = \begin{cases} \frac{1}{S_{ii}} & \text{for } S_{ii} > 0 \\ 0 & \text{otherwise} \end{cases} \quad (4.19)$$

and \mathbf{T}^* as the damping factors of the transformed parameters

$$T_{ij} = \frac{S_{ij}^2}{S_{ij}^2 + K^2} \quad (4.20)$$

Another advantage of this method is also that the inversion statistics come with the SVD as byproduct.

Resolution Analysis

The U and V matrices with the orthonormal data space and parameter space eigenvectors can be used to study the resolution of the individual model parameters namely the resistivities and thicknesses. In order to do this the following transformations are used:

$$\mathbf{p} \rightarrow \mathbf{q} = \mathbf{V}^T \mathbf{p} \quad \text{and} \quad (4.21)$$

$$\mathbf{g} \rightarrow \mathbf{r} = \mathbf{U}^T \mathbf{g} \quad (4.22)$$

Equation (4.21) describes a rotation in the parameter space. The transformed parameters are uncorrelated and the columns of the V matrix describe the linear combinations of the physical parameters for each of the transformed parameters.

The solution of equation (4.12) is obtained by multiplying equation (4.18) with \mathbf{V}^T :

$$\Delta \mathbf{q} = \mathbf{T} \mathbf{S}^* \mathbf{r} \quad (4.23)$$

The matrix \mathbf{T} is important for the progress of the inversion. To demonstrate this, the T_{ii} are normalized by the largest eigenvalue:

$$\text{with} \quad \lambda_{ii} = \frac{S_{ii}}{S_{11}} \quad (\text{normalized eigenvalue}) \quad \text{and} \quad (4.24)$$

$$v = \frac{K}{S_{11}} \quad (\text{normalized damping parameter}) \quad (4.25)$$

we obtain for the T_{ii} :

$$T_{ii} = \frac{\lambda_{ii}^2}{\lambda_i^2 + v^2} \quad (4.26)$$

The values of T_{ii} control the changes of the transformed parameters. They are dependent on the ratio of normalized eigenvalue and the normalized damping parameter. We thus distinguish between three possible cases:

1. case: $v \ll \lambda_i$

In this case T_{ii} is about 1 and the respective parameter combination is well resolved.

2. case: $v \gg \lambda_i$

This means T_{ii} becomes small which means that the parameter q_i is changed by only a small fraction. The influence of poorly resolved parameters is strongly damped. Thus the T_{ii} are called *damping factors of the transformed parameters*.

3. case: $v \approx \lambda_i$

In this case $T_{ii} \approx 0.5$ and the respective parameter is barely damped.

The above considerations show that v is taking the role of a threshold value for the relative eigenvalues λ_i . Thus v is commonly set to 0.1 during the initial stage of the inversion. This means that the parameter combinations with eigenvalues less than 10% of the maximum eigenvalues are being damped. The result is that initially only the well resolved parameters are being varied to obtain fast improvement of the fit. Between iterations of an inversion, v is decreased to consider also the influence of the less resolved parameters. For standard LOTEM inversions we often define 0.01 as lower limit of v , which means that parameter combinations with less than 1% of the maximum are considered irrelevant.

Jupp and Vozoff (1975) define a class of inversion procedures by setting:

$$T_{ii}^{(N)} = \frac{\lambda_{ii}^{2N}}{\lambda_{ii}^{2N} + v^{2N}} \quad (4.27)$$

For $N = 1$ the above described method is obtained. This method is also known as *Marquardt-Levenberg* method. Figure 4.4 shows $T^{(N)}$ as a function of λ for $v = 1$.

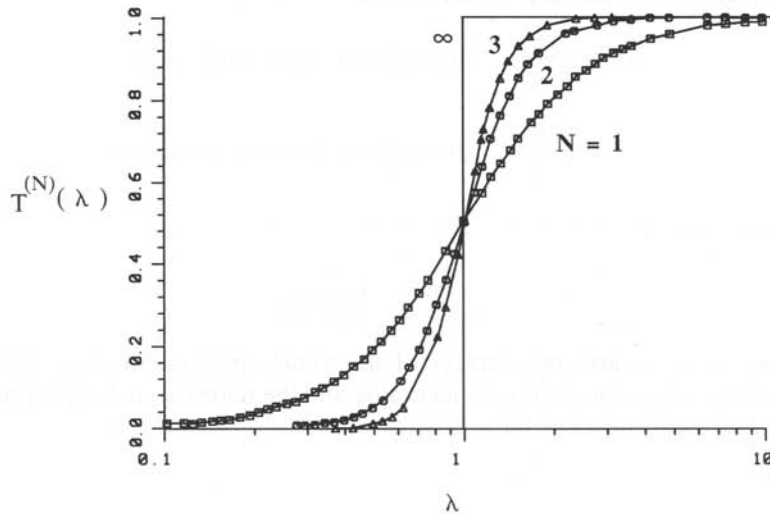


Fig.4.4: The function $T^{(N)}(\lambda) = \frac{\lambda^{(2N)}}{1 + \lambda^{(2N)}}$ for $N = 1, 2, 3, \infty$ (after Jupp and Vozoff, 1975).

For increasing N higher orders are obtained up to $N = \infty$ when the influence of parameters with eigenvalues smaller than v is completely damped.

For LOTEM inversion we use mostly $N = 2$ which can be termed the *Marquardt-Levenberg method* of second order.

In order to see how well resolved the original parameters are, the damping factors of the transformed parameters are transformed back.

$$\mathbf{T} \rightarrow \mathbf{R} = \mathbf{VT} \quad (4.28)$$

The diagonal elements of \mathbf{R} are then the *damping factors of the original parameters*. They lie between 0 and 1 and are called *importance* in the inversion statistics. An importance of 1 means that the parameter has strong influence on the fit of the model curve. A small value means that the parameter has little influence on the fit.

Another important quantity for the evaluation of the inversion result is the *number of effective parameters*. It is defined as the sum of the damping factors of the parameters and it is a measure for how many parameters the inversion really resolves.

The solution of the inversion problem depends on the starting model \mathbf{p}_0 . The reason is that the error function χ^2 can have different minima. This means that quite different earth models satisfy the data equally well. This becomes even more difficult, since there is always noise on the data and the best fit model is not always the one closest to the truth.

Thus, one spends a great deal of time in obtaining as much *a priori* information as possible to eliminate unreasonable solutions. The next step beyond simply comparing the results with well log information is the incorporation of the *a priori* information in the mathematical concept and reduce the bias in the inversion by incorporating other geophysical techniques.

Joint Inversion

In this section the above inversion concepts are extended to inversion of two data sets simultaneously and obtaining only one earth model which satisfies the data set. This type of inversion is called joint inversion. The two data sets may be in principle any type of data which can be interpreted with the same model. For practical purposes we use joint inversion either of two different components of the LOTEM electromagnetic fields or magnetotelluric data and one LOTEM data component.

Using the data sets of two different methods improves in general the results, provided that each data set contains complementary information. Sometimes this means that both data sets must have a large overlapping depth investigation range, sometimes it means that the overlap is small. Since it is possible to obtain different results by the individual interpretation of the components, only careful evaluation can answer the above uncertainty. One always hopes to combine the resolution capabilities of the two methods. Here we have selected the joint inversion of magnetotelluric and LOTEM data because both techniques complement each other well in depth resolution. The

overlap of LOTEM and MT data can readily be compared using the *skin depth* for the MT and the *diffusion depth* for the LOTEM (Spies, 1989).

The mathematical combination of the two methods is obtained by the combination of the matrices but maintaining only one parameter vector (resistivities and thicknesses) such as:

$$\mathbf{y} = \begin{pmatrix} \mathbf{y}_{(\text{LOTEM})} \\ \mathbf{y}_{(\text{MT})} \end{pmatrix} ; \quad \mathbf{J} = \begin{pmatrix} \mathbf{J}_1 (\text{LOTEM}) \\ \mathbf{J}_2 (\text{MT}) \end{pmatrix} ; \quad \mathbf{f} = \begin{pmatrix} \mathbf{f}_1 (\text{LOTEM}) \\ \mathbf{f}_2 (\text{MT}) \end{pmatrix} \quad (4.29)$$

where \mathbf{y} is the data vector containing the field observations, \mathbf{J} is the Jacobian matrix containing the derivatives with respect to the model parameters, and \mathbf{f} is the model function vector containing the forward calculations for a specified model at the same points as the field data.

A problem arises when weighting the data sets: If realistic standard deviations for both data sets exist, none of the data points will be given preference when each data point is weighted with its standard deviation.

With real data, it is often difficult to obtain a realistic error estimate and thus the weights in the weighting matrix are all set equal to 1. Since during the inversion dimensionless parameters are used, both data sets will contribute equally to the solution.

For LOTEM data it is important to include the standard deviation in the inversion because the relative error of the data often deviates by several orders of magnitude. For the joint inversion, if you would like to include the standard deviation for one data set but have no reliable error estimates for the other method, you must normalize the weights. One practical way is to normalize the weights of both data sets by the average of the weights of each data set. This will guarantee an average of the weights which is equal to 1. This means that the data sets are equally weighted against each other but each data set in itself contains its proper weights. For the LOTEM the induction currents at early time are more focused at a certain depth in the subsurface. At later times the induction currents are more spread out and the value at each individual time is more influenced by the values at times before. Thus abrupt weight changes can occur at early times but should not occur at later times.

Next, we will test the joint inversion with synthetic data to demonstrate its usefulness and drawbacks. First both data sets are inverted individually and then jointly. The resolution criteria of the proceeding discussions in this chapter are used. Since below case histories are shown, at this stage synthetic data without noise are used.

The first synthetic data were calculated for a K-type model (low – high – low resistivity, $\rho_1 \leq \rho_2 \geq \rho_3$):

$$\begin{array}{ll} \rho_1 = 10 \, \Omega \, \text{m} & h_1 = 2000 \, \text{m} \\ \rho_2 = 500 \, \Omega \, \text{m} & h_2 = 500 \, \text{m} \\ \rho_3 = 10 \, \Omega \, \text{m} & \end{array}$$

In this model, a more resistive layer is embedded between two conductors. Since the magnetic field component of LOTEM has little sensitivity to resistive layers we use the electric field component. We hope for an increased resolution for this type of model with joint inversion, since the MT data will resolve the lower conductor better than the LOTEM data, but MT has little information on the resistive layer which the LOTEM has.

Figure 4.5 shows the synthetic data for the LOTEM (top left) and MT (bottom left). For LOTEM the response of the electric component (in x-direction) was calculated for an offset of 7000 m with the receiver being located on the dipole equator. It shows little structure due to the embedded resistor. The MT apparent resistivity and phase curves show even less structure than the LOTEM curve. The solid line through the data curves shows the result of the joint inversion. The starting model for the individual inversions and the joint inversion was:

$$\begin{array}{ll} \rho_1 = 50 \, \Omega \, \text{m} & h_1 = 1800 \, \text{m} \\ \rho_2 = 50 \, \Omega \, \text{m} & h_2 = 1000 \, \text{m} \\ \rho_3 = 50 \, \Omega \, \text{m} & \end{array}$$

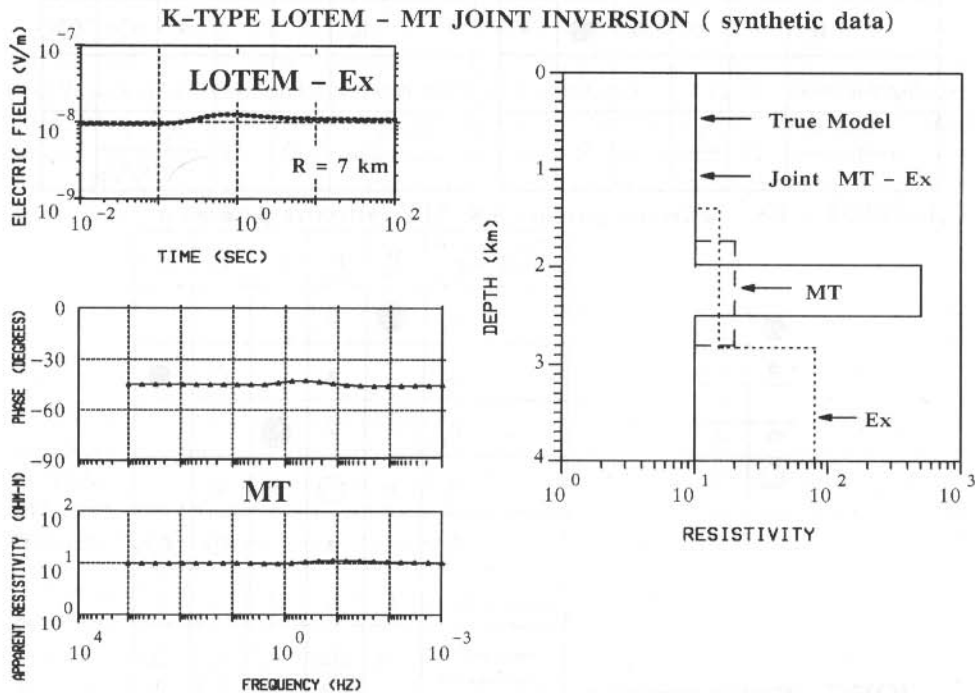


Fig. 4.5: Synthetic data example for LOTEM and MT joint inversion for a K-type model (left) and inversion results on the right. The joint inversion result here is the same as the true model (after Hördt, 1989).

The comparison of the results is shown in Figure 4.6. The MT data sees a thick slightly resistive layer whereas the LOTEM electric field is sensitive to an increase in resistivity. The LOTEM reaches higher resistivities than the MT, but never penetrates through the resistor. Only the joint inversion resolves the resistor. A difference between the original model and the inversion result is not visible. The fit for all three inversions is better than 1 %. If the interpreter had only one of the techniques available to him he would have difficulties finding the true model without the joint inversion. The higher quality of the joint inversion result can be shown using the V matrix (which relates the physical and the transformed parameters) as displayed in figure 4.6.

transform. original par. par.	P ₁	P ₂	P ₃	P ₄	P ₅
ρ_1	●	○			
ρ_2	•	●	○	•	●
ρ_3	•	•	●	•	•
h_1	○	○	•	○	●
h_2	•	○	○	●	•
Damping factor	1	1	1	0.8	0
resolved combination	ρ_1	$\frac{1}{h_1}$	ρ_3	h_2	

transform. original par. par.	P ₁	P ₂	P ₃	P ₄	P ₅
ρ_1	●				
ρ_2			○	○	●
ρ_3		●			
h_1			●	○	•
h_2			○	○	○
Damping factor	1	1	1	1	0
resolved combination	ρ_1	ρ_3	$\frac{h_1}{\rho_2}$	$\frac{1}{\rho_2 h_1 h_2}$	

LOTEm - Ex effective param.: 3.8 MT effective param.: 4

●	1
•	0.5
	0
○	-0.5
○	-1

transform. original par. par.	P ₁	P ₂	P ₃	P ₄	P ₅
ρ_1	●	○			
ρ_2		•		○	●
ρ_3		•	●		
h_1	○	○	•	○	
h_2		•		○	○
Damping factor	1	1	1	1	1
resolved combination	ρ_1	$\frac{1}{h_1}$	ρ_3	$\frac{1}{\rho_2 h_2}$	$\frac{\rho_2}{h_2}$

JOINT effective param.: 5

Fig. 4.6: V matrices for the individual and joint inversion of LOTEM and MT data using K-type synthetic data (after Hördt, 1989).

The relation between the transformed parameters P and the original parameters of the model is obtained by adding the logarithms of the original parameters multiplied by the coefficient. In figure 4.6 for the LOTEM electric field and the first transformed parameter P_1 we obtain:

$$P_1 = 0.88 \log(\rho_1) + 0.25 \log(\rho_2) + 0.11 \log(\rho_3) - 0.33 \log(h_1) - 0.19 \log(h_2) \quad (4.30)$$

This means that the parameter combination
$$\frac{\rho_1^{0.88} \rho_2^{0.25} \rho_3^{0.11}}{h_1^{0.33} h_2^{0.19}}$$
 is resolved.

The circles in figure 4.6 represent the coefficients of the transformed parameters. The circle diameter is proportional to the coefficient which is between 0 and 1. Open circles mean negative coefficient. The dominating parameter is the resistivity of the first layer. From the matrix of the electric field it can also be seen that the electric field sees the increasing resistivity but not the structure. This effect is independent of the starting model and even when the starting model is close to the true model the resistive layer will not be resolved. The joint inversion combines the resolution of both individual inversions and more parameters are resolved as can be seen at the bottom of the figure.

The second case considers an A-type (increasing resistivity with depth, $\rho_1 \leq \rho_2 \leq \rho_3$) model and the combinations of LOTEM magnetic field data with MT. This is a less favourable condition as the last one because neither the MT nor LOTEM magnetic field have full capabilities to resolve resistors. However, the combination should bridge the typical gap in the MT signal around 1 Hz. Both data sets the MT data and the LOTEM magnetic component have similar sensitivities to the subsurface resistivity. The model consists of three layers:

$$\begin{array}{ll} \rho_1 = 10 \, \Omega \, \text{m} & h_1 = 800 \, \text{m} \\ \rho_2 = 100 \, \Omega \, \text{m} & h_2 = 2000 \, \text{m} \\ \rho_3 = 1000 \, \Omega \, \text{m} & \end{array}$$

The model type is very typical because the resistivity often increases with increasing depth for a depth range between 1 and 20 km. Figure 4.7 shows the synthetic data for LOTEM magnetic field (top left) and the MT measurements (bottom left). For the MT, the data around 1 Hz (0.25 Hz to 8 Hz) has been eliminated, because in this frequency range the natural source signal is generally very weak.

The inversion results are presented on the right of figure 4.7. The MT inversion did not change the parameters of the second layer which is caused by the gap in the data. The LOTEM magnetic field and the joint inversion give approximately the same results. In order to better evaluate this, one can consider the damping factors of the original parameters – also called importances – as shown on the bottom right of figure 4.7. The joint inversion resolves more layer parameters. Contrary to the previous example, this result depends upon the starting model, in particular the values of the

importance of the second layer. In this case this dependence can be explained by the non-linearity in the solution and the instability of linearized inversion.

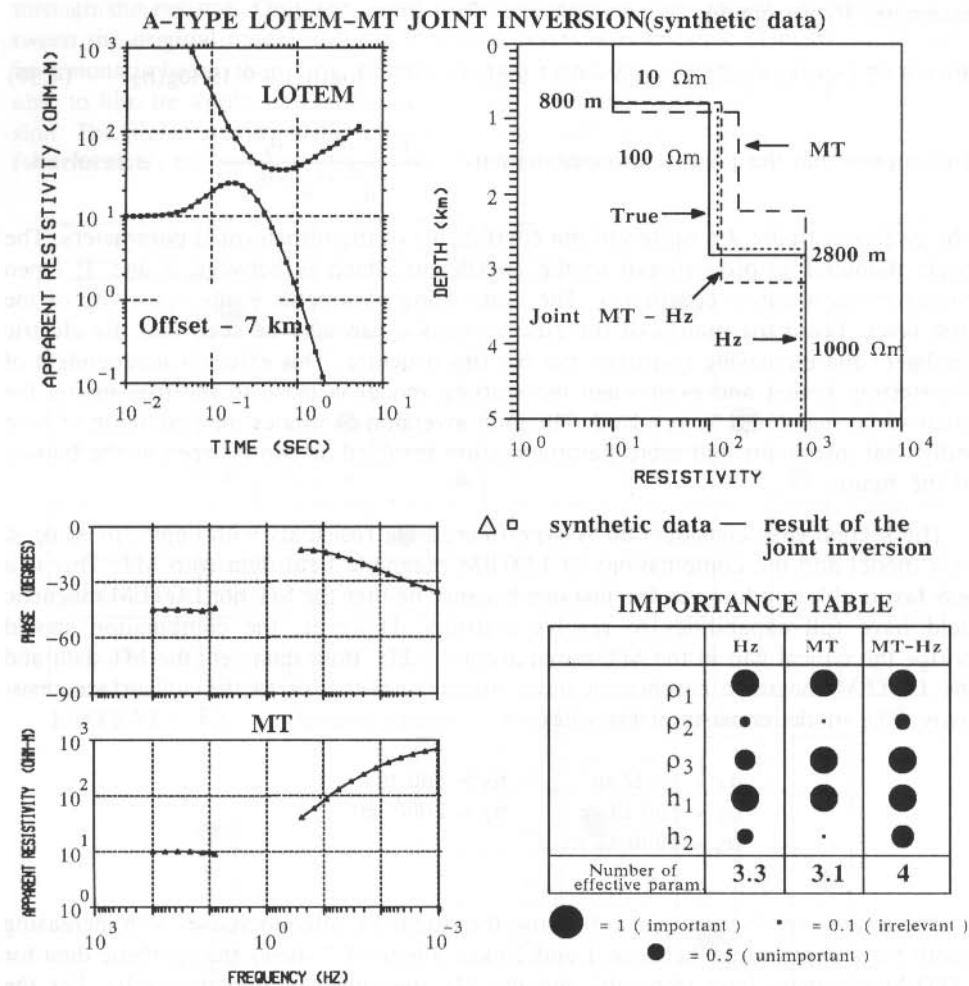


Fig. 4.7: LOTEM (top left) and MT (bottom left) synthetic data for an A-type model. On the right inversion result are shown with the parameter importances below (after Hördt, 1989).

Apart from the above shown examples, further tests were done for Q-type (decreasing resistivity, $\rho_1 \geq \rho_2 \geq \rho_3$) and H-type (imbedded conductor, $\rho_1 \geq \rho_2 \leq \rho_3$) models. In both cases the joint inversion did not improve the result. On the other hand, it was also not worse than the individual interpretation.

Following, one brief case history of jointly interpreting MT and LOTEM data is shown. Both data sets were measured in the area around the Münsterland borehole in

North-Western Germany (Hördt, 1989). A more detailed interpretation case history is shown later on. Here, only methodological aspects are considered. Figure 4.8 shows the real field data for the LOTEM magnetic field measurements. The MT consists of a combination of controlled source audio magnetotelluric (CSAMT) and MT data. The solid lines through the data represent the results of the joint inversion. In both cases – the MT and LOTEM – a better fit could be obtained with the individual inversions. However, it is not certain that the resulting model would be more realistic.

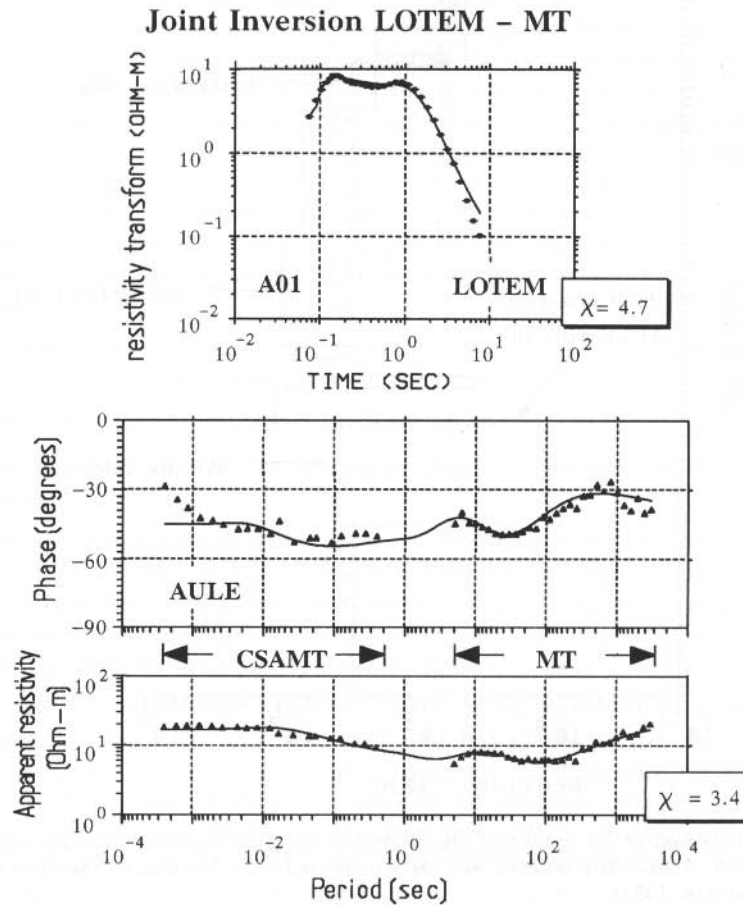


Fig. 4.8: Field data for LOTEM (top) and MT (bottom) measured at the same site in North-Western Germany with the synthetic curves for the joint inversion result (after Hördt, 1989).

Figure 4.9 compares the individual inversion and the joint inversion results with the well log. The joint inversion result fits the well log best and MT and LOTEM complement each other in depth investigation range. Still, there is some deviation from the well log which can be explained with three-dimensional structures. They lie

mainly in the gradual resistivity increase (see well log), where the layered earth model is inappropriate and will be discussed in more detail later on.

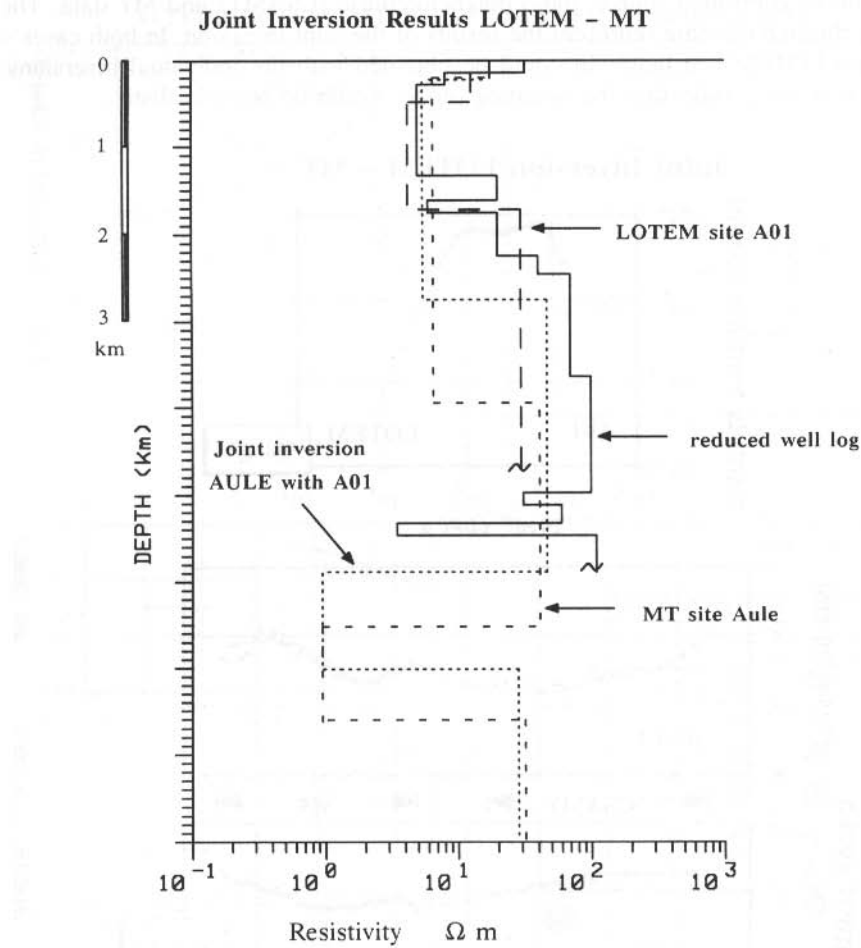


Fig. 4.9: Comparison of the individual inversions and the joint inversion with the well log (after Hördt, 1989). The reduced well log was derived from blocking of the original laterolog (Büchter, 1983).

Profile Inversion

When interpreting several soundings along a profile, the interpreter is comparing the individual inversion results with the results of the adjacent soundings. In a sedimentary environment, one mostly interprets the data in terms of layered earth models and is searching for deviations from the layering. If the inversion result of one station varies only slightly from the adjacent ones, the interpreter moves onto the next sounding. If the inversion result at one station varies significantly from the available adjacent stations, there is either a problem with the data (such as processing, scaling or noise) or the geology (e.g. 3-D structure, fault). These soundings take up most of the interpretation time since one has to make sure the problem with this particular data is analyzed and all possible inversion models have been tried. This is a very slow process requiring significant user interaction. Automatically, one requests a technique to carry out the inversion along a profile on the computer and thus reduce the user interaction to the data set where the standard inversion is not successful. We call such a procedure *profile inversion*.

The goal for such kind of procedure is to derive a more objective criterion to aid the interpreter. To achieve this, two tasks can be defined:

- One must find a reliable model for a profile.
- The results from one station must be objectively transferred to the next station.

The derivation of a reliable model for a station can be done in many different ways. The best way is the use of a good complete well log and an exemplary cross check with one station. If no additional information is available the interpreter is left to his own judgement and needs to find the reliable model on a trial and error basis. Once the model has been defined the *profile inversion* can be used.

The transfer of information from one station to the next in the inversion process can be done in many different ways. The simplest way is to use the last inversion result as input for the next station. The checks can be done with simple parameter comparison. This procedure will, however, only be successful in areas with very simple geology and not save much interpretation time. Here, we also consider two approaches to integrate the results from one station for the next station more thoroughly. The first approach is called *inversion with soft bounds* and the second *inversion with hard bounds*. The latter will mainly be considered theoretically, since not enough experience exists in applying the hard bounds inversion to field data. The derivation is following closely Petry (1987) with a more mathematical description given by Lawson and Hanson (1974).

In the derivation we start with a simplification of equation (4.10)

$$W J \Delta p = W g \quad (4.31)$$

If we define a weighted Jacobian such as $\mathbf{WJ} = \mathbf{J}_w$ we obtain

$$\mathbf{J}_w \Delta \mathbf{p} = \mathbf{W} \mathbf{g} \quad (4.31)$$

where \mathbf{J}_w is an $n \times m$ matrix and Δ the parameter difference vector containing m values for the parameters. We now append to the Jacobian an $n \times n$ diagonal matrix, \mathbf{D} , which contains the parameter weights on the main diagonal normalized by m/n . To the discrepancy vector a Nullvector, $\mathbf{0}$ of length n , is appended. Equation (4.31) converts then to:

$$\begin{pmatrix} \mathbf{J}_w \\ \mathbf{D} \end{pmatrix} \Delta \mathbf{p} = \begin{pmatrix} \mathbf{W} \mathbf{g} \\ \mathbf{0} \end{pmatrix} \quad (4.32)$$

where

$$\mathbf{D} = \text{diag} \left(\frac{m}{n} u_i \right) \quad i = 1, \dots, m \quad (4.33)$$

contains the non-negative weights of the i -th parameter u_i . The boundary condition – meaning that the parameter changes between stations are small – is described by:

$$\mathbf{D} \Delta \mathbf{p} = \mathbf{0} \quad (4.34)$$

This is exactly what we wanted: parameters with large weights are changed little and parameters with small weights can be modified more during inversion.

For hard bounds one would like to constrain the parameters explicitly within a given range. This range can be derived from well logs or other information. For a start parameter \mathbf{P}_0 , an upper and lower bound is defined such as upper bounds: $\mathbf{P}_0 + \mathbf{P}^u$ lower bounds: $\mathbf{P}_0 + \mathbf{P}^L$ (Weidelt, pers. comm.).

The i -th component of the parameter vector \mathbf{P} is then calculated in the k -th iteration by

$$P_{k,i} = P_{0,i} + \frac{P_i^u - P_i^L}{2} + \frac{P_i^u + P_i^L}{\pi} \arctan(a x_{k-1,i}) \quad (4.35)$$

where x_k is the sum of the undamped parameter variations during the k iterations. Instead of inverting for the parameter change during one iteration, $\Delta \mathbf{p}$, the inversion is now done with the total parameter change of x_k . Including the arcus-tangent function in this way guarantees that \mathbf{P} does not penetrate the bounds. The new Jacobian consists then of:

$$\frac{\delta f_j(\mathbf{P})}{\delta x_i} = \frac{P_i^u + P_i^L}{\pi} \frac{a}{1 + a^2 x_i^2} \frac{\delta f_j(\mathbf{P})}{\delta p_i} \quad (4.36)$$

The factor, α , directs the convergence. A large factor causes fast move away from the starting value but a slow convergence when the result is close to the final solution.

The first *profile inversion* case history uses data from a sedimentary basin in Europe. The basin is known to be approximately horizontally layered. Figure 4.10 shows three different inversion results for the same survey line. The field data was of average quality and a representative for the area. For the top of figure 4.10 the same starting model was used for the inversion of all soundings. This model was:

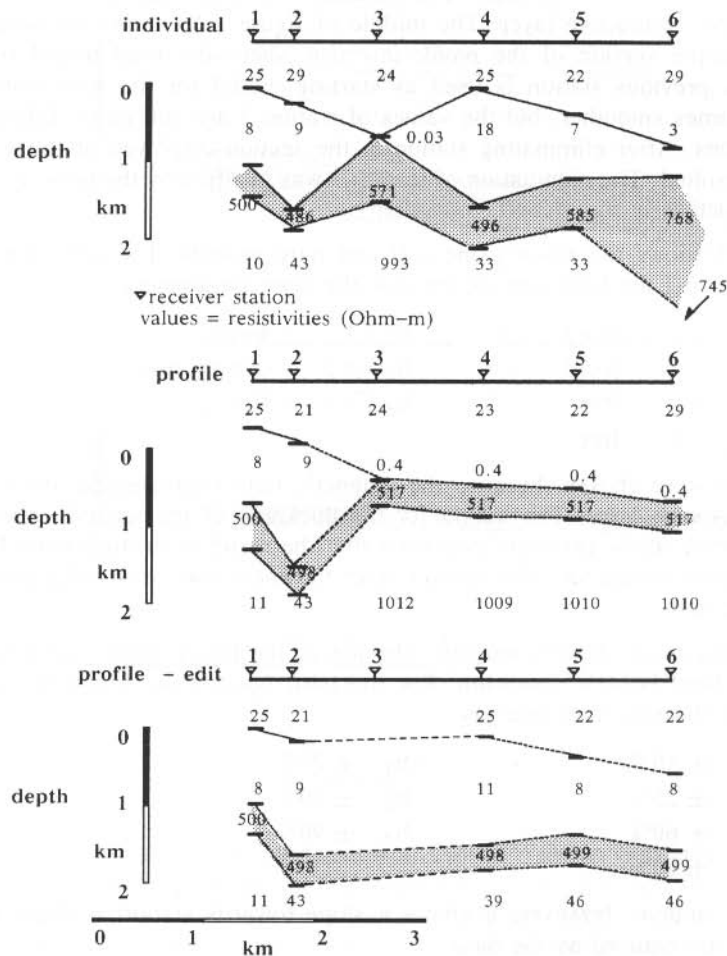


Fig.4.10: Inversion results for the same survey line. The top shows the results of the individual inversions using the same starting model for all data. The middle is the same line when the inversion result of the previous station was used as starting model for the next station. The bottom frame shows the results of the same procedure after eliminating station 3 (after Petry, 1987).

$\rho_1 = 20 \text{ } \Omega\text{m}$	$h_1 = 800 \text{ m}$
$\rho_2 = 10 \text{ } \Omega\text{m}$	$h_2 = 1100 \text{ m}$
$\rho_3 = 500 \text{ } \Omega\text{m}$	$h_3 = 400 \text{ m}$
$\rho_4 = 30 \text{ } \Omega\text{m}$	

Notably, the structure from the inversion models is erratic when using the shaded area as tracing layer. In particular, the result from station 3 is different from the expectations (known from well logs). The conductive second layer has been reduced to a very thin very conductive layer. The middle of figure 4.10 shows the results after applying a simple version of the *profile inversion* where the final model (inversion result) of the previous station is used as starting model for the next station. The structure becomes smoother, but the values of station 3 are still quite different from the expectations. After eliminating station 3, the section displayed at the bottom of figure 4.10 resulted. The elimination of station 3 was justified by the noise level in the data. The structure is significantly smoother.

Figure 4.11 shows the result using soft and hard bounds. The soft bounds (top) were applied using the following weights for the layer parameters:

$\rho_1 : 1.$ – fixed	$h_1 : 1.$ – fixed
$\rho_2 : 1.$ – fixed	$h_2 : 0.5$ – constrained
$\rho_3 : 0.05$ – free	$h_3 : 0.1$ – free
$\rho_4 : 0.1$ – free	

These weights were chosen, because the magnetic field measurement does not well resolve the resistive layer. The weight for the thickness of the second layer was derived after seeing in the previous inversions that the result is strongly biased towards the well resolved conductor. The second layer thickness was reasonably well known from well log data.

The resulting model is very smooth. The top of the figure shows the results after applying the hard bounds algorithm. For the hard bounds the following tolerances were used for the model parameters:

$\rho_1 : \pm 50\%$	$h_1 : \pm 25\%$
$\rho_2 : \pm 25\%$	$h_2 : \pm 50\%$
$\rho_3 : \pm 60\%$	$h_3 : \pm 90\%$
$\rho_4 : \pm 90\%$	

The result is smooth, however, it shows a slope towards station 6 which could be systematic or is required by the data.

These values were derived from the knowledge of the results in figure 4.10 and the true resistivities of the subsurface measured in a borehole. For both cases, the structure is now very smooth and represents closely the true resistivity distribution, but deviates in the thicknesses. The hard bounds force the data to a higher degree to match the preconceptions of the interpreter.

The sections using the hard and soft bounds are more realistic compared with the results in figure 4.10. They were also automatically calculated without user interaction. However, the data fit in both sections is worse than for the section in figure 4.10. Thus extreme care should be taken when applying this procedure and it should only be used when good structural constraints (i.e. well logs) exists.

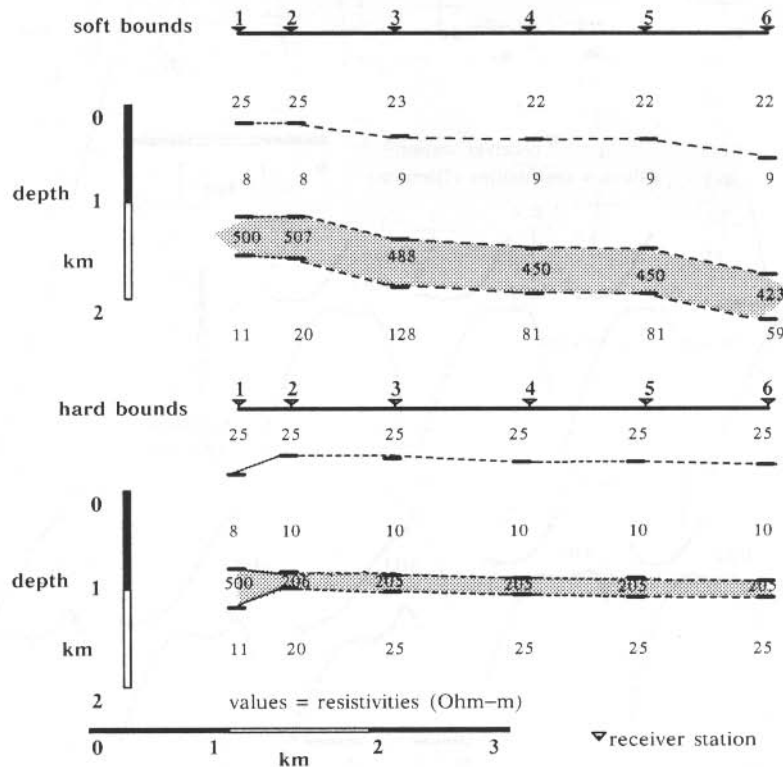


Fig.4.11: Inversion results for the same data as in figure 4.10 using soft bounds (bottom) and hard bounds (top) profile inversion (after Petry, 1987).

The next case history is for a data set from North-Western Germany. The data was interpreted using the above inversion procedures. Figure 4.12 shows the interpreted resistivity section from the one-dimensional inversions without consideration of the adjacent stations. For all stations the following starting model was used:

$$\begin{aligned}
 \rho_1 &= 13 \, \Omega\text{m} & h_1 &= 300 \, \Omega\text{m} \\
 \rho_2 &= 5 \, \Omega\text{m} & h_2 &= 1000 \, \Omega\text{m} \\
 \rho_3 &= 15 \, \Omega\text{m}
 \end{aligned}$$

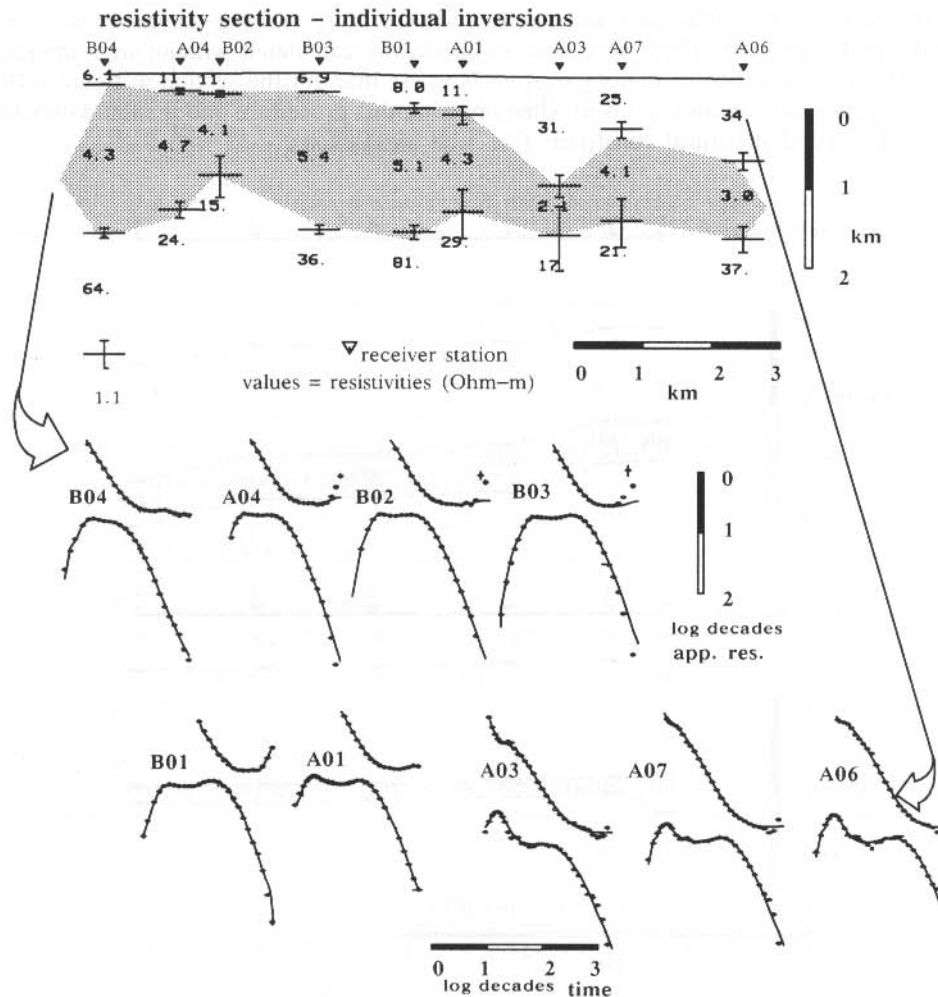


Fig.4.12: Interpreted resistivity section using the individual inversion results (top). At the bottom of the figure the data (squares) and synthetic curves are shown sequentially starting from the left side of the profile.

This model was derived from well log reduction of a 6 km deep borehole and subsequent forward modeling to obtain the minimum number of resolvable layers. The six stations on the left of the figure give reasonably consistent results whereas the resistivity section is jagged on the right side of the figure (inconsistency of the model). Below the section, the data (squares) is displayed with the solid lines representing the synthetic curves for the corresponding earth model. The three stations at the right side of the profile, A03, A07 and A06 are influenced by distortion in the field data which

can be seen in the high bend at early times. Most likely this distortion is caused by a three-dimensional effect. The data are, however, well fit by a one-dimensional model.

Figure 4.13 shows the results of the simple *profile inversion* when the final model of the previous station was used as starting model for the next station. The structure in

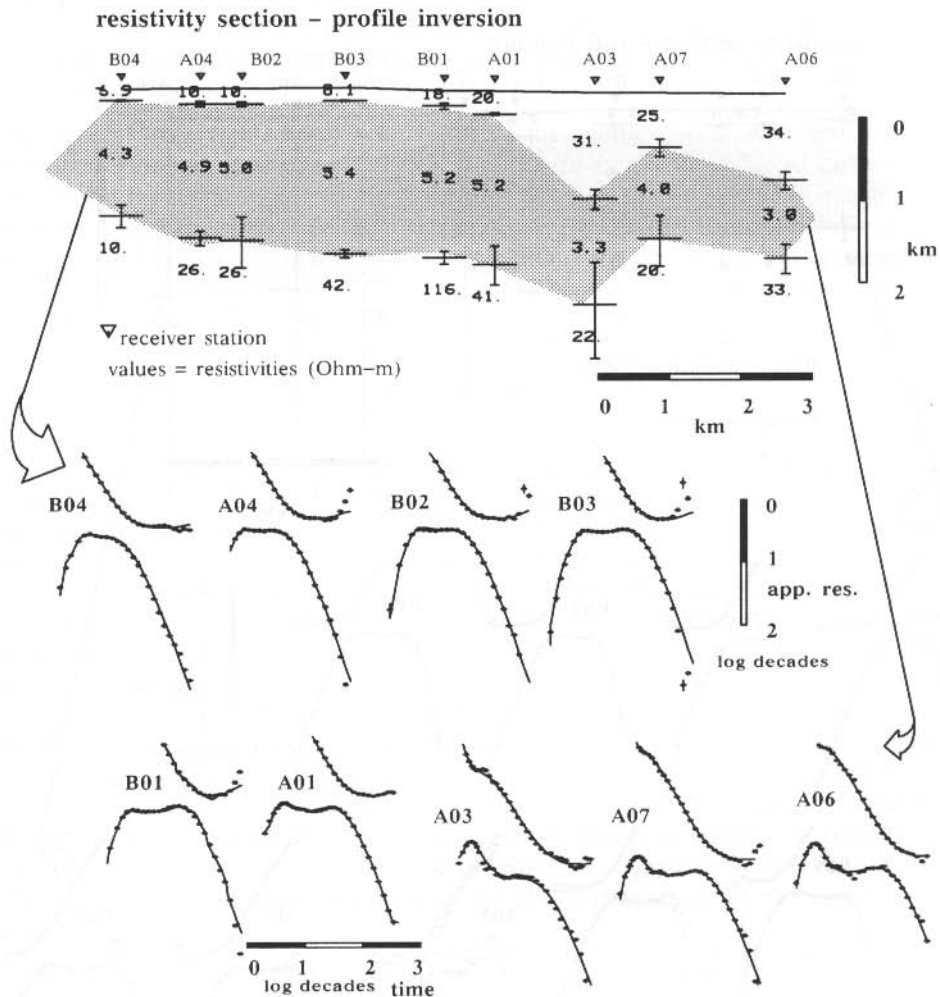


Fig.4.13: Interpreted resistivity section for the *profile inversion* without parameter bounds. At the bottom of the figure the data (squares) and synthetic curves are shown sequentially starting from the left side of the profile.

the resistivity section becomes already smoother including the right part of the profile. The data at the bottom of the figure shows only slightly worse data fits at later times.

The error bars for the layer thicknesses have essentially stayed the same except for station A03.

Figure 4.14 shows the resistivity section for the *profile inversion* when soft bounds were used. Since the resistivity of the second layer is well known, this layer has the highest weights. The detailed weights for the model parameters are:

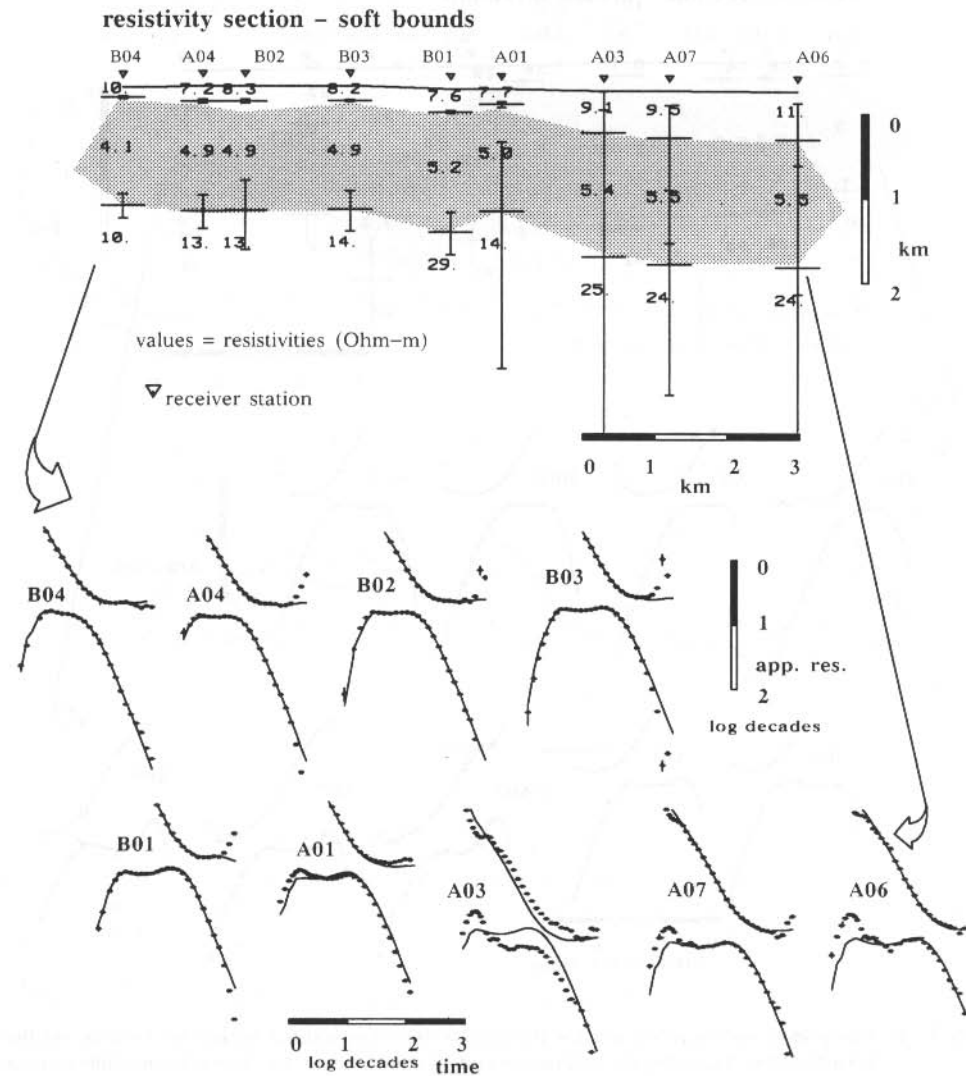


Fig.4.14: Interpreted resistivity section using the profile inversion with bounds. At the bottom of the figure the data (squares) and synthetic curves are shown sequentially as indicated by the arrows.

$$\begin{array}{ll} \rho_1 : 0.5 & h_1 : 0.5 \\ \rho_2 : 2. & h_2 : 1. \\ \rho_3 : 0.5 & \end{array}$$

The starting model was consistent with the borehole measurements. The result is even smoother than the section shown in figure 4.13. However, the data fit is not as good. In many instances the inversion terminated at the maximum number of iterations and not upon convergence. This is also expressed in the larger error bars for almost all curves.

In general the weighted *profile inversion* fits the geology better than the individual inversions. However, one cannot neglect that this fit is somehow forced and extreme care should be taken. In particular, a detailed analysis of the inversion statistics and the noise characteristics of the data becomes essential. When three-dimensional geology exists the *profile inversion* may serve to continue the underlying 1-D geology over the local 3-D anomaly. This procedure must be backed by 3-D modeling.

Occam Inversion

In the above chapter we have seen that we can interpret the field measurements along a profile and thus give the interpreter another tool to derive his/her more objective judgement. However, one needs a tool which shows which kind of information is actually in the data, and which is a result of the interpreters influence. Thus we are still looking for an even more objective tool to interpret the data. While searching for this, we must also consider the problems in our assumption. When inverting data to a minimum error, we are assuming that a specific number of layers will fit the data. However, the geology consists – if at all layered – of many layers and in most instances the resistivity changes between the layers are discontinuous on the scale of centimeters, but when the layers are lumped together in tens or hundred of meters they are, in sedimentary areas, mostly continuous. This assumption is no longer valid when a strong contrast of thick units exists (e.g. salt-sediment boundary; sediments above basement; crystalline units). For a smooth resistivity model we consider the concept of *Occam Inversion* which was first reported by Constable et al (1987). We will follow their concept closely and demonstrate the usefulness of *Occam inversion* with some case histories.

The *Occam Inversion* is based on the assumption that the resistivity – depth structure should be as smooth as possible. This means one is trying to avoid the jagged structures and is simply trying to fit the data with a smooth model. Even before looking at the mathematics it becomes evident that this will significantly increase the computation time. The assumption of a minimum model will, however, reduce the possibility of overinterpretation.

When inverting data we are generally speaking of a least squares process under boundary conditions. This means the functional to be minimized, F , consists of a

quantity to be minimized, Q , and an expression, P , describing the boundary conditions.

$$F = Q + P \quad (4.37)$$

The boundary condition term is multiplied with the Lagrange multiplier. The choice of the boundary condition determines the method used. For the Marquardt inversion, Q is the weighted least squares error, and P restricts the parameter change during the iterations. For the *Occam inversion* one requires smoothness of the resistivity – depth function in terms of roughness. The roughness is the integrated square of the first or second derivative with respect to depth (Constable et al, 1987).

$$Q = \chi^2$$

$$P = R_1 = \int \left(\frac{dm}{dz} \right)^2 dz \quad (4.38)$$

or

$$P = R_2 = \int \left(\frac{d^2m}{dz^2} \right)^2 dz \quad (4.39)$$

where R_1 and R_2 are the respective roughness of first or second order; $m(z)$ is here the resistivity versus depth function. The roughness should be as small as possible during inversion. As in the above chapters, one must minimize the χ^2 . However, since perfect fits are almost never achievable with real data the iterative process continues until the χ^2 value falls below a predefined threshold value. As one approaches small values of χ^2 , a substantial increase in roughness is required for little improvements (Parker, 1984). For further detailed derivation of the mathematics the reader is referred to Constable et al (1987).

The first case history is from a basalt covered area in Western Europe. Very little is known about the geology below the basalt, except that there are some sediments below. Without borehole information, the interpretation of LOTEM data becomes difficult, since one does not know how many layers one needs for the interpretation. Figure 4.15 shows a comparison of the *Occam inversion* with a three or four-layer model. The *Occam inversion* shows a smooth curve exhibiting a conductor. The center of the conductor is several hundred meters deeper than the center of the two-layer earth models. This indicates that either the assumption of layering in the Marquardt solution is insufficient or there are systematic problems in the data. Another possibility could be that the change from the top layer (basalt) to the strata below (interpreted as sediments) is abrupt. From this figure no judgement as to which one is correct can be made. Since the Occam model is unique, this example illustrates how the *Occam inversion* can be used to correlate the layered earth models and select the most likely result. In this case one should not trust any layered earth model without additional geological confirmation.

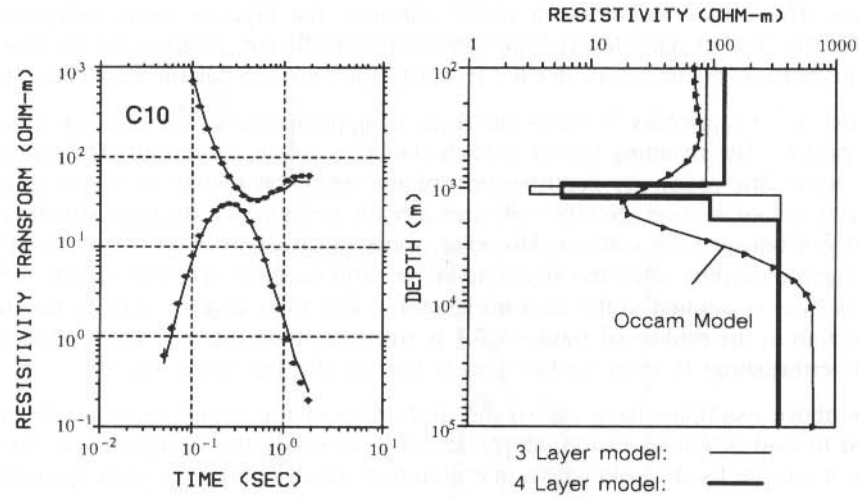


Fig.4.15: Comparison of *Occam inversion* with layered earth inversion. The left frame shows the field data (squares) with the theoretical curves for the inversion results on the right (smooth curve) (after Schruth, 1990).

Figure 4.16 shows an additional example of an *Occam inversion* for data from North-Western Germany. Since the display of a smooth earth model leaves the question open where to anchor the layer value on the graph, the Occam model is now

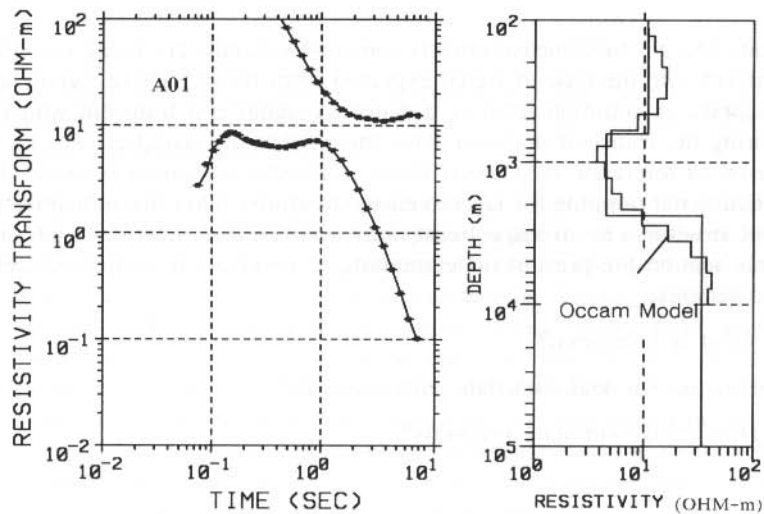


Fig.4.16: Example of an *Occam inversion* compared with the layered earth inversion result.

plotted as multi-layer model which is also the way it is calculated in the inversion program. Here, the Occam result nicely confirms the layered earth interpretation. Thus for this type of data, layered interpretation is sufficient, whereas for the previous example both inversions were needed to verify the existence of the conductive layer.

Figure A.7.1 (appendix 7) shows the result of applying the *Occam inversion* along an entire profile. The resulting model at each station is colour contoured. The top of the figure shows the resistivity depth section of the inversion results as output and displayed as colour section. Notably one can already recognize a detailed structure and consistency between the stations. However, some inconsistencies in particular at later times (greater depth) when the signal-to-noise ratio becomes worse is visible. Thus a lowpass filter is applied to the data horizontally. The filter width is half of the depth. The section in the middle of figure A.7.1 is smoother than the top. The overall structure (overthrusting) is more visible than in the top display of the figure.

The above examples have shown the usefulness of the *Occam inversion*. It can be applied to find problems in the interpretation or to verify the interpretation. Along a profile it can be used to obtain an interpretation which honors the data more than a layered earth interpretation. However, since many layers are used in the forward algorithm and the inversion goes through many iterations, the *Occam inversion* is very computation time intensive and cannot be used as a routine tool (figure 4.17 took about 50 hours CPU time on a MicroVax II; 12 hours with array processor).

INTERPRETATION OF DISTORTED TRANSIENTS (REVERSALS)

When carrying out field measurements sometimes signals are being recorded which do not conform with the type of signal expected from theory. These signals are called distorted signals. A common form of a distorted signal is a transient which changes polarity during the transient duration. This means that the signal crosses its DC level which is used as reference zero level. These transients are called *reversals*. Reversals are theoretically not possible for layered earth structures. They are indicative of three-dimensional structures or strong cultural noise sources (i.e. pipelines, railroad tracks, etc.). In this section the present understanding of reversals is addressed yielding the following questions:

- ☐ What is a reversal?
- ☐ How do we deal with data with reversals?
- ☐ How do we simulate reversals?

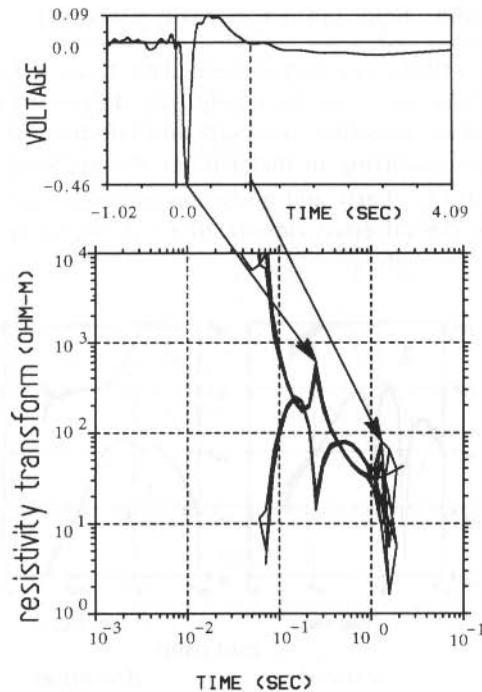


Fig.4.17: Display of observed field data showing a reversal. The top is the linear display of the stacked transients and the bottom a logarithmic display after apparent resistivity conversion. The crosshatching represents the 95% confidence interval.

So far, as field data interpretation is concerned, reversals have only been qualitatively interpreted. Two examples of interpreting reversals taken from Stoyer and Dameron (1986) and Stephan (1989) are given.

A distorted transient is a transient which behaves differently from the expected exponential decay over a layered earth. Sometimes when it crosses the reference level it is difficult to decide which part of the transient is the reverse part and which part is the non-reverse part. Figure 4.17 shows an example for a transient which has a sign reversal. The top of the figure shows the linear voltage versus time display of the stacked transient as recorded and observed in the field, the bottom figure displays the data after further poststack processing and conversion to early and late time apparent resistivity transforms. This reversal is a strong onset-reversal which means the reversal starts directly after the onset. Sometimes a reversal consists of a small onset reversal which is significantly smaller than the transient. In figure 4.17 the second reversal at later times could be either caused by incorrect reference level determination or additional three-dimensional effects. The insufficient reference level determination is sometimes the result of strong cultural noise and a reversed onset which can make an

objective judgement of the DC-level for the interpreter almost impossible. Reversals are easily recognized in the field, but not so easily classified.

Stoyer and Damron (1986) interpreted field data from a LOTEM survey in the Milford Valley, Utah. They classified their field data distortions into early time reversals, mid-time depressions, mid-time reversals and late time reversals. Late time reversals are sign changes occurring in that part of the apparent resistivity transform which should decay with $t^{-5/2}$. Early and mid-time reversals occur before the roll over time. Example data for the different classifications is shown in figure 4.18.

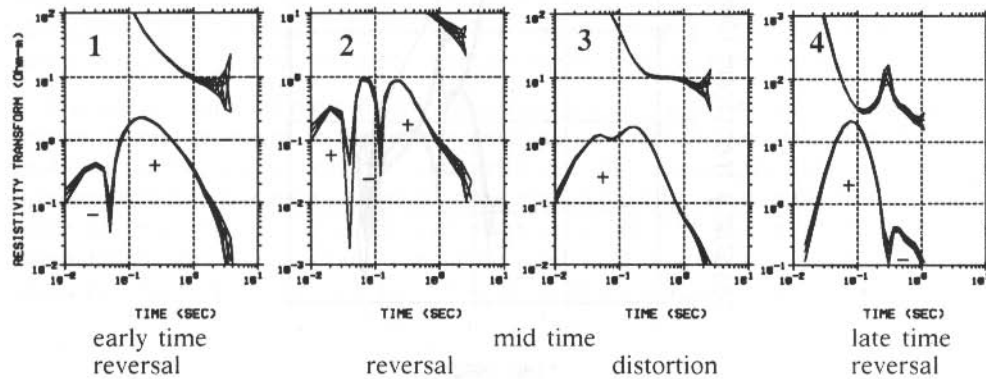


Fig.4.18: Classification of the field data distortions of a LOTEM survey in Utah. The left curve shows a reversed voltage at early times (1) and the right curve at late times (4). The two middle curves show mid-time distortions with a reversed voltage on the left (2) and a strong depression on the right (3) (modified after Stoyer and Damron, 1986).

The classifications are based on the time range when voltage reversals occur. In addition to the reversals there are also strong depressions in the signal which cannot be explained with layered earth interpretation. Stoyer and Damron (1986) used two different approaches to interpret their data. For late time reversals the geology could be explained using an axial conductor in a numerical modeling program (Tsubota, 1979). Figure 4.19 shows the results of Tsubota's calculations inferred for the field data. The axial conductor is buried in a homogeneous half-space. One curve shows the homogeneous earth response (upper curve) and below is the response of the axial conductor. The total field curve is a combination of both. The difference between the total field in figure 4.19 and the late time reversal in figure 4.18 is caused by the system response which has not been removed in figure 4.18 for the resistivity transforms. In figure 4.19 the synthetic data do not consider any system response. Furthermore, the synthetic data were obtained for a half-space host whereas the field data represents a layered host with three-dimensional structure. Considering this, the real field data of figure 4.18 (the late time reversal curve (4)) matches the synthetic results of figure 4.19 well.

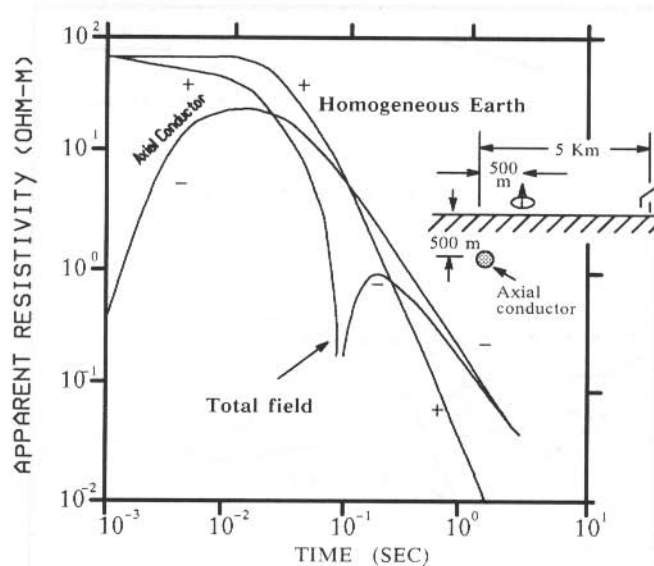


Fig.4.19: Synthetic distorted curve inferred for the Milford data (after Tsubota, 1979; Stoyer and Damron, 1986). The response of the conductor is negative for all times and responsible for the late time reversal. The conductor response is superimposed on the half-space response which is positive for all times.

Using the data classification in figure 4.18 and the synthetic data of Tsubota (1979) in figure 4.19 the soundings at the sites shown in figure 4.20 could be interpreted. A conductor was placed where shown in the figure (right side). The calculated homogeneous earth response, the response of the conductor and the total response are drawn. The total response shows a sign reversal at times when the negative response of the conductor becomes stronger than the homogeneous earth response. This axial conductor is very close to the Negro Mag Fault which is known to contain saline fluids from the geothermal field in the area. Due to the presence of these fluids a conductive anomaly can be expected. Numerical modeling results for this data set is shown below.

Other parts of the field data could not be interpreted in the same manner, because the geologic situation was different. To interpret these data, Damron (1986) built an analog scale model. For normalization and data comparison purposes he used a scaled transmitter – receiver array in a varying offset mode. This means the transmitter is kept fixed while the receiver is moved. The array was moved over a fault simulated by a soldering joint between two metal plates. The soldering joint simulates a more resistive fault zone. Figure 4.21 summarizes Damron's results. The early time curves are asymmetric with respect to the solder joint. When approaching the fault (curves 2 and 3 in figure 4.11) first a depression is seen growing to a mid-time reversal. As the receiver crosses and passes beyond the solder joint, the disturbances change character

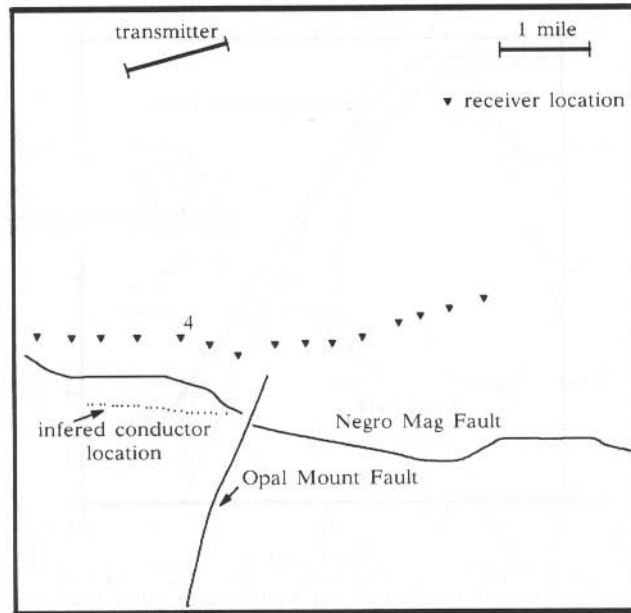


Fig.4.20: Station locations, faults and location of the modelled conductor for the Milford LOTEM survey (after Stoyer and Damron, 1986). Sounding 4 exhibiting a late time reversal is shown as example.

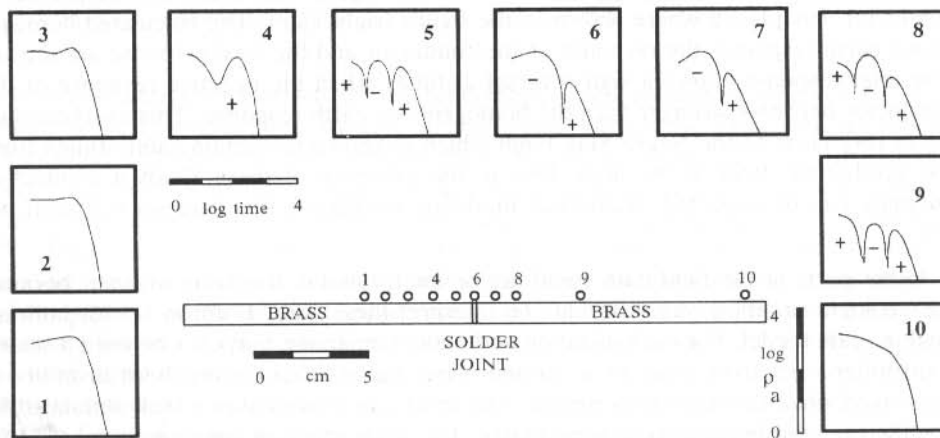


Fig.4.21: Simulation of a fault zone using an analog modeling experiment. The resulting shapes of the signal are used to classify the distorted responses (Stoyer and Damron, 1986). The station numbers are used as classification reference.

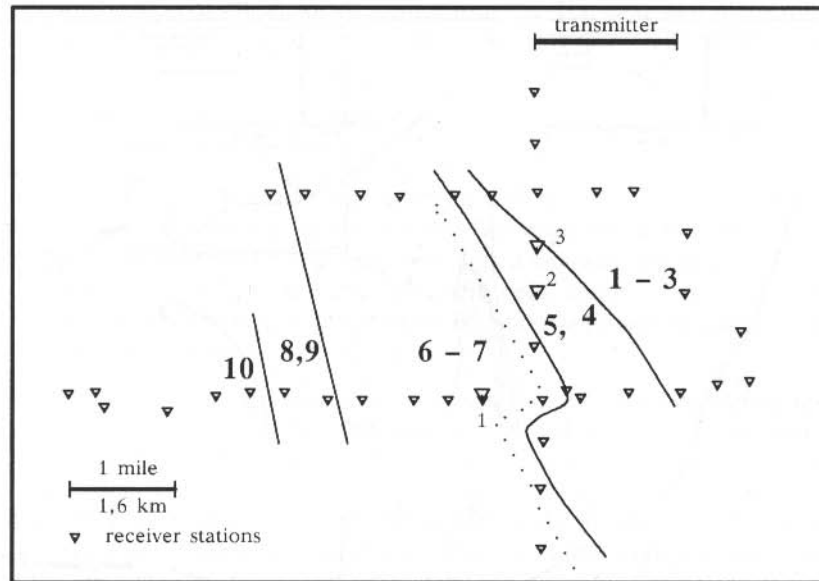


Fig.4.22: Interpreted *fault zone map* using the classification (bold numbers) for the distorted transients from figure 4.21 (after Stoyer and Damron, 1986). The large numbers refer to the curves shown in figure 4.18. The dotted line shows Stoyer and Damron's 1986 interpretation of the location of the fault.

and disappear more slowly (curves 6 to 10). The effect is expected to be stronger in the analog model, since the induction currents are more confined within the plate. Using the classification from the analog modeling results, part of the Milford data was interpreted yielding the interpretation shown in figure 4.22.

The analog modeling classification allowed the definition of possible fault zones. Resulting from this the location of the western boundary fault was inferred. There was also some geologic evidence for the existence of such a north-northwest trend. This geology is also numerically modeled and the results are shown below.

Stephan (1989) used the same approach and Damron's analog modeling results to classify his data from a survey in North-West Germany (Haltern). In parts of the survey area distorted transients were observed (see figure 4.23). Only in the north-eastern corner of the survey area could the reversals be attributed to geological structure. In other parts of the survey area the reversals were most likely caused by cultural noise (railroad tracks, pipelines etc.). The two sample transients displayed in the figure show different characters. The left transient has first a positive spike followed by a small narrow reversal. The right transient starts with a strong narrow reversal directly after the start of the signal. Using Damron's classification in figure 4.21 a possible fault map was prepared and is displayed in figure 4.24.

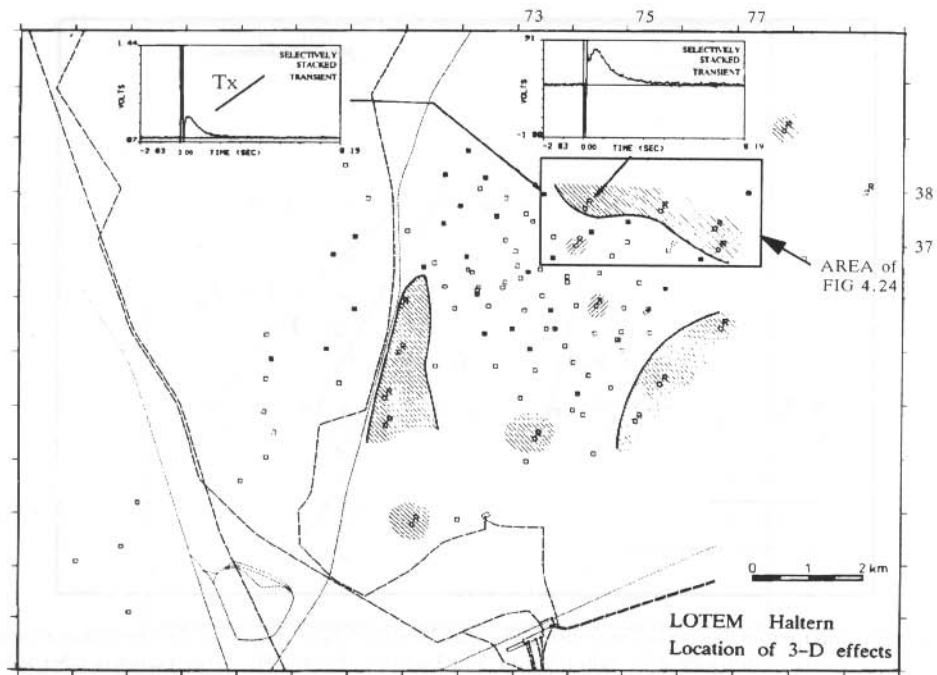


Fig.4.23: Survey map showing the location of distorted data (shaded areas). The shaded area in the north-eastern part exhibits reversals, two examples of which are shown in the figure (after Stephan, 1989). The dashed lines make the railroad and power lines.

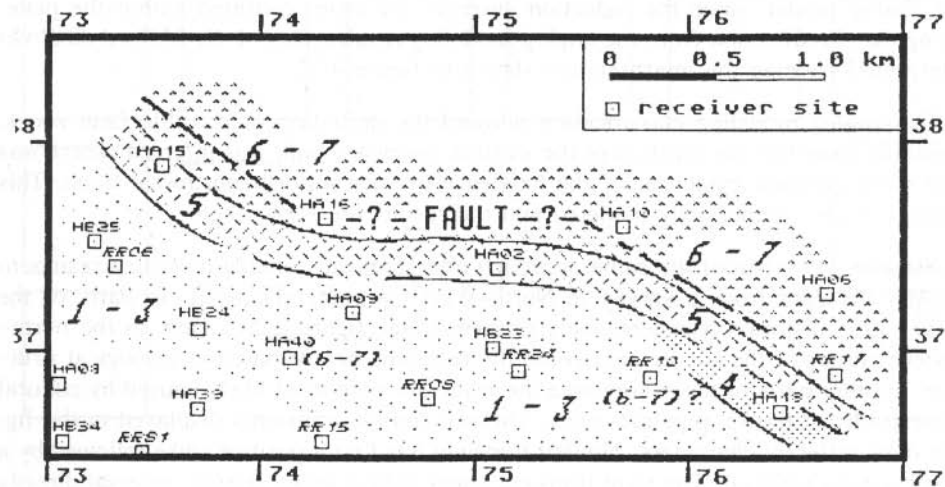


Fig.4.24: Possible fault maps for the Haltern Survey area using Damron's classification for distorted signals from figure 4.21 (after Stephan, 1989).

Using this kind of qualitative approach in combination with the field data allows an easy first classification of the distorted field transients. The next step is the integration of more elaborate modeling programs in the interpretation of real field data.

Numerical Simulation of Reversals

The numerical modeling of reversals is not an easy task, since *a priori* knowledge of the model structure is required. In this section two different numerical modeling approaches will be discussed. The first approach uses a laterally inhomogeneous conductive plate model to simulate the reversal (Weidelt, pers. comm.; Vasseur and Weidelt, 1977). The second approach uses the integral equation approach to calculate the 3-D response of an anomaly (Newman, 1989).

In the past, it was assumed that a reversal was caused by a conductive resistivity anomaly close to the receiver. This assumption was mainly based upon field experience and current channeling concepts. The conductive anomaly can be looked upon as a single conductor. The induction currents in this conductor remain strong for a long time and depending on what side of the conductor one places the receiver, the signal is positive or negative. Figures 4.25 and 4.26 show an example for a thin conductive plate model simulating such reversals (Weidelt, pers. comm.). The model is reduced to a thin plate with a conductance of 100 S located 100 m below the surface. Thickness and resistivity of the plate itself remain undetermined. The host rock has a resistivity of 10 Ωm . The resistivity values were selected from a real case history in Germany (see figure 4.24) simulating a resistive body. The offset between transmitter and receiver is 8 km. Figure 4.25 shows the time derivative of the vertical magnetic field for the receiver location marked in the upper part of the diagram. Reversals can be observed for the three stations on the far edge of the conductor and for three of the stations behind the conductor. The dashed lines on the graphs indicate the response for the earth without the conductive anomaly. The induction currents flow in the center of the plate causing on one side a positive and on the other a negative signal. The signal due to the anomalous conductor prevails with increasing distance from the transmitter. The anomalous response then adds to the normal response and depending upon its strength, reversals appear at different locations around the anomalous body.

The next model in figure 4.26 describes a more complicated field situation (Weidelt, pers. comm.). Now the conductive plate separates a 20 Ωm half-space from a surficial 12 Ωm layer. Part of the plate has a conductance of 10 S and the rest of 150 S. The layer above the plate has a resistivity of 12 Ωm and the one below of 20 Ωm . The corners of the conductivity anomaly are aligned with the equator of the dipole transmitter. In the plan view the conductivity anomaly is 3 km on the side and between 7 to 10 km away from the transmitter. The resulting time derivatives for the receiver stations are shown below. The response without anomalous zone is marked by the dashed line and differs strongly from the lower stations of the array. The station in the centre of the conductivity anomaly shows very little deviation between one- and three-dimensional curves. Again reversals occur only near the edge of the conductivity

anomaly. Again the specific occurrence of a reversal seems to be directly related to the strength of anomalous and normal fields with respect to the receiver position.

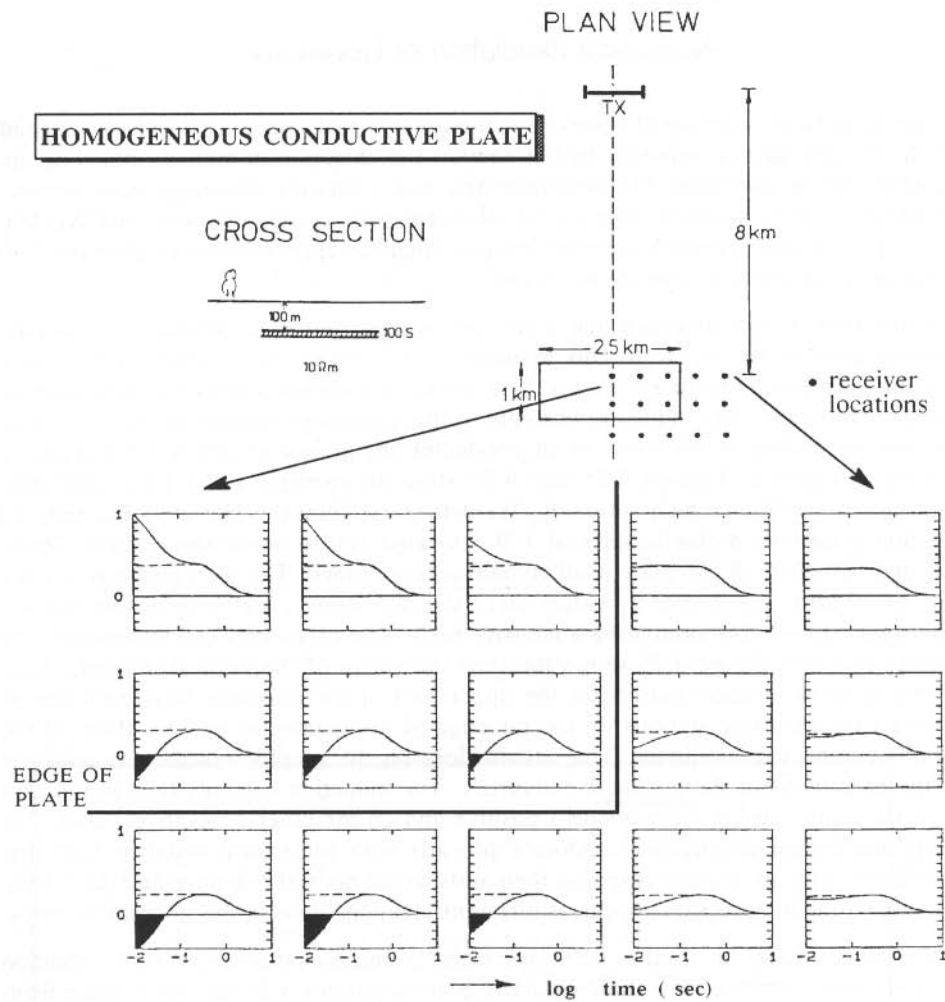


Fig.4.25: Field array and model for the conductive plate program simulating a sedimentary environment and the synthetic transients (semi-logarithmic axes) at the respective receiver sites. The conductive plate is laterally homogeneous (Weidelt, pers. comm.). The negative signals are displayed by area fill.

The second type of example uses Newman's 3-D (Newman, 1989) program to simulate a difficult field situation. The basic model and results are displayed in figure 4.27.

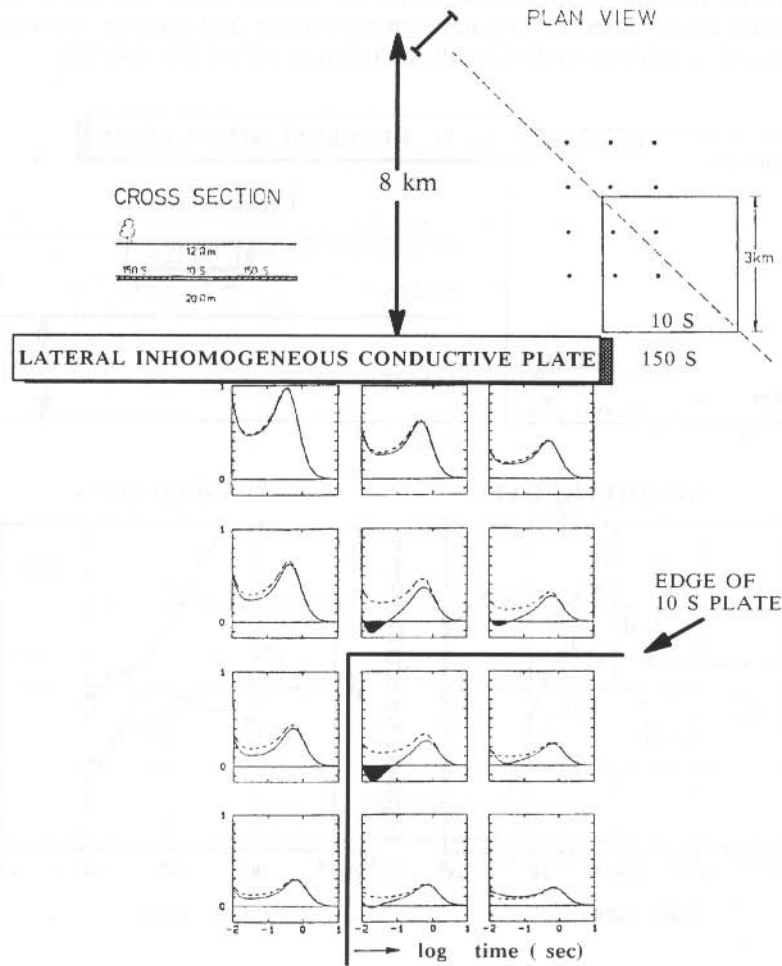


Fig.4.26: Geometric setup for the conductive plate program with lateral inhomogeneities. The model parameters simulate a sedimentary environment. The resulting synthetic transients (semi-logarithmic axes) are shown at the bottom.

This particular model simulates LOTEM measurements carried out in a crystalline environment with very high resistivities. The synthetic 3-D data (squares) are compared with a 1-D curve (solid line). The 1-D curve is the curve without the conductive anomaly (early time reversal). It can clearly be seen that the 3-D curve deviates very strongly from the 1-D curve until rather late times. On the right are the resistivity transforms of a field data set displayed which exhibits similar behavior. The difference in the zero crossing of the reversal is attributed to different scaling between the numerical model and the real geology under the receiver location where the data set

was acquired. The difference to the model of figure 4.26 is that the reversal was obtained with the conductive body between transmitter and receiver, whereas in the previous figure a resistive body beyond the receiver causes the anomaly.

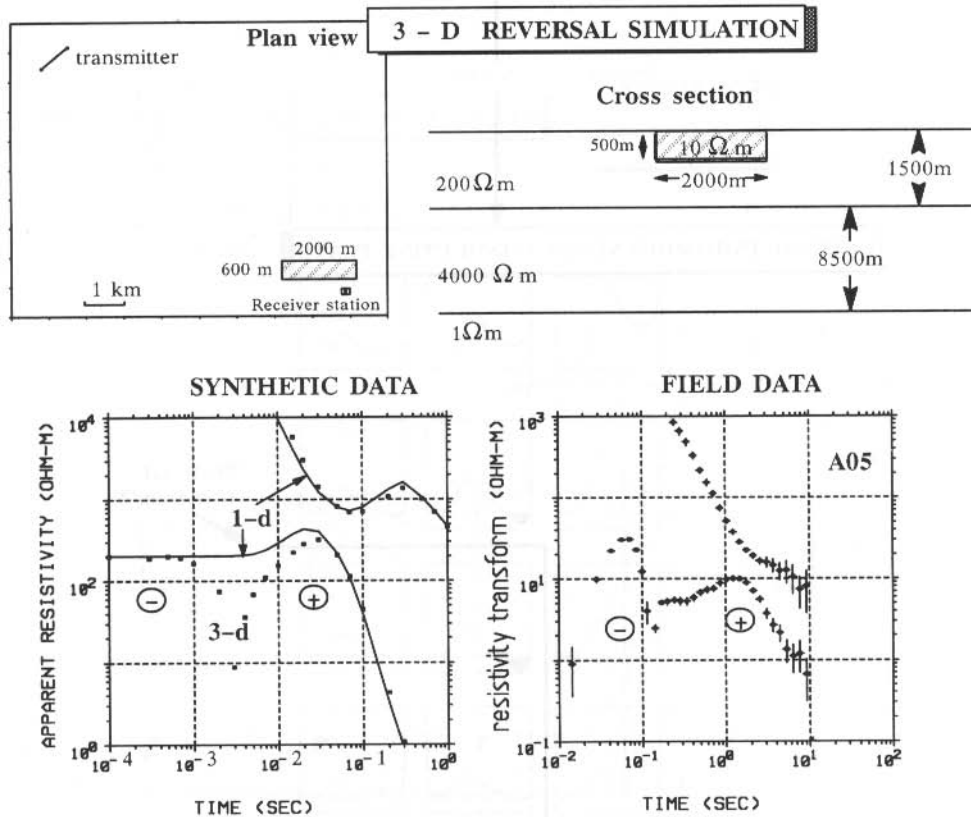


Fig.4.27: The three-dimensional response of a conductor near the receiver is calculated using the integral equation method. The top shows the section and plan view of the earth model. The data set on the bottom left shows the synthetic data for the 3-D model in comparison with the respective one-dimensional curve. On the bottom right a real field data set exhibiting the same characteristics is shown. The different location in time of the notch in both diagrams is caused by the model scaling and the fact that the detailed resistivity structure underneath the three-dimensional measurements is not known.

In order to evaluate the position of the reversals with respect to the location of the body further, Newman (1989) calculated the 3-D response for a profile across a conductive body. His results are displayed in figure 4.28. Two reversals can be seen in receiver location 3 and 5. The signals are distorted from receiver location 3 to 6. At site 3 the signal exhibits a sharp notch which is not yet a reversal. This is an indicator that we are approaching an anomalous zone. Similar behavior was also shown in

figure 2.19 where synthetic data of a 3-D structure was imaged. The location of the reversal behind the conductive body clearly indicate that the reversals occur near the conductivity anomaly when the response of the anomaly is larger than the layered earth response.

The above examples have shown two different ways of explaining reversals using analog and numerical modeling. In particular, they have demonstrated that reversals can be caused on either side of the conductivity anomaly. Also, reversals can be caused by resistive faults. Thus, for each particular survey where such reversals occur one should carefully eliminate all impossible options and pinpoint the conductivity anomaly by getting as much field data as possible to narrow down. Only then can successful 3-D modeling be done.

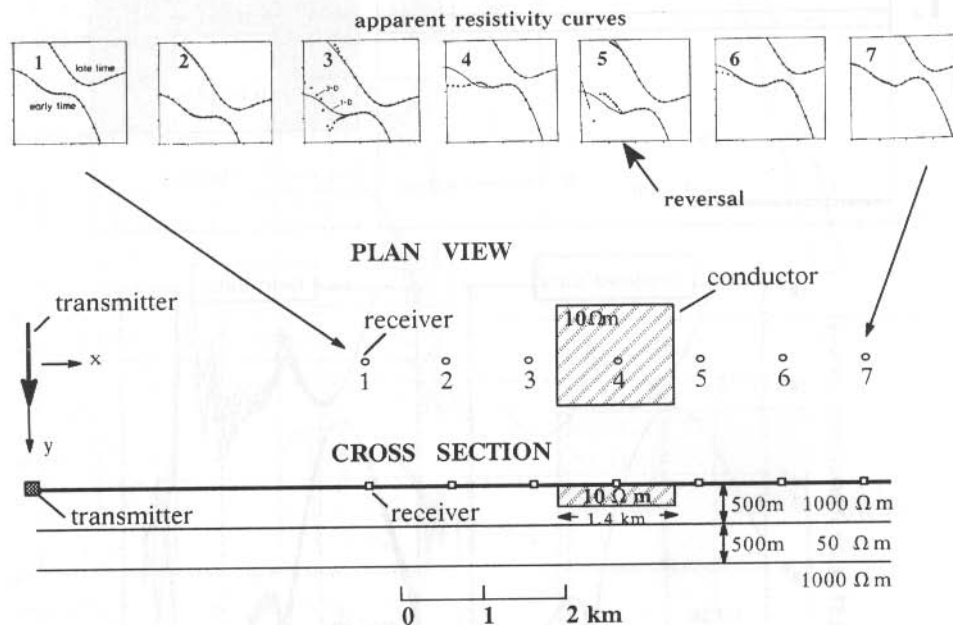


Fig.4.28: Model profile over a conductive body from 3-D modeling (after Newman, 1989).

With the above considerations, Kriegshäuser (1991) calculated two numerical models for the data from the Milford area, Utah. Based on Stoyer and Damron's (1986) interpretation the Negro Mag fault zone was simulated by a two-dimensional structure. From the above modeling results the conductor was placed at a similar depth the authors interpreted. The axial conductor has a very high conductivity to obtain the sign reversal at approximately the same time. Figure 4.29 shows the model setup and a comparison of a selected field data set with the respective numerical modeling data. For the modeling the finite difference program by Druskin and Knishnerman (1988) was used. The shape and amplitudes of the modeled and field data are very similar indicating that a very realistic model was selected. The remaining deviation between

the time of the sign reversal can be improved when changing the depth and conductivity of the axial conductor.

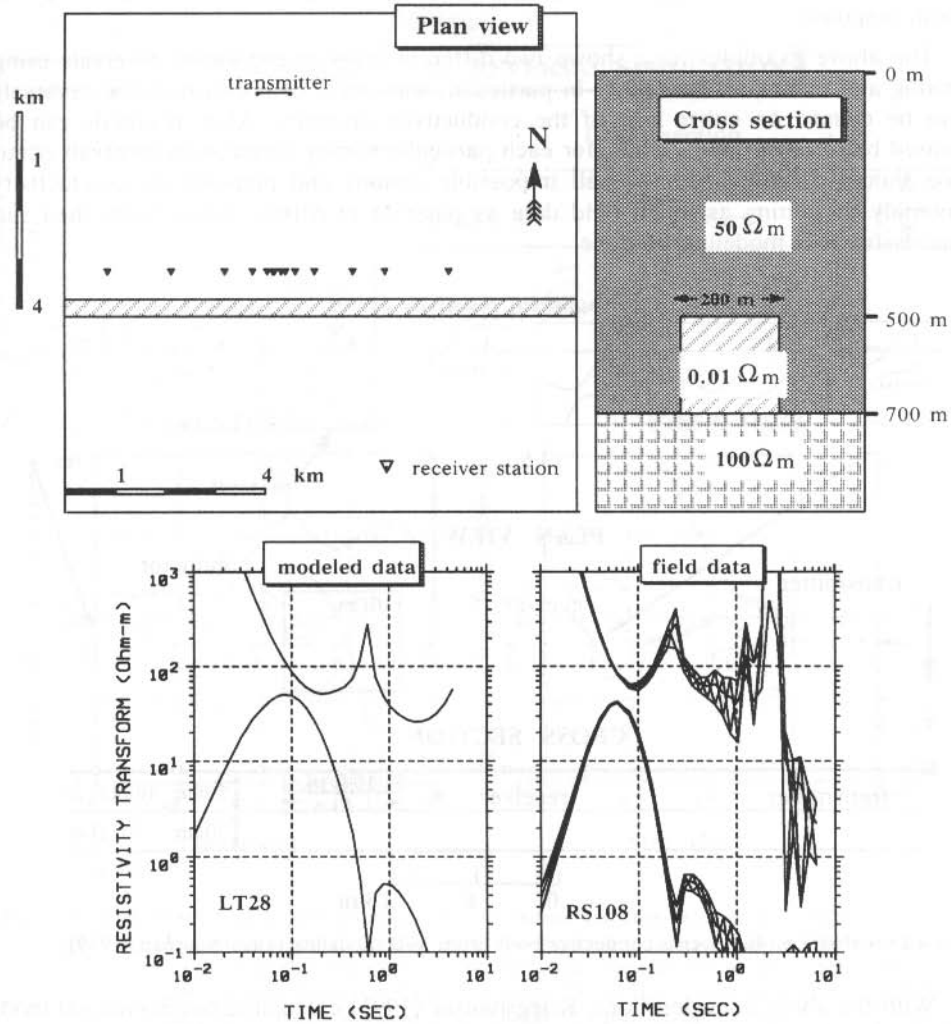


Fig. 4.29: Two-dimensional model setup for the axial conductor model of the Milford area, Utah. At the bottom of the figure a comparison between the synthetic and field data is shown. Both data sets are displayed as resistivity transforms. (after Kriegshäuser, 1991).

Another more detailed example is also from the Milford area but from the part of the survey which could previously only be interpreted with analog models. A three-dimensional model was constructed based on the one-dimensional interpretation of all data in the area with a resistive dike superimposed on it. The depth values for the 1-D

background model were selected from one-dimensional interpretation and the depth to the top of the dike and its width from the numerous different model runs. Figure 4.30 shows the survey plan with the dike outlined as well as a cross section of the model. On the left side of the figure characteristic transients are selected for the field data

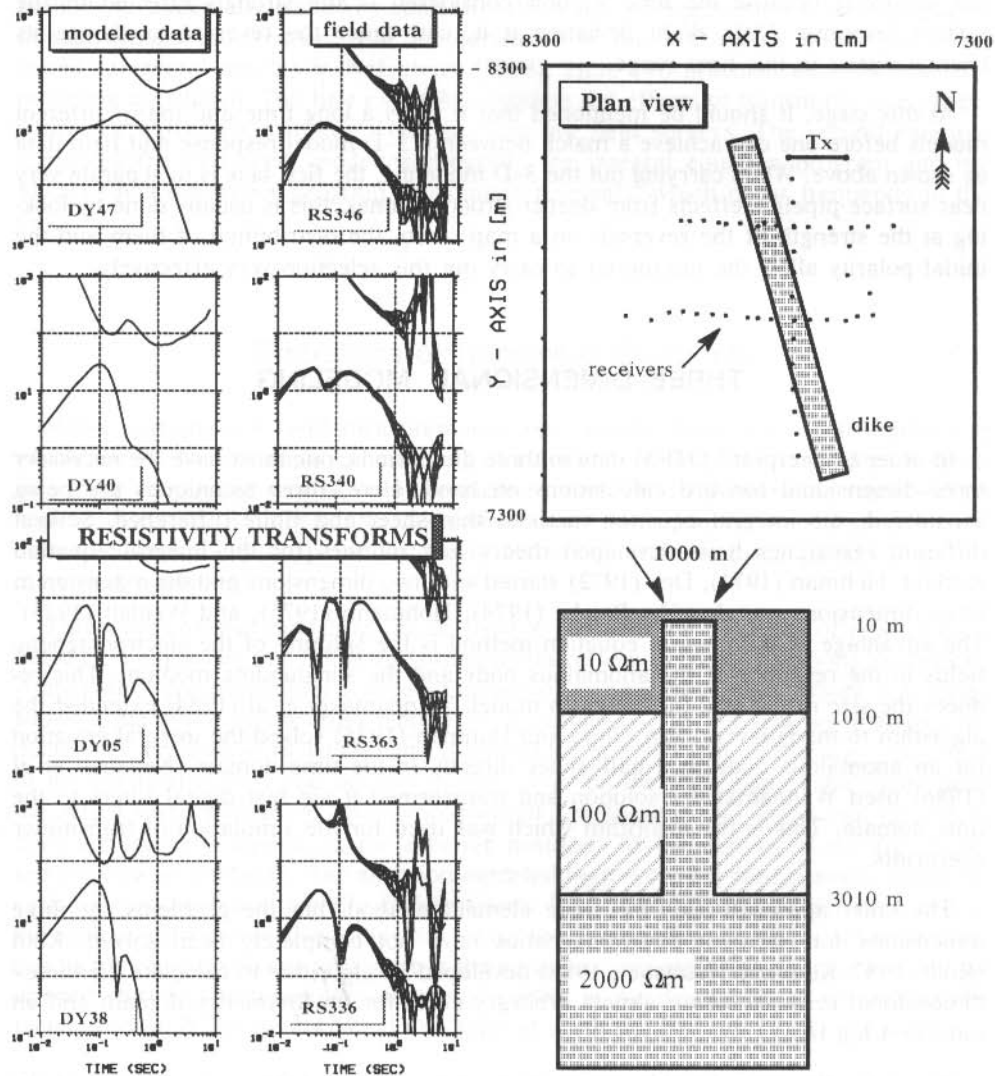


Fig. 4.30: Three-dimensional model setup (right) for part of the Milford survey. On the left the resistivity transform are shown for the modeled and field data.

and for the calculated data sets. The early time depression (top frames), the double reversal (third row of frames) and the intermediate time reversal match very nicely. The early time depression shown in the second row of frames is clearly exhibited by the field data but not so clearly by the modeled data. In fact, the modeled data shows the depression at significant later times. Although this appears to be a discrepancy, it is not so strong because the time window considered is still strongly effected by the system response. Only slight deviation in it, can cause the reversal to change its characteristics in this time range.

At this stage, it should be mentioned that it takes a long time and many different models before one can achieve a match between a 3-D model response and field data as shown above. When carrying out the 3-D modeling, the first task is to separate very near surface pipeline effects from deeper structural ones. This is usually done by looking at the strength of the reversals on a map. Also, the distribution of them and the initial polarity allow the interpreter to carry out this selection very effectively.

THREE-DIMENSIONAL MODELING

In order to interpret LOTEM data in three dimensions, one must have the necessary three-dimensional forward calculations on hand. Here, three techniques are being considered: the integral equation method, thin-sheet and finite difference. Several different researches have developed theory and routines for the integral equation method. Hohman (1971), Dey (1972) started with two dimensions and the extension to three dimensions was done by Raiche (1974), Hohmann (1975), and Weidelt (1975). The advantage of the integral equation method is the splitting of the electromagnetic fields in the response of the anomalous body and the surrounding medium. This reduces the size of the grid for the earth model. Wannamaker et al (1984) extended the algorithm to many layers. San Filippo and Hohman (1975) solved the integral equation for an anomalous body in a half-space directly in the time domain. Newman et al (1986) used Wannamaker's solution and transformed it via fast digital filters to the time domain. This is the algorithm which was used for the simulation of transmitter overprints.

The other approach uses the finite element method, but the problems for three dimensions for transient electromagnetics have not completely been solved. Kuth (Kuth, 1987; Kuth and Neubauer, 1988) developed an algorithm to calculate the three-dimensional response of an almost arbitrary earth for the frequency domain and an induction log tool.

Presently, the most flexible approach is using a finite difference scheme and the spectral Lanczos decomposition method (SLDM). The method was derived by Druskin and Knizhnerman (1988) and applied to real data for the first time by Hördt et al (1992). It can simulate very complex geology and calculate the 3-D response within a reasonable amount of computer time.

The first three-dimensional modeling for grounded wire TEM was done by Gundersen et al (1986). Their results gave the first insight into the 3-D current flows around a grounded wire. In all of their models the receiver was located less than four times the dipole length away from the transmitter and thus does not quite represent the LOTEM method. The first LOTEM modeling was done by Newman (1989). However, both above papers use resistivity contrasts which are not representative for exploration in sedimentary environment. For the derivation of the 3-D theory the reader is referred to several articles in Nabighian (1988). Here two practical examples of 3-D modeling are shown: The first example considers the effects of transmitter overprints, which are extremely common when carrying out field surveys. The second example compares the thin-sheet modeling program, the integral equation program and the SLDM finite difference program to simulate reversals, which occur frequently in the field.

Simulations of Transmitter Overprints

When carrying out field measurements, one usually looks for a transmitter site which allows the best electrical coupling of electrodes. Often, the transmitter is setup in a more conductive area or on a conductive patch. This will cause the signals to be slightly distorted. Routinely, the calibration factor (see chapter 3) is applied to the data to correct for this type of distortion. Here, this effect is investigated using 3-D numerical modeling.

Three-dimensional modeling can be used to simulate the influence of near surface inhomogeneities. In the following example the effect of field situations is demonstrated when the transmitter is located on top of a conductive body. Figure 4.31 (top) shows a plan view and a cross section for a simple 3-D model. The anomalous conductor has a resistivity of $10 \Omega\text{m}$ and is embedded in a $300 \Omega\text{m}$ half-space. The effect of the conductive body can be seen in the curves on the right side of the figure near the actual surface location. The comparison of site one and two shows that the effect does not strongly depend on the receiver position. At the bottom of the figure the section view is displayed. The situation modeled here is typical for German conditions such as encountered in the Black Forest area. The transmitter is usually deployed in the valleys with conductive valley fill while the surrounding is highly resistive. The conductor causes a downwards shift in the early time apparent resistivity curve and an upward shift at late times. As mentioned earlier in the discussion on the calibration factor, this shift can be corrected and layered earth models can be obtained.

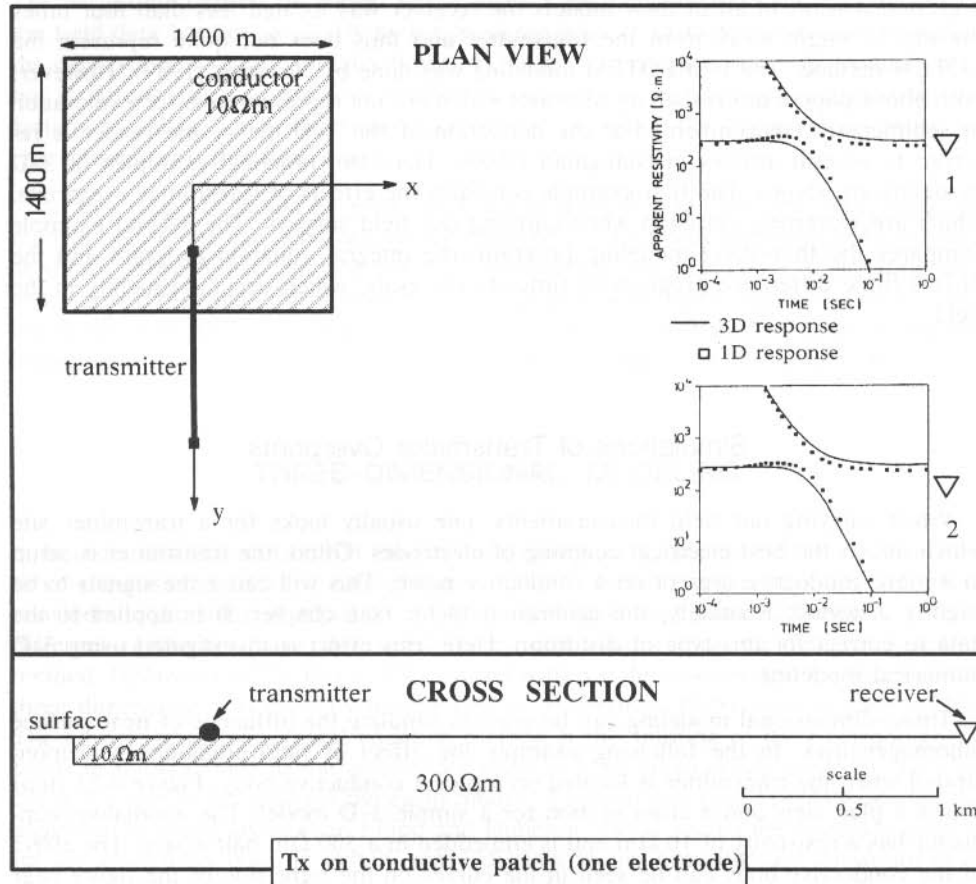


Fig.4.31: Plan view and cross section of the 3-D model to test the effect of conductive bodies underneath one electrode of the transmitter. For two stations the 3-D response (squares) and the 1-D response (solid lines) is shown on the right (after Newman, 1989).

Newman (1989) describes the results of interpreting the above model as yielding a biased layered earth model. Figure 4.32 shows the results of inverting the data from the 3-D model using a 1-D inversion algorithm. The inversion contained an additional parameter, the calibration factor, which is multiplied with the curve and thus shifts the curves vertically. The calibration factor was left floating during the inversion. The 3-D response is presented as data points in this figure. The solid lines through the early and late time curves are the synthetic curves for the inversion results. On the right side of the figure, the inversion models are shown in comparison with the true earth. The dashed line is the true earth model. Except for the upper part of the section

where an additional layer was introduced the resulting resistivity matches the true model. The data fit is quite acceptable. When using real field data, the model will in most instances be biased in the upper part of the section due to the effect of the system response. One thus needs a calibration well or additional information to make sure the interpretation is correct.

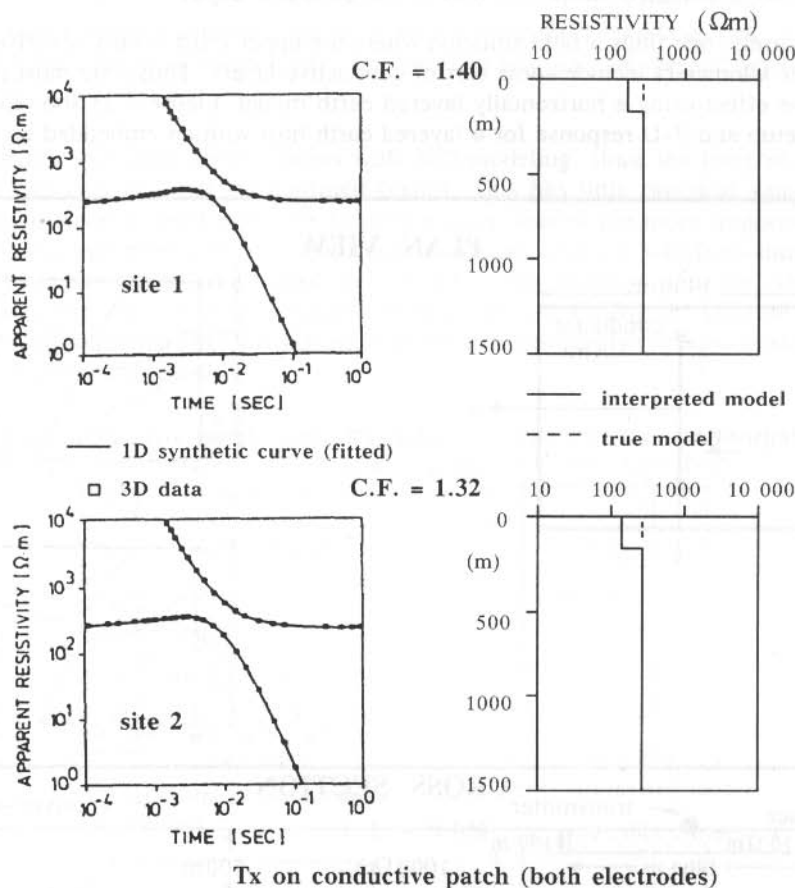


Fig.4.32: Interpretation results for the 3-D data of figure 4.31 using a 1-D inversion program (after Newman, 1989).

The system response must be considered in the interpretation because it masks the upper part of the section. In this case, when assuming that the model is typical for the Black Forest area (compare chapter 9), one would consider the following: In the Black Forest area, one is forced to use 16 2/3 Hz analog notch filters to obtain a useful signal. This restricts the reliable frequency content of the signal to below 10 Hz. One can use the diffusion depth $d = (2t\rho/\mu_0)^{1/2}$ (Spies, 1989) as a rough estimate for the depth when reliable data was acquired. For this case using a resistivity of 300 Ωm and

earliest time 0.1 sec (equivalent to 10 Hz), one obtains $d = (2 \cdot 0.1 \cdot 300 \cdot 107/4\pi)^{1/2} = 6900$ m. If the resistivity is to be slightly lower ($200 \Omega\text{m}$) and the analog filters to effect the data from only 13 Hz onwards, this depth would be $d = 4900$ m. Since the diffusion depth represents the extreme case and usually the deconvolution removes some of the filter effects, one can assume for practical purposes that reliable information is obtained starting at half of the diffusion depth.

Very rarely, one finds a field situation where the upper crust is only resistive. Often the upper kilometers include some sort of conductive layers. Thus, one must consider the above effect using a horizontally layered earth model. Figure 4.33 shows the geometric setup and 3-D response for a layered earth host with an embedded conductor

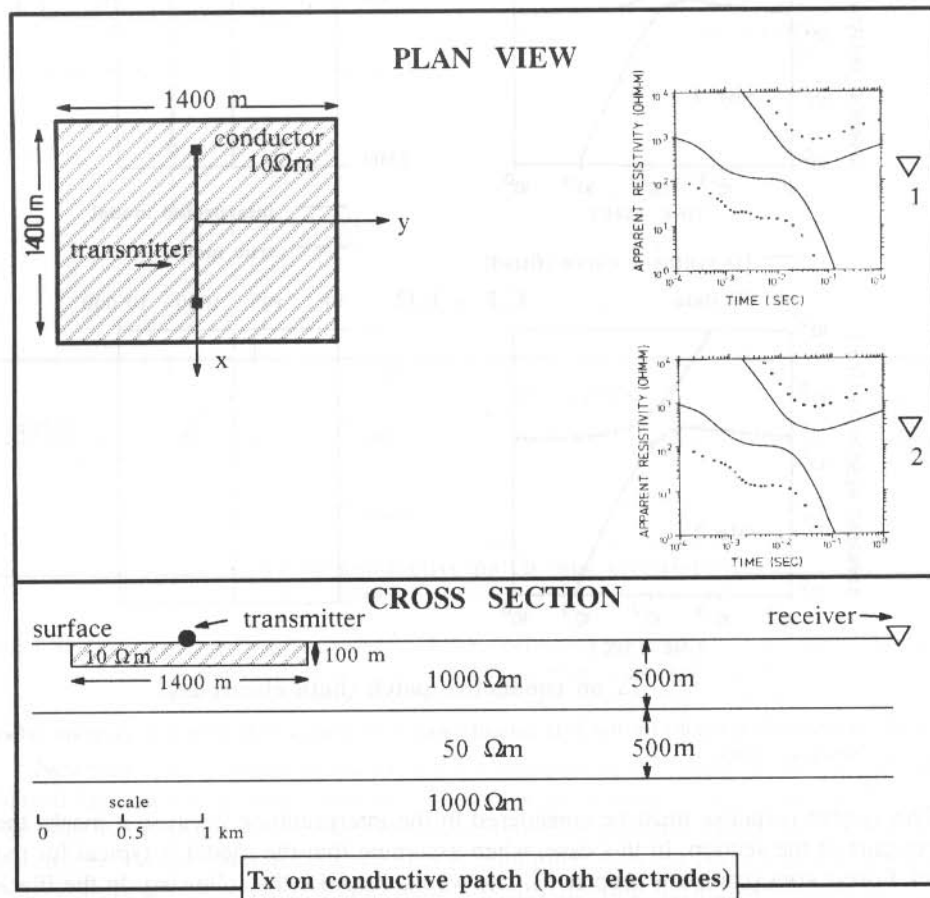


Fig. 4.33: Geometric setup and calculated data for a conductor embedded in a layered earth with the transmitter located on top of the conductive patch (after Newman, 1989).

when both electrodes are located on a conductive plate. This is a very typical situation since one is always looking for the most conductive place to plant the transmitter. For both receiver locations the data is essentially parallel shifted at early and late times. When inverting the 3-D data with a 1-D inversion program (figure 4.34), an additional near surface layer is required for the interpretation. Also, the depth to the conductor is slightly wrong; its resistivity, however, is correct. Since the floating calibration factor in the inversion program has forced the data to be matched by a model one must be extremely careful when interpreting any part of the section below the conductor.

There are still some serious limits with 3-D modeling, since the integral equation method can only be used for confined bodies. This has little practical value for oil exploration since in most instances layered quarter-spaces are more important. Here one can envisage more use of layered quarter-spaces and a 2.5-D (two-dimensional earth and three-dimensional transmitter) model seems more appropriate. This is the reason why the application of a finite difference program using the spectral Lanczos decomposition method (SLDM) (Druskin and Knizhnerman, 1988) was considered for more complex structures.

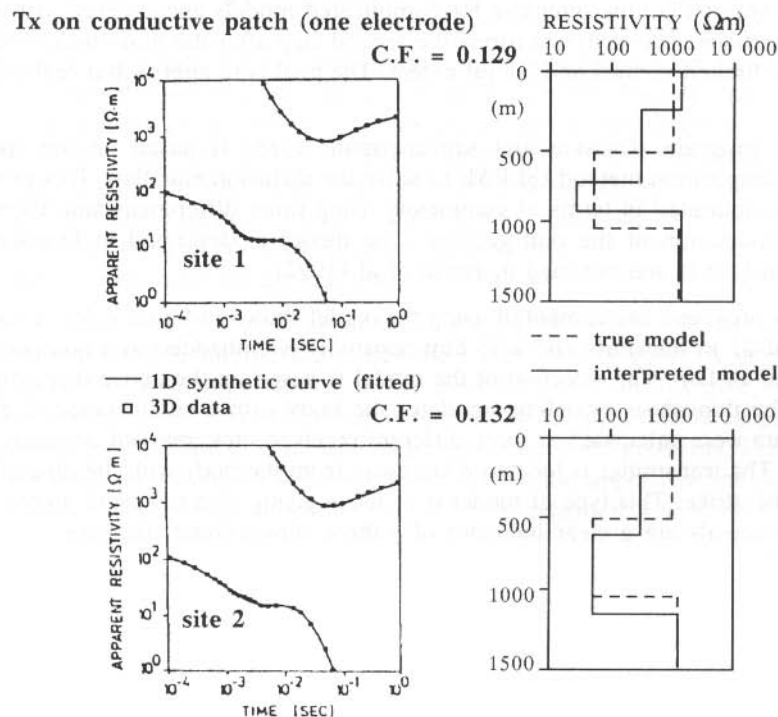


Fig.4.34: Interpretation results for the 3-D data of figure 4.33 using a 1-D inversion program (after Newman, 1989).

Comparison of Different 3-D Modeling Programs

In this section different 3-D programs are compared using a similar field situation as described in the chapter about reversals. The first program is a so called "thin-sheet" modeling routine. It calculates the transient response of an infinitesimally thin horizontal sheet, which is embedded in a layered half-space. The conductance, the product of thickness and conductivity, is finite. The algorithm is based on an integral equation (IE) technique (Vasseur and Weidelt, 1977). The main advantage of the program is its computational speed (about 5 min CPU time on a MicroVax computer for one earth model), allowing an inversion to obtain a rapid first order fit of the data. Since the resulting model is restricted to anomalous bodies of finite horizontal extent, which may not be appropriate to the current problem, it is used to develop a starting model for more complex 3-D simulations.

The second program used is an integral equation program (Newman et al, 1986). It calculates the transient response of confined bodies in a layered half-space. There are theoretically no restrictions concerning the number and the shape of the bodies, but it can become very CPU time intensive for complicated models encountered in real exploration situations. This program forms the second step after the thin-sheet modeling for bodies of limited vertical and lateral extent. The goal is to approach a real geological model.

The third program (Druskin and Knizhnerman, 1988) is based on the spectral Lanczos decomposition method (SLDM) to solve the diffusion equation. This program is practically unlimited in terms of complexity using finite differences and allows the closest approximation of the real geology. The theory is described in Druskin and Knizhnerman (1988) and outlined in Hördt et al (1992).

The three programs are compared using the model shown in figure 4.35. A conductive body of 25 m thickness and 0.25 Ωm resistivity is embedded in a homogeneous half-space of 10 Ωm . The selection of the model is based on the above discussion on reversals. The thin-sheet modeling simulates the body with a conductance of 100 S. Synthetic data were calculated at three different receiver sites, marked on the right in figure 4.35. The transmitter is located 8 km away from the body with the dipole being parallel to the strike. This type of model is of those giving sign reversals. In the field, these sign reversals are a clear indicator of a three-dimensional structure.

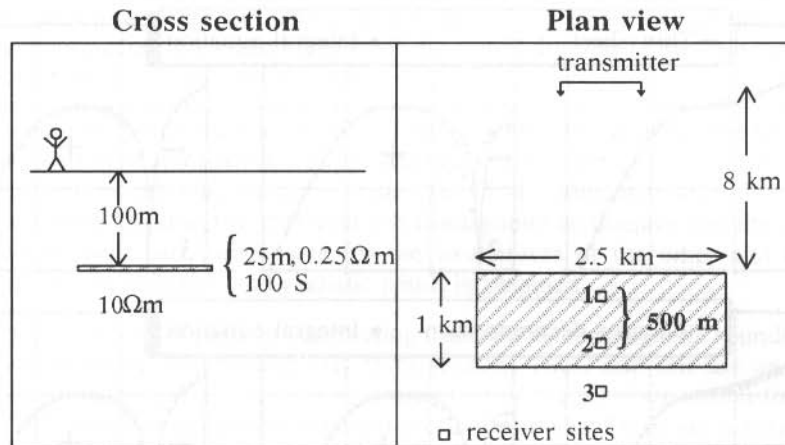


Fig. 4.35 The 3-D model used to compare the forward modeling routines. For the thin-sheet program the conductive body is infinitesimally thin, with a conductance of 100 S. For the two other programs (integral equation and finite difference, SLDM) the body is 25 m thick, with a resistivity of 0.25 Ωm (after Hördt et al., 1992).

The modeling results for the different programs are compared in figure 4.36. In the upper row the thin-sheet modeling is compared with the integral equation program. For all three receiver sites the two curves match well at late times (greater than 500 ms). For site 1 the curves diverge only at very early times. The greatest difference occurs for site 2. The deviations may be caused by the slightly different model, because the thin-sheet program uses an infinitesimally thin body, whereas the body is 25 m thick for the integral equation program. Considering this, the discrepancies may be regarded as small; and the general characteristics are similar between the models.

The second row shows the comparison of the SLDM results with the integral equation program. Again, for the late times the match is very good. A deviation of the curve occurs for early times and is the greatest for site 2. In this case, we also must consider that the earth model is difficult for the SLDM algorithm because the anomalous zone is confined to a small area and causes high field gradients. For the integral equation program the model is almost ideal. As for the upper row the difference can be considered negligible, confirming that all three programs give comparable results.

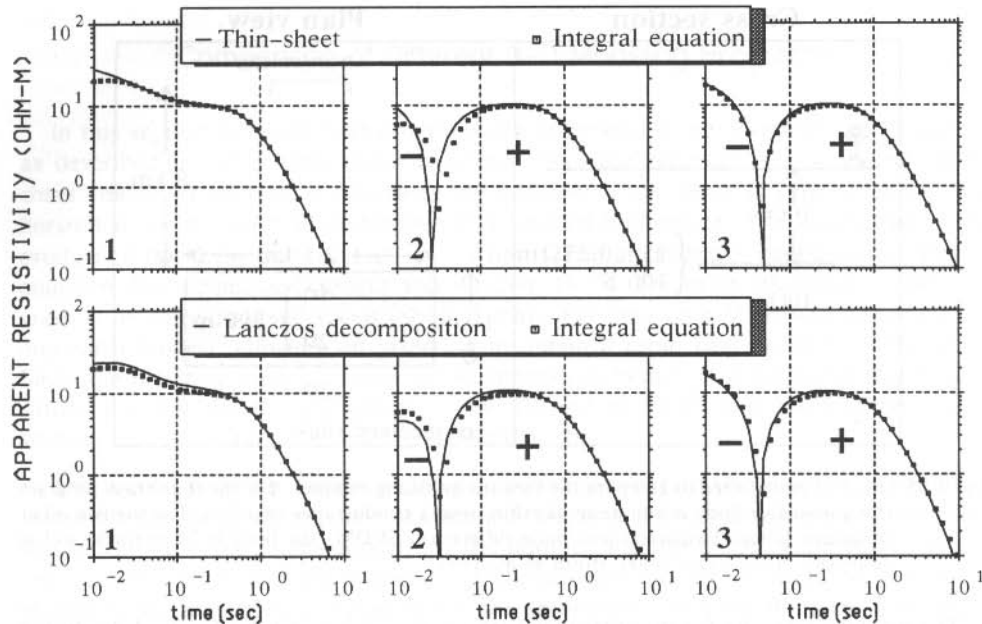


Fig. 4.36: Comparison of calculated data for the configuration of figure 4.35. Upper row: The solid line is the result using thin-sheet modeling. The squares are the results using the integral equation (IE) method. Lower row: The solid line is the result using the spectral Lanczos decomposition method (SLDM). The squares are the results using the IE method (after Hördt et al, 1992).

SUMMARY CHAPTER 4

The standard interpretation of deep transient electromagnetic soundings is done using one-dimensional inversion algorithms. The interpretation is "trying" to derive from the measured data the most likely subsurface resistivity as a function of depth. One-dimensional inversion can be used in several different ways to obtain a more objective estimate of the subsurface resistivity: individual inversion at each site; joint inversion of several components or different electromagnetic measurements; automatic inversion along a profile; or inversion of the data yielding a smooth resistivity versus depth function (Occam inversion). When applying all these different inversion techniques one is still left with a small number of anomalous soundings which have to be interpreted initially in a qualitative way until quantitative three-dimensional modeling can be done.

Most routinely inversion is applied to a single sounding at one station. To obtain estimates for the reliability of the inversion results, the statistics and its analysis are just as important as the inversion itself. In most real field situations in sedimentary

environment this type of inversion will already give sufficient information about the resistivity structure of the subsurface. Sometimes, this type of interpretation does not yield the information requested because of the sensitivity bias in the component (electric or magnetic field) selected for inversion.

To reduce the bias in the sensitivities of the individual electromagnetic field components, two different components can be inverted at the same time in a joint inversion. A joint inversion can also be done using one TEM component together with magnetotelluric data. Joining two different electromagnetic techniques has the advantage that each of them can compensate for the weaknesses of the other and in a joint inversion a more objective and realistic result is obtained.

One of the important parts in interpreting transient electromagnetic soundings is the time spent inverting similar data sets from scratch. Thus, one can use an inversion procedure which integrates the *a priori* information of the previous station for the next station. This inversion procedure is called profile inversion. There are several ways of choosing how this *a priori* information is being integrated and one should carefully apply it depending upon the problem of the specific target area. With this type of inversion extreme care should be taken, because one can also force the data to match the expectations of the interpreter.

In order to cross-check the interpretation results one is searching for a unique resistivity versus depth function. This type of unique result can be obtained using the Occam inversion. The Occam inversion is based on the assumption that the resistivity versus depth distribution is smooth. This works well in sedimentary environment with no abrupt resistivity changes in the subsurface. In those cases the Occam inversion which is very computer time intensive can be used to cross check the interpretation results.

When applying the different inversion techniques the interpreter sometimes faces the problem that specific transients behave abnormally and cannot be interpreted. One type of these abnormal transients is when the measured voltage crosses the reference level. These transients are called reversals. Due to the limitations of three-dimensional modeling it is very difficult to quantitatively interpret these reversals. Thus, one first tries to use the reversals to obtain a map of this three-dimensional geologic structure in the survey area. Once the interpreter understands the nature of the three-dimensional structure simple three-dimensional models can be calculated and a more quantitative estimate of the structure obtained. The different techniques for three-dimensional modeling include asymptotic formulations, reduction of the three-dimensional anomaly to a thin inhomogeneous conductive plate, and integral equation methods. All of the techniques yield interpretations of resistive fault zones or conductive patches between the transmitter and the receiver.

The selection of the appropriate 3-D modeling routine is very important. One should always evaluate different routines using characteristic effects in the field data. In this chapter, using the different routines gave comparable results for the interpretation of a characteristic reversal.

PROBLEMS CHAPTER 4

1. Explain the process of inversion.
2. What is the Jacobian and what does it mean?
3. Explain the difference between the *Marquardt–Levenberg* method and the gradient method.
4. Why does the inversion often use logarithmic parameters?
5. How do the transformed parameters relate to the original parameters?
6. Why do we use *joint inversion*?
7. How do you determine a correlation between model parameters?
8. What would you use *profile inversion* for?
9. In what geological environment should we not use the *Occam inversion* philosophy?
10. What would you do when you start observing reversals on a walkaway profile in the field?
11. How do we routinely compensate for transmitter overprints in the magnetic field signal?
12. Explain possible applications for the three 3-D programs discussed here.

KMS Technologies – KJT Enterprises Inc.
6420 Richmond Ave., Suite 610
Houston, Texas, 77057, USA
Tel: 713.532.8144

Please visit us
<http://www.kmstechnologies.com>

This material is not longer covered by copyright. The copyright was released by Elsevier to Dr. Strack on November 5th, 2007.

The author explicitly authorizes unrestricted use of this material as long as proper reference is given.

KMS Technologies – KJT Enterprises Inc.

An EMGS/rxt-company

Chapter 3 Distortions of the Signal and their Compensation

extract from

Strack, K.-M., 1992, reprinted 1999
***Exploration with deep transient
electromagnetic:*** Elsevier, 373 pp.

This material is not longer cover by copyright. The copyright was released by Elsevier to Dr. Strack on November 5th, 2007.

The author explicit authorizes unrestricted use of this material as long as proper reference is given.

Chapter 3

Distortions of the Signal and their Compensation

After considering the physical background of deep transient electromagnetics, one needs to be aware of possible problems encountered when measuring, processing and interpreting real field data. These problems can be overcome by either carefully correcting for them or by avoiding them as much as possible. For better evaluation and selection of the tools required, the possible errors are categorized in three classes.

- Errors caused by the choice of the hardware system such as transmitter input waveform and receiver filters.
- Errors caused by external anthropogenic influence introducing electromagnetic noise into the signal recorded.
- Errors caused by the local geology such as unknown near-surface lateral resistivity variations.

In this chapter, possible solutions are given for the above errors. One way of correction for the transmitter input waveform and receiver system filters is a careful consideration of the system response. After measuring this response, one can deconvolve it from the data. Anthropogenic (man made) electromagnetic noise can be removed using digital signal processing techniques. The digital processing of the field data is the area where most of the signal-to-noise improvements can be obtained. This is emphasized in this chapter. Distortions caused by 3-D geology are not considered in this section because these signals are the wanted information. Most of the typical distortions are from near-surface lateral resistivity inhomogeneities which cause transmitter overprints. Using some insight into the physical behavior of electromagnetic fields, most of these can be corrected in the magnetic field measurements.

Only the combination of all techniques and careful evaluation of the data behavior guaranties that LOTEM can be applied in most environments. In very noisy environments one often has to apply the filters prestack to get optimum signal-to-noise ratios.

THE FIELD PROBLEM

During field data acquisition, the output signal consists of the input signal combined somehow with the effects of the entire data generation process. This can be

visualized through the *Black Box* concept with the *true signal*, the earth response, going into a *Black Box* where it is modified. The output is the measured signal. In the field, the *Black Box* is a combination of distortions in the data acquisition and transmitter systems. The transmitter system introduces distortions due to imperfections in the transmitter waveform and coupling effects (induced polarization etc.) with the subsurface. The data acquisition system introduces distortions from the receiver side (amplitude response, temperature drifts, receiver misorientation, etc.).

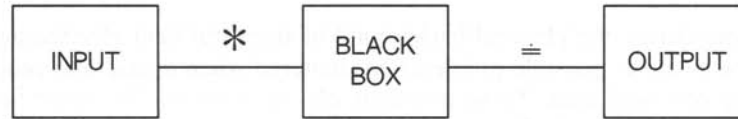


Fig. 3.1: *Black Box* concept for the signal path.

Mathematically, the *Black Box* concept can be described as convolution of

$$\text{Input} (t) * \text{Black Box} (t) = \text{Output} (t) \quad (3.1)$$

or

$$\text{Output} (t) = \int_{-\infty}^{\infty} \text{Input} (t - \tau) \text{Black Box} (\tau) d\tau. \quad (3.2)$$

The *convolution* process can be performed by taking the time series *Input* and *Black Box*, reversing *Black Box* and performing a serial multiplication of *Input* with the reversed *Black Box* (Bracewell, 1978). The effect of the systematic distortion of the signal can be removed from the measured earth response by using the inverse of the *convolution* called *deconvolution*, which will be described later on.

In addition to the transformation by the earth and the recording system, different sources of noise are superimposed on the signal. Whereas above system distortions are convolutions, this noise is added to the signal as shown in figure 3.2.

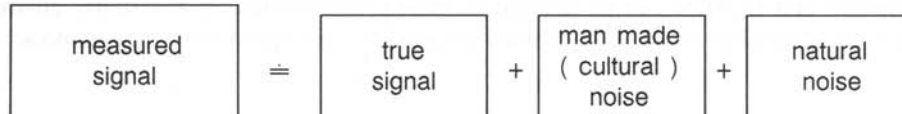


Fig. 3.2: Combination of noise sources with the true signal.

Noise can be classified into *periodic* and *sporadic noise*. *Periodic noise* can be removed with digital filters and *sporadic noise* by using selective stacking techniques.

Periodic noise is mainly generated by power lines, telephone lines and the power consumers. *Sporadic noise* is caused by current surges in the power network, machinery, motion of magnetic material near the receiver and external magnetic field variations. Natural noise caused by ionospheric currents and geologic structures can severely distort the signal. In most instances it will be unrecoverable unless special natural noise compensation techniques are used. To date, one way of overcoming the natural noise is to increase the transmitter moment to a level where the signal can be measured with the field system. Other ways of overcoming the noise are for frequency domain EM systems remote referencing (Clarke et al, 1983), or pseudo random binary sequence (PRBS) systems which use encoded signals (Duncan et al, 1980). For LOTEM field applications we found a transmitter moment increase or local noise compensation (LNC) (Stephan and Strack, 1991) work best to overcome the noise problem. New multichannel systems integrating field procedures, newest data processing principles and state-of-the-art electronics can further improve the signal-to-noise ratios.

At this stage, the reader is referred to some classic papers and textbooks (Shanks, 1967; Kulhanek, 1976) for the derivation of the digital recursive filters. In this chapter, only the results necessary for understanding the LOTEM data processing and filtering are included.

DECONVOLUTION OF THE SYSTEM RESPONSE

The ideal theoretical response of a polarity reversing transmitter at the receiver is influenced by the following effects:

- Deviation of the current waveform from a step (ramp) function.
- Off-time between the polarity reversals.
- Polarization effects near the electrodes and sensors.
- Inductance of transmitter wire.
- Near-surface lateral resistivity inhomogeneities.
- Misalignment of the receiver.
- Frequency response of the receiver.
- Analog electronics of the amplifier and preamplifier (notch filters).
- A/D converter temperature drift.

All of these yield the *true* system response when convolved with each other. They must be eliminated from the measured signal in order to obtain the *true* signal. Using conventional digital signal processing principles would mean that one can measure the system response accurately, when inputting a spike (delta function) and measuring the output. Since a delta function in practice can not be realized as input, a square wave is input and the derivative of the output is calculated. Three of the items in the above list cannot be included into the system response measurements, namely near-surface lateral resistivity variations, the misalignment errors of the receiver, and the temperature

drift of the A/D converter. We assume that the temperature drifts of the state-of-the-art A/D converter are small and are statistically included by measuring the system response many times and then averaging it. The receiver misalignment and lateral inhomogeneities can give us a static shift of the signal, which is removed from the magnetic field using the MMR correction or calibration factor (see below). The remaining system influence is measured by using the switchbox to generate the square wave which is then input into the data acquisition system.

Rewriting the input/output equation 3.1 with $x(t)$ being the *input*, $y(t)$ the *output*, and $s(t)$ the *Black Box*, we obtain:

$$y(t) = s(t) * x(t) \quad (3.3)$$

The deconvolution of the *system response* $s(t)$ (the *Black Box*) can be done in three different ways:

First, using the convolution theorem (Bracewell, 1978), the above equation can be transformed to the frequency or z -domain yielding a simple multiplication:

$$Y(z) = S(z) * X(z) \quad (3.4)$$

If we divide $Y(z)$ by $S(z)$ we obtain $X(z)$. For transient data this procedure becomes very difficult, since the frequency content of the system response is too similar to the frequency content of the transient signal. Also, the frequency spectrum of the signal and the system response contains holes in them when analog notch filters have been used during data recording. Calculation of the inverse of $S(z)$ thus can cause instabilities due to the inverse of numbers close to zero. To date, nobody has successfully implemented the above method for transient data (Bond et al, 1981; Strack, 1981; Rossow, 1987). This principal problem can also be understood by using the time-frequency equivalent. The transient system response is designed to be as narrow as possible in time domain, in order to have the least influence on the signal. Narrow in time, however, means broad in frequency which is why frequency deconvolution will always increase the noise on the signal.

Second, one can use a deconvolution scheme in time domain similar to the one in the frequency domain, but using numerically stable procedures. This convolution scheme was developed by Stoyer in 1981 (Stoyer and Strack, 1984; Strack 1985), and although specifically developed for transient data, it is very similar to the one developed by LaCoste (1982) and Ioup and Ioup (1983). The algorithm is based on the van Cittert iteration:

$$\begin{aligned} A_0 &= y(t) \\ A_1 &= A_0 + (y(t) - A_0 * s(t)) \\ &\dots \\ A_m &= A_{m-1} + (y(t) - A_{m-1} * s(t)) \end{aligned} \quad (3.5)$$

It can be shown that, if m goes to infinity, A_m approaches $x(t)$ (see proof in appendix 1). When doing the above deconvolution, the convergence to $x(t)$ is often reached after 3 to 5 iterations. A side effect of this type of deconvolution is the signal-to-noise ratio improvement, whereas the frequency domain deconvolution amplifies the noise. Figure 3.3 shows an example of a signal with and without the time domain deconvolution.

The left side of the figure shows the data set after deconvolution in a linear stacked data display and as early and late time apparent resistivities. Note the amplitude recovery at early times in comparison to the stacked data on the right side of the figure. The flair up of the 95% confidence level in the early time apparent resistivity curves is caused by the noise around the onset (first data point after the $t=0$ vertical marker line) which often brings this data point below the zero level causing stability errors in the logarithmic display.

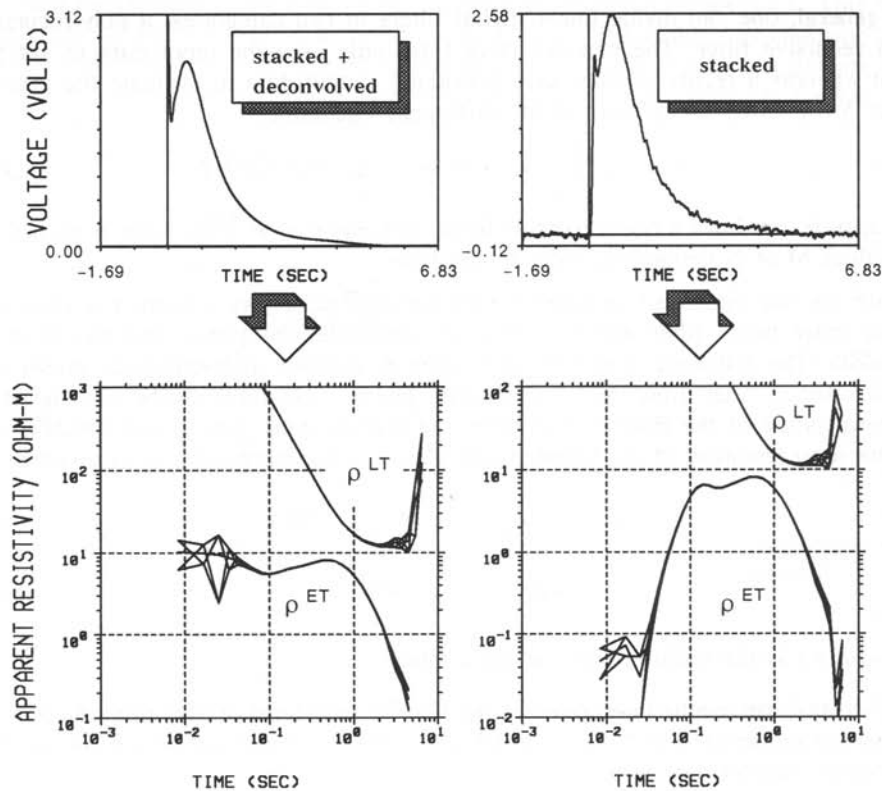


Fig. 3.3: Example of a selectively stacked transients with (left) and without (right) time domain deconvolution of the system response.

Third, one can replace the deconvolution in the data processing sequence by a convolution of the synthetic data with the system response in the inversion/for-

ward modeling phase. This must be done when the length of the system response is more than one third of the length of the transient (rule of thumb). We recommend that this and the second method be carried out for each survey and the best (most stable) and fastest way selected.

RECURSIVE DIGITAL FILTERS

Since we know how to remove distortions due to systematic errors in our own system, we can now consider the distortions due to external influences. One kind of distortion is caused by periodic noise, which can not be completely filtered out using analog filters. However, it can be significantly reduced using digital recursive filters. Following is a description of the *true amplitude recursive filters* (Strack et al, 1988).

In general, one can divide linear digital filters in two categories: a non-recursive and a recursive filter. The non-recursive filter only uses the input data to get the output whereas a recursive filter uses previously output data to evaluate the present output. More easily this is seen in the difference equation:

$$y(n) = \sum_{k=1}^M a_k y(n-k) + \sum_{k=0}^N b_k x(n-k), \quad (3.6)$$

If all $a_k \equiv 0$, we have a non-recursive filter, whereas if $a_k \neq 0$ the filter is recursive. The values M or N denote the order of the filter.

Since we are interested in filtering out periodic noise, we construct a recursive second order notch filter which is true in amplitude and phase and has a small bandwidth. The following shows the derivation of a phase and amplitude preserving digital recursive filter using the z -transform. The z -transform can be considered as a generalization of the Fourier transform for discrete time series $x(n)$ which is the discrete representation of the function $x(t)$. The z -transform of $x(n)$ is given by

$$X(z) = \sum_{n=-\infty}^{\infty} x(n) z^n; \quad z \in \mathbb{C} \quad (3.7)$$

$$\text{with} \quad z = r e^{-i\omega} \quad (3.8)$$

where r is the radius vector in the z -plane.

The z -transform can be interpreted as the Fourier transform of $x(n)$ multiplied by an exponential sequence. For $r = 1$, (i.e. $|z| = 1$), the z -transform of $x(n)$ is equal to the Fourier transform of $x(n)$.

The convolution theorem is used for the construction of a filter by taking the difference equation and performing a z -transform, giving:

$$Y(z) = \sum_{k=1}^M a_k z^k Y(z) + \sum_{k=0}^N b_k z^k X(z). \quad (3.9)$$

With this form of the difference equation we get the relationship between the filter coefficients and the filter response function:

$$H(z) = \frac{Y(z)}{X(z)} = \frac{\sum_{k=0}^N b_k z^k}{\left(1 - \sum_{k=1}^M a_k z^k\right)} \quad (3.10)$$

The frequency response of the above $H(z)$ can be evaluated on the unit circle where $|z| = 1$. We choose $(1,0)$ to be 0 frequency and $(-1,0)$ to be the Nyquist frequency, f_N .

Since $H(z)$ is a rational function we must consider poles and zeroes of $H(z)$ which are the values where $H(z)$ is infinite and zero, respectively. With a notch filter in mind we want the frequency response of $H(z)$ to be 0 at the notch frequency f_0 . This means that a zero of $H(z)$ is located at $z_n = (\cos \phi, \sin \phi)$. This is done by choosing the a_k and b_k such that $H(z_n) = 0$. A filter with small bandwidth is obtained by placing a pole right next to the zero z_n , which assures us that $H(z)$ is only zero for a small range around the notch frequency f_0 . The nearer the pole z_p and the zero z_n , the smaller is the bandwidth of the filter.

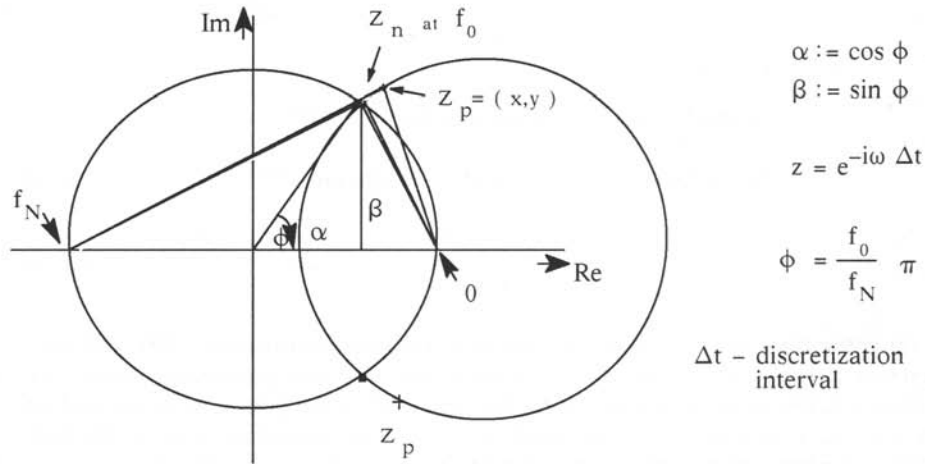


Fig. 3.4: Schematic of the pole-zero technique in the complex plane for the construction of a digital recursive filter.

However, since the amplitude and shape of the transient contains most of the resistivity information, it is essential that the digital filter should not only suppress the noise but maintain the amplitude. This gives us a further condition for the placement of the poles and zeroes, since this can be only achieved when the pole is located on the Appollonian circle, which means that:

$$\frac{|z_n - 1|^2}{|z_n + 1|^2} = \frac{|z_p - 1|^2}{|z_p + 1|^2} \quad \text{or} \quad (3.11)$$

$$\frac{(1 - \alpha)^2 + \beta^2}{(1 + \alpha)^2 + \beta^2} = \frac{(1 - x)^2 + y^2}{(1 + x)^2 + y^2}.$$

In other words, the ratio between the vectors to the pole and zero will remain the same and yield a recursion formula in the z -plane.

$$H(z) = \frac{Y(z)}{X(z)} = \eta \frac{(z - z_n)(z - z_n^*)}{(z - z_p)(z - z_p^*)} = \eta \frac{z^2 - 2\alpha z + 1}{z^2 - 2\alpha\eta z + 2\eta - 1} \quad (3.12)$$

$$\text{with } \eta := \frac{z_p - 1}{z_n - 1} \quad (3.13)$$

is the normalization for gain 1.

$$\text{If we define } x := \eta\alpha, \text{ we obtain} \quad (3.14)$$

$$y^2 = \frac{2x}{\alpha} - (1 - x^2) \quad (3.15)$$

$H(z)$ is the filter function given by the ratio of the output function $Y(z)$, and the input function $X(z)$; z_n and z_p are the positions of the zero and poles respectively; η is the proportionality factor which combines the real part of the pole x , with the real part of the zero α ; η is also called the bandwidth, y is the imaginary part of the pole. To eliminate phase shifts, the recursive filter is applied twice to the data: first in the forward, and then in the reverse direction.

If we remember that multiplication with z means a shift by one step in the time domain, we obtain after simple reformulation of the above equations

$$Y_n = \frac{1}{(2n-1)} \left[\eta X_{n-2} \alpha \eta X_{n-1} + \eta X_{n-2} + 2 \alpha \eta Y_{n-1} - Y_{n-2} \right] \quad (3.16)$$

where

$$Y_{-1} = Y_{-2} = X_0 \quad \text{can be chosen as starting values.}$$

In figures 3.5a-c, this recursive true amplitude notch filter has been applied to three different sets of synthetic data. For all curves in figures 3.5a-c, the superimposed, solid line is the noise-free synthetic input signal. The top curves in figures 3.5a-c show this synthetic signal plus 16 2/3 Hz periodic noise, which is characteristic of the German railroad power grid. The middle curves in figures 3.5a-c have been filtered with a bandwidth of $\eta = 1.02$, whereas the bottom curves have been filtered with a bandwidth of $\eta = 1.08$.

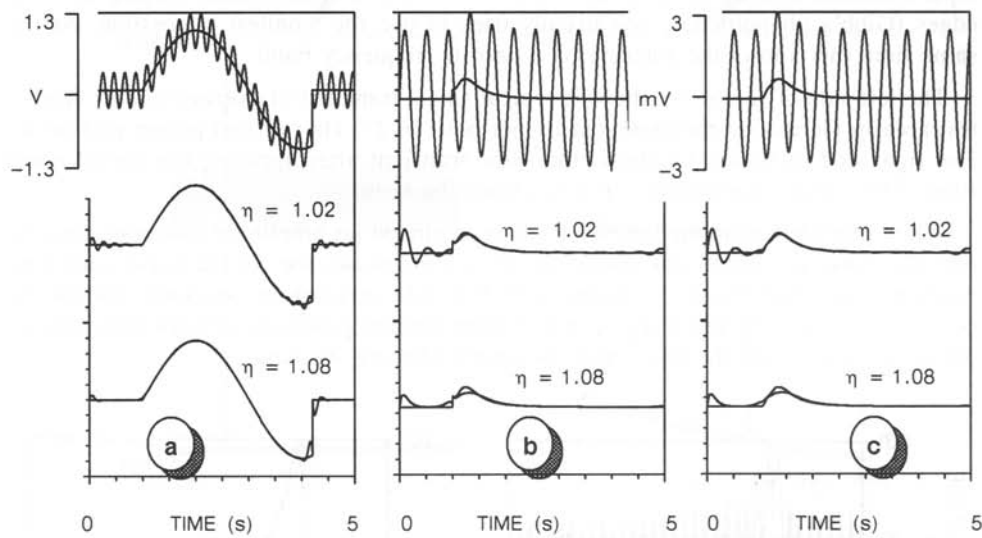


Fig. 3.5a-c: Example of a digital recursive notch filter applied to synthetic data. For all figures the noise-free synthetic input signal is superimposed for comparison. The bottom two curves are the results of applying the digital notch filter with different bandwidths to the top curve. For figure 3.5a, periodic 16 2/3 Hz noise is added to a sinusoid which abruptly starts, and ends with a step discontinuity. The synthetic curve in figure 3.5b represents an ideal theoretical transient. Figure 3.5c is the theoretical transient from figure 3.5b convolved with the impulse response of the recording system and transmitter, thus representing a real transient (after Strack et al, 1989).

In figure 3.5a, the synthetic signal is a sinusoid which abruptly starts and then ends with a step. The filtered curves show that due to the modest slope at the start of the sinusoid there are only minimal ringing effects. Ringing does occur at the step discon-

tinuity due to the Gibbs's phenomenon. The ringing at the onset of the time series becomes less with increasing bandwidth and at the step, the ringing becomes greater with increasing filter bandwidth. In this example, there is almost no amplitude distortion.

The synthetic input signal of figure 3.5b represents an ideal transient where the signal rises instantaneously to its maximum. As with the step discontinuity in figure 3.5a, Gibbs's phenomenon causes ringing at the onset of the transient. The filtered sinusoids also show the same correlation of bandwidth to ringing as those in figure 3.5a. Again, there is little or no amplitude distortion.

Figure 3.5c shows a realistic transient obtained from convolving the synthetic input curve of figure 3.5b with the impulse response of the receiver and the transmitter current waveform from our field system. The ringing due to filtering at the rise of the transient is much less than in figure 3.5b, since there is no longer a step discontinuity. For these data, there is almost no visible difference between the filtered signal and the input synthetic without noise. Since for $\eta = 1.08$, the filter introduces ringing at sharp edges (Gibb's phenomena), one usually tries to use the smallest η possible. At the same time this allows the filtering of a narrow frequency band.

The left side of figure 3.6 shows a typical single transient of average quality from a test area in Germany, contaminated by periodic 16 2/3 Hz railroad power grid noise. The right side of figure 3.6 shows the same transient after applying the digital notch filter. The signal information can now clearly be seen.

When this filter is applied prestack, there is almost no amplitude distortion and the periodic noise is filtered out. Since the 16 2/3 Hz noise, the 50 Hz noise, and their harmonics are not phase-correlated with the data acquisition, stacking smears the power line frequency and a digital notch filter applied poststack can not eliminate all the noise. Therefore, the filter must be applied before stacking.

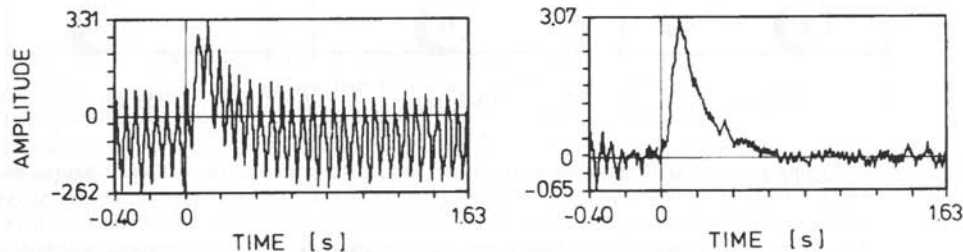


Fig. 3.6: Digital recursive, true amplitude notch filter applied to transient data. The left curve shows the original field data and the right curve the same data after filtering (after Strack et al, 1989).

One drawback of the digital recursive filters is the ringing when the transient rises sharply as can be seen in figure 3.5b. When using the new generation of acquisition hardware the signal is usually highly oversampled. Also, less analog filters are used

because of the high dynamic range. When in addition solid-state transmitters are used, the signal rises sharply (depending upon the subsurface resistivity) between the sample points. This gives significant problems because the above described recursive filters can, in some cases, ring so strongly that no transient can be recovered from the signal. In this case, a different filtering approach must be used. This approach is termed *lockin filter*, because it calculates from the data before the start of the transient the optimum periodic noise, locks to the phase of the noise and subtracts the noise from the single records prestack. The *lockin filter* consists of a series of sine and cosine functions which match the periodic component of the noise in a least squares sense. Figure 3.7 shows an example of a single record acquired with the TEAMEX multi-channel system which has a high dynamic range of 204 dB. The data were recorded

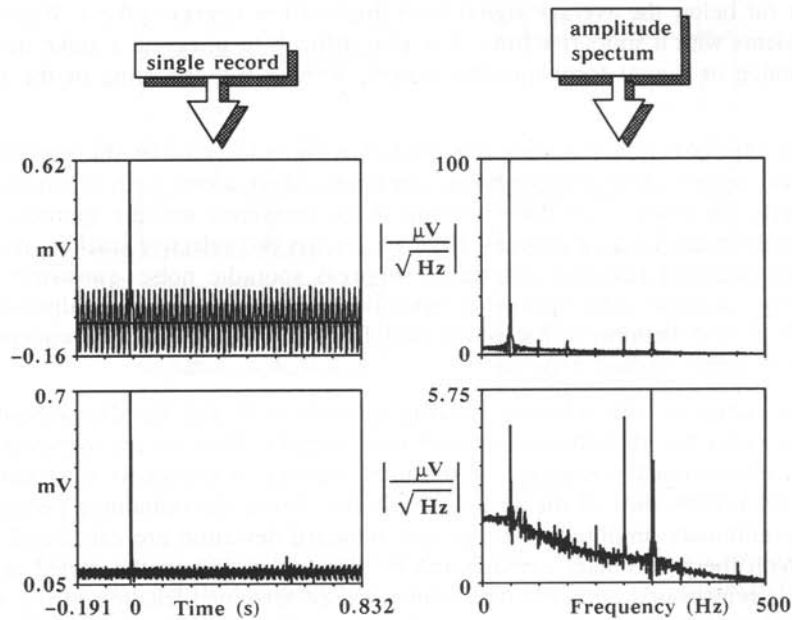


Fig 3.7: Example of a single transient contaminated with periodic noise. The left column shows the single record before and after filtering with a lockin digital filter. On the right side the respective amplitude responses are shown.

over highly resistive terrain in South Africa which explains the short length of a signal. On the left of the figure the single records are shown with the periodic noise (top) and after applying the digital *lockin filter* (bottom). Note that the noise has been reduced significantly. On the right side of the figure the respective amplitude responses are shown. Before filtering, the 50 Hz periodic noise is strongest with odd and even harmonics following. After applying the *lockin filter* the periodic noise up to 300 Hz has been significantly reduced (i.e. by approximately 20 times for 50 Hz). A very narrow signal was selected because it would be more distorted than a wider one. The narrow

signal is hardly effected by the *lockin filter* which would not be possible with a recursive filter. It should be emphasized that this filters should not be applied poststack because stacking smears the line characteristic of the noise.

SELECTIVE STACKING METHODS

Sporadic noise such as spikes may be caused by natural sources such as lightening and by many different cultural sources such as water pumps, electric fences, trains, factories and vehicles passing by the receiver. Once this noise is recorded and not recognized, it can severely distort the stacked results, since its amplitude is either far above or far below the average signal level (high or low energy spikes). When acquiring transients with a short rise time, it is also difficult to integrate a spike detector in either analog or digital form into the system, without the distorting of the transient itself.

A safe approach to eliminating this kind of noise is to consider the statistics of all signals and analyse their corresponding amplitude distributions, both of which become increasingly important when there are only a few transients and the sporadic noise is not canceled in the stacking process. Here we discuss two selective stacking techniques which use different rejection criteria to suppress sporadic noise: *symmetric* and the *area-defined rejection*. The symmetric selective stack, also known as alpha-trimmed mean (Watt and Bednar, 1983; Naess and Bruland, 1985), is less frequently used because of computational expense.

The first step in both selective stacking schemes is to sort the data amplitudes in ascending order for all transients at each time sample. Then for the symmetric rejection, a predetermined percentage of the total number of transients is symmetrically rejected from both ends of the sorted amplitudes. From the remaining percentage of data, a preliminary amplitude average and standard deviation are calculated (Stoyer, 1981). With the preliminary average and its standard deviation the sorted amplitude data set is reinspected and only data within a predetermined fraction of the standard deviation are kept. This procedure is very robust with respect to changes in the symmetric cutoff percentage which may be varied over a wide range (between 10 and 40%) where the low and high amplitude noise are removed.

For the area-defined rejection, amplitude frequency distributions are calculated by sliding overlapping windows over the sorted amplitude curves for each time sample of all transients. With this kind of rejection criteria, a percentage of the area under each distribution curve symmetric about the maximum is calculated, and all data within that area are kept.

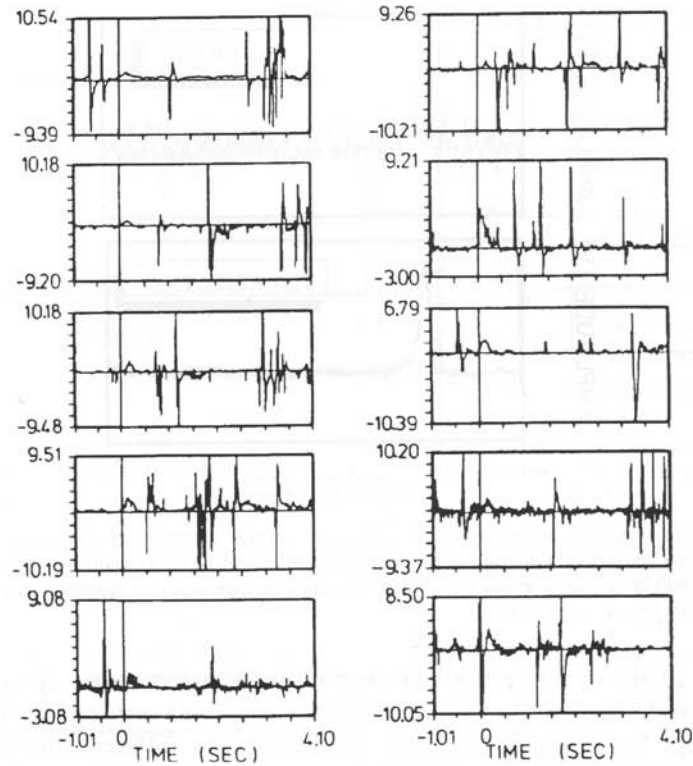


Fig. 3.8: Ten raw transients from Germany distorted by sporadic noise (after Strack et al, 1989).

An example of ten individual transients distorted by sporadic noise is given in figure 3.8. The elapsed time between the individual frames is approximately 20 seconds. Although the transient can be recognized directly after the vertical $t=0$ marker line, the predominant feature in the records are the spikes. These build parts of the data base (96 records) for the results shown in figures 3.9 through 3.11. The upper transient of figure 3.9 is the output of a straight average summation which did not cancel out the high and low energy noise. After calculating a preliminary amplitude average and standard deviation from all the field data, the data lying within two standard deviations of the average were then stacked. The lower transient of figure 3.8 is the result of this procedure. The high and low energy noise are now reduced and the signal-to-noise ratio improved.

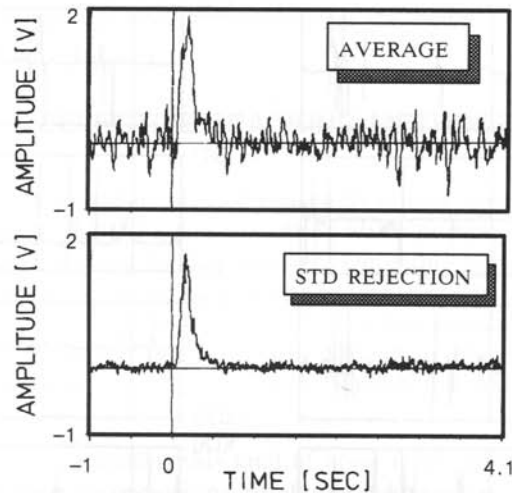


Fig. 3.9: Upper transient is the result of a straight average summation with poor signal-to-noise ratio. This stacking technique is improved by eliminating all amplitudes outside two standard deviations of the average ($-\sigma$, $+\sigma$) from the selective stack as shown in the lower transient (after Strack et al, 1989).

Figure 3.10 shows a selectively stacked transient based on the *symmetric rejection* criteria, using a 20% cutoff at both ends of the amplitude distribution. The frames at the right show two example amplitude distributions for different time samples. This transient displays an even higher signal-to-noise ratio than the transient shown at the bottom of figure 3.9. Similar results are obtained using the *area-defined rejection* selective stack with 60% of the area, as shown in figure 3.11. Amplitude frequency distribution curves are shown at the right where the shaded part of the curve is 60% of the kept area.

Figures 3.10 through 3.11 show that both the *symmetric rejection* and the *area-defined rejection* selective stack significantly improve the signal-to-noise ratio compared to the summation process which eliminated all data which lie outside of two standard deviations of the average (figure 3.9). This is because the average is already corrupted by the outlying sporadic noise amplitudes which, for the selective stacking schemes, are rejected before the average is calculated. For LOTEM soundings, our experience has been that the *symmetric rejection* stack gives us the best signal-to-noise ratios for the data from most survey areas.

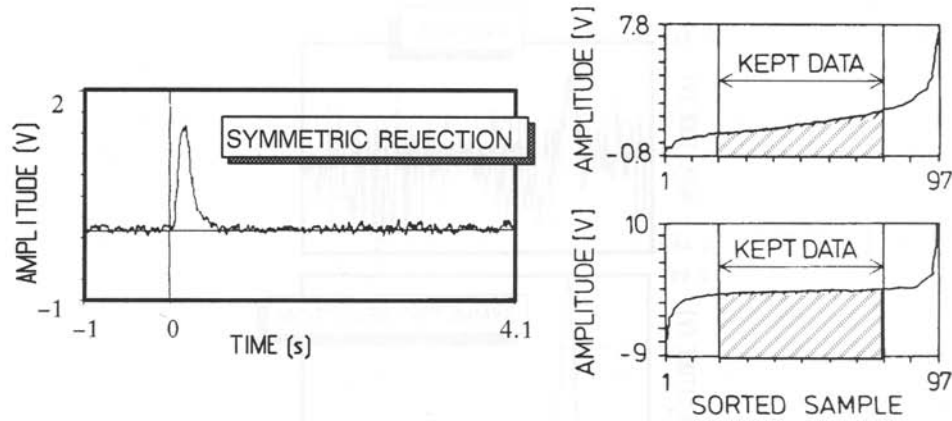


Fig. 3.10: Stacked data using the *symmetric rejection* selective stack technique with a cutoff 20% at both ends of the sorted amplitudes. The shaded areas represent the amplitudes which are all kept, all others are rejected (after Strack et al, 1989).

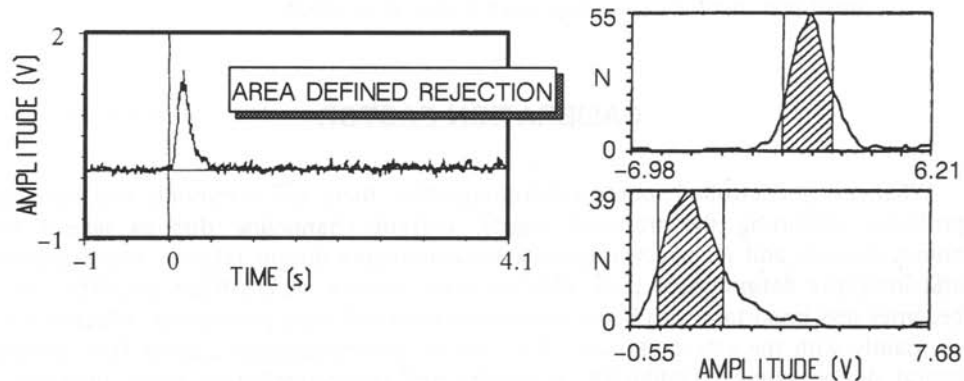


Fig. 3.11: Stacked data using the *area-defined rejection* selective stack technique with an area (shaded) defined as 60% to keep (after Strack et al, 1989).

Another more impressive example is shown in figure 3.12, where approximately 20 transients were used to derive the different stacks. The top of the figure displays the stack using a straight average of all data points without rejecting any of the high and low energy spikes. The bottom transient results from the same data set using the selective stacking algorithm with a 20% cutoff on either side of the sorted amplitude distribution. The improvement in signal-to-noise ratio is significant.

For computational speed reasons and operational ease, one can use the quartile values as rejection criteria and restrict the selection of the different stacking methods to the data sets which are still noisy after stacking.

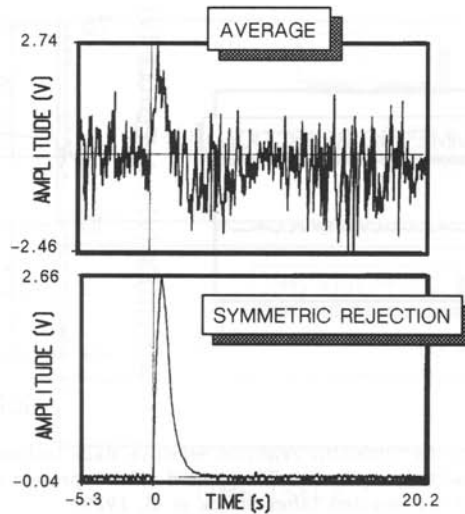


Fig. 3.12: Comparison of the selective stacking algorithm (bottom) with a straight averaging of the signal (top) using the same data (after Walker et al, 1982).

CALIBRATION FACTOR

When using controlled source electromagnetics, there are commonly two possible problems distorting the transient signal: current channeling due to lateral inhomogeneities, and incorrect amplitude measurements due to receiver misalignment and improper definition of gain, receiver area, current, A/D offsets etc. The latter becomes less important with better instrumentation and field procedures, which leaves us mainly with the effect of *static shifts* due to inhomogeneous current flow around lateral discontinuities. Unlike DC-resistivity and magnetotellurics, every interpreter finds it is difficult and often impossible to match TEM curves with *static shift* to a realistic layered earth model. This is mainly because of the stronger coupling of controlled source electromagnetic methods to the subsurface resistivity. In other words, a change in layering will not only shift the curves along the ordinate, but also distort the frequency or time scale. Vertical shifts in the apparent resistivity curves can be corrected with a correction factor which is called in this book *calibration factor*. Sometimes this factor is called *fudge factor*, or also *MMR* (magnetometric resistivity) *correction factor* (Edwards, 1978; Gomez-Trevino and Edwards, 1983) or *scale factor*, which is used as extra parameter in the inversion. It can be derived for the frequency domain from the known DC ($\omega = 0$) limit (Kaufmann and Keller, 1983; Le Roux, 1987). Stoyer applied this factor first in 1981 to transient data and subsequently it was called *calibration factor*, due to its compensation of receiver area error, which was at that time a big problem when superconducting magnetometers (SQUIDS) were used.

$$\int_0^{\infty} u(t) dt \quad \text{proportional to} \quad H_z$$

and also that

$$\int_0^{\infty} \rho_a^{ET} dt \quad \text{proportional to} \quad H_z$$

We now consider the integral beneath the measured voltage curve and would like to find

$$\int_0^{\infty} u(t) dt = ?$$

$$\text{where } u(t) = \frac{1}{2\pi} \int_{-\infty}^{\infty} \tilde{u}(\omega) e^{i\omega t} d\omega. \quad (3.25)$$

The time-frequency equivalents are obtained by separating Fourier transform terms into a delta function:

$$\int_0^{\infty} u(t) dt = \frac{1}{2\pi} \int_{-\infty}^{\infty} \tilde{u}(\omega) d\omega \underbrace{\int_0^{\infty} e^{i\omega t} dt}_{2\pi \delta(\omega)} = \tilde{u}(\omega=0) \quad (3.26)$$

$$\text{where } \int_{-\infty}^{\infty} \delta(\omega' - \omega) f(\omega) d\omega = f(\omega') \quad (3.27)$$

If we now calculate $\int_0^{\infty} \rho_a^{E.T.} dt$, we obtain:

$$\begin{aligned} \int_0^{\infty} \rho_a^{E.T.} dt &= \int_0^{\infty} \frac{2\pi r^5}{3AD_0 y} u_z(t) dt = \frac{2\pi r^5}{3AD_0 y} \mu_0 A H_z(\omega=0) = \\ &= \frac{2\pi r^5}{3AD_0 y} \mu_0 \frac{AD_0 y}{4\pi r^3} = \frac{\mu_0 r^2}{6} \end{aligned} \quad (3.28)$$

For a layered earth we obtain

$$\tilde{H}_z(\omega) = \frac{D_0 y}{4\pi r} \left\{ \frac{1}{r^2} - \int_0^{\infty} \frac{B_E(k) - k}{B_E(k) + k} J_1(kr) k dk \right\}. \quad (3.29)$$

For $\omega = 0$, the $B_E(\kappa) = \kappa$ is at the boundary to the bottom half-space. The recursion through the layers results in $B_E(\kappa) = \kappa$ for each layer boundary including the surface. The integrand is therefore = 0,

$$\text{or } \tilde{H}_Z(\omega = 0) = \frac{D_0 y}{4\pi} \frac{1}{r^3} \quad (3.30)$$

which is the same as the magnetic field of the half-space. In other words, for very low frequencies or very long recording times the electromagnetic response of a layered earth approaches the response of a half-space with the resistivity of the bottom layer.

Thus the *calibration factor* will be the same for a layered earth and the half-space. This means if we integrate the early time apparent resistivity curve, we obtain a constant which depends only on the transmitter-receiver separation and no other factors. This was first developed by Stoyer in 1981 and was subsequently tested through his students at many places around the world.

Another way of deriving the *calibration factor* is the consideration of symmetry in current flow within the subsurface (Edwards et al, 1978). Figure 3.13 illustrates this concept using a DC-monopole. The top of the figure shows a vertical section. The current flows into a conductive half-space through the monopole. Current flow is rotationally symmetric. The receiver is located at the observation site P. The bottom sketch shows a plan view of the same situation. An induction loop is located at P and the rate of change of the vertical magnetic field is measured. Each current density vector can be split into horizontal and vertical components. Only the horizontal component will yield a contribution to the vertical magnetic field in the receiver loop, because the magnetic field lines from the vertical component of the current density vector do not cross the receiver loop. The fields from the horizontal components have opposite sign and thus cancel. When using grounded wire, one can substitute it with two monopoles connected by a wire. Due to the fact that the magnetic field of a monopole is zero ($\text{rot } \mathbf{E} = 0$), at the receiver only the magnetic field from the wire connecting the two electrodes remains. This can be calculated using Biot Savart's law and the resulting value must be equal to the integral:

$$H_z^{\text{static}} = \frac{D_0}{4\pi r^2} \sin \phi = \int_0^\infty \dot{H}_z(t) dt \quad (3.31)$$

Since \dot{H}_z is proportional to $\rho_a^{\text{E.T.}}$, we can now integrate the early time apparent resistivity curve and obtain:

$$\int_0^\infty \rho_a^{\text{E.T.}} dt = \frac{\mu_0 r^2}{6} \quad (3.32)$$

Due to the symmetry the same derivation is true for layered earth models.

This integral allows us to define a *correction factor* or *calibration factor* as:

$$\text{C.F.} = \frac{\mu_0 r^2}{6 \int_0^\infty \rho_a^{\text{E.T.}}(t) dt} \quad (3.33)$$

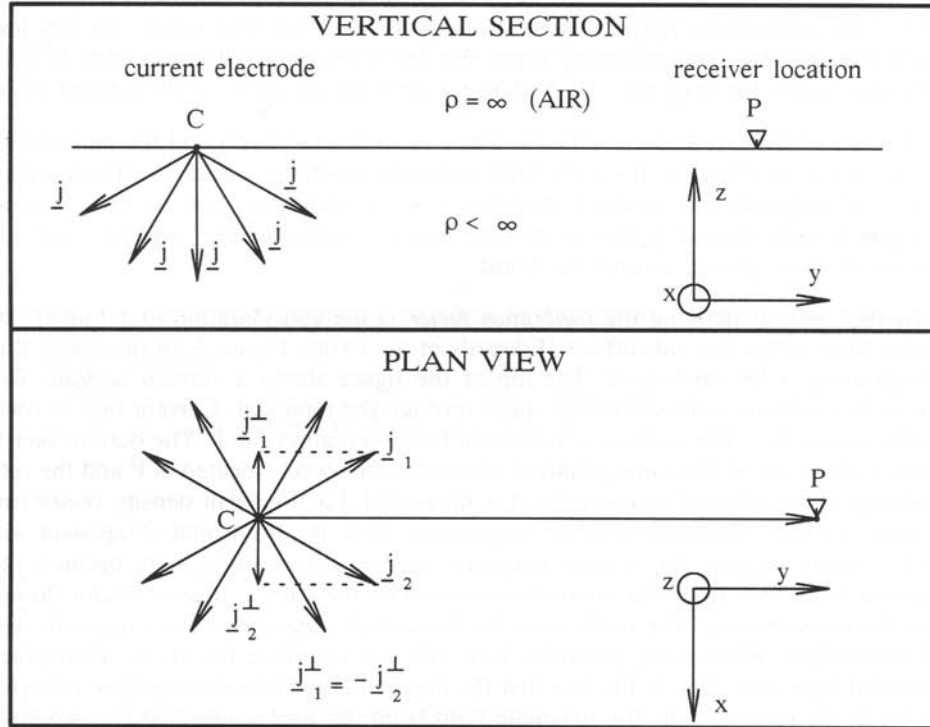


Fig. 3.13: Sketch of the symmetry within the current behavior of a DC-monopole used to visualize the effect of the calibration factor (after Hördt, 1989).

When this factor is applied it will correct the data so that the static limit is correct. We observe that for the vertical magnetic field component the above quantities only depend on the distance between transmitter and receiver. Hence the subsurface resistivity distribution has no effect on the *calibration factor*.

For real data correction the calibration factor is applied in the following manner:

- Calculate the integral with respect to time over the measured $\rho_a^{\text{E.T.}}$ curve.
- Calculate the theoretical value for that integral from the offset.
- Compare the two values and multiply the $\rho_a^{\text{E.T.}}$ curve by the ratio in case the two values do not match. This is a vertical shift of the curve on log-log coordinates.

After the above correction has been applied the distortions which manifest in vertical shifts of the apparent resistivity curve are corrected. These shifts are called *static shift* similar to seismics. Usually the word *static shift* as used in electromagnetics refers strictly to vertical parallel shifts which can be interpreted with an equivalent earth model. There may still be distortions of the transient signal through current channeling around lateral inhomogeneities in the ground which give a time dependent shift. These distortions can be called *pseudo-static* shifts which are vertical shifts for only a certain time window and the shifting factor varies between time windows. They cannot be interpreted with an equivalent model. Since this is not known before interpreting a sounding curve, the *pseudo-static* shifts are usually referred to as *static shifts*. They appear in many cases in the early time apparent resistivity curve as shifts to higher or lower resistivities leaving the impression that incorrect voltages were measured. In order to handle these shifts, an additional scale factor is provided in the inversion. Usually, one lets this factor float to compensate for minor effects caused by data editing and noise in the data.

However, if this factor is large you must be extreme care must be taken. Following is a procedure to indicate whether the *static shift* problem is present in the data set or not. At the same time it can be used to provide first order correction of the data:

- Apply the *calibration factor* to the data set. Now you are certain that any remaining shifts are not due to improper amplitude calibration.
- Use the scale factor in the inversion as a free (floating) parameter. A change required during the inversion means that the curve needs to be shifted up or down in order to obtain a satisfactory fit.
- If the *calibration factor* was changed during the inversion (larger than 20%), then this data set should be treated with great caution, because there could be some current channeling or three-dimensional effects present. For this data set it is not sufficient to rely on the validity of the first order correction which was introduced through shifting the curve. When the same behavior can be found in adjacent stations, the effect is probably caused by geologic feature. Consider this case multi-dimensional modeling.

Similar corrections may be derived for the two horizontal magnetic field components. However, their value to real data interpretation is not yet completely understood. For the electric field components, the static fields depend upon the subsurface resistivity and thus a simple *correction factor* cannot be applied. Electric field measurements are shifted in the same sense as MT data. When applying scale factors with electric fields in the inversion process, extreme care should be taken. A good way for scaling the electric field is to use an undistorted magnetic field and jointly invert the data set while keeping the scale factor for the electric field floating.

PRESTACK AND POSTSTACK PROCESSING

The above corrections build the core of a LOTEM data processing system. Most other electromagnetic systems stack the data directly at the receiver. However, we found that for deep transient electromagnetic signals, this will not work in areas with high cultural noise (Strack et al, 1989). The only way to obtain reasonable signal-to-noise ratios in those areas are prestack processing techniques. Apart from the above mentioned filter numerous simple data processing algorithms are required to correct for distortions in the signal. Table 3.1 gives a summary of most processing modules. The removal of a DC-step between the transient leader and the transient trailer should not be done prestack because the steps can only be caused by the selective stacking when the reference amplitudes are not accurately known. If this step exists in prestack data, there is a problem with the acquisition system. Notch filtering and lockin filtering should only be carried out prestack, because the periodic noise loses its line characteristics through stacking. The deconvolution of the system response can only be done prestack when the system response for the corresponding transmitter switching has been recorded. Since mostly the recorded system response is taken as average of a statistical representative number of transmitter pulses, it should usually be done poststack.

Table 3.1: Data processing modules which can be applied to LOTEM data. The X marks when this module should be applied prestack or poststack.

MODULE	PRESTACK	POSTSTACK
DC-leveling	X	X
linear drift correction	X	X
header editing	X	X
calculate amplitude spectrum	X	X
interactive data editing	X	
DC-step removal		X
pick transient onset	X	X
notch filtering	X	
lockin filtering	X	
Hanning window smoothing	X	X
time variant smoothing		X
recursive lowpass filtering	X	X
sign reversal of the data	X	
system response deconvolution		X
differentiate data	X	X
apparent resistivity transform	X	X
apply calibration factor	X	X

Figure 3.14 shows an example of prestack and poststack processing. The top frame shows a representative single transient out of 50 consecutive records recorded at a site

in central Germany. The data are strong contaminated by periodic noise. The left column shows the direct stack of the 50 records without any significant prestack processing. However, the DC-level must be removed prestack to obtain a proper reference level for the selective stacking. The stacked data set exhibits still a significant amount of noise. The data are the poststack filtered and the $16\frac{2}{3}$ Hz and 50 Hz periodic noise removed. Subsequently, the data are converted to apparent resistivity transforms displayed at the bottom of the figure. The right column shows the single record after applying the recursive filters for $16\frac{2}{3}$ Hz and 50 Hz, followed by selective stack and conversion to resistivity transforms.

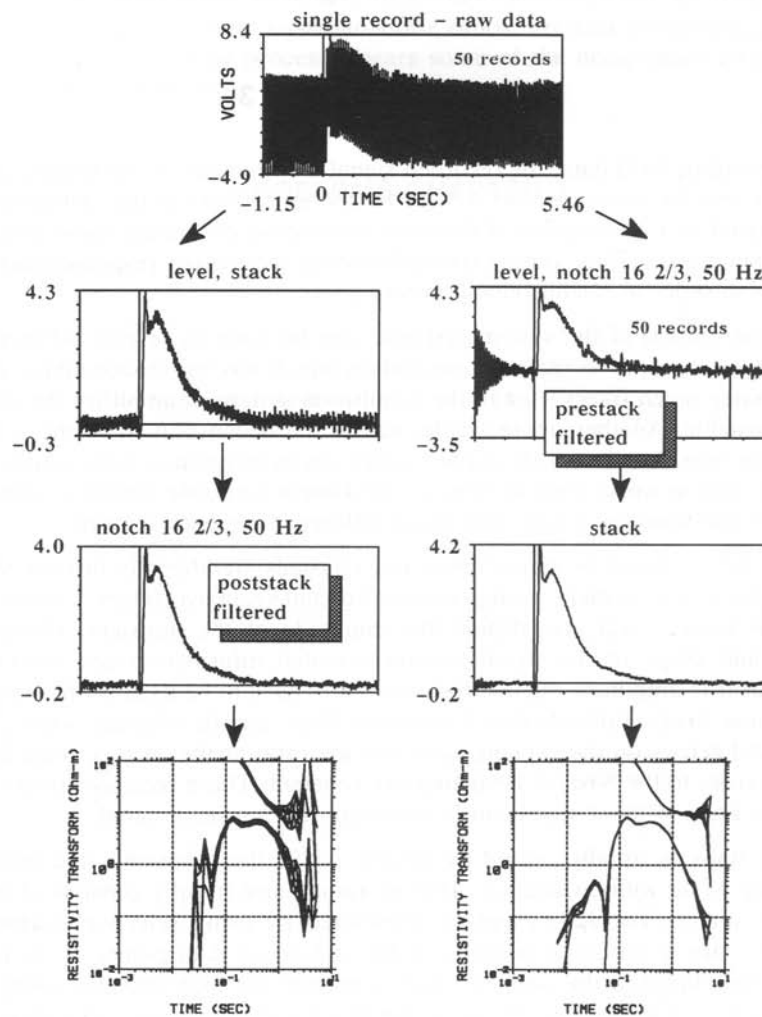


Fig. 3.14: Prestack and poststack processing example. Detailed explanation is given in the text.

After applying the digital filters poststack, some high frequency noise remains. Also, at later times in the poststack filtered data one can see some low frequency noise which is not present in the prestack filtered data (compare third row frames). The resistivity transforms of the poststack filtered data are not as smooth as the ones of the prestack filtered data. Also the error (95% confidence envelope) is significantly larger for the poststack filtered data. This is because the errors are derived from the selective stacking algorithm. A realistic error estimate is important, when one wants to use these errors as weights in the inversion. The prestack filtered data do not only appear smoother, but have also significantly smaller errors. For this example, prestack processing is the better choice to improve the signal-to-noise ratio.

SUMMARY CHAPTER 3

When recording field data, the recorded signal is influenced by systematic errors of the receiver and the transmitter as well as by sporadic errors in the instruments. The recorded signal is a convolution of the system response containing these effects with the true input signal. Thus, during data processing the system response must be accounted for in order to obtain reliable information.

The deconvolution of the system response can be done in several different ways. One way is a frequency domain deconvolution which has the disadvantage that, because of analog notch filters used in the acquisition system, it amplifies the noise and becomes unstable. Another, more stable, way is the deconvolution of the system response in the time domain which can be carried out in an iterative least squares sense. This deconvolution works well as long as the system response length is significantly shorter than the transient length and has a different frequency content.

Periodic noise caused by power lines and railroads significantly distorts the data. Since this noise is extremely strong, standard digital recursive filters – when used to remove this noise – will also distort the amplitude of the transient. However, the amplitude and shape of the signal contain essential information and must be preserved. Thus true amplitude digital recursive filters have to be used for the removal of periodic noise. True amplitude digital recursive filters can be obtained when choosing the poles and zeroes on the z -plane such that the ratio of the vectors going from the poles and zeroes to the Nyquist frequency are constant. These recursive filters remove the periodic noise without significantly distorting the transient signal.

Sporadic noise is usually caused by electric power line transients and many other effects going along with civilization. This sporadic noise usually consists of high and low energy spikes. The spikes can be eliminated by using selective stacking techniques. They are a statistical analysis of the individual data points of all recorded transients and eliminate the outliers which represent the high and low energy noise. Using this selective stacking technique a significant signal-to-noise ratio improvement can be obtained in a robust way. For different noise environments different rejection criteria for the selective stacking techniques give the optimum result.

Furthermore, the resulting signal can be distorted by current channeling near the transmitter (which is caused by small lateral inhomogeneities) or slight current channeling between the transmitter and receiver. Since the static limit of the magnetic field is independent of the resistivity of the subsurface, a characteristic scale factor for the magnetic field signal can be obtained and the resulting apparent resistivity curves can be scaled accordingly. For the electric field measurements this kind of characteristic factor cannot be derived, since the electric field depends on the resistivity of the subsurface. In this chapter the theoretical foundation was laid for the demonstration with 3-D models and field data in the following chapter.

In areas with high cultural noise level one must apply digital processing techniques often prestack to get optimum signal-to-noise ratios. Prestack processing gives better results because the stacking process smears some of the noise characteristics, which makes the noise harder to be removed poststack.

PROBLEMS CHAPTER 3

1. The following data set is given:

RECORD:	1				
0.2755908	0.0119920	0.0000030	2.3900363	0.5832117	-0.0380386
0.1928412	0.3573927	0.1526969	0.20133	0.2706927	
RECORD:	2				
-1.5540766	-1.6780542	-1.8991159	-0.2161476	0.2473381	0.4385308
0.8813409	0.9375696	0.3787163	-0.5645440	-1.2707208	
RECORD:	3				
-1.0341588	-1.1320440	0.0740108	2.0977080	1.4319669	1.0603390
0.1261196	-0.3070775	-1.2292424	-1.3732855	-1.3503211	
RECORD:	4				
0.2017749	0.8703387	0.9356464	2.7415242	-1.2459029	-0.0844801
-1.4686812	-2.2912827	-1.3721312	-0.1848829	0.5837787	
RECORD:	5				
-2.1118524	-2.0408990	-1.3452507	2.4703624	2.9146221	2.2398403
5.0405531	-1.8007256	-1.1418511	-2.7388361	-2.8436639	
RECORD:	6				
-2.3441656	-2.5334892	-1.0664327	2.3691602	-1.0777242	-0.0351673
-1.5888555	-1.6748388	-2.0209844	-2.9484138	-0.7456929	
RECORD:	7				
-1.6146545	-0.4482726	1.0428545	3.9444280	1.5758060	-0.9646301
-1.6764526	-1.9360046	-2.6586609	-1.7716675	0.4748080	
RECORD:	8				
-2.3276727	-3.0785196	-4.3858929	-1.0590187	-0.4985634	0.6217370
-1.4811532	0.0647912	2.6683986	0.0751671	0.4168114	
RECORD:	9				
-3.1864831	-2.3261542	-1.8513770	-0.9439368	-0.9474463	-0.9302039
1.0502346	-1.8462653	-1.4414496	-2.0959754	-0.7333655	
RECORD:	10				
-1.6225488	-2.5334988	-2.2142847	0.8845467	1.1036630	1.7215295
1.6822000	0.9217781	-0.7886559	-1.9777735	0.0725502	
RECORD:	11				
1.6127090	2.2853165	1.2950211	2.4119644	-0.4884264	-1.9182514
-2.8122258	-2.0249104	-0.3581164	1.3807755	-0.8517382	

RECORD:	12				
1.8469988	2.4987781	2.3358905	3.2498157	0.4743562	-0.9259812
-0.9009567	0.0024018	1.4670550	2.0931232	2.2414386	
RECORD:	13				
-0.2569095	0.5355940	0.6386671	2.2935593	-0.2292147	-1.7735569
-2.8649800	-2.4438374	-1.4358799	-0.3457156	0.9185896	
RECORD:	14				
-0.9805466	0.5012346	2.6479175	5.4910116	3.4184101	2.1564319
-0.1822448	-1.4537216	-2.0488145	-1.5449692	0.0188661	
RECORD:	15				
-3.3838344	-3.3142543	-2.9539180	0.5495003	0.7615975	0.9481363
1.6817789	1.2588053	0.2600411	-1.3739847	-2.7665401	

Each record represents a coarsely digitized measurement (like a transient). Sequentially, each number in a record is the i -th data sample.

- Stack the above data set using the standard average. Also, calculate the standard deviation of the stack.
- Now apply the following stacking algorithm.
 - Read in the i -th sample of each record, average them and calculate the standard deviation of the read in data.
 - Sort the data points by amplitude.
 - Eliminate the outliers of the data in two possible ways
 - 20 % of all points from the lower and upper sorted data.
 - All points outside of one standard deviation.
 - Calculate from the remaining points the new average and standard deviation.
 - Read in the $(i+1)$ -th data point of each record and repeat the above procedure.

What is the meaning of the different stacking algorithms? Can you identify what they are being used for?

2. Derive the *calibration factor* for the horizontal magnetic field components H_x and H_y .
3. Explain in detail (mathematically) why the calibration factor for the electric field components is different from the magnetic field components.
4. Take an arbitrary early time apparent resistivity curve. Calculate the calibration factor for it. Then cut off some data points at the beginning and the end of the original curve and calculate the calibration factor. Doing this several times you can study the error introduced by editing or not editing the data.
5. Write a Fortran program to carry out deconvolution in the frequency domain. Make sure you keep the array length of the transient signal and system response variable so that you can apply it later to real data. Select a test data set (synthetic) and try out your program on the data.
6. Write a Fortran program which implements the deconvolution in the time domain. Compare the results with the results of problem 5.

KMS Technologies – KJT Enterprises Inc.
6420 Richmond Ave., Suite 610
Houston, Texas, 77057, USA
Tel: 713.532.8144

Please visit us
<http://www.kmstechnologies.com>

This material is not longer covered by copyright. The copyright was released by Elsevier to Dr. Strack on November 5th, 2007.

The author explicitly authorizes unrestricted use of this material as long as proper reference is given.

KMS Technologies – KJT Enterprises Inc.

An EMGS/rxt-company

Chapter 5

The Field System and Field Procedure

extract from

Strack, K.-M., 1992, reprinted 1999
***Exploration with deep transient
electromagnetic:*** Elsevier, 373 pp.

This material is not longer cover by copyright. The copyright was released by Elsevier to Dr. Strack on November 5th, 2007.

The author explicit authorizes unrestricted use of this material as long as proper reference is given.

Chapter 5

The Field System and Field Procedures

The previous chapters explained the physical background, the data processing and interpretation of LOTEM data. In this chapter, the system hardware and field procedures are described. First, the individual system building blocks of a conventional acquisition system are considered leading to more advanced multichannel systems. Multichannel systems will move electromagnetic techniques into a technological state common to seismics. In the future, the large amount of data will bring the development of new multichannel processing techniques. These require new imaging methods and finally yield a subsurface image of much higher resolution.

After considering the general system concept, specific problems are addressed. The selection of them is strictly based on field experience and where most misunderstandings and errors occur. When synchronizing different receiver and transmitter systems, one is often faced with incompatible synchronization circuits. By properly designing the synchronization clocks one can easily circumvent this problem with little additional effort. At the same time, by choosing a proper synchronization design, one can incorporate safety devices into the system at a small additional cost.

Further, the mobile processing systems are discussed which are essential to maintain an optimum quality control during the ongoing survey. The quality assurance always grants continuous adjustment to the survey condition yielding a very high productivity.

When discussing the field procedures, emphasis is given at all stages to avoid a breakdown in the field and increase the amount of acquired data. The same objective guides us when systematically preparing the transmitter side. Systematic preparations can save several field days. In addition to the increased productivity, one should always consider special field techniques which allow an additional improvement of the signal-to-noise ratios. Special field procedures can also save significantly in the hardware cost and operation expenditures. Considering that a signal-to-noise ratio improvement by a factor of two can only be obtained by either increasing the transmitter current by a factor of two or decreasing the noise by twofold. An increase in current by a factor of two requires the generator power to be increased by a factor of four which soon reaches the practical limits. Thus, an improvement of the signal-to-noise ratios using improved processing principles and field procedures seems to be the more logical and less expensive way to go.

SYSTEM CONCEPTS

A deep transient EM system uses a grounded wire transmitter and a receiver system. Figure 5.1 shows a typical field setup of the **long offset transient electromagnetic (LOTEM)** sounding system. A grounded wire transmitter of approximately 1 to 2 km length, is laid out on the earth surface and earthed on both sides. Through this transmitter, a square wave current of several tens to several hundreds of Amperes is injected into the ground. The current step induces induction or eddy currents in the subsurface which propagate downwards and outwards with increasing time. A mobile receiver located at some offset (2–20 km) is used to record the electromagnetic response of the secondary currents in the form of the time derivative of the magnetic field and the electric field components. The signals appearing at the receiver caused by the induction currents in the subsurface are called transients. This is because when the current is switched abruptly, it starts at a high value and then decays with time to a constant level. Repetitive current switching cause transients to appear at the receiver site. They can then be stacked on top of each other to obtain an optimum signal-to-noise ratio using digital data processing techniques similar to those of the seismic industry.

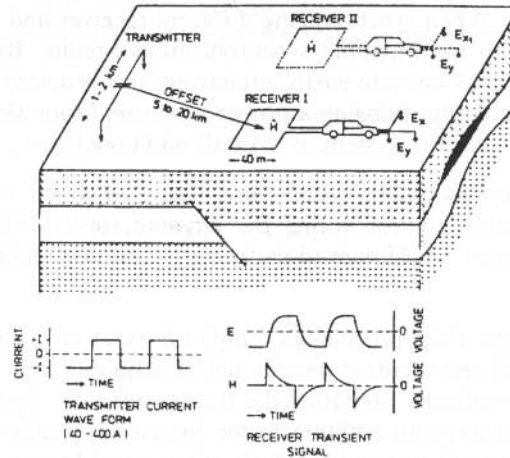


Fig. 5.1: Typical setup of the long offset transient electromagnetic sounding system.

A block diagram of the transmitter and receiver hardware components is given in figure 5.2. The transmitter consists of a standard three-phase generator which supplies the rectifier-current-switch assembly with 220–880 Volts AC. Other generators such as 400 Hz generators may also be used. The current switching after rectification is synchronized with the receiver with a high precision crystal clock. The receiver consists of magnetic and electric field sensors which send the signal directly to the

preamplifier. Then via the amplifier it goes into the digital part of the data acquisition system. The data acquisition system described here is called DEMS IV (Digital ElectroMagnetic System, 4-th generation). It has the feature to record all the raw data on a removeable hard disc. It also allows real time quality control of all signal using a graphics display. The entire data acquisition system is portable and operated by a 12 Volt automobile battery. DEMS IV is a development based on the field systems described by Strack (1985) and is a single site system meaning that one receiver site is recorded at one time with one acquisition system. A newer multichannel data acquisition system, the TEAMEX system block diagram is shown at the bottom of the figure.

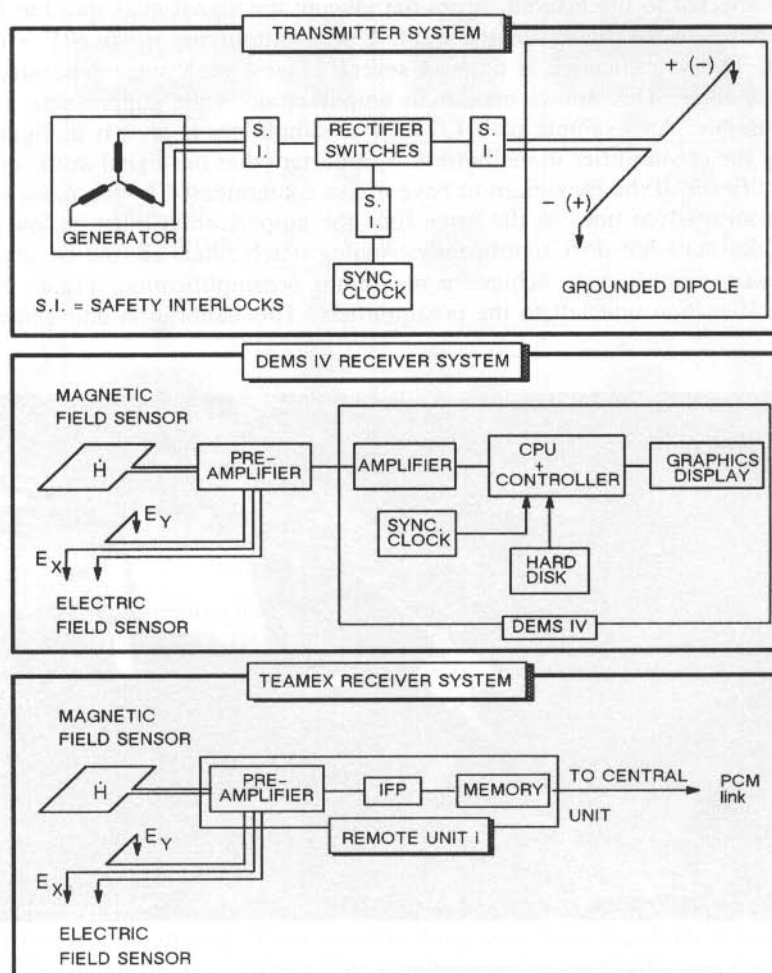


Fig. 5.2: Block diagram of the hardware building blocks for a LOTEM transmitter and receiver systems.

Routinely, copper–copper sulphate electrodes for the electric field and a large air loop as induction coil receiver for the magnetic field are used. For more rugged terrain one can use flux gate magnetometers (3 components) or induction coils. Only during recent years have the noise characteristics and the price of the latter sensors come within an acceptable range. Compared to air coils, ferrit core magnetometers are about twice as expensive and flux gate magnetometers about five to eight times. Figure 5.3 shows a picture of the induction coil takeout. The induction coil consists of a seismic cable with approximately 100 conductors connected in series. Its length may vary between 120 m to 200 m. The coil can either be laid out as large square loop (30 m to 50 m on the side) or with a smaller side length (10 m with several turns). Both ends are connected to the takeout. From the takeout the signal goes into the pre-amplifier shown in the figure on the right. Before amplifying it, the RF – noise is filtered out. The amplification is done in several stages, each stage separated by an analog notch filter. This allows maximum amplification while suppressing as much noise as possible. An example of a LOTEM preamplifiers is shown in figures 5.4. When using the preamplifier in the field, it is important that the signal at the output of the preamplifier is at the maximum to have it less contaminated by the noise entering the signal transmission line. At the same time the amplification must be low enough that the signal does not drift significantly. Analog notch filters should be placed between the gain amplifiers to achieve a maximum preamplification. Figure 5.4 also shows the calibration unit left to the preamplifier. This calibration unit generates a

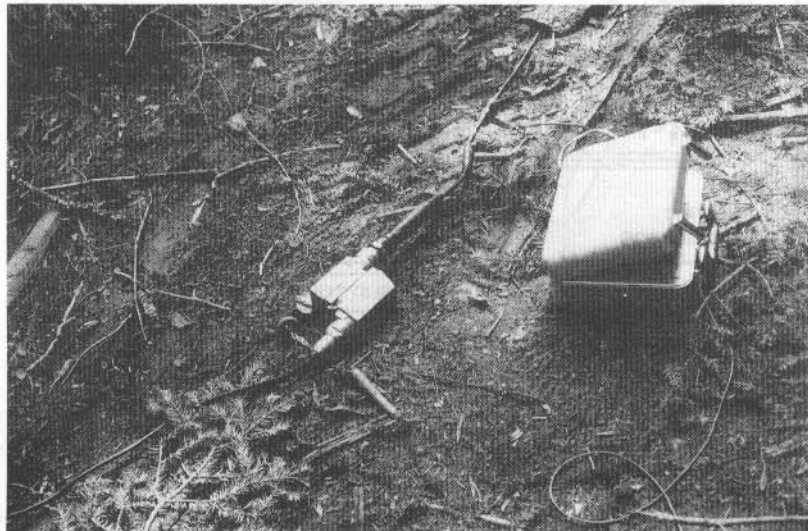


Fig. 5.3: Takeout and connector of the LOTEM induction coil which is made up of a 160 m long seismic cable. On the right side of the figure the preamplifier is displayed.

square wave signal which can be attenuated in binary steps. Using the output of the calibration unit as input to the amplifier allows a quick check of the gain factors. The calibration unit can be triggered by the synchronization clock to allow the recording of several stacks for system response evaluation.

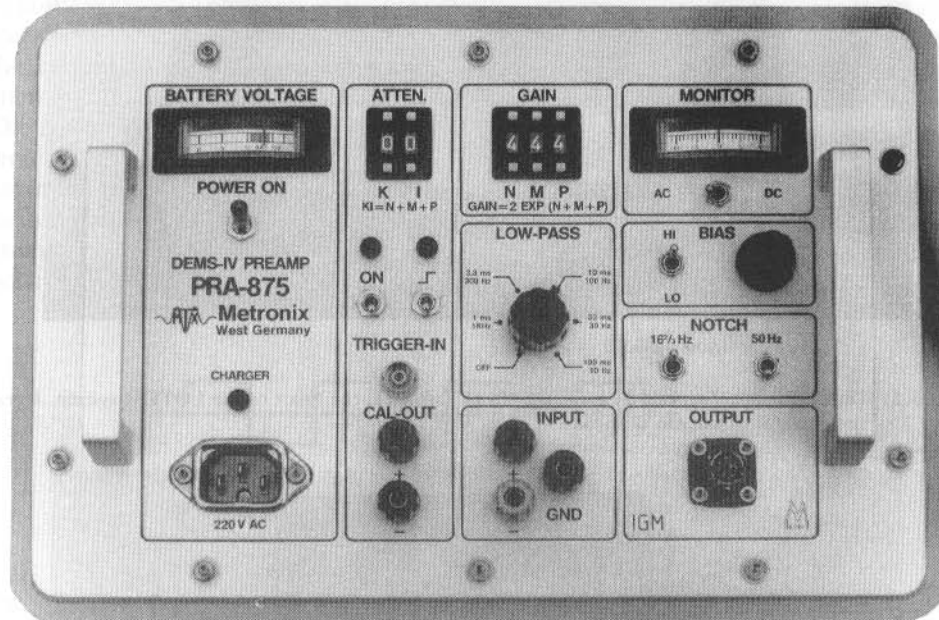


Fig. 5.4: LOTEM preamplifier showing on the left side of the preamplifier the calibration unit and on the right side the preamplifier control panels.

A 20 to 50 m long cable connects the preamplifier with the amplifier at the site of the digital data acquisition system. The acquisition system is located at a distance from the sensors because generally the receiver vehicle and the movements of the operators can cause unnecessary electromagnetic noise in the sensors. Figure 5.5 and 5.6 show examples of different single site acquisition systems of the DEMS IV generation. In figure 5.5 the original prototype version is shown (only the digital part). Figure 5.6 shows the commercial version of DEMS IV which also integrates the analog amplifier and the graphic display. Both systems have removable hard discs and especially modified for harsh field conditions. The comparison between both systems shows how rapid the size is reduced with new technology within only 2 – 3 years time. Multichannel remote units are only one sixth of the size of the DEMS IV system in figure 5.6 with twice the capability.

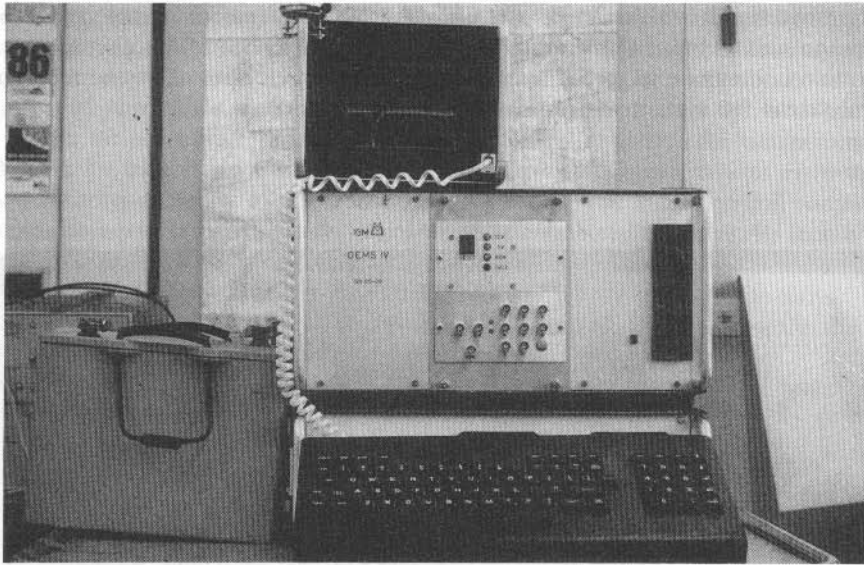


Fig. 5.5: Digital ElectroMagnetic System (DEMS IV) which is the heart of the LOTEM system. Here the original prototype is shown.

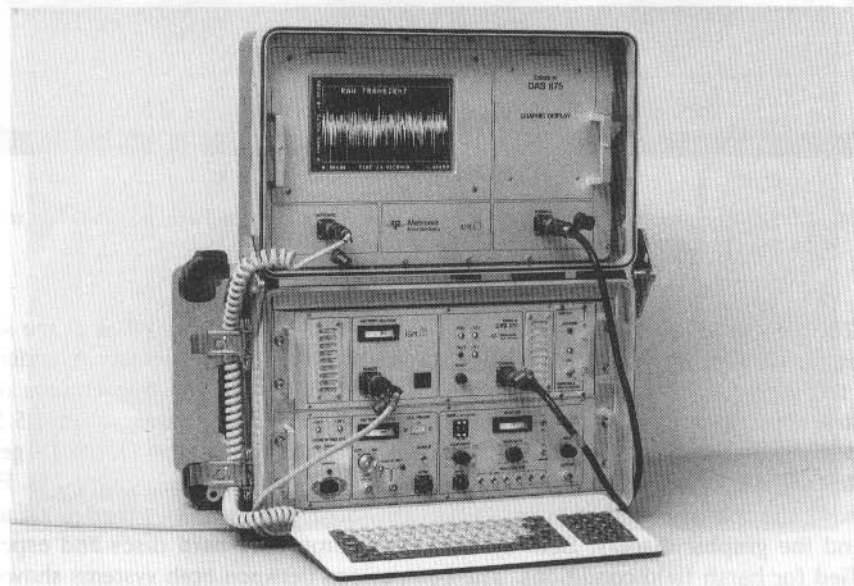


Fig. 5.6: Digital ElectroMagnetic System (DEMS IV) in a commercial version.

Transmitter Systems

The objective of the transmitter is to produce a direct current which is then turned off or reversed. Figure 5.7 shows two possible transmitter *wave forms*. Here, only bipolar current waveforms have been selected because the averaging of the signal of opposite sign is essential to avoid effect caused by the polarization of the transmitter electrodes. The bipolar continuous current waveform has the advantage of using twice the current to obtain a maximum source moment. Furthermore, larger generators show significant wear when used under changing load as with the bipolar waveform. The *bipolar continuous waveform* is sufficient when using larger offsets ($> 5\text{--}7\text{ km}$) and large investigation depth. In that case the ripple on the current from the rectifier assembly is negligible. When requiring higher resolution at shallower depth, the *bipolar waveform* is more appropriate, because one can eliminate the ripple from the generator when recording only during the off-time. The time between cycles of the same polarization is called the *repetition rate*.

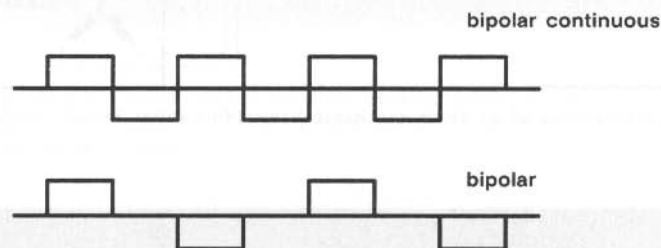


Fig. 5.7: Two possible bipolar transmitter current waveforms.

Hereto, it is still difficult to obtain a perfect square wave current waveform and a large output current. Although solid state transmitters delivering currents of up to 100 Ampere (peak-to-peak) are available, field reliability and safety are of major concern. One is thus sometimes forced to use electromechanical switches and to measure the system response carefully. Deconvolution of the system response including the ramp time will in most instances compensate for the effects. Figure 5.8 shows a schematic of an electromechanical *switchbox*. When designing a switchbox one should not forget to include safety devices (not included in the figure) which turn off the current once it falls below 10% of its maximum level. This can be accomplished using window comparators. The safety device is disabled just before the current reversal and it is enabled again immediately after the switching. From the field operations point of view, the easiest and most reliable generator is a standard three phase 380 V generator as used at any construction site. They are readily available anywhere in the world and can be replaced when problems occur. Figure 5.9 shows a picture of such a generator as we commonly use in Germany. For mining applications the use of 400 Hz aircraft generators is very common. They are significantly smaller and give a cleaner DC-

current. Their drawback lies in the availability of spare parts which can be an essential factor for field operations.

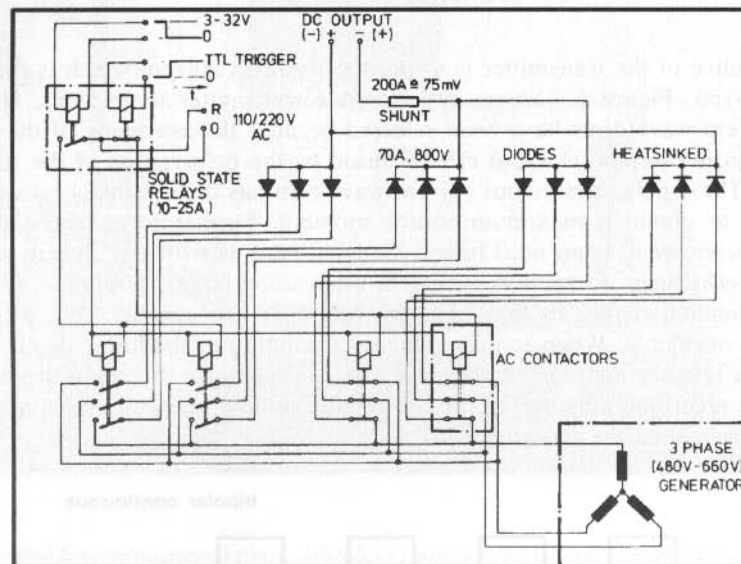


Fig. 5.8: Principal schematic of an electromechanical switchbox (after Strack, 1985).



Fig. 5.9: Standard construction generator used for LOTEM test surveys in Germany.

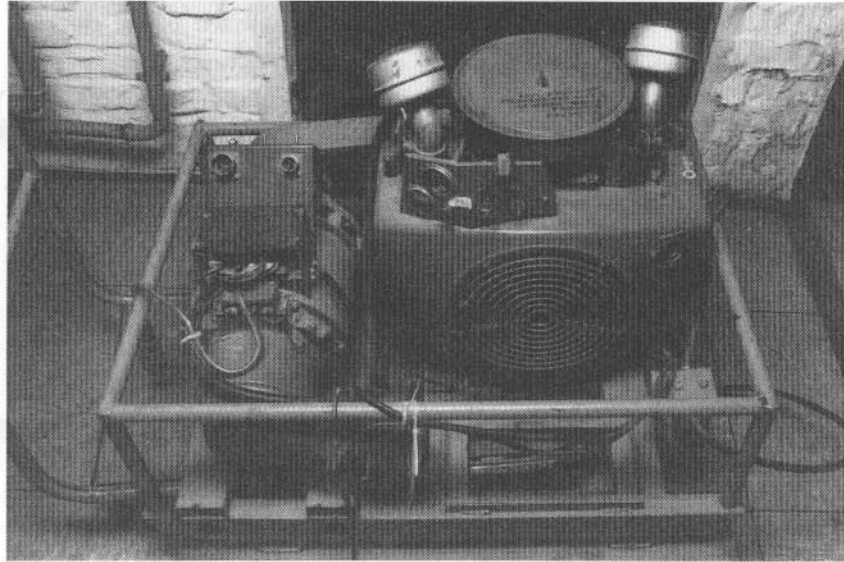


Fig. 5.10: 400 Hz 30 KVA generator as commonly used for mining applications. Connected to the generator can be solid state 25 KVA switchbox giving maximum output current of up to 50 Ampere (peak-to-peak).

Synchronization between Transmitter and Receiver

Synchronization between transmitter and receivers is an essential task. Because of the large distance between transmitter and receiver, the synchronization can either be done using satellite clocks or remote clocks which operate independently and are synchronized just before leaving the base camp. Satellite clocks have the advantage of an absolute time reference, however their functionality depends greatly on the availability of the units. The least expensive and most practical way is the use of remote clocks. Oven controlled clocks are generally more accurate but require significantly more power than temperature compensated crystals. The latter can be obtained with a relative accuracy of one part in 10^{-7} . The clock designer should consider the following:

- Minimum length of operation without recharging should be 2 days in case the nightly recharging is forgotten or the receiver crew has to stay overnight away from the basecamp.
- Relative tuning output of the crystals should be provided at a frequency high enough for the required accuracy (about 300 kHz or 100 kHz) but low enough to be monitored with simple field oscilloscopes.

- Clock rate is externally selectable.
- Various output signals should exist to allow flexible use of the clocks.
- The clocks should operate as master and slave.

A principal schematic of the synchronization clock is shown in figure 5.11. When selecting the components extreme care must be taken to guarantee reliable operation over a large temperature range.

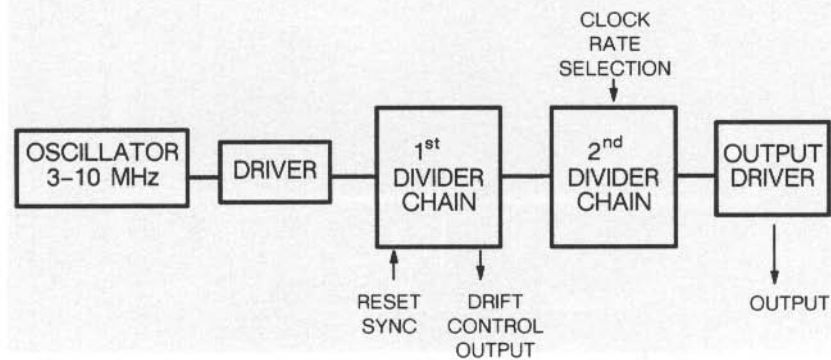


Fig. 5.11: Principal block diagram of a synchronization clock.

Figure 5.12 shows a picture of a synchronization clock as used with DEMS IV. The key switch for the power is essential to avoid accidental turn off and synchronization loss while operating. Below the dip switch, the code for the different clock rates is shown. Output is a 5 V TTL signal which is also provided in reversed form in case each trigger separately controls one of the two halves of switching assembly. Above the synchronization connector two LEDs are shown. Only one of them will only be lit when the two clocks to be compared are out of synchronization.

Figure 5.13 shows a diagram of the front panel of a more elaborate synchronization clock. This clock was developed after long field tests and accommodates most field requirements. Design criteria are:

- Low power consumption and operation for longer than 72 hours allowing the field crew to be away two or three days from the base camp.
- Input voltage for charger between 110 to 250 V, switching automatically.
- Charge status indicator to show the operator when he needs to go back to the basecamp.
- Clock rate selected as displayed on the switches to avoid errors due to false translation of switch setting tables.
- Two different high frequency outputs (3kHz and 300 kHz) for coarse and fine relative adjustment of the crystal drift.
- Pretrigger for safety interlocks at the transmitter and pretrigger for the acquisition systems. The pretrigger should be selectable in percent of the clock rate.

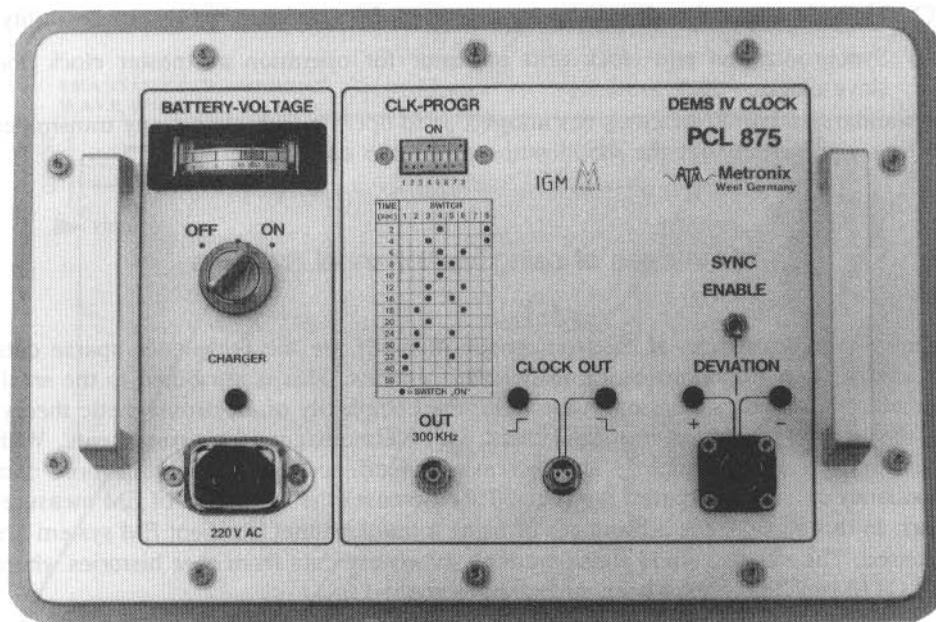


Fig. 5.12: Front plate of a simple synchronization clock.

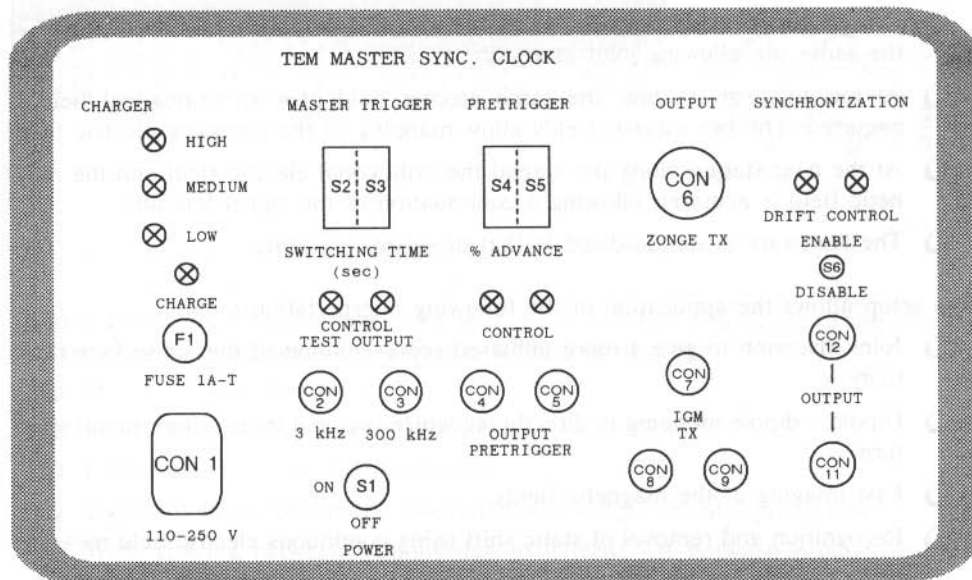


Fig 5.13: Front panel diagram of a multi-purpose synchronization clock.

- Multiple output for all standard transmitters for maximum hardware flexibility.
- Synchronization and clock drift indicator for operation as master clock and slave clock.

The standardization of the clock has allowed us to operate with almost any transmitter and thus significantly cut the mobilization and setup cost.

Advantages of using Multichannel Systems

One of the drawbacks of electromagnetic methods are the prevalence sparse data sets and the lack of sophistication in field instruments. This is attributed to the small number of researchers working in the field, the complexity of electromagnetic theory, and the limited resolution one can obtain with electromagnetic measurements. With the advancement of technology and increasing experience, one can obtain more data redundancy and denser spatial sampling. This increases the resolution of EM measurements. In this section, the advantages of using a multichannel transient EM system are discussed. The examples and considerations shown use data from case histories where the LOTEM technique has been successfully applied.

Figure 5.14 shows a typical field setup for a multichannel transient EM system. Many digital remote units (RU) are connected via a digital telemetry line. Each RU acquires two channels simultaneously. The reasons to use two channels in one unit are:

- One magnetic field component and one electric component can be acquired at the same site allowing joint inversion.
- At the adjacent stations, the same electric field plus an orthogonal field is acquired. The two electric fields allow mapping of the complete electric field.
- At the next station along the spread the orthogonal electric field and the magnetic field is acquired allowing a continuation of the signal laterally.
- The hardware is standardized to that of seismic systems.

This setup allows the application of the following interpretation tools:

- Joint inversion to give a more unbiased representation of the subsurface resistivity.
- Dipole – dipole mapping to directly recognize regional three-dimensional structure.
- Fast imaging of the magnetic fields.
- Recognition and removal of static shift using continuous electric field measurement in combination with magnetic fields.
- Noise compensation techniques for time synchronous measurement.

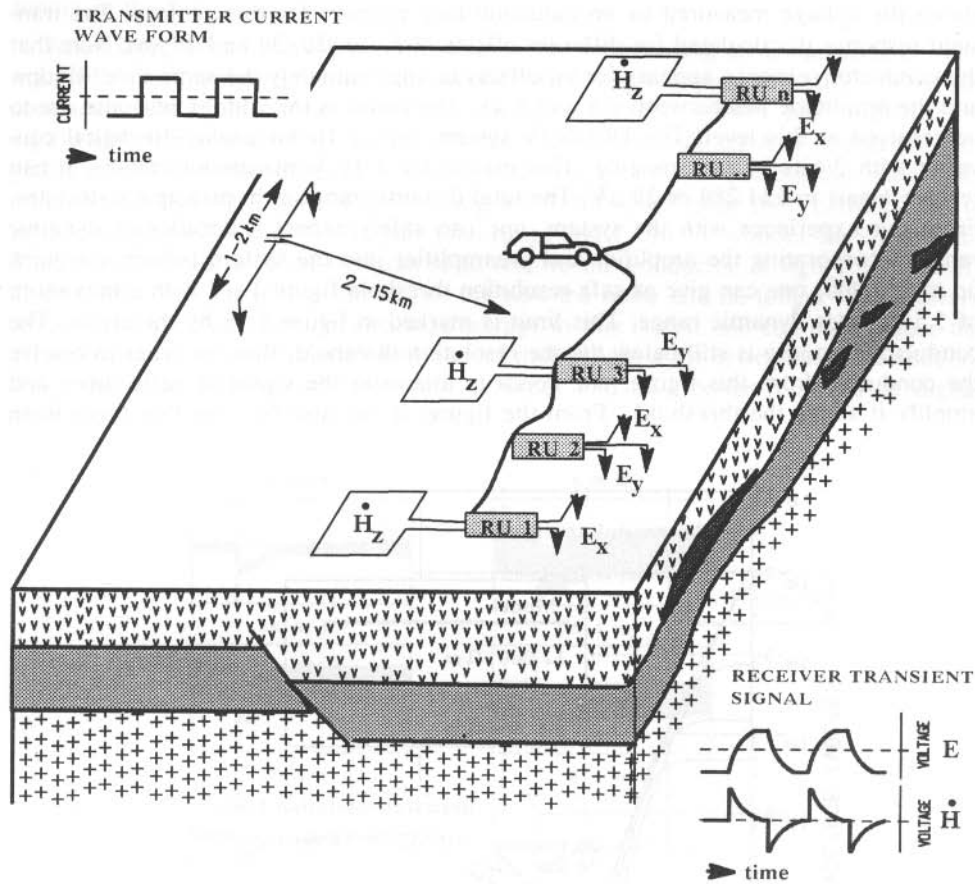


Fig. 5.14: Typical field layout for a multichannel transient EM system.

To fully appreciate the advantages of a multichannel system, one needs to consider the drawbacks of present single site systems. Among them are:

- Dynamic range limitation.
- Inaccuracies due to slight signal drifts.
- Limitations in noise and bandwidth.
- Signal-to-noise limitations associated with single channel processing.
- Wide spacing between stations due to a trade off between productivity and lateral resolution.
- Maintenance and cost per site.

The *dynamic range* problem can be illustrated using a deep crustal application where a conductor is to be found below a 20 km thick highly resistive layer. Figure 5.15 shows the voltage measured by an induction loop receiver for this geology. The transient response is calculated for different offsets of 5, 10, 20, 30 and 40 km. Note that the conductor response appears for all offsets at approximately the same time window and the amplitude lies between 0.1 and 1 μV . Deviation in the voltage response are to be resolved at this level. The DEMS IV system uses a 16-bit analog-to-digital converter with 3 bits of gain ranging. This means for a 10 V maximum voltage, it can resolve 1 part in 524 288 or 20 μV . The total dynamic range is in principle 6 decades. From our experience with the system, one can safely expect 4 decades of dynamic range. Incorporating the amplifier and preamplifier into the system (which use gains up to 500 000) one can give as safe resolution threshold figure 1 μV with a maximum of 3.5 decades dynamic range. This limit is marked in figure 5.15 by the arrow. The conductor response is still below the the resolution threshold, thus, in order to resolve the conductor from this figure, one needs to attenuate the signal at early times and amplify it above the threshold. From the figure, it can also be seen that there is an

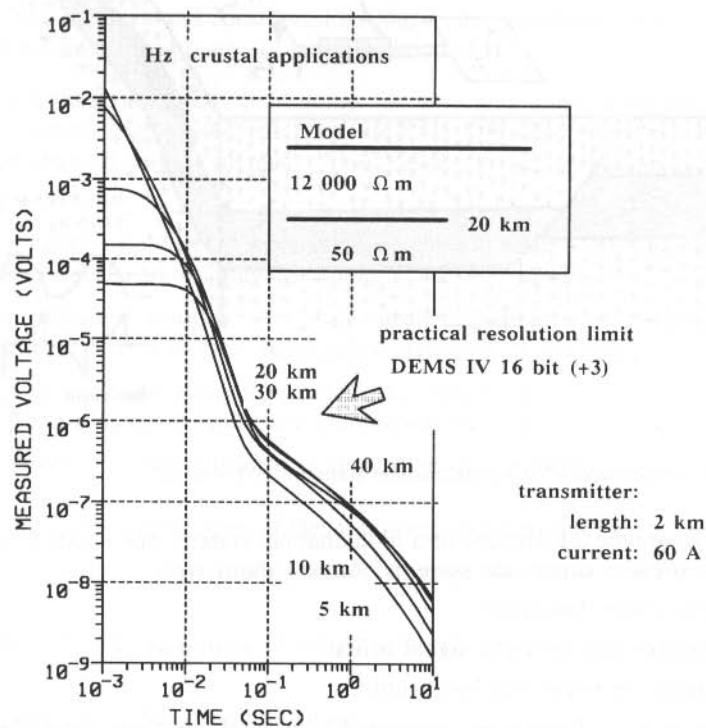


Fig. 5.15 Voltages responses for different offsets for deep crustal application.

optimum offset (20 to 30 km) at which the response from the conductor is strongest. All of this requires in the necessity for very careful survey design and survey fine tuning in the field.

When integrating state-of-the art seismic technology using an instantaneous floating (IFP) point amplifier, one can simplify the survey design and still resolve the conductor. The multichannel system we use, the TEAMEX system, has 90 dB (15 bit equivalent) IFP amplifier, 42 db (7 bit) initial gain and a 12 bit A/D converter. This yields a total dynamic range of 34 bits (or 1 part in 10^{10}) or without the initial gain amplifier 27 bits (or 1 part in 10^8). Using a 5 V full scale value the TEAMEX can in principle resolve $5.8 \cdot 10^{-11}$ V for the total range and $7 \cdot 10^{-9}$ V without the initial gain. This is far beyond of what is required to resolve the conductor in figure 5.15 at *any* given offset. The remaining limitations are now the noise and no longer the hardware dynamic range. The most important advantage in this is that one can now reduce the offset between transmitter and receiver and thus obtain a lot better lateral resolution. Also, the noise can be measured with accuracy and thus better removed by digital filters.

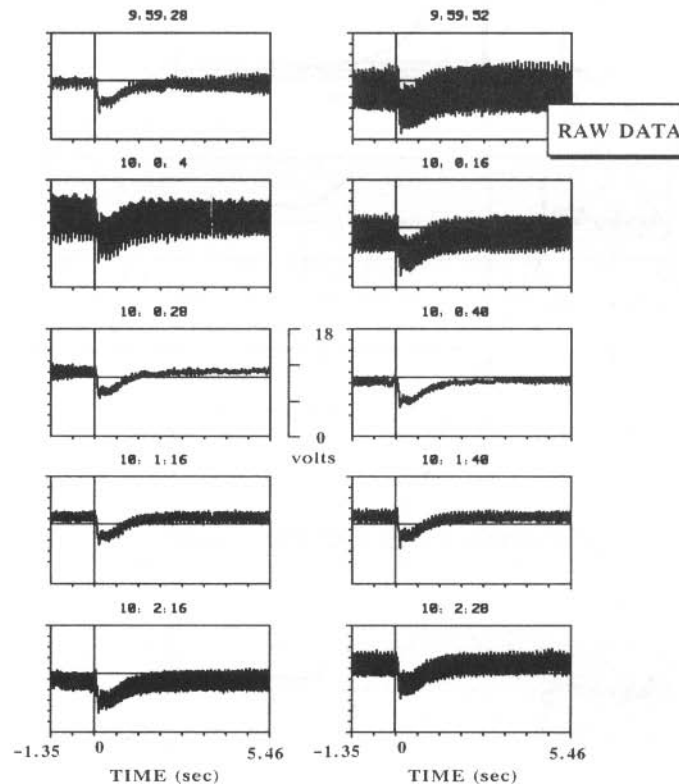


Fig. 5.16: Ten single magnetic field measurements (time derivatives) recorded consecutively.

When recording transients the signal is sensitive to *DC-drifts* because the TEM amplifiers usually do not contain low cut filters. The drift may be of external origin or from the connections of the instruments (thermal drift etc.). Figure 5.16 shows 10 consecutive single records for the induced voltage response of the magnetic field. Above the individual frames, the time of the recording is displayed. Within several tens of seconds the data drifts considerably. Because of this drift it is essential that an accurate reference level is calculated before selectively stacking the data.

For the illustration of *drift-induced* offset on the interpretation the following experiment was done. The data set of all records acquired at the same site (as in figure 5.16) was first digitally processed and the DC-level for each record removed and then

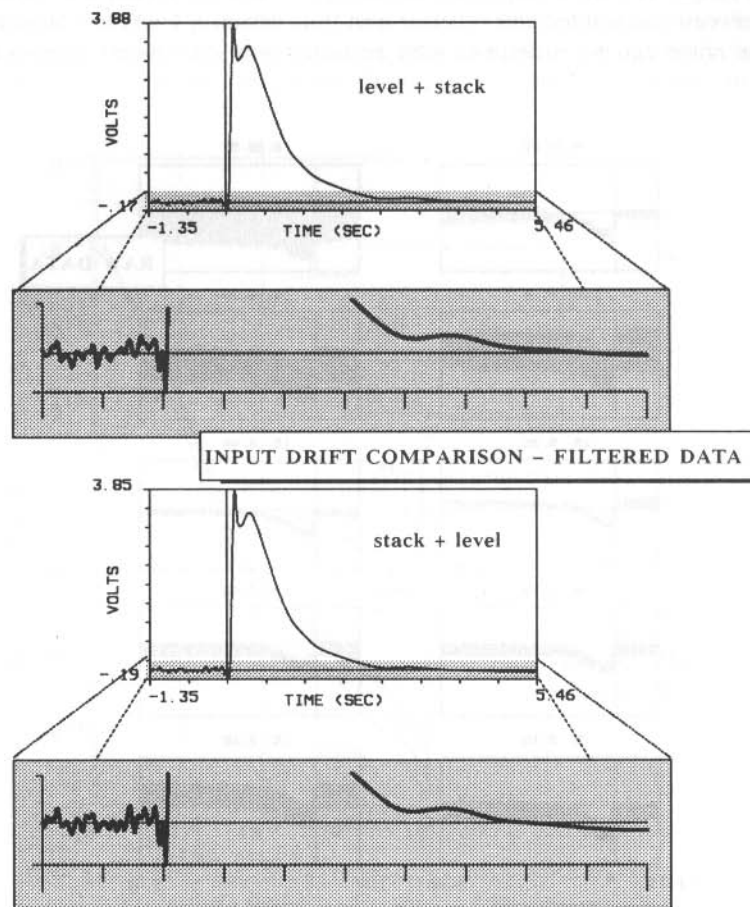


Fig. 5.17: Example of the experiment for comparison of the DC-level effect before and after stack.

selectively stacked. The same data were also selectively stacked and the DC-level removed. The result is shown in figure 5.17. The top graph in the figure displays the data which was DC-leveled prestack and then selectively stacked and the bottom the same data which was leveled poststack. Both data sets were filtered poststack with the same filter to visualize the difference in processing. Below both curves, a zoomed window of the shaded area is shown. The top curve stays about 0.8 seconds longer above the reference zero line. Since only positive transient data can be used for interpretation, the top has 0.8 seconds more usable data. The result from this experiment is that very accurate DC-level or reference level in the data is required before stacking.

To visualize the importance of an accurate DC-level even further, the synthetic apparent resistivity curves for a realistic earth model are calculated and displayed in figure 5.18. Superimposed on the theoretical curve are the early and late time resistivity curves from the same data after the DC-level has been perturbed by 1% or 1‰. Note that perturbed curves flair up from about 2 seconds for the $\pm 1\%$ DC-level perturbation and from about 3 seconds for the 1‰ DC-level change. In both cases false high resistive or conductive layers would result during interpretation.

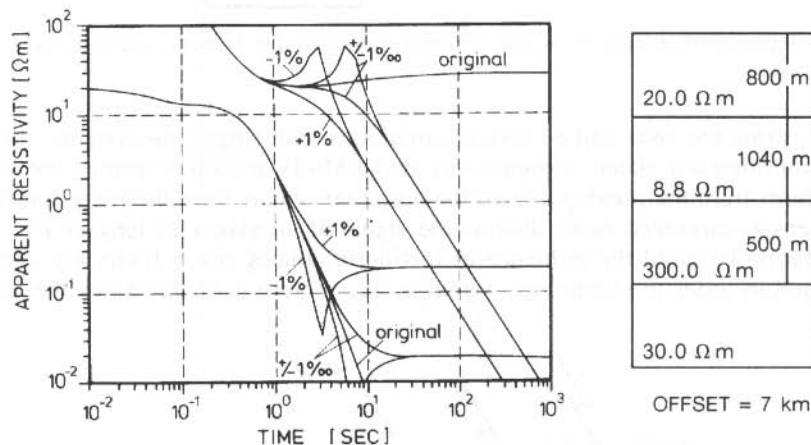


Fig.5.18: Effect of slight inaccuracies in the determination of the DC-level on the apparent resistivity curves. The notches in the perturbed curves represent the times when the signals become negative (negative values are displayed as absolute values).

The TEAMEX system significantly improves the reference level by integrating a microprocessor controlled leveling procedure which is done just before the transmitter clock switches using a pretrigger (either software or hardware). A block diagram of the procedure is shown in figure 5.19. The bias is calculated after analog-to-digital conversion. From the microprocessor, the bias voltage is fed back into the input after digital-to-analog conversion. The difficult part in this concept is to time exactly when the bias control is being done, because no bias control must be done while the

recording is going on or any useful signal is present. In addition to the bias control just before the recording of a transient, the individual operational amplifiers are also drift controlled on operators request. This significantly improved the problems with the DC drift in the signal and also reduces the processing time.

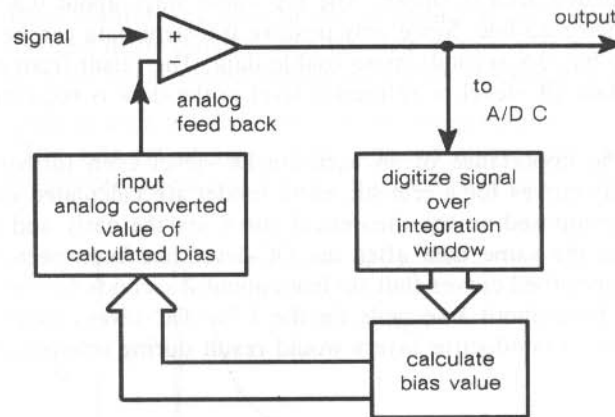


Fig.5.19: Principal block diagram of the microprocessor controller DC-bias circuit of the TEAMEX system.

To illustrate the *noise* and *bandwidth* limitations with single site systems, the signal path is considered in detail. Systems such as DEMS IV usually transmits the signal in analog form from the preamplifier to the amplifier. Apart from the noise interference at the sensor, unwanted noise distorts the signal at all stages as long as it is still in analog form. To avoid the influence of this noise, analog notch filters are commonly being used in order to obtain any signal at all. Figure 5.20 illustrates the different

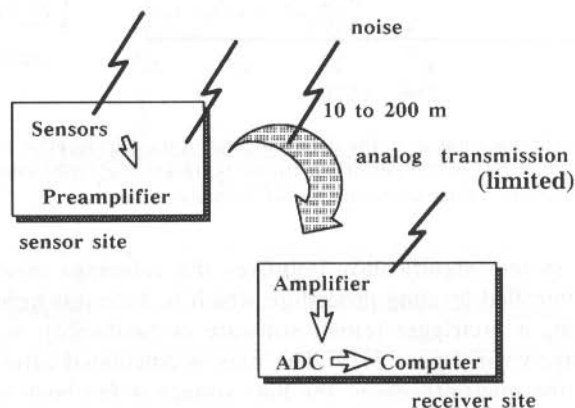


Fig.5.20: System units for a single site LOTEM system where electromagnetic noise can influence the signal.

building blocks where the noise gets into the system. Although extreme care is taken during data acquisition and processing even further improves the signal-to-noise ratio, the noise is not always satisfactorily removed. In these cases the interpreter has to accept noise in the final results. This noise exhibits itself in the large error bars of the inversion results and the scattering of the inversion models between adjacent stations.

An example for an interpretation where the noise can still be seen in the final results is shown in figure 5.21. Here, LOTEM measurements were done for crustal applications in an extremely noisy area in Germany. Even 68% confidence levels for the error calculation yields large error bars. The stations 26 and 27 in the middle of the profile in figure 5.21 show an additional layer at shallower depth with the other stations do not show this layer. This does not mean that this layer is not there. It was simply filtered out of the signal to obtain any useful information at these sites. Thus, the data for this profile is restricted in bandwidth due to the strong noise. The information on the shallow part of the section was outside the remaining bandwidth of the signal.

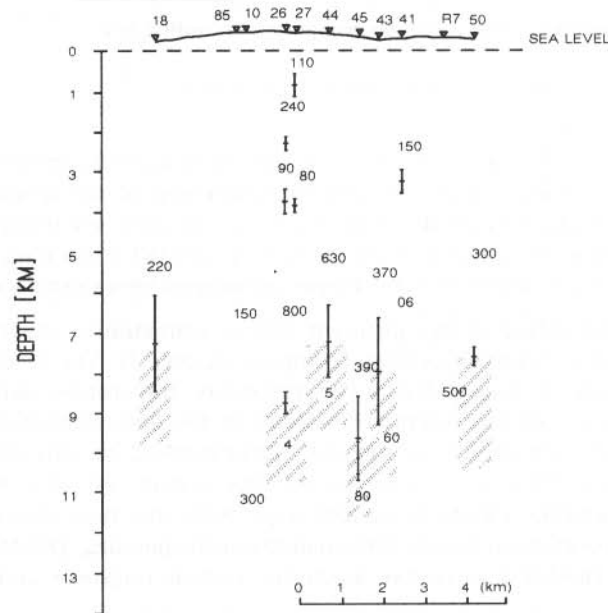


Fig.5.21: Example of an interpreted resistivity depth section where the noise in the signal can still be seen in the scattering of the depth to the conductor (shaded) (after Strack et al, 1990).

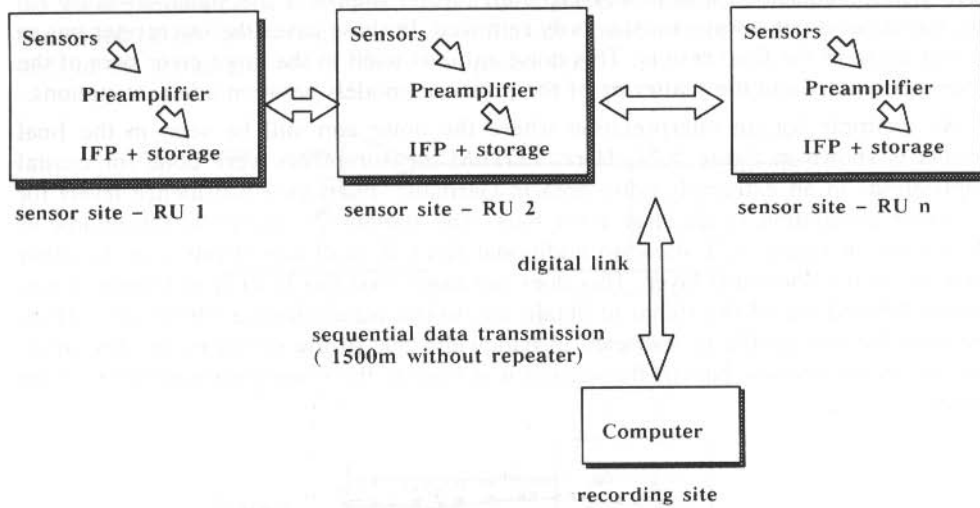


Fig. 5.22: Block diagram of the TEAMEX multichannel system.

The limitation due to *bandwidth* and *noise* can be reduced by minimizing the number of analog filters used in the system, by shortening of the analog transmission circuitry, and by digitizing directly at the receiver. The only remaining noise is entering into the system at the sensors. After the remote unit (RU), the data is in the digital form (see figure 5.22) and is thus no longer influenced by external noise.

To illustrate the effect of the different filters, comparative measurements were taken at a test site with known geology (compare chapter 7). The results of this comparison are shown in figure 5.23. The resistivity transforms derived from the TEAMEX, which are the logarithmic transforms of the data without system response deconvolution, data are shown as squares. Superimposed on this are the synthetic curves of the true earth model convolved with the system response of the TEAMEX system (bottom) and the DEMS IV system (top). Note that the curve with the DEMS IV system response starts at a later time than the corresponding TEAMEX curve. This means that the TEAMEX data has a shorter system response and thus a larger bandwidth.

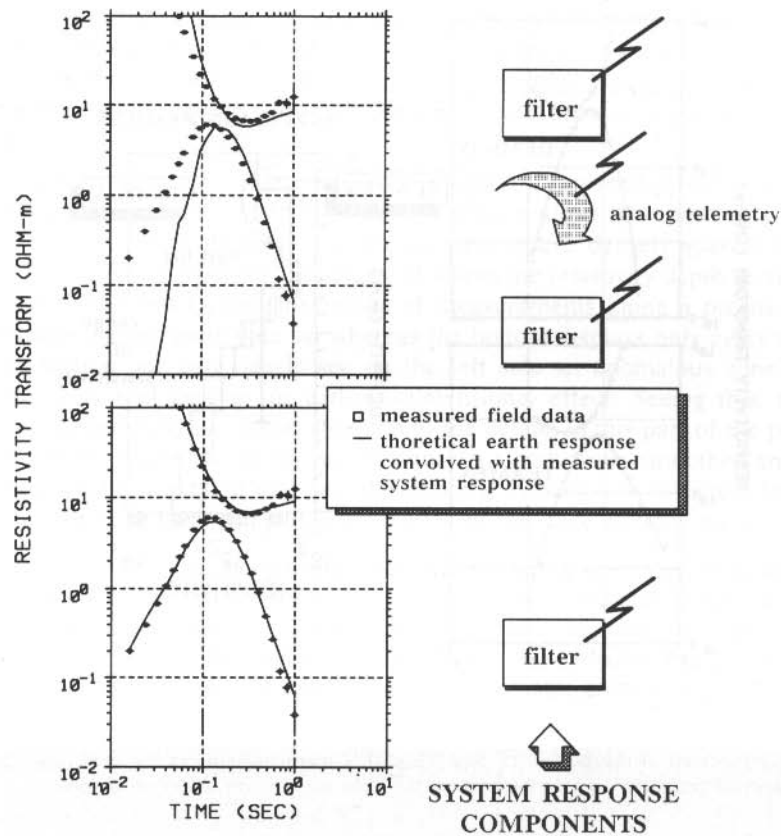


Fig. 5.23: Comparison of the different system responses of the DEMS IV and the TEAMEX systems. The graphs show the TEAMEX data in comparison with the real earth model convolved with the TEAMEX system response (bottom) and the DEMS IV system response (top).

Figure 5.24 shows the comparison of the interpretation of both data sets. The top displays DEMS IV data and the bottom the TEAMEX data. On the right are the respective Occam inversion results shown superimposed on the true earth model derived from well logs. The overlapping depth investigation range is shown cross-hatched. The match of the two interpretations is striking. Apart from the good fit the TEAMEX shows an additional layer at shallower depth. This layer might be attributed to the increased bandwidth of the TEAMEX system.

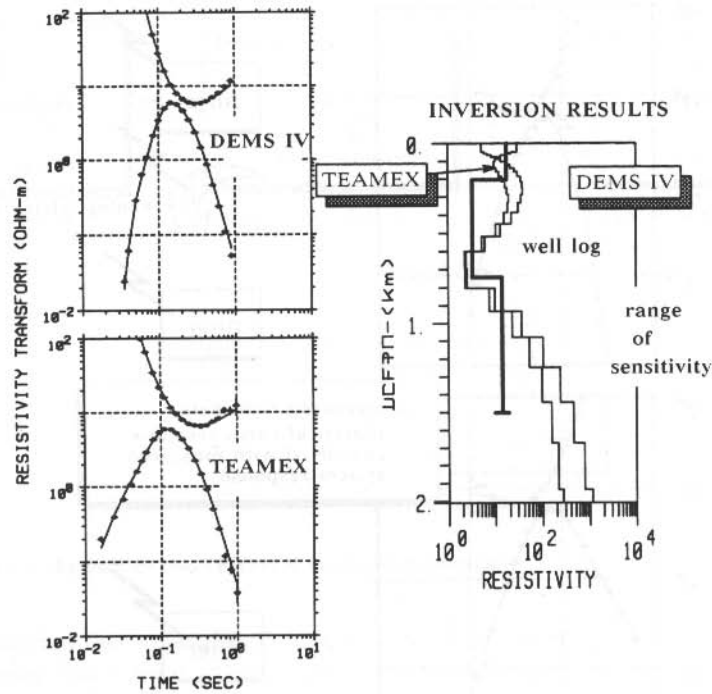


Fig.5.24: Comparison of the DEMS IV and TEAMEX measurements at the same site. On the left are the resistivity transforms and on the right the Occam inversion models.

When acquiring data with a single site system, signal-to-noise improvements can only be made using the data from this site. When using time synchronous multichannel measurements complete new noise cancellation techniques can be developed. Figure 5.25 (left) shows an example of a data set which was processed using only the

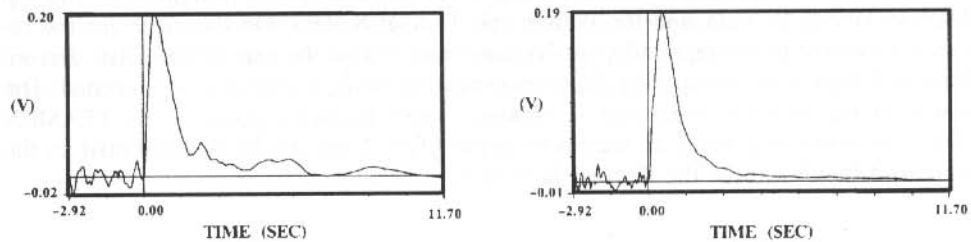


Fig. 5.25: Comparison of a single site processed data set (left) with the same data after noise processing (right) using multiple receivers.

data at this site. the right side of this figure shows the same data after the remaining noise in it was canceled using the local noise compensation technique which is based on time synchronous measurements and time dependent noise definition. The local noise compensation technique is described in more detail below. This type of noise compensation is only feasible with multichannel system because accurate synchronous timing of all receivers is required.

Even a careful designed survey, requires a trade off between productivity and lateral resolution. When interpreting the data, one often realizes that more data had to be taken at closer spacings. Following is an example where densely spaced data were acquired. Figure A.7.1 (bottom) (appendix 7) shows the resistivity depth section (color contours) derived from Occam inversions of measurements along a profile. The top frame displays the complete data set whereas the bottom displays only every third site. In the top section one can clearly see on the left side an anomalous zone which is either caused by real geology or a three-dimensional effect. Seeing this, the interpreter must immediately pay more attention to the details in this part of the profile. At the bottom of the figure this particular structure is significantly smoothed and from it one would probably conclude that one-dimensional inversion is sufficient for it. This structure would have been simply overlooked with too wide station spacing.

Last but not least, the *maintenance* and *cost* per site govern the applicability and success of a survey in many cases. Using many small identical remote units (RU) reduces the amount of spares which have to be carried, since the RUs are essentially non-user repairable and the failure of one means that only one trace less is being recorded. A photograph of a TEAMEX remote unit is shown in figure 5.26.



Fig.5.26: Photograph of a remote unit of the TEAMEX multichannel system.

Mobile Processing Systems

When acquiring field data continuous quality control is essential for optimum survey results. The quality control can be done in two different ways:

- Quality control directly at the site.
- Quality control in a mobile processing center at the *base camp*.

Quality control at the basecamp is the most reasonable option, because carrying out this task at the receiver site would result in lower production. For the mobile processing center one can either use PCs or workstations. Because of the tremendous amount of data and the need for batch processing and multitasking, the workstation option is favorable because it allows the interpreter the simultaneous control of all the processes. The advantage of using a workstation-based mobile processing center lies clearly in the ease of field operations. All data are maintained and handled by one system and additional data transfer and bookkeeping greatly reduced. Figure 5.27 shows the data processing and interpretation system as used by the University of Cologne. The units of the mobile processing system are marked by a bold border. The field system can easily be updated to a full mainframe system allowing communication with different computer systems.

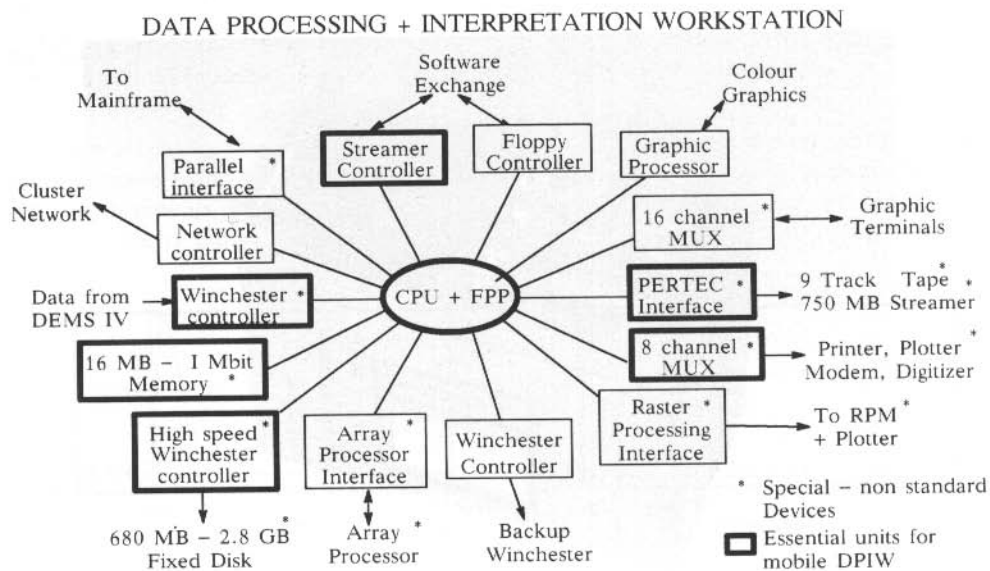


Fig. 5.27: Block diagram of the principal building blocks of the LOTEM data processing and interpretation workstation.

For very remote operations where transport and spare availability are important, the PC version may be preferable because PCs are more widely distributed than workstations.

FIELD PROCEDURES

Apart from the continuous bookkeeping during the data processing stage, significant care must be taken when carrying out the field measurements. In particular careful transmitter preparation can save significant time. Very meticulous bookkeeping of the synchronization and clock drifts can be vital for the survey and later interpretation. Complete control over the above may eliminate some of the questions when measuring the system response.

Transmitter Electrode Preparation

The data quality in LOTEM surveys can be improved by injecting the largest possible transmitter current into the ground. In dry areas or in areas with a resistive surface layer, the only way to achieve this is careful preparation of the electrode sites.

An electrode comprises several buried iron sheets which are all connected to the end of the transmitter cable as shown in figure 5.28. The individual sheets are separated by a distance a . If this distance is chosen too small, then the electric current density in the ground between the sheets is too high: the currents of an individual sheet would have little chance to spread out before they are hindered by the currents

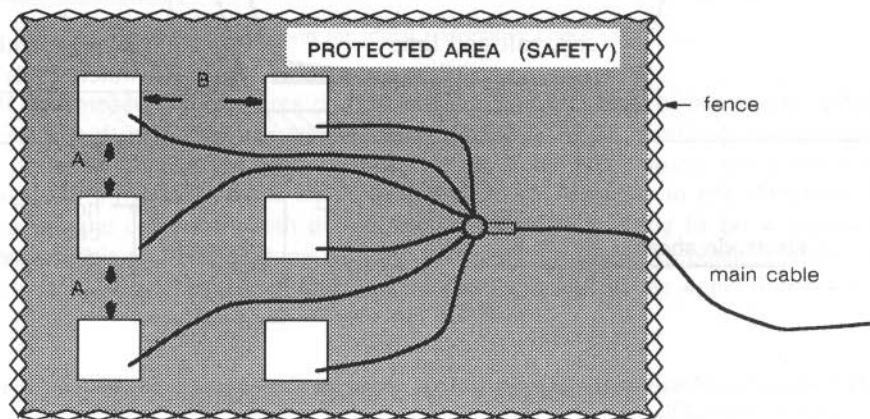


Fig. 5.28: Arrangement of six individual electrode pits at one end of the main cable. A fence is required to protect bystanders.

from the neighbouring sheet. In sedimentary environment, experience shows that the sheets should be separated by at least 5 m. Also, sometimes only 3 or 4 sheets suffice in order to achieve a small contact resistance and hence a high current. In an area with only a few meters of sediments overlying resistive units such as volcanics, sheet separations of 50 m may be required.

For connecting the sheets to the cables, a hole is drilled into the sheets and then the wire lug at the end of the cable is screwed onto the sheet as is shown in figure 5.29. The connection must be prepared very carefully because it will not be accessible once you cover the pit with soil.

The preparation of the pits for the individual sheets is shown in figure 5.29. First, a hole of sufficient size is dug until wet ground (water table) is reached; in Germany this requires 1–2 m depth. The bottom is then covered with a mixture of soil, salt, and lime: the salt increases the ground conductivity and the lime helps to keep the humidity which is important in dry areas. The use of bentonite is also possible, but bentonite tends to be more expensive than salt and lime. The iron sheet with the short piece of cable connected to it is then placed horizontally into the hole and covered with the same mixture of soil, salt and lime. When environmental concerns are important, one can use potassium or a mixture of potassium and salt. Next, the hole is watered and covered with the soil. For each hole a maximum about 50 kg of salt and 50 kg of lime is required, depending on the local conditions. For emergencies you can use a mixture of salt and laundry detergent, but for environmental reasons this is not advisable.

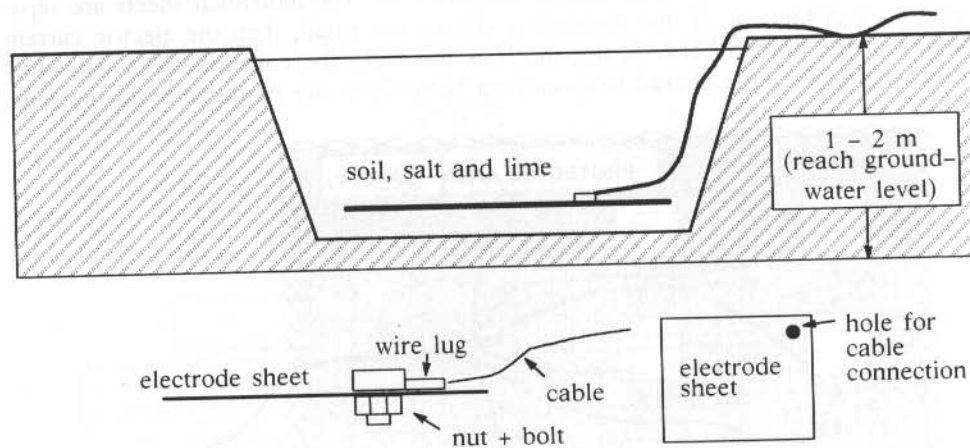


Fig. 5.29: Preparation of transmitter electrodes. Top: preparation of electrode pit. Bottom: connection to main cable.

The electrode sites should be prepared one day before the start of operations. During operations it is extremely important to secure the area of the electrodes with fences and with a watch person, because touching any part of the assembly cou

from the neighbouring sheet. In sedimentary environment, experience shows that the sheets should be separated by at least 5 m. Also, sometimes only 3 or 4 sheets suffice in order to achieve a small contact resistance and hence a high current. In an area with only a few meters of sediments overlying resistive units such as volcanics, sheet separations of 50 m may be required.

For connecting the sheets to the cables, a hole is drilled into the sheets and then the wire lug at the end of the cable is screwed onto the sheet as is shown in figure 5.29. The connection must be prepared very carefully because it will not be accessible once you cover the pit with soil.

The preparation of the pits for the individual sheets is shown in figure 5.29. First, a hole of sufficient size is dug until wet ground (water table) is reached; in Germany this requires 1–2 m depth. The bottom is then covered with a mixture of soil, salt, and lime: the salt increases the ground conductivity and the lime helps to keep the humidity which is important in dry areas. The use of bentonite is also possible, but bentonite tends to be more expensive than salt and lime. The iron sheet with the short piece of cable connected to it is then placed horizontally into the hole and covered with the same mixture of soil, salt and lime. When environmental concerns are important, one can use potassium or a mixture of potassium and salt. Next, the hole is watered and covered with the soil. For each hole a maximum about 50 kg of salt and 50 kg of lime is required, depending on the local conditions. For emergencies you can use a mixture of salt and laundry detergent, but for environmental reasons this is not advisable.

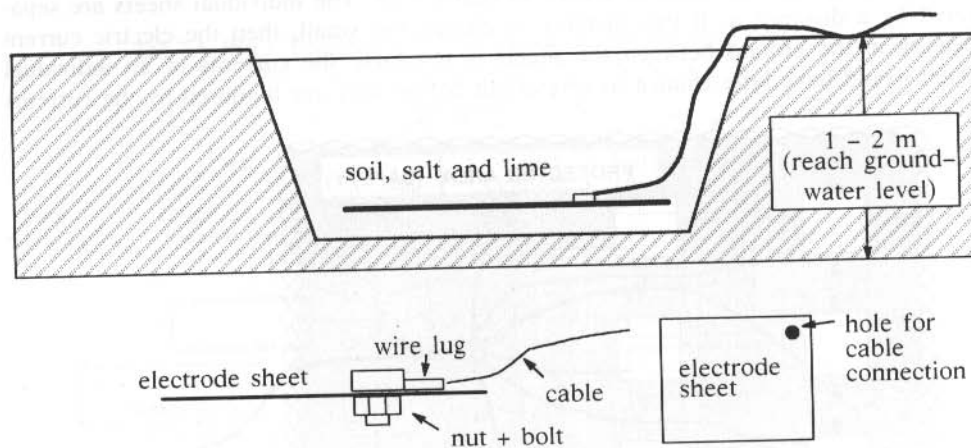


Fig. 5.29: Preparation of transmitter electrodes. Top: preparation of electrode pit. Bottom: connection to main cable.

The electrode sites should be prepared one day before the start of operations. During operations it is extremely important to secure the area of the electrodes with a fence and with a watch person, because touching any part of the assembly could

possibly injure a person. For the same reason, it is also important to insulate all open metal parts with electric tape – for protection of the crew as well as safeguard against other people who could become injured by touching any non-insulated parts.

For low current (less than 30 A) operations, you can also use steel mesh as electrode material when you have the option to increase the output voltage on your transmitter. Significantly less electrode preparation is required when you use different output voltages of the transmitter.

Initial Transmitter Check Out

It has been our experience that it is possible to achieve very high currents with many different generators. In some instances these currents were so high that the switchbox suffered damage. Thus, we strongly recommend that you check out the transmitter, when you connect it for the first time.

This is done by connecting a 12 V battery to the transmitter instead of the switchbox and generator. Make sure the battery is fully charged. You then measure voltage and current as shown in figure 5.30, in order to calculate the earth resistance.

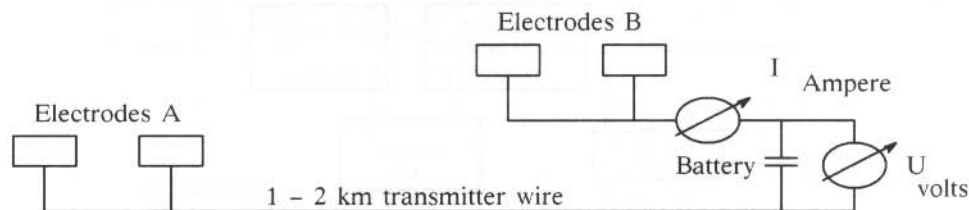


Fig. 5.30: Simplified circuit diagram for initial transmitter check out.

If you measure 2 Amperes current and 11.8 Volts potential across the battery, the resistance of the earth plus transmitter is $11.8/2 = 5.9 \Omega$. Similarly you can calculate the predicted current for the DC voltage of the switchbox (mostly 510 V when using 3 phase 380 V). In the above example this is 86.45 Amperes in one direction. We always use the current in both directions for our current rating to get a representative average. This test can be done without having the generator in place. For the convenience of the reader a transmitter control sheet is given in the appendix 3.

Routine Daily Synchronization Check

Although clock synchronization seems to be a simple matter, extreme care is required because unrecognized clock drift can cause significant problems in later interpretation. Shifting of the data by even one sample point can change the data fit and

matching of adjacent stations along a profile. Also, when deconvolving the system response improper synchronization can cause unpredictable results. The importance of proper synchronization is the main reason why the synchronization clocks have so many different outputs. To get a consistent record of the drift, the clock synchronization must be recorded in the morning and the drift at night. When using a clock for the first time during a survey it may also be advisable to record the drift of the clock just before synchronizing it. This way one can observe the aging of the crystal oscillator and retune the clocks before failures occur. A drift between two clocks in the range of 1 to 2 ms over a whole day is reasonable.

When recording the clock drift, one must make sure that the same trigger source is used for the measurement in the morning and also in the evening. Figure 5.31 is a block diagram showing how the clocks are connected to the acquisition system. The recording of the trigger signal with the remote unit of the same clock allows you to determine the delay between the time when the clock triggers and when the remote unit receives the trigger. This delay is caused by software and digital connections. The recorded signal is then used as reference to the signal from the second clock which allows you to determine the drift. When storing the records make sure you use a logical name assignment for the file and data such that you can find the records later for statistics. An example for a clock drift record sheet is given in appendix 3.

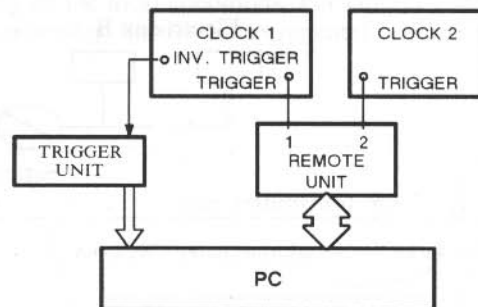


Fig.5.31: Block diagram of the daily synchronization control setup.

Measuring the System Response

One of the important tasks during a field survey is the careful record keeping of which analog filters are used at each station. The system response must be measured for each of these settings in order to remove the distortion due to the field system itself. The removal of the system response is done by deconvolution and was described earlier. In general, there are two different procedures which allow to obtain a careful estimate of the effect of the recording system.

The first procedure can be done in the laboratory and is sufficiently accurate, if the transients are long enough (i.e. longer than 1 second) and the ramp time of the trans-

mitter is sufficiently short. Another alternative to this procedure can be done in the field using the transmitter switching unit (switchbox) to put a calibration signal into the analog electronics. The output of this first setup is equivalent to the current output in the field under the assumption that the switching characteristics do not vary much under load (which we found to be true for most switchboxes). The two switching units which are responsible for the current reversing are connected to a clean direct current power supply (a battery) in such a fashion that they simulate the output current wave form. A sketch of the system component setup is shown in figure 5.32. The output from the calibration gear is fed into the preamplifier and from there via the amplifier

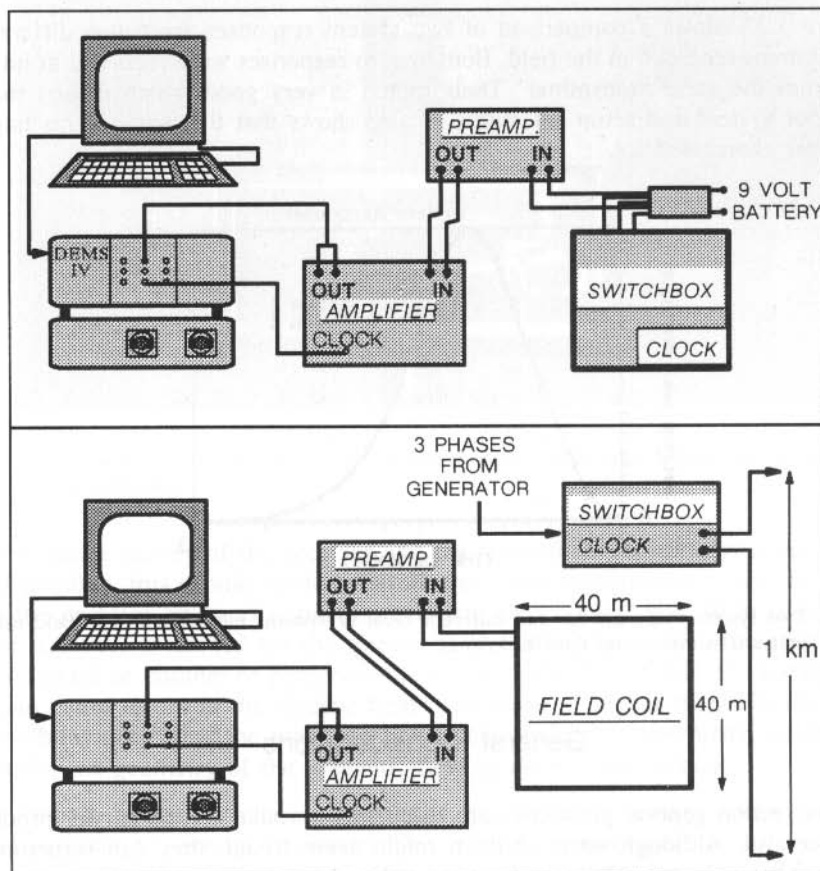


Fig. 5.32: System setup of the LOTEM equipment to record the system response. The top shows the setup using only the switchbox which is done in the laboratory and the bottom shows the setup including the entire system.

directly into the digital data acquisition system. The step output is being recorded in the same fashion as a transient, stacked and stored onto disk. Later, this output is

differentiated, filtered, and windowed for deconvolution of or convolution with the system response.

The second procedure is similar to the first, except that now the entire system including the transmitter switching time (ramp time) including the electrode plants is taken into account. A system setup is displayed in figure 5.32 (bottom). The receiver in the field is placed directly next to the transmitter allowing you to record solely the system response of the transmitter. We recommend trying both methods in the field, and selecting the more stable method for each particular survey. It has also been our experience that for current controlled transmitters and short (less than one second) the second procedure is more reliable.

Figure 5.33 shows a comparison of two system responses from two different receiver systems recorded in the field. Both system responses were recorded at different times from the same transmitter. Their match is very good which means that the transmitter system and setup are stable. It also shows that the two systems have the same filter characteristics.

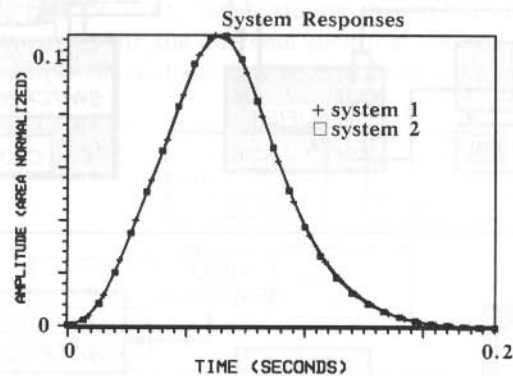


Fig.5.33: Two system responses for two different receiver systems measured in the field using the entire transmitter and receiver system.

General Considerations

In this section general guidelines are discussed to make a field survey productive and successful. Although some of them might seem trivial, they can sometimes be crucial for the success or failure of a survey. Emphasis is given to safety and smooth logistics. On the transmitter site extreme care is required because the high current (several hundred Amperes) and the high voltages (500–800 V) can easily injure a person. Apart from the safety features, one should also have additional staff to watch the transmitter wire and electrodes. When laying out the cable in the morning nobody should be near the wire on the back of the truck because the wire can make loops which could hit a person or in the worst case pull him/her off the truck. For pickup of

the wire cable, winding devices called spitters can be very helpful because they allow the wire to be picked up at 10–15 km/h speed. A picture of such a cable winding device (spitter) is shown in figure 5.34. Using a spitter rather than a cable reel avoids the cutting and splicing of the heavy transmitter wire which takes time and creates possible error sources.

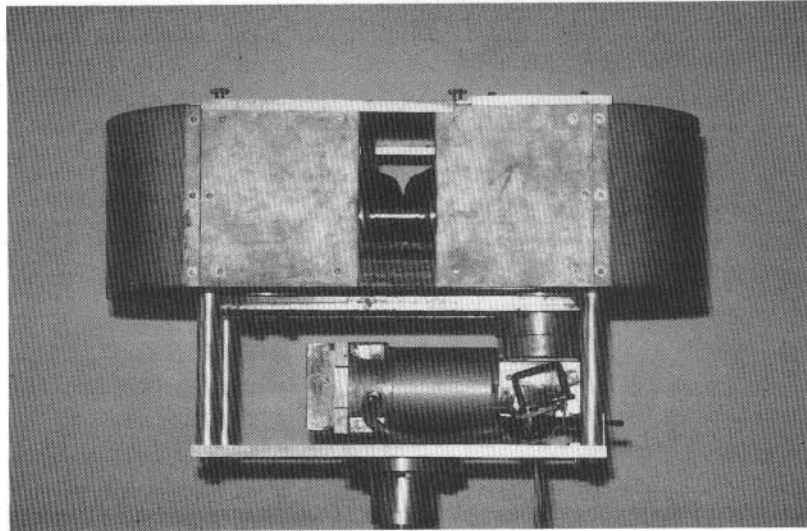


Fig.5.34: Cable winder ("spitter") which permits the pick-up the 25 mm² transmitter cable (1–5km) in ten minutes.

The accurate survey of the receiver and the transmitter coordinates is very important. If possible, this should be done before the actual measurement time. In general, unless the problem on hand requires otherwise, an accuracy of ± 10 m is sufficient. Greater accuracy is needed for the directions of the electric fields. The electric field dipoles should be parallel or perpendicular to the transmitter within 1° . Larger deviations can cause errors in the electric field calculation of higher than 5%. Because of the possibility correcting the magnetic fields using the *calibration factor*, as described previously, the geometry of the magnetic field sensors is less critical.

For smooth operation it is recommended that for each survey a task list as described in table 5.1 should be made. This allows the field staff to concentrate on problem solving rather than remembering what they could forget. To avoid unnecessary down times constant radio communication between transmitter and receiver is highly recommended.

Table 5.1: Task list of the daily routine tasks of a LOTEM crew.

MORNING:

- ☐ Synchronize receiver and transmitter clocks
- ☐ Get receiver coordinates for the day and possible transmitter current
- ☐ Check receiver for completeness and charging status
- ☐ Fuel check, radio check, map check

EVENING:

- ☐ Transfer data,
- ☐ Check coordinates of receiver sites and transmitter currents
- ☐ Is the system response available?
- ☐ Measure clock drift
- ☐ Charge all batteries
- ☐ Do all bookkeeping including field log
- ☐ Data backups

SURVEY TECHNIQUES

Different survey techniques for single site and multichannel systems are sometimes required for the selection of the survey task. The objective of the different field layouts is always to get as much data as possible with the best resolution. Further, a different noise cancellation technique, the local noise compensation technique (LNC) will be discussed because one of the key tasks is the improvement of the signal-to-noise ratios. The latter can be obtained by either increasing the signal or reducing the noise. An increase in signal can be achieved by an increase of the transmitter current. However, a current increase by twofold increases the generator power and fuel consumption by a factor of four. The same results can be obtained by decreasing the noise by only a factor of two.

Single Site Field Procedures

For single site systems one distinguishes between continuous electric field measurements and continuous magnetic field measurements (see figure 5.35). For the latter one or more magnetic field components are being measured at every site, while for the continuous electric field measurements the magnetic field components are only being measured every other site. The decision which one of the two modes to use is based on the exploration target. If the target is very conductive in a moderately resistive sedimentary environment (average resistivity: 5–10 Ωm), the magnetic field components are sufficient for the target resolution. In this mode the electric fields should be

measured every other station only to make sure that no obvious 3-D structure distorts the interpretation. Crosschecks of this are being done by using the electric fields for dipole-dipole mapping and the magnetic and electric field joint inversion. The results from this should give a clear indication about the complexity of the interpretation. When preliminary field results indicate that the subsurface can be sufficiently imaged with the magnetic fields, the distance between the electric field site can be increased. Under no circumstances should the distance between the magnetic fields be increased because this could result in the missing of a geologic feature as illustrated in figure A.7.1.

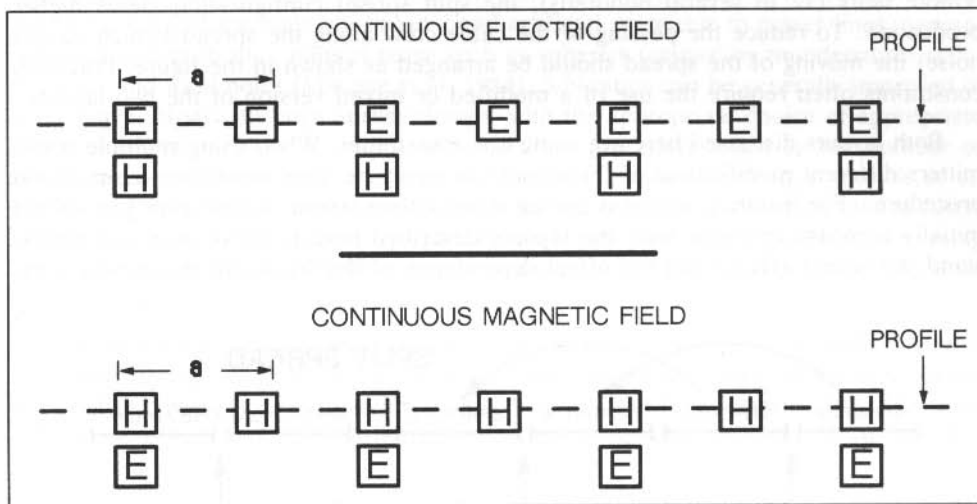


Fig.5.35: Receiver site for single site systems for continuous electric field and continuous magnetic field measurements.

The distance, a , between the sites is always a compromise between productivity and lateral resolution. We found for targets at a depth of 1 to 4 km, a distance between sites of 250 m to be the most reliable one. Larger distances often cause problems in the correlation of the results between adjacent stations and make the interpretation very lengthy and expensive.

When the target is more resistive, it is preferable to use the continuous electric field mode, because its electric field measurements are more sensitive to resistive structures. However, in this mode one must record the magnetic component at every other station to be able to correct for static shifts in the electric field.

Although novice operators always think differently, the production can be significantly increased by laying out the magnetic field receivers and electric field electrodes beforehand. The receiver operators should restrict themselves only to the recording and not handle the sensors themselves. A minimum production increase of 30% is not unusual when using this leapfrogging technique.

Multichannel Field Procedures

Using a multichannel system is very similar to carrying out a seismic survey. The maximum number of remote units is usually six given a 12 channel system. Figure 5.36 shows a split spread setup and a roll along layout for the multichannel system. For a small number of remote units the roll along technique provides higher productivity and also yields a higher number of vertical stacks at the overlap. When using more remote units (12 to several hundreds), the split spread configuration yields higher production. To reduce the passing of the cable crew along the spread (which causes noise) the moving of the spread should be arranged as shown in the figure. Practical constraints often require the use of a modified or mixed version of the two layouts.

Both layouts discussed here are using one transmitter. When using multiple transmitters different modification of the layout can easily be done similar to seismic field procedures. For instance, you may use an inline-offset layout. In that case you should initially compare this type with the layouts described here to make sure you understand the lateral effects and the offset dependence of the signal for the survey area.

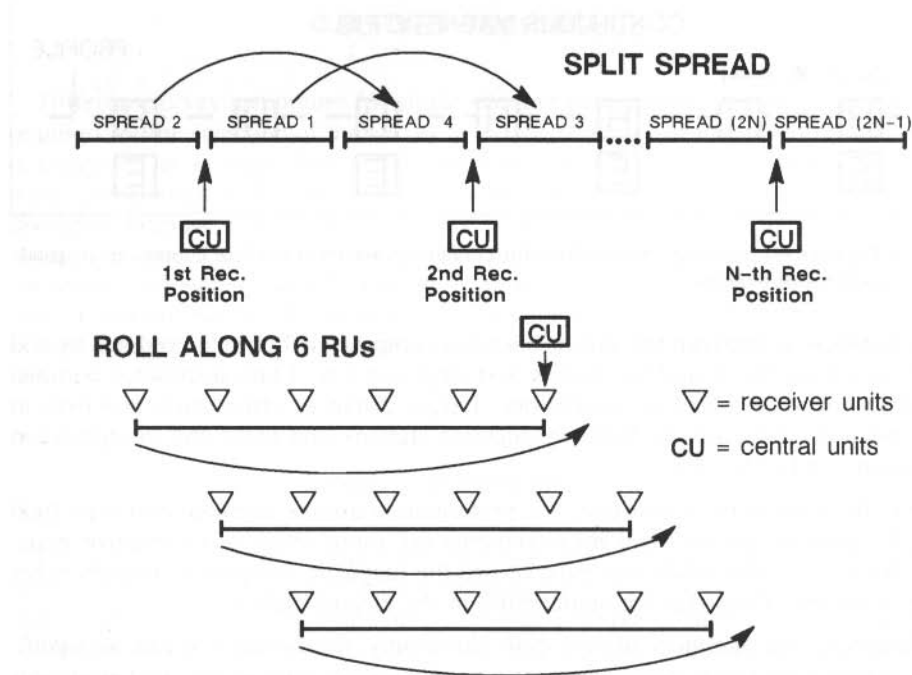


Fig.5.36: Multichannel layout for split spread and roll along configurations.

Local Noise Compensation Technique

One of the practical problems for all electromagnetic methods is the improvement in signal-to-noise (S/N) ratios, the objective being to achieve a higher data quality and to increase the depth of investigation. A way of improving the S/N ratios is to utilize artificial EM fields as done in frequency and transient EM (TEM) sounding methods (Nekut and Spies, 1989). Under the assumption that instrument noise of modern equipment is small and geologic noise is part of the information desired, the main problems for EM methods are broad-band artificial noise due to power lines, generators, railroad grids etc., natural noise such as spherics (caused by thunderstorm activity, etc.) and wind noise (Macnae et al, 1984). S/N ratios can be generally improved in three ways. Firstly, through survey design, with the appropriate choice of appropriate transmitter and receiver locations, of acquisition procedure (such as the number of single records acquired for stacking), and of the stacking technique (Strack et al, 1989). Secondly, in very noisy environments the noise can be reduced by analog filters implemented in the acquisition system and the signal can be increased by increasing the transmitter moment. Thirdly, after data acquisition the S/N ratio can be improved by digital data processing techniques.

Assume that we want to increase the S/N ratio by a factor of ten by either increasing signal strength or reducing the noise. A signal strength increase of ten requires the transmitter power or the acquisition time to be increased by a factor of 100. The same S/N improvement can be achieved by reducing the noise by a factor of 10 (see also Spies, 1988).

For controlled source EM methods, stacking is the standard noise reduction method. In very noisy areas extensive stacking is needed which requires long acquisition times. Analog filters generally cause problems due to their influence on the usable part of the signal spectrum. Thus, one must find new field procedures for very noisy environments to improve productivity and to increase the S/N ratio at the same time. In the magnetotelluric method (MT) the remote-reference technique is used to overcome the noise problem, provided that the noise in the MT array is uncorrelated with the noise in two additional components of the MT signals measured at a remote site (Gamble et al, 1979; Clarke et al, 1983).

Recently, for the in-loop transient electromagnetics (TEM) the *local noise prediction filtering* (LNPF) has been developed for noise reduction (Spies, 1988). LNPF is based on simultaneous measurements of three orthogonal magnetic field components at the same site and the calculation of a time domain filter which predicts the vertical noise component from the two horizontal components. This noise can be subtracted from the measured vertical component in the subsequent processing.

The *local noise compensation* (LNC) technique was developed specifically for the long-offset transient electromagnetic sounding (LOTEM). LNC differs from the LNPF technique in that a base station is used as reference site. Unlike LNC to the remote-

reference MT technique, where the noise must be uncorrelated, the LNC requires the noise to be correlated. Since the validity of this premise varies significantly with most noise sources, environments and geology, it must be tested on the beginning of the survey. The objective for the development of the LNC technique was to provide a noise cancellation technique for a multichannel TEM acquisition system with dense station spacing.

In very noisy areas a large number of single records must to be acquired to get sufficient data quality, especially, if the noise characterization is similar to the one of the signal. A low productivity results because of long recording time. Sometimes even with a high number of stacks the data quality is poor, as the noise characteristic is not strictly sporadic or periodic but a combination of both. When the noise is specific to the survey area, often no filters for the data set are available to the interpreter. Thus, the LNC technique was developed to reduce the number of poor data sets containing the above type of noise and to allow the application of LOTEM in very noisy environments, where it would be otherwise not possible.

The principle receiver setup is shown in figure 5.37. The transmitter is assumed to be several kilometers away. The base station is fixed and measurements are taken at this base station all day long. To take advantage of the correlated noise, measurements are made simultaneously at the various other mobile stations. These mobile measurements are much shorter in acquisition time, because fewer transients are recorded. During the subsequent signal processing the actual noise at the base station is obtained and thus – when the noise is spatially constant – also at the mobile stations. The noise from the base station at any particular time is then subtracted from the data, recorded at the mobile station at that particular time.

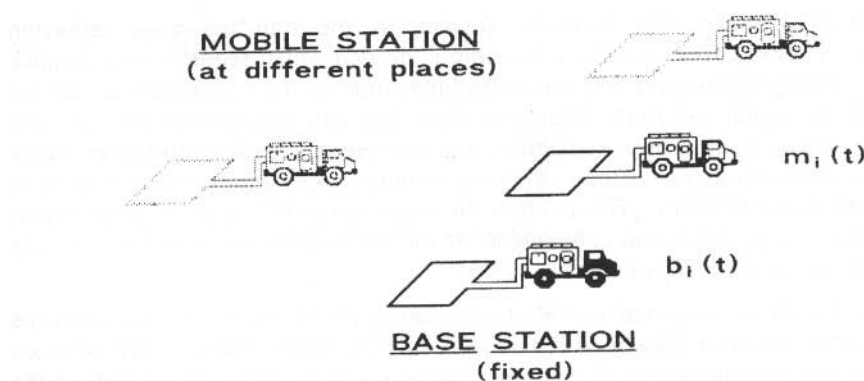


Fig. 5.37: Basic field setup for the LNC technique using two receivers (after Stephan, 1989).

Since, with controlled source EM methods the transmitter signal is present over the entire survey area, it is not possible to observe the noise at one receiver site while a signal is observed at another. In order to get only the noise at the base station, the following procedure has to be applied: initially, the stack of the base station data gives

a very smooth stacked transient S , because a very large number of single signals $b(t)$ exist as a result of the long acquisition time. This final stacked transient is termed 'base stack' and is essentially the local signal as shown in figure 5.38. Now, this accurate base stack is subsequently subtracted from each single record $b(t)$ at the base station and the noise remains. An example for this noise is shown on the first row in figure 5.39. The left column in the figure shows an example of sporadic noise and the right side is an example of periodic noise. The two recordings are only 3 minutes apart demonstrating the time variability of the external noise.

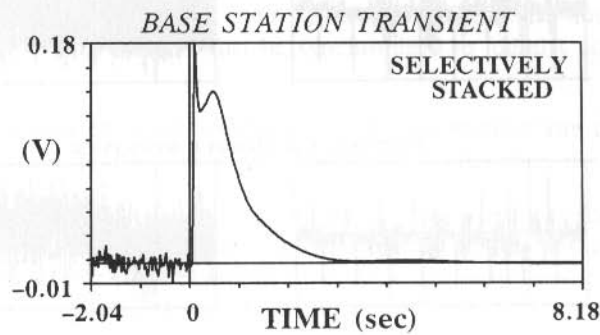


Fig. 5.38: Selectively stacked transient at the base station, which is termed 'base stack' (after Stephan and Strack, 1991).

$$n(t) = b(t) - S. \quad (5.1)$$

Once the noise $n(t)$ at the base station is known, this noise can be subtracted from the single records $m(t)$ of the mobile stations (the second row of figure 5.39) and a noise-compensated signal $c(t)$ can be calculated by

$$c(t) = m(t) - n(t). \quad (5.2)$$

This noise-compensated signal is shown at the third row of figure 5.39. In both cases the noise can be successfully reduced.

Sometimes, under certain field conditions (i. e. different temperatures, vibrations, etc.), the synchronization clocks of the mobile and the base receiver systems drift apart a few milliseconds over the whole day. This time drift results in a phase shift of the periodic noise. In this case a simple point by point subtraction can increase the noise. To overcome these difficulties the clock drift is corrected by a time shift derived from the cross-correlation

$$CC(T) = \sum_i m_{i+1} n_i \quad (5.3)$$

as a function of the time displacement T between the mobile station signal and the noise of the base station. If the cross-correlation has its maximum for a certain dis-

placement T' , the noise in the two signals should be in phase. If now the noise of the base station is shifted by the displacement T' , the clock drift is corrected without changing any of the timing reference of the mobile station data.

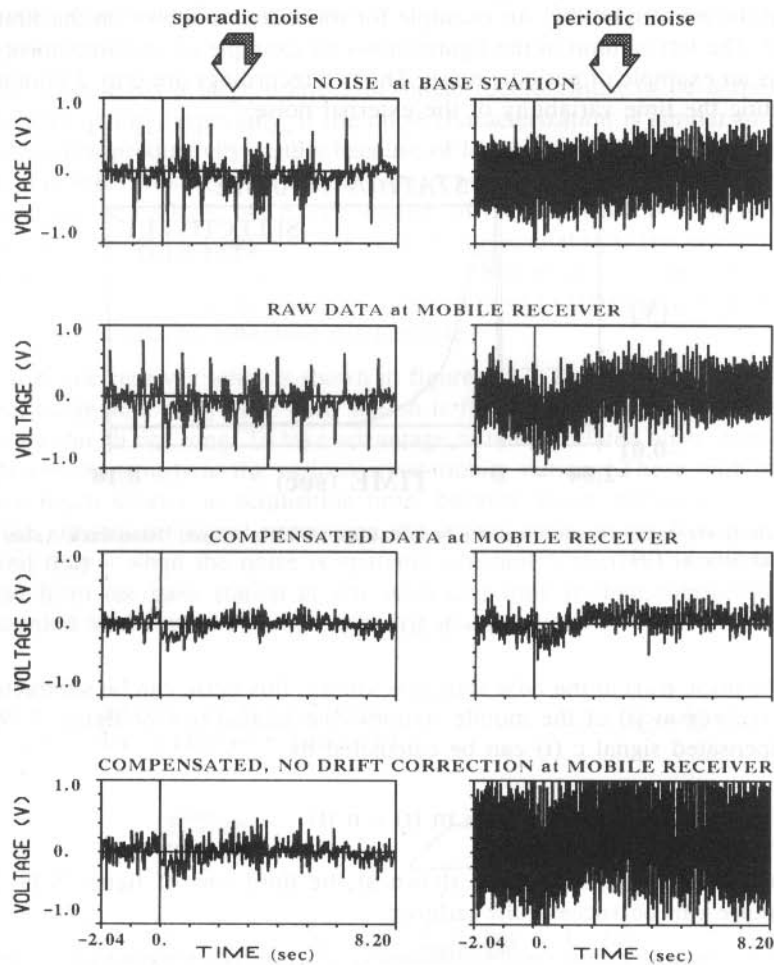


Fig. 5.39: Two examples of the processing sequence for the LNC technique (left column: sporadic noise; right column: periodic noise; data taken in Germany). Top: noise at the base station. Second row: raw transient of control measurement with a different receiver system. Third row: noise-compensated data. Bottom: compensated data without clock drift correction (after Stephan and Strack, 1991).

To illustrate the effect of clock drift, two compensated signals without clock drift correction are shown in the bottom row of figure 5.39. The periodic noise has been amplified (right side) and even the sporadic noise (left side) could not be as well

reduced as shown in the third row of the figure. Thus, if this clock drift correction is routinely done before noise compensation, the noise compensation will work well. With these noise compensated signals the routine subsequent processing can be done.

To apply the LNC, the following conditions must be met and tested at the beginning of the survey:

- The noise must correlate over a certain range around the base station and this regional noise can not easily be reduced by standard processing.
- The receiver systems at the base station and at the surrounding mobile stations must be identical in their system characteristics, and the recording times in the data header must be synchronized to identify corresponding records.
- The very localized noise belonging to only one receiver site (i. e. wind noise or noise from nearby power lines) must be smaller than the regional noise.

The correlation of the noise in the survey area is the principal criterion needed to check whether or not the LNC can be applied. The last two conditions are technical problems or a task of the field planning (i. e. to avoid power lines). When using a multichannel system with central synchronization the second condition no longer applies.

Signal processing tests, i.e. with synthetic noise, were not considered useful to rigorously prove the methodology, because they can not simulate the complexity of problems occurring under real field conditions. Therefore, two survey areas with noisy environment were chosen to test the technique.

In the case histories below the measurements were done to check the applicability of the method. In each new survey area a control measurement is carried out in parallel at the site of the base station. It is observed with a completely different acquisition system using a second receiver coil laid on top of the base station coil. The objectives for this control measurement are as follows: First, to verify that the receiver systems have identical noise characteristics and second, to verify that the LNC technique yields an improvement in the S/N ratio of stacked data (and in interpretation). If this test is positive the next step is to move the mobile receiver several kilometers away (we have tested up to 4 km) to define the range where the LNC technique is applicable. Case histories are shown below for a survey area where LNC does not increase the S/N ratio of the stacked data although it apparently improved the single records, and for an area where LNC is successful.

The first field test was carried out during 1988 at the University of Cologne test area in Germany (Stephan et al, 1991). This is an extremely noisy area north of the Rhine-Ruhr industrial district with mainly manmade noise caused by nearby dense industrialization. Measurements undertaken at the beginning of the survey showed that the noise looked very similar at receiver sites several hundred meters apart.

The first LNC step was to process the base transient. Although a large number of stacks were observed, the base stack could only be obtained as smooth as shown in

figure 5.38 after prestack filtering and smoothing. Even with extreme care it could not be guaranteed that the shape and amplitude of this base transient was not distorted by these filters. Consequently, the calculated noise at the base station could still contain some signal and the compensated data could be influenced by this signal.

For this survey, the control measurement (see figure 5.39) took only 30 minutes. In this area the noise characterization greatly varied with time, but the high frequency noise dominated. Thus, the normal prestack processing of these data such as low pass filtering, notch filtering and time variant smoothing and the selective stacking method (Strack et al, 1989) could reduce the noise level to such a degree, that the LNC technique yielded no further improvement in the quality of the stacked data. Figure 5.40 shows the comparison between the uncompensated (upper frame) and the noise compensated (lower frame) data of the control measurement. The data quality is low in both cases and a decision can not be drawn as to which data set should be used for further interpretation.

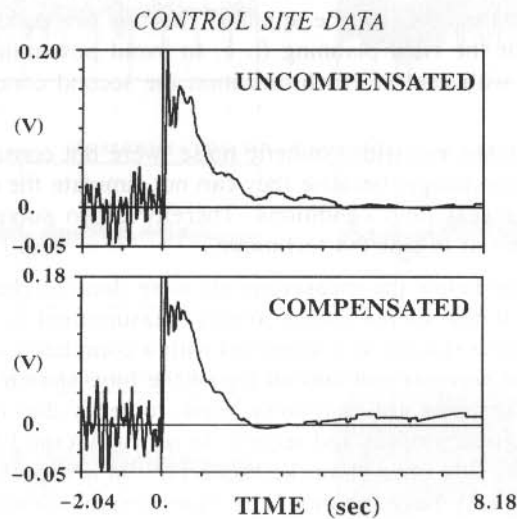


Fig.5.40: Comparison between uncompensated (upper frame) and noise compensated (lower frame) stacked transients of the control measurement at the base station (German survey) (after Stephan and Strack, 1991).

Although the LNC could successfully reduce the noise level in the single records (not shown) of the two examples above, there is no improvement visible in the stacked data. The same results were obtained at other mobile measurement sites located around the base station. Thus, the survey area was not suitable for the application of the LNC technique.

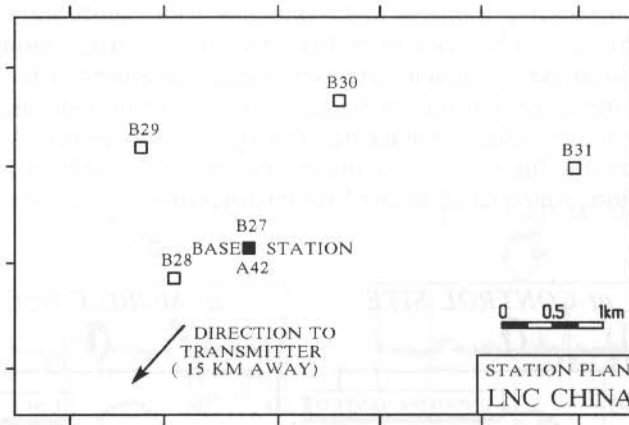


Fig.5.41: Receiver location map of the field test in China (after Stephan and Strack, 1991).

The second field test was carried out in a coal mining area in the Peoples Republic of China in 1988. In this area the mining equipment produced very strong sporadic noise which was very coherent over the entire survey area. The site location map of

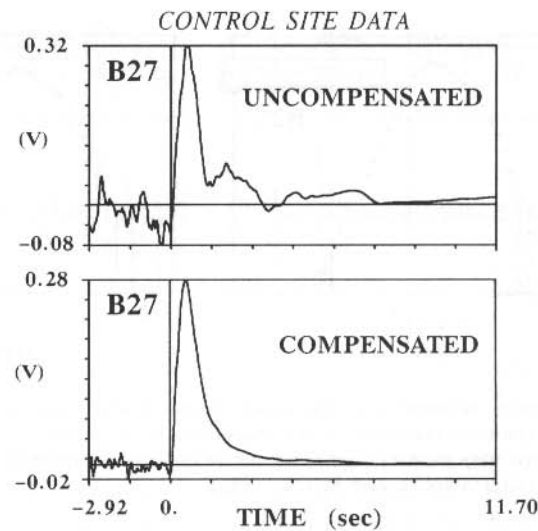


Fig.5.42: Comparison between uncompensated (upper frame) and noise – compensated (lower frame) stacked transients of the control measurement at the base station (China survey) (after Stephan and Strack, 1991).

these test measurements is shown in figure 5.41. Again, first a control measurement (location B27) at the base station site was processed. The uncompensated (upper

frame) and the noise compensated (lower frame) stacked transients are shown in figure 5.42. The compensated transient looks smoother with significantly improved S/N ratio. The advantage of LNC can be better seen after transformation to apparent resistivities in bilogarithmic domain. The early stage transforms of the two curves in figure 5.42 are shown on the left in figure 5.43. The error bars are the standard deviations derived from selective stacking. The noise-compensated data have much smaller error bars and the curve looks much smoother. Especially at later times, the range of data points, which could be used for interpretation, is increased by about one decade in time.

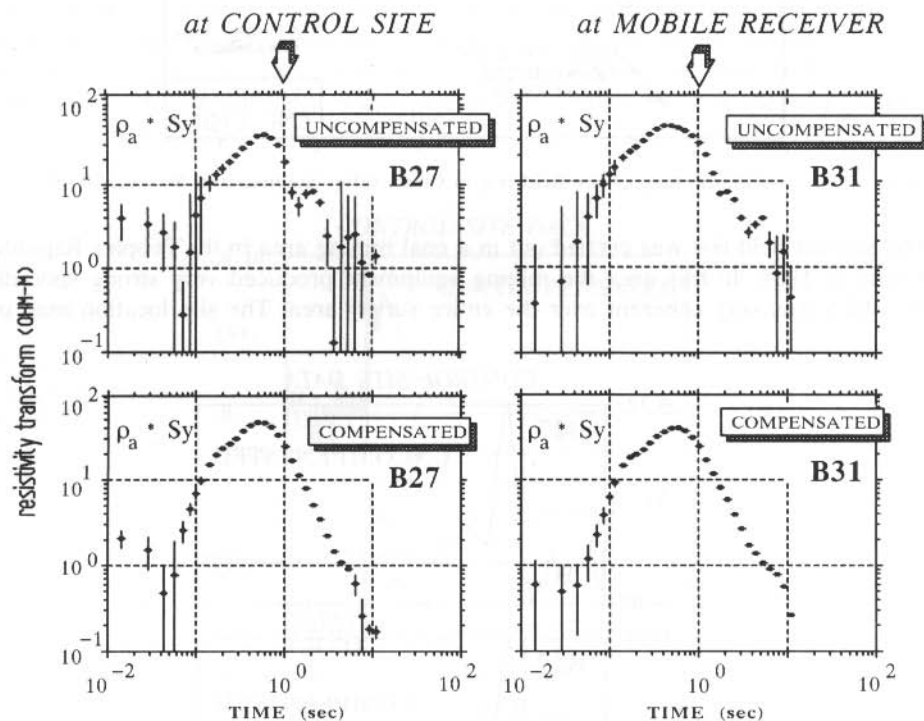


Fig. 5.43: Comparison between uncompensated (upper frame) and noise - compensated (lower frame) resistivity transform of two measurements in China. Left side: control measurement B27 at the base station. Right side: mobile receiver station B31, 3.3 km away from the base station (after Stephan and Strack, 1991).

On the right of figure 5.43, a comparison between noise-compensated and uncompensated data is shown for the mobile station B31 located 3.3 km away from the base station. Even at this distance from the base station the LNC works very well. Figure 5.44 shows four single records from station B31. The original raw data are displayed on the left column, the noise-compensated data on the right column. Most of the high amplitude noise could be reduced. Only a few residual high amplitude spikes remain.

In addition, high frequency noise of low amplitude is increased, which is incoherent noise (i. e. wind noise) at the base station or the mobile site. Another effect increasing the high frequency noise is clock drift less than one sample interval, which can not be corrected by a time shift with respect to the cross-correlation maximum. However, this kind of high frequency noise can easily be reduced in the subsequent data processing such as low pass filtering, smoothing and stacking.

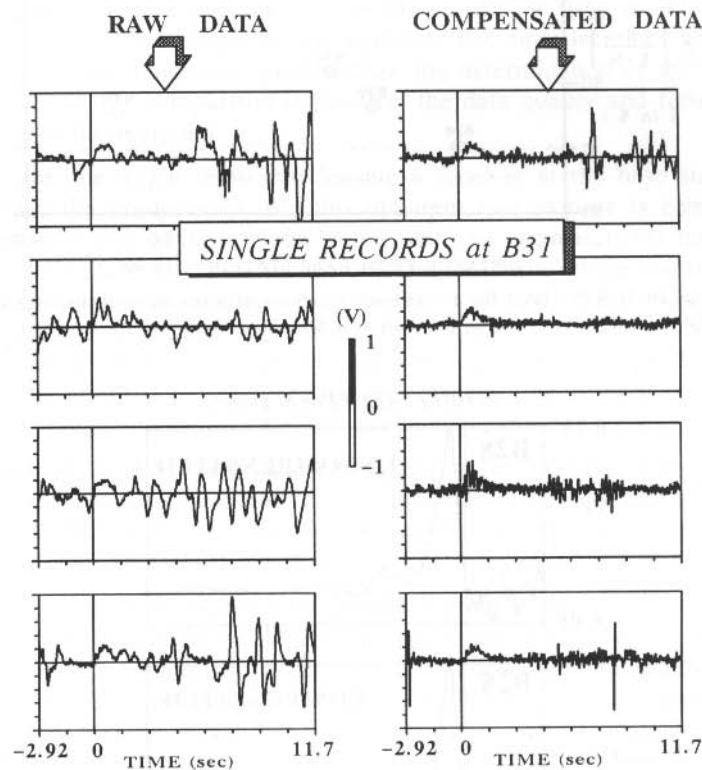


Fig.5.44: Comparison between four examples of the raw data (left column) and compensated data (right column) of the mobile station B31 (after Stephan and Strack, 1991).

For quantitative evaluation of the noise reduction, the $S/(S+N)$ amplitude ratio is used. The $(S+N)$ are the maximal amplitudes of each individual record averaged over all records of each station, because the individual records are dominated by noise. This $(S+N)$ is calculated for the raw data and the noise-compensated single records. The signal S is the maximal amplitude of the final stacked transient. In figure 5.45, the improvement of this $S/(S+N)$ ratio for all stations is plotted as a function of distance to the base station. For the control measurement B27 at the base station an improvement of 118 % could be achieved. For the other stations except of station B28 the improvement is between 26 and 60 %. The station B28 has to be considered sepa-

rately, because at this site additionally high amplitude local noise from a telephone line was present. For this type of localized noise the LNC technique will not yield much better $S/(S+N)$ ratios. But even at this station the time window of reliable data, which could be used for later interpretation, was increased (compare with figure 5.46).

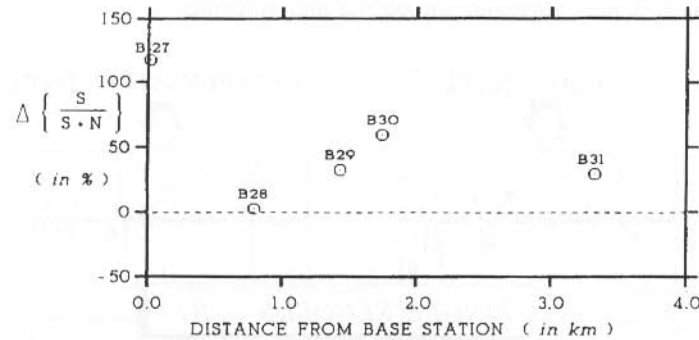


Fig. 5.45: Change in $S/(S+N)$ ratio for all receiver locations as a function of distance from the base station (China survey) (after Stephan and Strack, 1991).

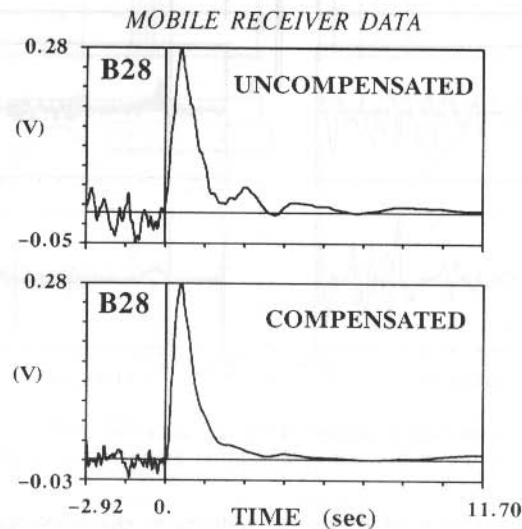


Fig. 5.46: Comparison between uncompensated (upper frame) and noise compensated (lower frame) stacked transient of site B28, which was disturbed by telephone line noise (after Stephan and Strack, 1991).

In the first case history the noise could be successfully reduced in the single records, but there was no increase in data quality after stacking in comparison to data without LNC application. Standard filtering and selective stacking were robust and powerful enough for this mainly periodic, only sometimes sporadic noise. The LNC

worked well on the raw data, but the amount of interpretable data was not increased for this survey area.

For the second case history, the LNC technique reduced the noise to such a degree that additionally one more decade in time of data was available for interpretation. This result could be obtained at all mobile stations, which were as far as 3.3 km away from the base station.

The two examples show that the LNC technique can be used in selected areas to increase the data quality. Comparing the signals at two close locations with respect to coherency of sporadic noise will quickly allow the determination of the suitability of the survey area. If this comparison is positive, the data quality and furthermore, the productivity, can be increased.

At first sight one might think that leaving a receiver at the base station all day would decrease the productivity. But this apparent loss in time is compensated by shorter acquisition time at the various mobile stations, because fewer transients have to be recorded for stacking. Thus, for the test area in China, where two receivers were used, the same number of stations were observed with LNC using a base station and one mobile receiver as with two mobile receivers and no LNC. Also, LNC yields one stacked transient at the base station with an extremely good data quality because of the high number of single records used for selective stacking. If more receiver systems are used with a multichannel system, the productivity can be increased even further.

A drawback of the LNC technique can be the slight increase of processing time, because first the base transient has to be completely processed, the noise has to be calculated and LNC applied to the mobile stations, before standard processing can start. However, the increase of available computation power removes this drawback.

The LNC technique should only be applied in areas where the regional correlation of noise is proven. This must be done at the beginning of each survey. Furthermore, extreme care must be taken with calculation of the base stack to obtain a noise-free signal. If this is not obtained, the noise that is subtracted from the mobile measurements may contain some signal and the interpretation results could be false. It has been our experience that LNC never decreases the quality of the data. In some cases – as in China – it was the only available remedy easily implemented in the field to obtain useful data.

SUMMARY CHAPTER 5

In this chapter, the general system design concept for deep transient electromagnetic sounding systems are outlined. A deep transient EM or LOTEM system consists of independent transmitter and receiver systems. Both are linked using high precision remote synchronization clocks. The acquired field data is generally interpreted using a mobile processing center at the base camp. This allows a very fast turn-around and continuous quality control of the survey data.

When preparing for a LOTEM field survey, one needs to consider very carefully the preparation of the transmitter electrodes. In order to inject a maximum current into the subsurface the preparation should be done using a mixture out of salt (or potassium), lime and soil directly around the electrode plates. Before starting the transmitter system the transmitter can be checked out using a battery. After preparing the transmitter and getting the transmitter operational the deviation of the current switching from a perfect square wave should be measured and included in the system response. Combining the transmitter system response with the receiver system response gives high quality data for later interpretation.

The survey techniques can be classified as single site survey procedures and multichannel procedures. For both setups the main objective is the highest possible data production to obtain a higher data redundancy and better quality data. To improve the data quality even further, one can use noise reduction techniques which permit the improvement of the signal-to-noise ratio significantly. Initial field tests have shown that *local noise compensation* can extend the signal by one decade, which would be equivalent to increasing the transmitter power by a factor of one hundred. Considering all these different field configurations one can very easily deploy multichannel acquisition systems and obtain data volumes and productions similar to those of a seismic survey.

PROBLEMS CHAPTER 5

1. Please list the principle building blocks of a LOTEM field system. Separate between transmitter and receiver system.
2. Why is the 'bipolar continuous' waveform the most used one?
3. What forms of synchronization between transmitter and receiver do you know (including the ones described in this chapter)?
4. Discuss the difference in dynamic range between DEMS IV and the TEAMEX. What are the consequences?
5. Explain the advantage of measuring the time derivative of the magnetic field using the DC-level.
6. What are the advantages in the noise reduction of the TEAMEX over conventional systems?
7. Please outline the setting up of a transmitter starting with the arrival on site and ending with the turn on of the current.
8. Explain the different concept in measuring the system response. How do they influence the processing and interpretation of the data?
9. Assume you have a 12 channel TEAMEX system and you would like to make sure that you have no gaps in the spread (RU fails while recording). How would you lay out the spread? Please use the maximum number of soundings as additional criterion.
10. How would you layout the spread if you wanted to do *local noise compensation* at the same time without losing production?

KMS Technologies – KJT Enterprises Inc.
6420 Richmond Ave., Suite 610
Houston, Texas, 77057, USA
Tel: 713.532.8144

Please visit us
<http://www.kmstechnologies.com>

This material is not longer covered by copyright. The copyright was released by Elsevier to Dr. Strack on November 5th, 2007.

The author explicitly authorizes unrestricted use of this material as long as proper reference is given.

KMS Technologies – KJT Enterprises Inc.

An EMGS/rxt-company

Chapter 6 Survey Feasibility Studies

extract from

Strack, K.-M., 1992, reprinted 1999
***Exploration with deep transient
electromagnetic:*** Elsevier, 373 pp.

This material is not longer cover by copyright. The copyright was released by Elsevier to Dr. Strack on November 5th, 2007.

The author explicit authorizes unrestricted use of this material as long as proper reference is given.

Chapter 6

Survey Feasibility Studies

This chapter describes two main tasks during the preparation of a LOTEM survey: *feasibility studies* and *survey design*. The same kind of work is done for both tasks but the aims are different:

The feasibility study determines whether or not a specific exploration problem can be solved with the LOTEM method. Once this is decided positively, the same tools that were used for the feasibility study are now used to design a survey and to optimize the survey parameters such as transmitter – receiver distance (offset) and time window for the data acquisition.

The first step is the construction of a simple geoelectric model consisting of layers with thicknesses and electrical resistivities assigned to each layer from a well log or other geophysical *a priori* information. Next, each of the thicknesses and resistivities is changed within a reasonable range. For each of the changes, LOTEM field data are simulated and compared. If the curves are different, then there is a chance to detect the changes and in many cases also the actual values of thickness or resistivity.

Two types of feasibility studies are shown for real field situations. The first case history is a synthetic example for a field situation from China where a thick carbonate unit at a depth between 4 to 6 km had to be resolved. The second case history uses real exploration data as input for an investigation in an production environment in Australia. The last case history considers the possible application of LOTEM to an exploration problem in Japan.

SURVEY DESIGN BASED ON WELL LOGS

The goal of the reduction of electrical logs to obtain a suitable model for the LOTEM method is:

Using the given detailed log of resistivities and depths (e.g. from well logs), derive geoelectric boundaries and equivalent resistivities such that they can be resolved with the LOTEM method.

- First, the emphasis should be on finding the simplest geoelectric model (least number of layers) that is resolvable with LOTEM and at the same time is the best representation of the geology.

- Second, you can incorporate other geophysical knowledge (such as structural information from seismic interpretation) to refine the layering and test the resolution using inversion techniques in your synthetic data.

In most cases there will be at least one well log of electrical resistivity available for the target area. Well logs have usually a much finer resolution of layers than can ever be expected from an electromagnetic surface method. In order to estimate the resolution capability of the particular surface method (in our case the LOTEM sounding method), the well log must first be reduced to an electrical model with only a few layers of different resistivities.

A reduction is basically an average and the way this average is calculated, introduces a bias into the subsequent resolution analysis. There are two ways to control this bias:

- Use simple layer equivalencing where the thickness of the layers is kept fixed and an average resistivity is being calculated. The procedure is designed so that the resulting reduced model is well adapted to the intrinsic resolution capabilities of LOTEM. This facilitates a subsequent resolution analysis greatly.
- In difficult cases, use an iterative procedure between layer equivalencing and forward modeling to optimize the reduction before you commence with the resolution analysis.

The following example illustrates the use of the layer equivalencing technique. We assume that a well log has already been blocked to reduce the number of data points normally contained in a digitized well log. The first blocking is usually done by maintaining the lithological boundaries as much as possible. Table 6.1 shows an example where from the well log the blocking was done based on the lithological boundaries. A graphic display of the blocked well log (squares) and the reduced models for a four layer and five layer case are shown in figure 6.1.

Table 6.1: Example for a simplified electric well log: resistivities, thicknesses and lithology.

Formation	Depth (m)		Resistivity Range (Ohm-m)		Average (Ohm-m)	Thickness (m)	Lithology
CRETACEOUS	0	- 101	20	- 100	30	101	SS
	101	- 285	33	- 86	50	184	SS
JURASSIC	285	- 335	35	- 230	100	50	marly LST
	335	- 1316	120	- 13000	3000	981	volcanics
TRIASSIC	1316	- 1700	200	- 800	600	384	SH, ANH
	1700	- 1750	15	- 60	50	50	SS
	1750	- 2050	400	- 2000	900	300	DOL, LST
	2050	- 2210	15	- 80	60	160	SS (target)
PERMIAN	2210	- 2480	100	- 600	150	270	SS (target)
PALEOZOIC	2480	- ...	20	- 2000	1500		granites

LST=limestone, SS=sandstone, DOL=dolomite, ANH=anhydrite, SH=shale

The values of depth and resistivity of the induction log are then used to calculate the *cumulative conductance*. The *cumulative* or *total conductance* of a layer-cake is ob-

tained from:

$$S = \frac{H_T}{\rho_{\text{average}}} = \sum_{i=1}^n \frac{h_i}{\rho_i} \quad (6.1)$$

H_T is the added thickness of all layers (total thickness), ρ_i and h_i are the resistivity and thickness of the selected piece of the layer-cake and ρ_{average} the average resistivity to be used in the modeling (Keller and Frischknecht, 1966). This resistivity is obtained under the assumption that the *total conductance* for the layers averaged remains constant. We obtain:

$$\rho_{\text{average}} = \frac{H_T}{\sum_{i=1}^n \frac{h_i}{\rho_i}} \quad (6.2)$$

Other ways of averaging such as using the *transverse resistance* or weights for the parameters can be applied, where necessary.

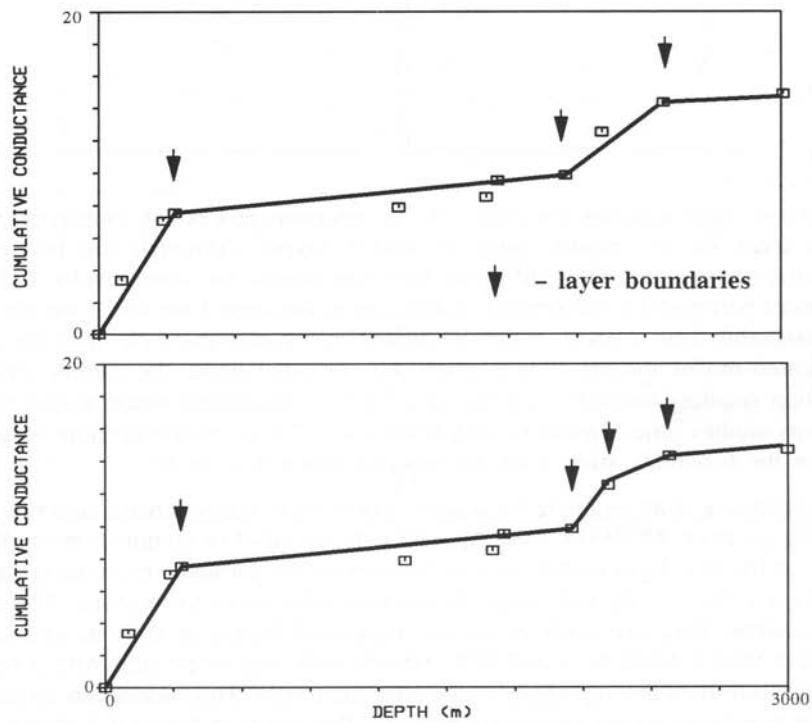


Fig. 6.1: Cumulative conductance for the blocked well log from table 6.1 for a four-layer model (top) and a five-layer model (bottom).

Most electromagnetic methods resolve just this function and not discrete layers of constant resistivity. The slope of this function is the resistivity and bends in the curve (if present) indicate layer boundaries. Reducing the well log further for use in LOTEM forward modeling consists in the following steps:

- Fit a few straight lines to this curve.
- Define the slopes of the lines as the resistivities of the layers.
- Define the intersections of the lines as the layer boundaries.

These steps can be done by hand or using simple computer programs. In table 6.1 the results of the coarse blocking of an electrical log is summarized. The lithology and resistivity ranges are also given to allow the interpreter to check the plausibility of the results. Table 6.2 lists the further reduced model obtained after layer equivalencing.

Table 6.2: Reduction models resulting from different degrees of reduction of the geoelectric model. Left: five-layer model, right: four-layer model.

5 LAYER MODEL			4 LAYER MODEL		
Layer No.	Resistivity (Ohm-m)	Thickness (m)	Layer No.	Resistivity (Ohm-m)	Thickness (m)
1	44	335	1	44	335
2	748	1715	2	748	1715
3	60	160	3	96	430
4	150	270	4	1500	
5	1500				

Figure 6.2 demonstrates the effect of the reduction process by displaying the synthetic curves for the models with 10 and 5 layers. Although the two modeled geoelectric sections are quite different, they give almost the same results. In fact, the differences between the two simulated data curves between 1 ms and 3 ms are outside the measurable time window. It will be difficult to resolve the difference between the complicated model and the simple model. On the other hand, the complicated model simulation requires much more CPU time for the calculation which would make the sensitivity studies time consuming and ambiguous. The normal procedure would be to continue the feasibility study with the reduced geoelectric model.

The following is an example for a case, where layer equivalencing and the forward modeling program MODALL (see Appendix 4) are used in conjunction to check the validity of the five-layer model. As can be seen on the cumulative conductance curves in figure 6.1, the two separate target layers have almost the same slope. The question arises whether they are resolved as two individual layers or only as one unit. An equivalent model could be found that contains only one target unit with a resistivity averaged from the two target layers (compare table 6.2). This model can be compared with the five-layer model previously derived. The result in figure 6.3 shows that the target is resolved only as one unit, because the curves using a five- or four-layer model cannot be distinguished.

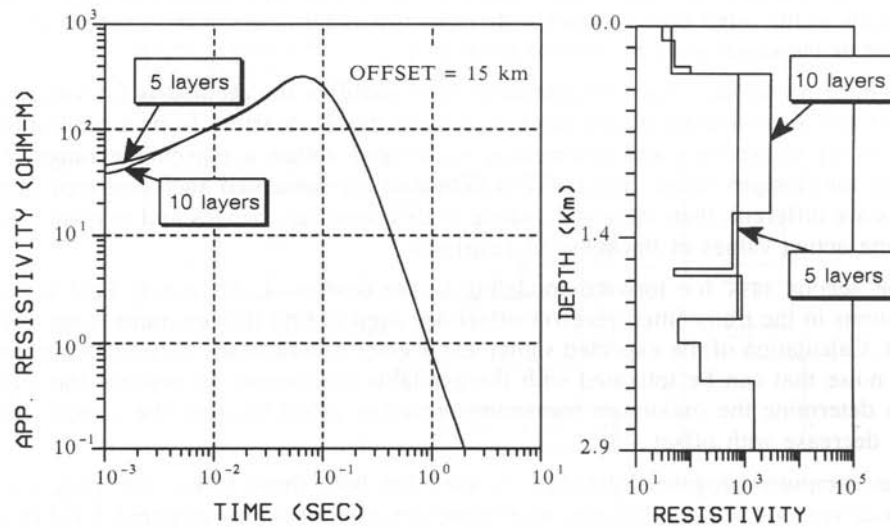


Fig. 6.2: Simulated LOTEM data for the blocked model without reduction (10 layers) in comparison with the reduced model (5 layers).

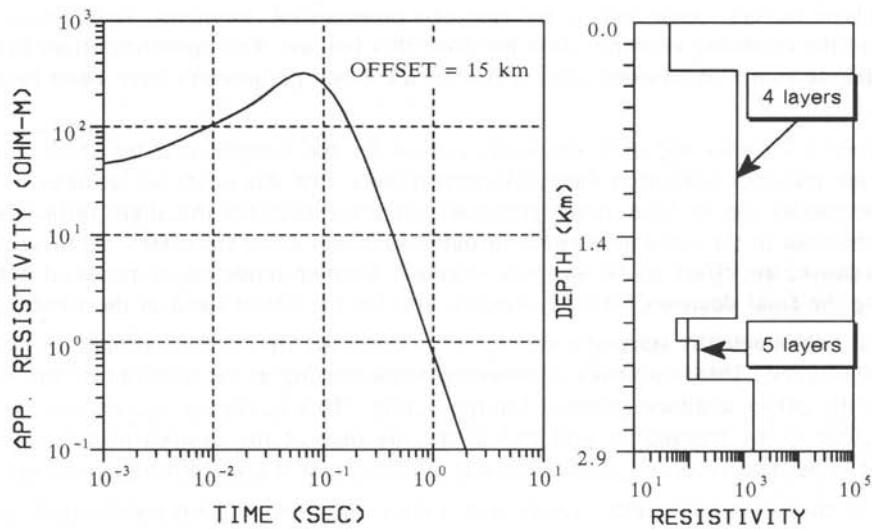


Fig. 6.3: Simulated LOTEM data for the two different reduction models (5 layers and 4 layers).

As consequence one should use a five-layer model for the sensitivity study because it is easier to assign realistic resistivity variations to each of the two geological target layers separately than to derive variations of the average resistivity of the combined units. The geophysicist/geologist must however keep in mind, that the variations he

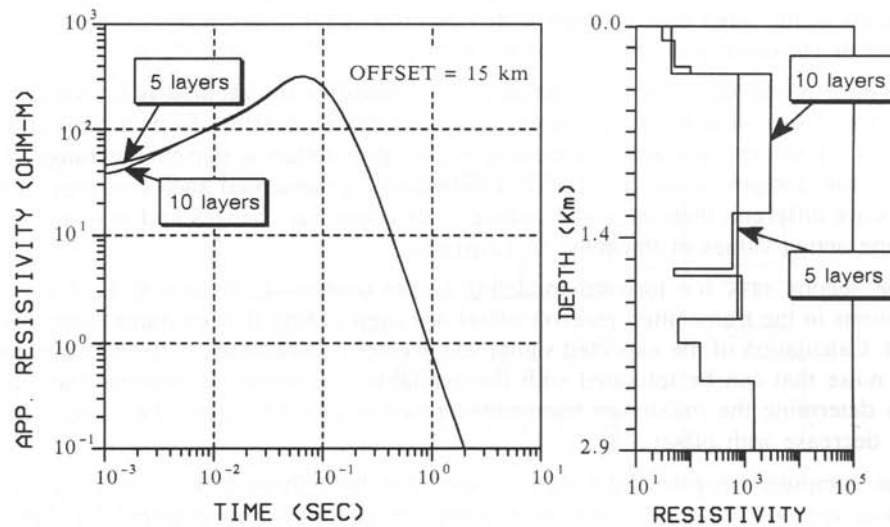


Fig. 6.2: Simulated LOTEM data for the blocked model without reduction (10 layers) in comparison with the reduced model (5 layers).

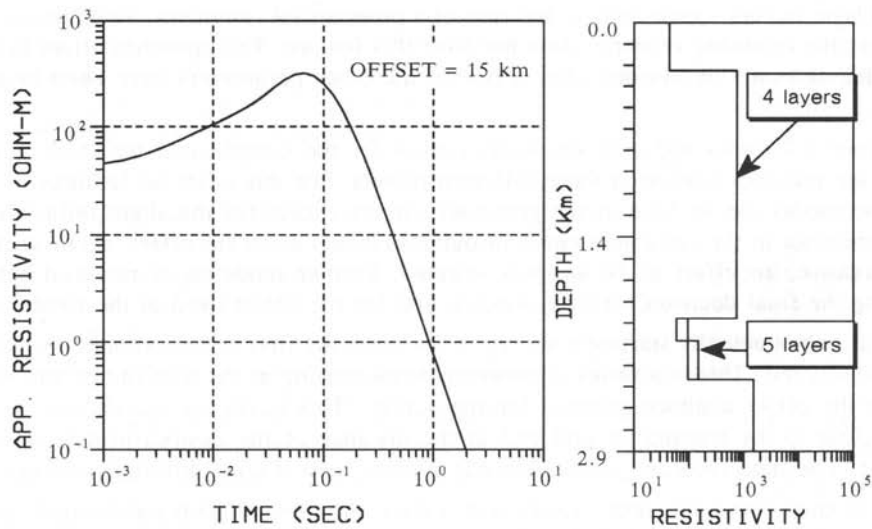


Fig. 6.3: Simulated LOTEM data for the two different reduction models (5 layers and 4 layers).

As consequence one should use a five-layer model for the sensitivity study because it is easier to assign realistic resistivity variations to each of the two geological target layers separately than to derive variations of the average resistivity of the combined units. The geophysicist/geologist must however keep in mind, that the variations he

introduces in one of the two target layers could just as well be replaced by similar variations in the other one. In other words: *the two target layers in this example are not resolved as individual units but only as a whole.*

Forward modeling is used to determine how sensitive the method is for variations of thickness or resistivity of any layer in a given model. Starting from a basic model each of the thicknesses and resistivities is changed within a reasonable range. For each of the changes, noise-free LOTEM field data are simulated and compared. If the curves are different, then there is a chance of detecting the changes and in many cases also the actual values of thickness or resistivity.

The second task for forward modeling is the design of the actual field survey. Variations in the transmitter-receiver offset are used to find the optimum value of the offset. Calculation of the expected signal levels gives a limit to the natural electromagnetic noise that can be tolerated with the available equipment. In practice the signal levels determine the maximum transmitter-receiver offset because the signals (voltages) decrease with offset.

The computer program MODALL is used for both these tasks. The program is menu-driven and self-explanatory so that the description is only required for difficult questions (see appendix 4).

Varying the transmitter-receiver offset is the first step in the analysis. In some cases it is obvious from the simulated curves in which time window the effect of the target layer occurs – especially in the case of a pronounced conductor. Since this is not the rule the following example does not have this feature. The optimum offset in this example can only be decided after a few of the other parameters have been investigated.

Figure 6.4 shows apparent resistivity curves for the complicated ten-layer model from the previous section at three different offsets. For this case, no features of the electric model can be seen in the generated curves except for the slight influence of the conductor in the early time curve (around 30 msec) at 15 km offset. To be slightly conservative, an offset of 10 km was selected. Further modeling is required before making the final decision for time window and for the offset used in the field.

Thus, when actually starting a survey in the field, the first activity should always be a *walkaway test*. This is a series of measurements starting at the transmitter and moving to the offset distance planned for the survey. This *walkaway test* should always start close to the transmitter and end at the distance of the desired profile or even further. The data recorded on a walkaway profile yield several different answers:

- It shows how the noise varies with offset and what system parameters (gain, number of stacks) should be used.
- If a significant 2-D or 3-D structure exists between transmitter and receiver, it will usually be seen as reversal in the *walkaway test*.
- For smooth 2-D or 3-D structure the measurements of both electric field components on the walkaway profile can give you some preliminary indication of the strike direction (current channelling) of the structure.

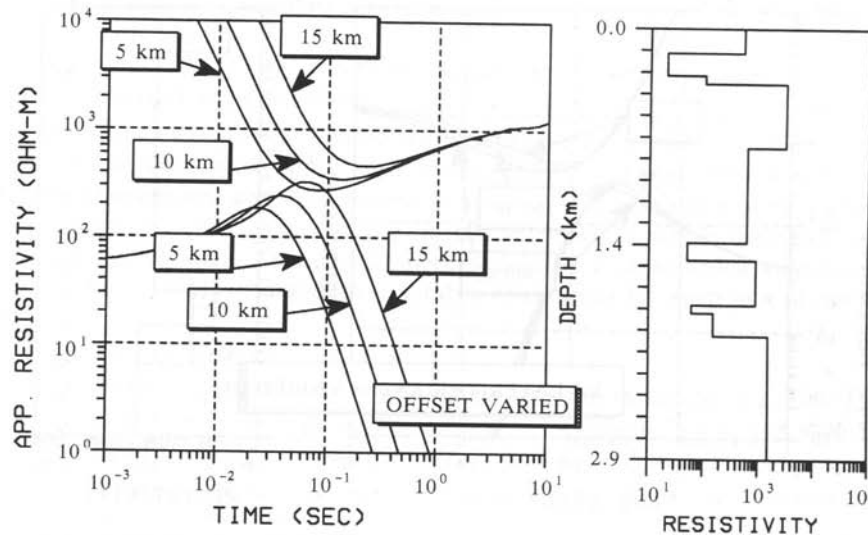


Fig. 6.4: Apparent resistivity curves for three different transmitter-receiver offsets (5, 10 and 15 km) for the ten-layer model.

Next, the resistivity of the lower target layer was varied within the range from 100 to 600 Ωm (see table 6.1). The result in figure 6.6 shows that this parameter is resolved, but the calculated curves do not vary as much as the curves in figure 6.5 for the thickness variations of the first target layer.

Examples for parameter variations are shown in the following figures (figure 6.5 to 6.7). First, in figure 6.5, the thickness of the upper part of the target was changed from 1 m (simulating the absence of the layer), 150 m, and 300 m. Often, 10 % of the depth is a rough first estimate for the thickness resolution of the LOTEM method. The calculated curves in figure 6.5 are well separated from each other so that we have a chance of resolving this parameter. However, it is not resolved uniquely, because a similar variation of the lower target layer could produce the same effect.

The next task in a feasibility study is to define the signal level which is important to know when predefining the field parameters. Figure 6.7 shows the same model variations as figure 6.6, but now the induced voltage in the receiver coil is displayed using typical field parameters. With the present system, the detection limit in the presence of moderate electromagnetic noise and assuming 0.5 hours averaging time at one station reaches down into the submicrovolt range (experience has shown that detectable signal limits lie between 1 and 0.001 μvolt). The signals in figure 6.7 are measurable up to about 0.5 seconds. The technically feasible, lower limit of the time window is at present a few tens of milliseconds. This results in a usable time window reaching from several milliseconds up to 0.5 seconds. Thus the variations shown in the previous examples lie within that measurable time window and can therefore be detected.

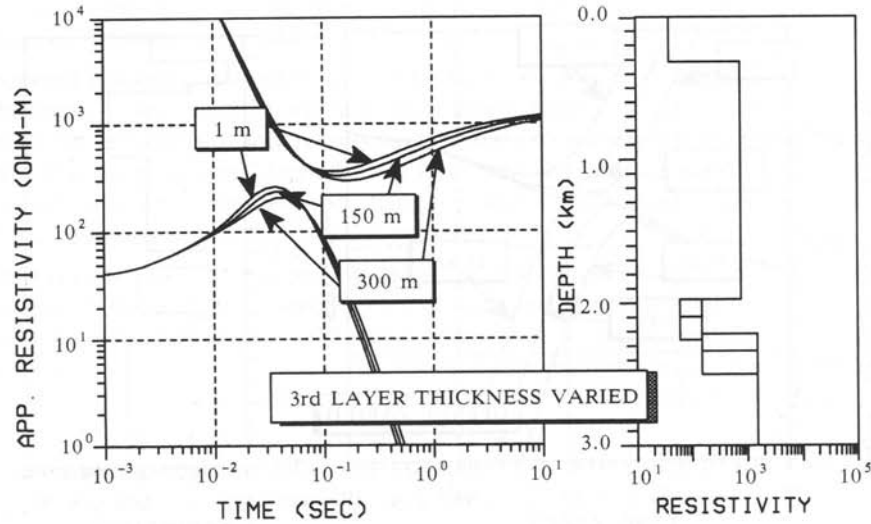


Fig. 6.5: Apparent resistivity curves for three different thicknesses of the third layer. The absence of this part of the target was simulated as an invisibly thin (1m) layer.

So far, the examples were calculated with a transmitter – receiver offset of 10 km. More model calculations are now required in order to check whether the offset could be optimized. For example, the same variations could be tried with an offset of 7 km and with 15 km. The points to observe when carrying out this fine tuning are:

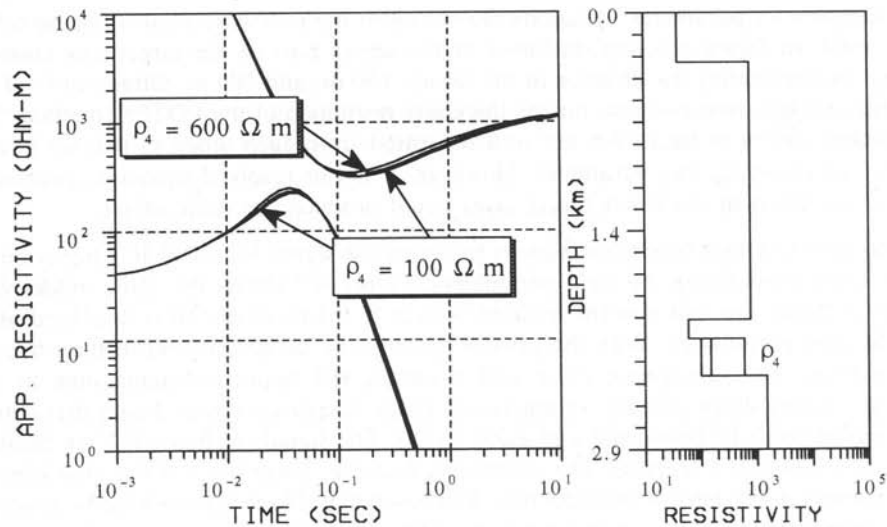


Fig. 6.6: Apparent resistivity curves for three different resistivities of the fourth layer.

- The signal level: it decreases rapidly with distance.
- The time window in which the variations are visible: it is shifted slightly with offset.
- The size of the variations: variations of deeper targets are generally stronger at larger offsets.

The previous examples introduced the well log reduction and the forward modeling for a *survey feasibility* study and for the *survey design*. The results from this preparation should be documented and summarized in a report well before the survey. The report is best structured chronologically, i.e. in the sequence in which the tasks were described in this chapter. At the end, there should be a table which summarizes the results of the forward modeling in a number of columns for each unit of the layered model:

- **LAYER NUMBER.**
- **RESISTIVITY (Ωm):** include here only the variations, e.g. 100, 150, 600
- **THICKNESS (m):** include here only the variations, e.g. 1, 128, 300
- **GEOPHYSICAL APPEARANCE:** describe the effect of the variations on the simulated curves, e.g. strong influence from 0.02 s to 10 s, displacement of late time minimum.
- **GEOLOGICAL MEANING:** interpretation of the variation, e.g. changes in thickness of sandstone target.
- **TARGET RESOLUTION:** decision whether the parameter is resolvable or not, e.g. resolvable by late time asymptote.
- **FIGURE NUMBER:** cross reference to the figures (in the appendix of the report) which display the result of the variation, e.g. 3–4.

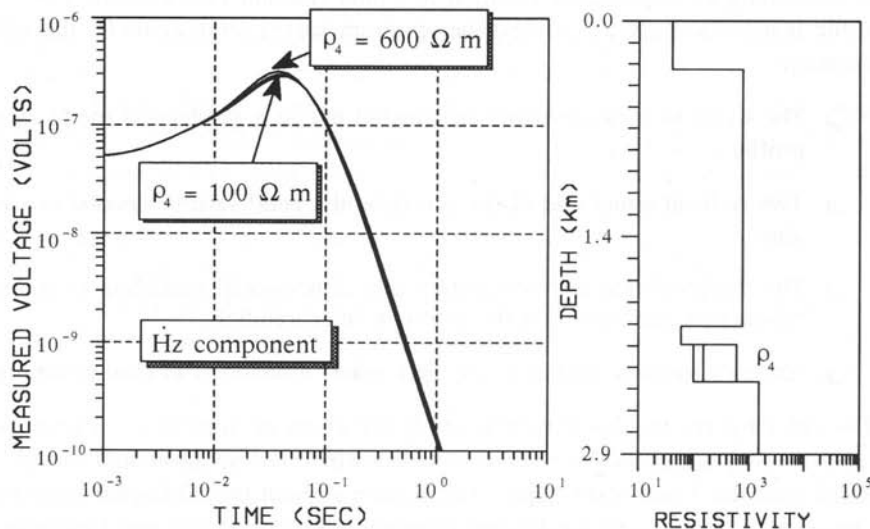


Fig. 6.7: Induced voltage in the receiver coil (signal level) for three different resistivities of the fourth layer.

With these data and the conditions in the target area, it is relatively easy to select an optimum survey layout. This should be done as final step to give input to the logistics operator for the survey design: optimum transmitter–receiver offset, optimum time window, required accuracy for the data. The latter always results in a tradeoff: the longer you stay at one receiver site the better your averaged signal becomes, but also the costs per station increase. The feasibility study can put limits on the required accuracy and therefore help in both, time–planning and in cost estimation.

You may refine the presurvey feasibility study even more, if you have more data available. If noise measurements from the survey area and the system response of your system exists, you may actually want to calculate synthetic, noisy, raw field data and simulate the whole interpretation process. The more time you spend on the feasibility study the more time you will save during the data acquisition and interpretation phase.

In the next section artificial noise is added to the data and the resolution is investigated under production conditions by looking at the inversion results.

RESOLVING A DEEP CARBONATE UNIT

A difficult target for EM techniques is the determination of resistivity and thickness of thick resistive units at a depth of 4 to 6 km. For production and exploration problems this is however very important because accurate porosity predictions can save money spent on dry wells. To simulate this situation we have selected a case history simulating an exploration situation in China (Baxian Depression). The objective of the feasibility study was to find the optimum survey strategy under the following conditions:

- The LOTEM measurements are carried out in a production mode along a profile.
- Two wells at either end of the profile and a good seismic section are available.
- The interpretation is restricted to one–dimensional modeling to maintain production and constrain the effort in interpretation.
- Archie's formula applies to the carbonates embedded in clastic sediments.

The color figures for this feasibility study are given in Appendix 7. Figure A.7.2 (top) shows an electrical section with three layers which has an additional fourth layer embedded between 4 and 6 km depth. The section without the additional layer represents the overall structure of the Baxian Depression according to Chen Leshou et al's (1988) interpretation of magnetotelluric data (table 6.3). The Baxian Depression is part of the Bohai Gulf Basin which has a great variety of different oil and gas pool

systems related to structural and lithological parameters (figures 1.1–12 and 1.1–20 in Schlumberger, 1985). The additional layer in the model simulates the effect of a variable porosities in the carbonate sequence in the conductive environment of the Baxian area. The variations in electrical resistivity (compare table 6.3) are indicated by the colour coding in the figure. The basic model is displayed as the top frame in the figure.

Table 6.3: Resistivity models used for the resolution study.

Layer No.	LEFT MODEL		3rd LAYER – VARIATIONS (Ohm-m)	RIGHT MODEL	
	Resistivity (Ohm-m)	Thickness (m)		Resistivity (Ohm-m)	Thickness (m)
1	21.0	770	–	21.0	770
2	4.4	3000	–	4.4	3000
3	4.4	2350	10, 15, 25, 50	100.0	2350
4	30.0	–	–	30.0	–

Synthetic LOTEM data and synthetic magnetotelluric data were calculated for eleven receiver stations along a profile which crosses the region of resistivity variations of the simulated carbonate layer.

Artificial noise was added to the synthetic data in order to allow a realistic resolution study. The resulting synthetic data sets were then inverted in terms of layered models at each receiver station and the results assembled into an interpreted electrical section. Ideally, the original section should be recovered after this procedure.

Figure A.7.2 shows the results of interpreting single synthetic data sets without imposing any constraints on the curve fitting process. The first frame is the model section which was used to generate the synthetic data. The next frames show results of the procedure for LOTEM magnetic data, LOTEM electric data, and (in the bottom row) for magnetotelluric data. The curve fitting process for each of the three data types was initialized once with a model without the additional layer (left column) and once with a model with the additional layer (right column). This procedure simulates that the well log is input into the interpretation process. The interpretations show a strong dependence on the initialization of the curve fitting: the left column is quite different from the right column. Also, the resistivity variations in the original model could not be recovered; instead they appear as structural variations. None of these results would be acceptable in a real exploration environment.

The use of structural information such as an interpreted seismic section was simulated in figure A.7.3 by forcing the curve fitting process to leave the layer thicknesses fixed and vary only the resistivities of the units. Of the resulting interpretations the LOTEM electric fields and the magnetotelluric data can now reproduce the variations to some degree. However, the LOTEM electric fields do not give consistent

information about the part of the section below the resistive unit. Also, all of the interpretations still depend on the starting model for the inversion.

Next, different data sets were combined using joint inversion. The result is displayed in figure A.7.4. The results in figure A.7.4 were obtained without *a priori* information about the structure. The results are equally unacceptable as for the independent inversions in figure A.7.2. Figure A.7.4 shows the joint inversion results when the structure is kept fixed. The first pair of frames shows the combination of LOTEM electric fields with LOTEM magnetic fields. The result has only marginally improved over the electric field interpretation in the previous figure. The center frames show the combination of LOTEM magnetic fields with magnetotelluric data. Since both data sets are more adapted to resolution of conductive targets, they are not successful in resolving the resistive target in this example. The last row shows the combination of LOTEM electric field data with magnetotelluric data. The result is an acceptable resolution of the resistive unit. The interpreted resistivity variations within that unit do not depend on the initialization of the curve fitting, and the part of the section below the resistive unit has little distortion left in it.

The resolution study with synthetic data and synthetic noise indicates that for the given exploration task the exploration strategy can be designed such that the resistive target layer is resolved. In the example the a variable resistive unit simulates a carbonate layer in the conductive sediments of the Baxian Depression. Its resistivity can be mapped when the structure is fixed on the basis of other information such as seismics, and when in addition a combination of the LOTEM electric field component with magnetotelluric data is measured and jointly interpreted.

HIGH RESOLUTION FEASIBILITY STUDY

A typical problem in exploration is the definition of porosity within resistive units at a depth between 1 to 2 km. Often these resistive units are either carbonates or diabase/dolerites. Following, a case history from Australia is shown where porosity variations are to be mapped within a dolerite unit. Above the dolerite are sandstones and silts of medium resistivity. A blocked well log is given in figure 6.8. The dolerite is clearly marked by a resistivity increase in the log at 1700 m depth.

The location of the well is marked in figure 6.9 which shows the two way travel-times for the survey area. Also indicated in the section is the location of the seismic profile (see figure 6.10) used to derive the structure used for the forward modeling. In the seismic section, the dolerite is marked.

For the structure synthetic data were generated and 1% noise added. Porosity variations from of 5%, 10%, 20%, and 30% were modeled with the respective resis-

tivity changes. This noise level is somewhat high for LOTEM data because the acquisition and processing eliminates most of the noise. However, during the forward model-

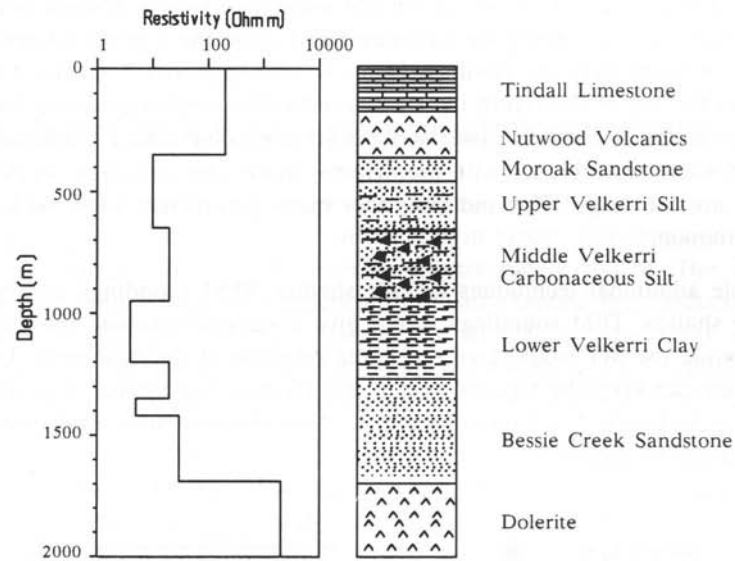


Fig. 6.8: Blocked electrical log for the well in the survey area in Australia.

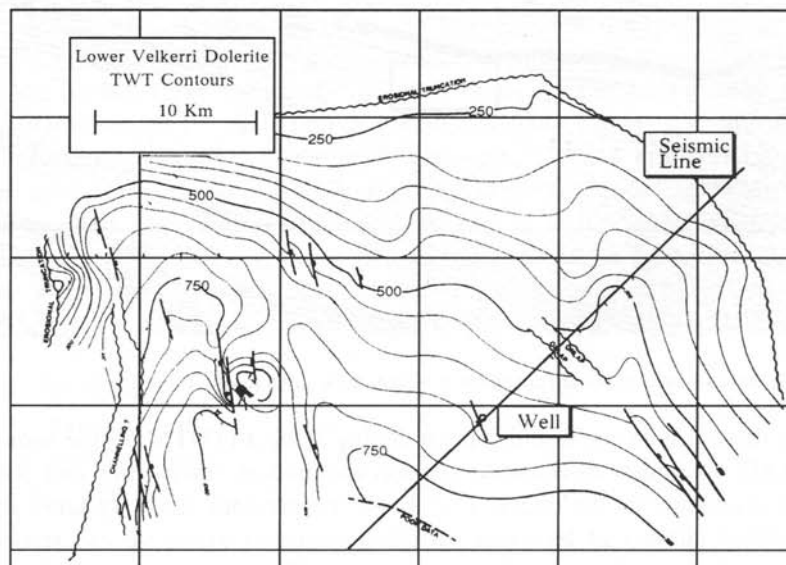


Fig. 6.9: Two way traveltime contours of the top of the dolerite unit.

ing process conservative estimates are usually used. The synthetic data were then interpreted and it was quickly concluded that the individual components would not yield the wanted results.

Thus, the feasibility study was continued using inversion as routine interpretation tool of the data. When keeping the structure fixed using the *a priori* information from the seismic in figure 6.10 the result in figure A.7.5 (Appendix 7 – color figures) was obtained. At the top of the figure the electrical models used to generate the synthetic data is shown. Below, are the inversion results are color coded. Although one can already see some resemblance with the original model the deviation on the edges of the profile are too large. This indicates that more parameters must be known as *a priori* information.

Possible additional techniques include shallow TEM soundings and magnetotellurics. The shallow TEM soundings would give a reliable estimate for the top layer resistivity while the MT would give a reliable estimate of the basement. Using these estimates one can keep the top and bottom resistivities fixed which was done for the computations in figure A.7.5 (bottom frame). Now the inversion result shows a close resemblance of the model.

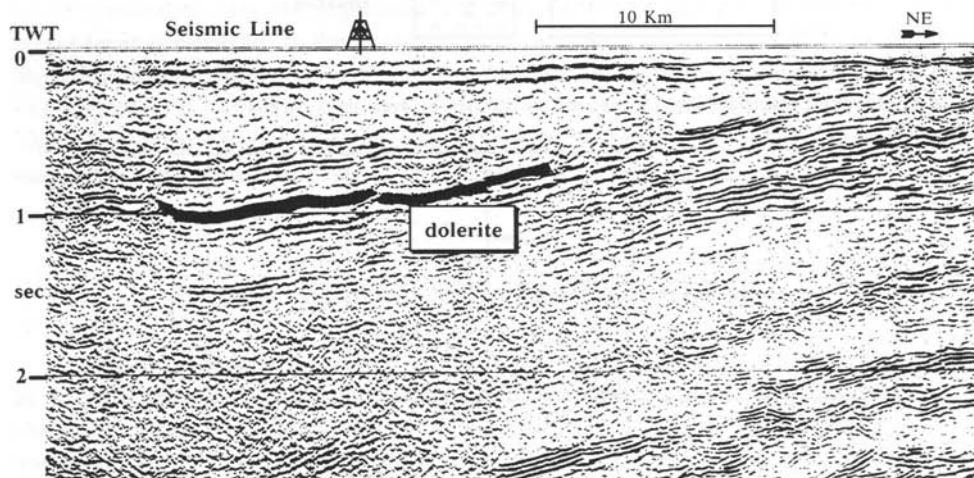


Fig. 6.10: Seismic section indicated in figure 6.9. the dark area marks the dolerite unit.

From these results one would suggest adding along a LOTEM profile some sparse TEM and MT soundings to constrain the top and bottom resistivities and obtain the maximum resolution for the target layer. From the previous study we know that only when a limited number of layers of sufficient thickness exists we can resolve deep target without high resolution shallow information. The study for an area in Australia suggests that one must be very careful when the section is only moderately more

complicated. not only does the approach for the interpretation change but one also needs additional measurements. It is very important that this is known before the survey is planned and not found out during the interpretation phase when it is often too late.

FEASIBILITY STUDY OF A TWO-DIMENSIONAL STRUCTURE

The next feasibility study considers a more complex possible application of LOTEM. The exploration problem is from an area in Japan. The objective was to map a swarm of conductive dikes at a depth of approximately 500 m. The structure is considered two-dimensional for a practical purposes. Around the conductive dikes is medium to high resistive material separated by fault zones. the entire structure is embedded in high resistive background material. the situation could simulate a variety of situation encountered in mineral exploration but also in geothermal exploration.

A two-dimensional model as constructed and the SLDM program (Druskin and Knizhnerman, 1988) (see chapter 4) was applied in a 2-D mode to calculate the response of a LOTEM setup. The model is shown in figure 6.11 and the plan view in figure 6.12. In figure 6.11 are also the receiver location above the model and several selected characteristic transients displayed in the top portion of the figure. The corresponding profile location is shown in figure 6.12. The electric field stations are coincident with the locations where the time derivative of the magnetic field is calculated (recorded). The surface projection of the 1 Ohm-m conductive dikes is also shown in figure 6.12. The anomalous body extends further to the sparsely sampled parts on the right of the profile. First, the electric field transients are shown and below the apparent resistivities (using the early time apparent resistivity formulation) of the time derivative of the magnetic field. The transient response at the far end of the profile show no anomalous behavior and are essential similar to the 1-D response. When approaching, one can notice anomalous behavior going over to sign reversals near the edge of the structure. Station 61 is the last non-reversed transient on the profile. In the corresponding electric field measurement (station 15) at the same surface location one can already see some change in signal behavior when comparing it with the signal at station 01. At station 62 the magnetic field transient contains a sign reversal (thus displayed as squares). In the electric field this reversal can only be observed one station further on the profile (station 17). At the magnetic field station 69 at the far end of the profile a sign reversal in the signal is observed again beyond the far edge of the anomaly. The corresponding electric field response is now shifted in the opposite direction.

If we consider that the objective is definition if LOTEM is applicable to this exploration target, we have to give a more modified answer as for the above feasibility

studies. Considering that the synthetic transients exhibit reversals, it is clear that one-dimensional interpretation will not give the wanted result. This means that at least 2-D and probably even 3-D interpretation must be used. For 3-D interpretation the key is

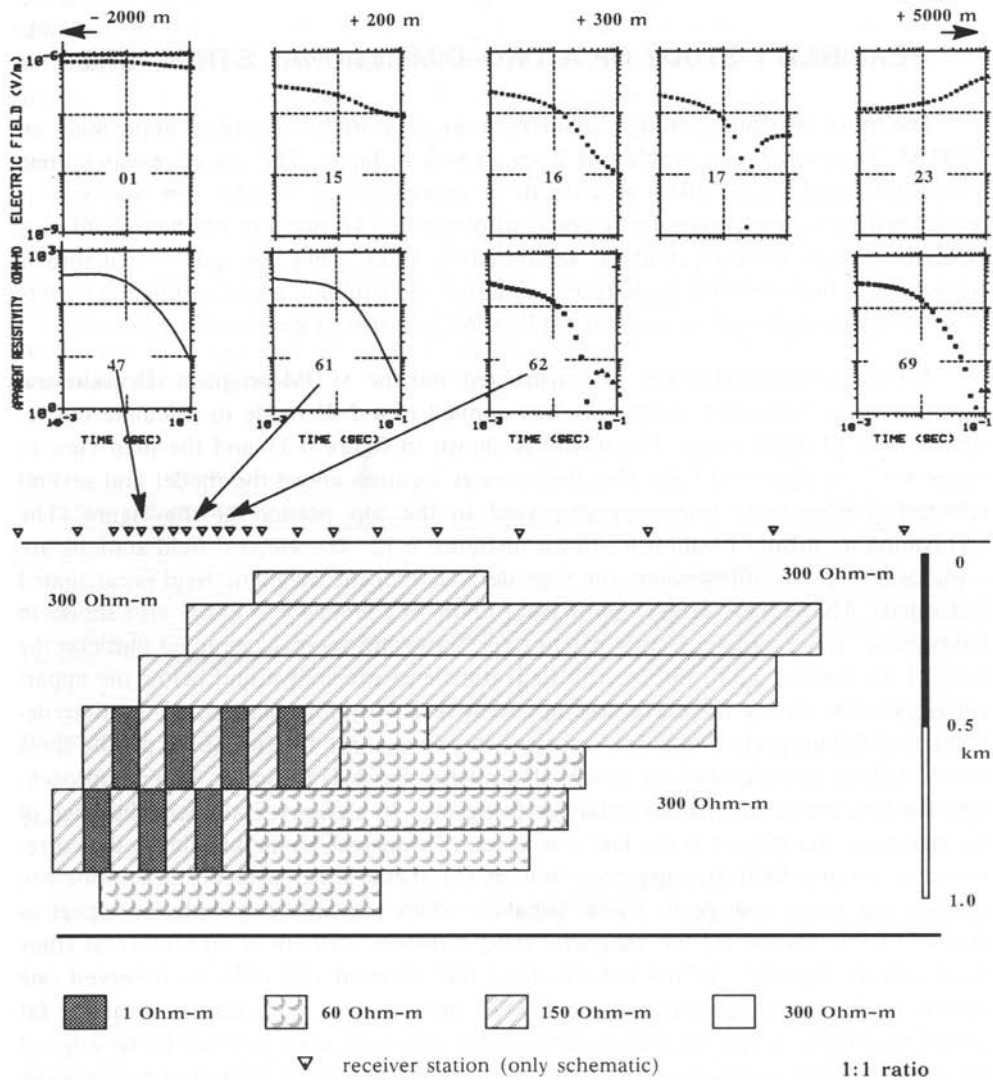


Fig. 6.11: Two-dimensional section view of the model used for the computation of the transient responses shown in the upper half of the figure.

to find a good starting model since 3-D modeling takes significant computational effort. This requires that the data are measured on parallel profiles or even better on a grid. The electric fields should be measured because the time difference between the occurrence of the first reversal in the electric and magnetic field data can give an additional indication on where the edge of the body is located. The operational mode in which the data should be collected is preferably a profiling mode similar to what is routinely used by the mining industry.

For this particular two-dimensional problem we can summarize results from the feasibility study:

- LOTEM electric and magnetic field should be measured at the same surface location to be able to locate the edge of the anomalous zone.
- The data should be collected at least on parallel profiles or even better on a grid to allow the best estimate of the starting model for the 2-D or 3-D modeling.
- The data should be initially displayed in a profiling sense and soundings on at selected parts of the profile where the 3-D anomaly is significantly weaker than the one-dimensional response.

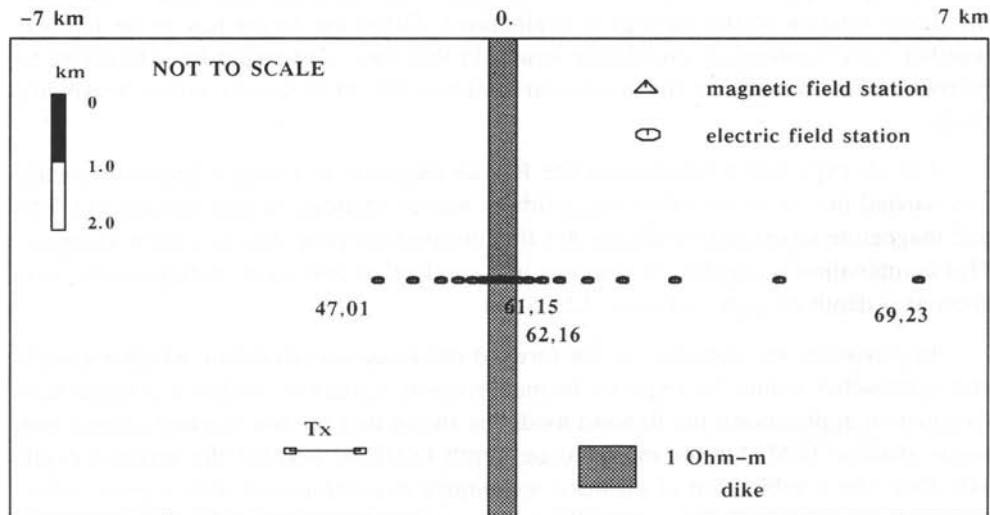


Fig. 6.12: Plan view of the two-dimensional section displayed figure 6.11 and the location of the profile of which selected data sets are shown.

SUMMARY CHAPTER 6

Before carrying out a field survey, the feasibility of the technique for the problem on hand must be investigated. In order to obtain a realistic estimate of the performance of the LOTEM technique in a new environment, it is important to consider all available information concerning the resistivity structure and the general geology is obtained.

The most common way of deriving a reasonable model for the LOTEM method is the layer equivalencing applied to well log (induction log) data. The log is blocked such that a minimum structure is obtained, but the general trend of the well log is still preserved. When further reduction in the number of layers is being made, one must make sure that the resulting responses in the electromagnetic field are identical.

Once the optimum model is found and the target parameter variations are known, the responses can be calculated and an optimum offset determined. For this optimum offset one can then calculate the actual received voltages to confirm that the acquisition system on hand can resolve the parameters.

During all phases of the modeling and feasibility study one must make sure that the direct relation to the geology is maintained. Often the target has to be lumped together with overlying or underlying strata. In that case, one might have to resort to inversions and analysis of the resolution statistics for an optimum survey feasibility study.

For an exploration situation in the Baxian Depression, China a feasibility study was carried out. It showed that the optimum survey strategy should include LOTEM and magnetotellurics and should use for the interpretation the structure from seismics. This combination is capable of mapping in a production operation bulk porosity variation at a depth of approximately 4 to 6 km.

In Australia, the objective of the forward modeling was to define which methods and approaches would be required to map porosity variations within a dolerite unit (production application). the forward modeling shows that for near surface control one needs shallow TEM, for the intermediate depth LOTEM, and for the greatest depth MT. Only the combination of all three techniques in combination with *a priori* information from seismics (structure) will give the required high resolution.

In Japan, are complicated two-dimensional anomaly had to be investigated. From 2-D modeling it is clear that sounding interpretation is not applicable in this case. However, a combination of LOTEM electric and magnetic field data collected on a densely spaced grid can delineate the zone of interest and allow the derivation of a model for the exploration target.

PROBLEMS CHAPTER 6

1. Conduct a survey feasibility study for a typical European situation (strong cultural noise). This should include:

- Well log reduction and deviation of the more reasonable geoelectric model, which shows the minimum structure but honors the geology.
- First reduce the well log to some number of layers between 6 and 10 and then cross check all further reductions to deep layers graphically. Stop your reduction when either geology contradicts to the layer boundaries or the deviation between the consecutive reductions becomes too large.

The data picked from the well log is (first depth then resistivities):

Problem 1 log

0,80.
725,80.
770,80.
810,6.
860,40.
1140,11.
1220,100.
1450,11.
1680,40.
1830,6.
1900,60.
1960,8.
2050,35.
2080,6.5
2100,45.
2200,6.
2250,30.
2800,4.
3000,4.

You also know from the borehole geology:

Table 6.4: Data of a blocked electrical log maintaining the lithological boundaries.

Depth	Approximate Resistivity	Lithology
0 – 700 m	medium high	limestone
700 – 2300 m	medium conductive	Mesozoic sediments
2300 – 3000 m	10 – 15 km conductive	
3000 – 4500 m	5km medium conductive	
4500 m	resistive	basement

The target is the conductive sedimentary unit between 2300 and 3000 m!

- ☐ Simulate resistivity variation for all units with emphasis on the target layer. Make sure you determine the optimum offset for the survey.
- ☐ Which component is more suitable, the vertical magnetic field or the electric field components?
- ☐ Give optimum survey parameters.
- ☐ Would you include another geophysical method? If so, why?

2. *Volcanic cover:*

A typical exploration situation is the definition of the thickness of sediments under volcanic cover (USA, India, Brazil, FRG etc.). Common resistivity values for the top volcanic layer is just below 100 Ωm (70 – 90 Ωm). These thicknesses range between 200 to 1500 m. The thicknesses of these sediments below is between 500 to 2500 m. They are underlain by resistive basement material.

- ☐ Define the optimum offset using MODALL of a LOTEM setup for thickness variations of the sediments of 800 to 2000 m.
- ☐ What source currents and receiver moments do you need to have the target response above 1 microvolt?

3. *Deep crustal applications:*

You have been asked to assess the applicability of LOTEM to deep crustal problems. You know that a low velocity zone is expected from 7 km (uncertain) to 12 km. The top layer (2 – 3 km) is made up of 150 Ωm material followed by 8000 – 20000 Ωm crystalline rock.

- ☐ Derive the possible model.
- ☐ Define possible variations of the parameters.
- ☐ What is the optimum offset?
- ☐ What noise level can you tolerate to resolve your target?

4. *Overthrust:*

An overthrust varies in thickness from 20 m to 2000 m over a distance of 25 km. Its resistivity is 150 Ωm . Below sediments (3 – 8 Ωm) with a maximum thickness of 2500 m are expected. Please design all survey parameters.

5. *Carbonates at depth:*

At 2 km depth is a carbonate unit of 200–700 m thickness. The overlying strata have a resistivity of 3 – 8 Ωm . The sediments below (to 5 km depth) about 15 Ωm . Design a survey which allows you to map porosity variations within the carbonates of 5, 10, 30, 50%.

6. You are asked to map a 20 m thick resistive (200 Ωm) unit within conductive sediments (5 Ωm) The resistive unit is at 2000 m depth. What would you do if you have to be successful?

KMS Technologies – KJT Enterprises Inc.
6420 Richmond Ave., Suite 610
Houston, Texas, 77057, USA
Tel: 713.532.8144

Please visit us
<http://www.kmstechnologies.com>

This material is not longer covered by copyright. The copyright was released by Elsevier to Dr. Strack on November 5th, 2007.

The author explicitly authorizes unrestricted use of this material as long as proper reference is given.

KMS Technologies – KJT Enterprises Inc.

An EMGS/rxt-company

Chapter 7 General Case Histories

extract from

Strack, K.-M., 1992, reprinted 1999
***Exploration with deep transient
electromagnetic:*** Elsevier, 373 pp.

This material is not longer cover by copyright. The copyright was released by Elsevier to Dr. Strack on November 5th, 2007.

The author explicit authorizes unrestricted use of this material as long as proper reference is given.

Chapter 7

General Case Histories

In the following chapters several case histories are presented, where LOTEM measurements have been carried out in conjunction with other geophysical techniques available well log information. In this chapter, the case histories not falling under a specific category are listed. These surveys were mostly carried out for test and calibration purposes. The first case history is from the University of Cologne test site north of the Ruhr area in Germany (Stephan, 1989). The survey area is a part of the "Rheinische Schiefergebirge", North-West Germany. The sediments are of upper Carboniferous and more than 5000 m thick. Two historic case studies follow: the geologic calibration of the method with the Group Seven Inc. system near the Colorado School of Mines test area and the first field tests of the method in Australia. The last case history in this chapter describes the first quantitative 3-D interpretation of LOTEM field measurements in the Münsterland Basin, FRG.

FIELD SURVEY NORTH OF THE RUHR DISTRICT, FRG

The test area is located approximately 100 km north of Cologne and about 10 km north of the Ruhr District, one of the most densely populated and industrialized districts in Germany. The area was selected for its closeness to Cologne with the following objectives in mind:

- Due to its closeness to the Ruhr district, the test area shows very strong cultural noise. It is an ideal site to test the noise compensation and data processing techniques developed for the LOTEM system.
- Because of the coal mining activities, the geology of the area is extremely well known. Several logged wells allow the comparison of the method with known geology to overcome these problems.
- In parts of the survey area, reflection seismic measurements have problems due to a thin water bearing layer. Thus a field survey in the area would be a good demonstration of the capability of the LOTEM method.

Figure 7.1 shows the base maps for two surveys carried out during 1987 and 1988. During the 1987 survey, only one transmitter was used in order to reach the above objectives. A total of 145 individual soundings at 100 different receiver locations were recorded. Because no significant resistive layer was expected in the survey area, observations of the time derivative of the magnetic field were sufficient to resolve the resistivity structure (Strack et al, 1989b). During the 1988 survey two different transmitters

were used in order to verify the results from the 1987 survey, and to address the question of repeatability of the field measurements using different systems and different field crews.

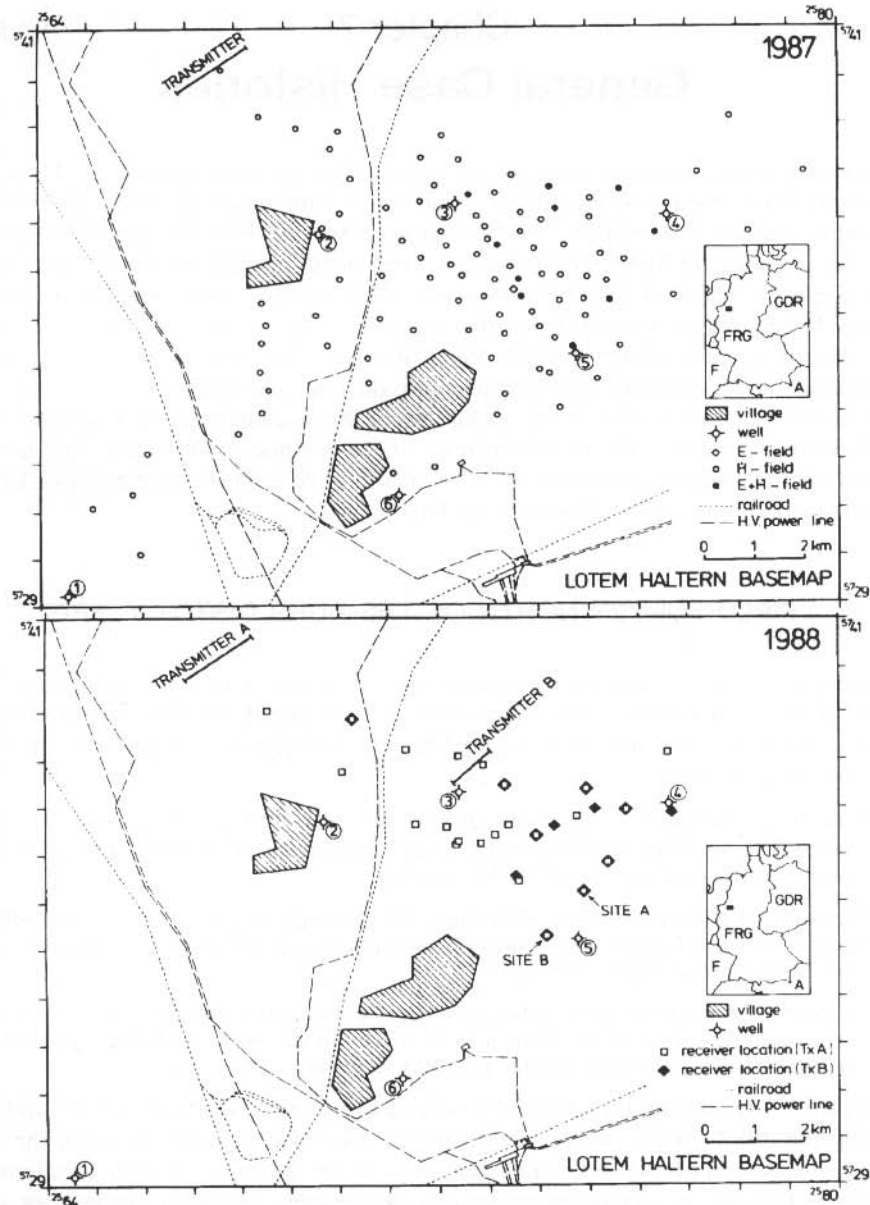


Fig. 7.1: Survey layout of the 1987 (top) and the 1988 (bottom) LOTEM survey.

Additional information from six boreholes was available; their respective locations are shown in figures 7.1. Figure 7.2 shows a representative well log for the area with a conductor sandwiched between two resistors. The change in resistivity to the third layer at 800 m depth is strong and abrupt, whereas the change between the first and the second layer is generally smooth. The exact depth of this boundary is not clearly defined in the original logs. Only the blocking lets it appear as strong as shown in figure 7.3. The upper 270 m are of medium resistivity of approximately $18 \Omega\text{m}$. The

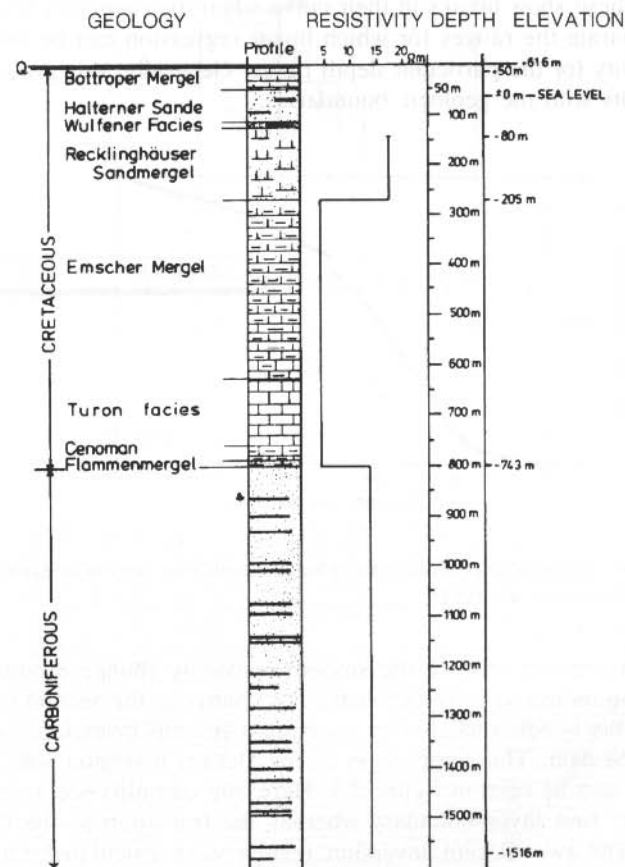


Fig. 7.2: Representative well log derived from borehole measurements within the survey area.

geologic units in this range consist mainly of Marl, sands and limestone of Cretaceous and Quaternary age. Some of the sands in the Haltern Sands are locally water-bearing and thus present problems with reflection seismics. Below this, a conductive unit follows which consists of Marls down to a depth of approximately 1800 m. The resistivity of this unit is approximately $3 \Omega\text{m}$. Below 700 to 800 m, Carboniferous strata has been found with the coal measures in cyclic sequences. In the extreme south of the

LOTEM survey area, two other formations intervene between the Carboniferous and the Cretaceous. These are the upper Permian ("Zechstein") with thin bedded shales, limestones and anhydrites up to 100 m thickness and the lower Triassic ("Buntsandstein") make up of sandstones up to 200 m thickness with high resistivities. The Carboniferous is again of medium resistivity of approximately $15 \Omega\text{m}$. The coarse resistivity model of figure 7.2 was used as a general starting model for the interpretation. This model was then refined using the individual well logs. The resistivities of the well logs were digitized and plotted in the form of cumulative conductance as shown in figure 7.3. These show breaks in their curve when the resistivity boundary changes. The breaks separate the ranges for which linear regression can be used to define the average resistivity for the particular depth range. Generally, this procedure gives very consistent results with the geologic boundaries.

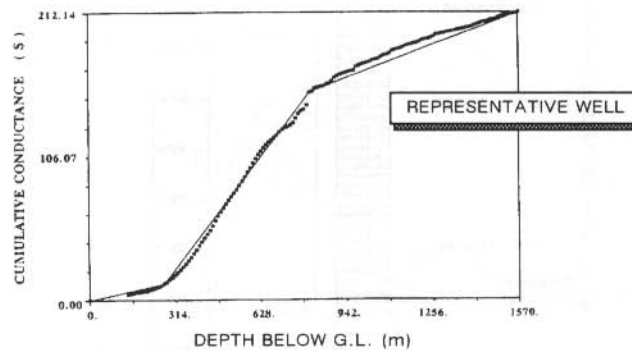


Fig. 7.3: Cumulative conductance analysis to define the resistivity layer boundaries from the well logs (after Stephan et al, 1991).

In figure 7.3 one can observe the smooth resistivity change around the first layer boundary as also indicated by the geology. The change at the second layer boundary is more abrupt. This is best modeled by applying a smooth inversion algorithm (Occam inversion) to the data. The comparison of the Occam inversion with a layered earth well log model can be seen in figure 7.4. Here one can also see a smooth change in resistivity at the first layer boundary whereas the transition to the Carboniferous is more abrupt. The two Occam inversion results were calculated for measurements taken at the same surface location with different receiver systems.

In addition, one seismic section of the area is available for inspection and is displayed in figure 7.5. It is partly interpreted and the thin line is only a general indication for the top of the Carboniferous formation. This section is low data quality and furthermore, the top of Carboniferous formation could not always be detected clearly, i.e. the three strong reflectors indicating the top Carboniferous boundary are not visible at the left and at the extreme right side of this section. This seismic section is mainly used to confirm the horizontal layering of the geological strata and to justify

one-dimensional interpretation for the LOTEM data. More detailed information can be found in Stephan et al (1991).

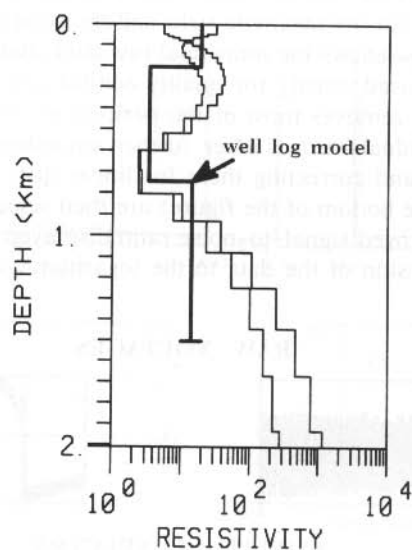


Fig. 7.4: Comparison of two Occam inversion results with a layered earth model.

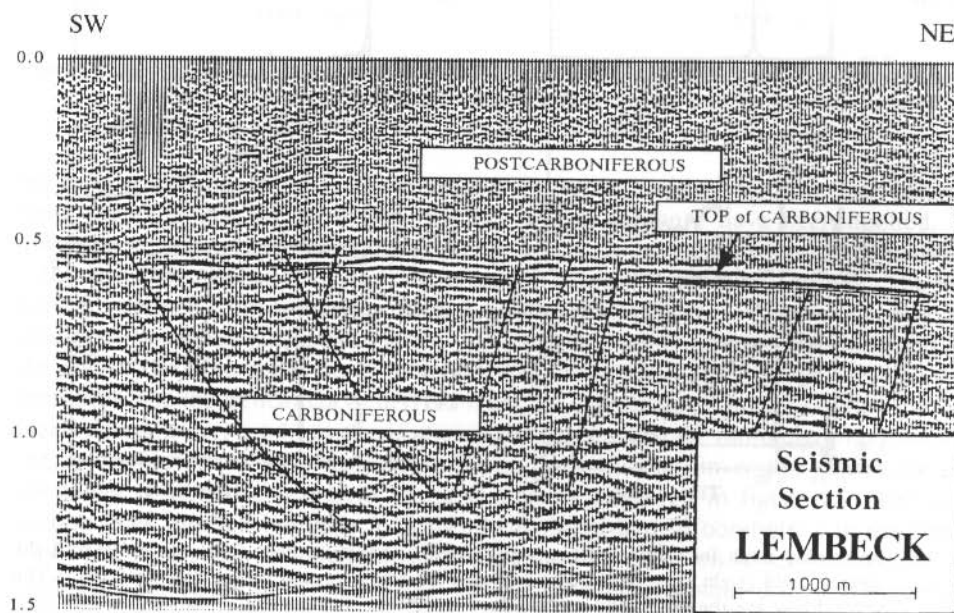


Fig.7.5: Seismic reflection line for the survey area (after Stephan et al, 1991).

The field data in the survey area were extremely noisy. Generally, between 50 to 150 stacks had to be acquired. Figure 7.6 shows the processing steps for two individual records for magnetic and electric field measurements respectively of the 1988 survey. The left column is for the magnetic field and the right one for the electric field measurements. The top row shows the individual raw data. Below, the amplitude spectra are shown which are used strictly for quality control and to design the optimum digital filter. The filtering removes most of the periodic noise in the signal. The bottom row shows the individual records after further smoothing the data with a time variant Hanning window and correcting them for linear drift. The individual records (like the ones shown at the bottom of the figure) are then selectively stacked and yield the signal with much improved signal-to-noise ratio displayed in the top of figure 7.7. At the bottom, the conversion of the data to the logarithmic domain is shown. Here

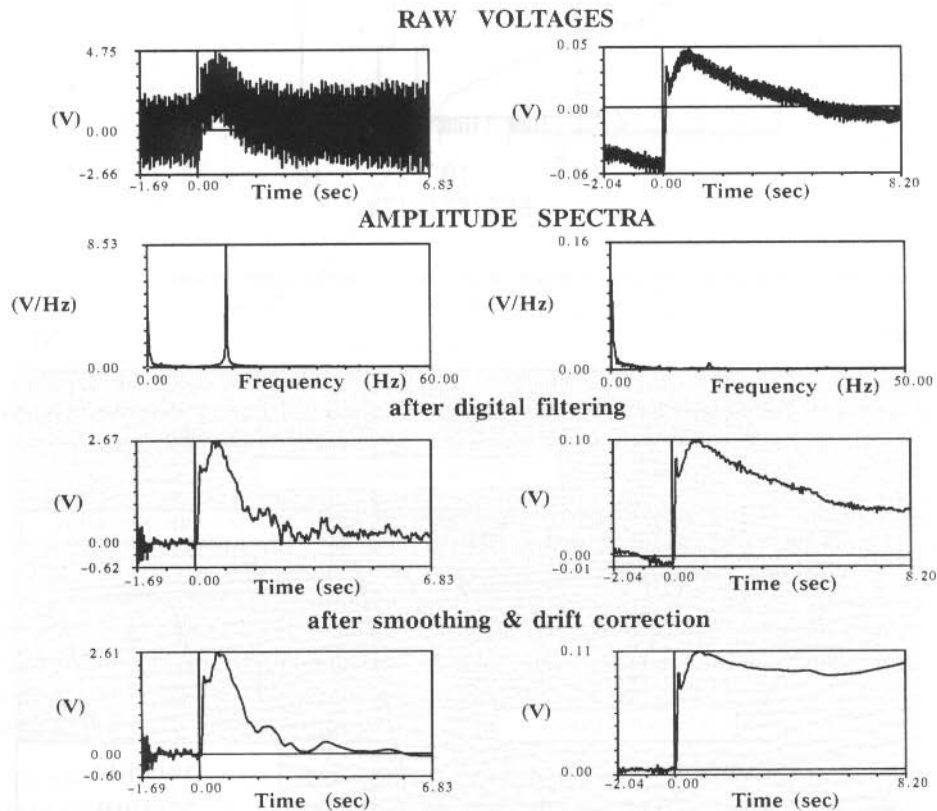


Fig. 7.6: Processing steps for individual raw signals of the magnetic field (left; site A09) and the electric field (right; site B11). The top shows a single record of the raw field data. The second row are the amplitude spectra used for the quality control. Following are the digitally filtered records. At the bottom the further smoothed individual signals are displayed (after Stephan et al, 1991).

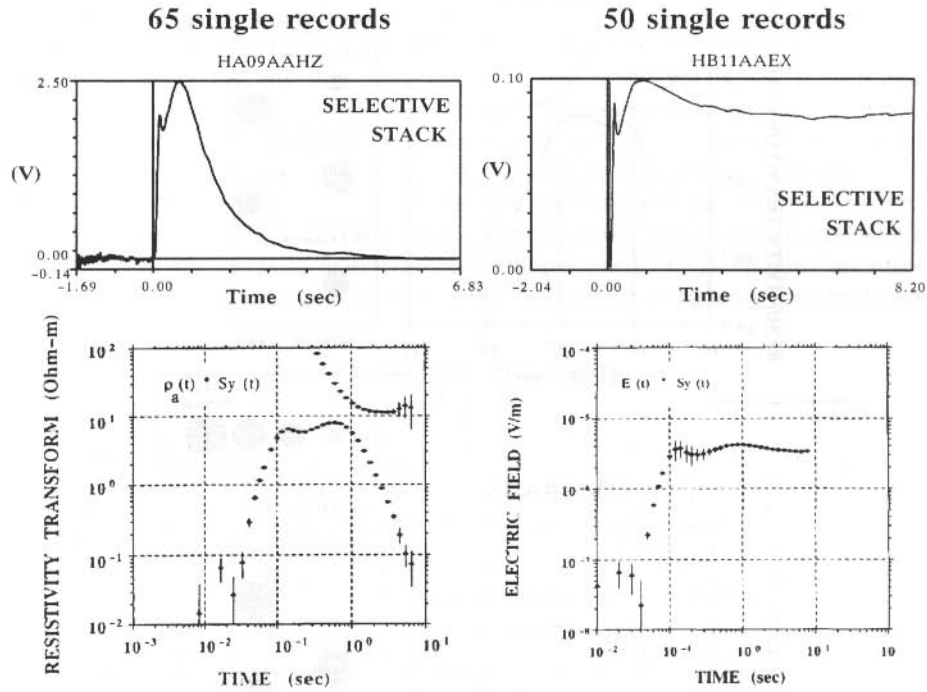


Fig. 7.7: Selectively stacked magnetic field transient from figure 7.5 and the corresponding resistivity transform curve (left). On the right the measured electric field transient is displayed both linearly and logarithmically (after Stephan et al, 1991).

the data are displayed as resistivity transform for the time derivative of the magnetic field, meaning that no corrections for the system response have been applied. The lower curve represents the transformation using the early time apparent resistivity formula and the upper one the transformation using the late time formula. The error bars are derived from the selective stacking algorithm. Figure 7.8 shows the inversion results of this station. The data points representing mainly noise at the beginning and the end of the time series have been edited out. The solid line through the data point represents the theoretical curve derived from the layered earth model on the right. The black dots are derived from the inversion statistics and their radius is proportional to the resolution of the individual parameters. The individual inversion results are then combined to obtain a resistivity cross section as displayed in figure 7.9. This cross section goes through borehole 1 in the South-West and to borehole 2 in the North-East. The inversion results clearly show that the interpretation is very consistent. The error bars in the depth mark the 95% confidence bounds obtained from the inversion statistics. Also, it should be mentioned that the individual model parameters were mostly uncorrelated and no conductance referencing was done.

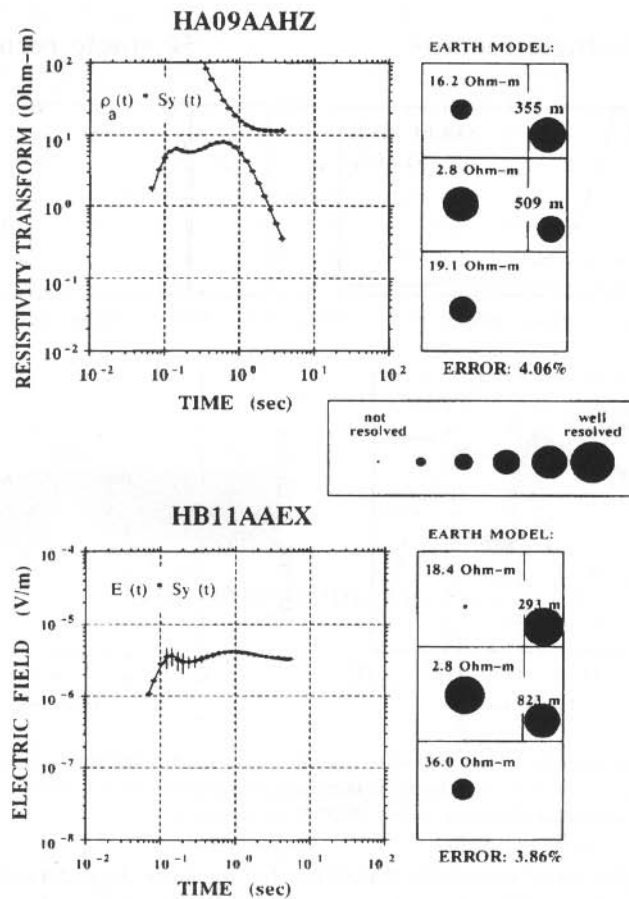


Fig. 7.8: Inversion results of the field data shown in figure 7.6 and figure 7.7 (after Stephan et al, 1991).

Consistency of soundings from different transmitters is a very common problem when carrying out controlled source EM surveys because of possible transmitter overprints (see chapter 4). Two common types of explanations of inconsistencies exist: one caused by inappropriate interpretation of inversion results and the other caused by geologic structure (3-D effect). Before selecting one of the causes and applying corrections through conductance (or transverse resistance) referencing or 3-D modeling as described throughout this book, one must eliminate the stations with data highly contaminated by noise.

The repeatability of the field measurements was checked using measurements from both surveys and all three transmitters. The results are displayed in figure 7.10 for the two sites marked on figure 7.2. In both cases the inversion results are very consistent.

They deviate a little in the resistivity of the last layer. It can be explained that the field data were obtained from magnetic field measurements and magnetic field measurements are not accurate in defining higher resistivities. Furthermore, the measurements at site A were noisier than the measurements at site B. When comparing the measurements of the individual electromagnetic field components (see figure 7.11) it can be seen that they are in general consistent. The deviation in the resistivity of the last layer is now less, since the electric field measurements can more accurately determine the resistivity of this layer (Strack et al, 1989b). At station 17 (right side of figure 7.11) a shift of approximately 50 – 70 m between the well log and the inversion results remains. The cause of this shift is not clearly known, but it could be attributed to a lack of resolution of the LOTEM technique in the upper parts of the section. Because the shift is constant throughout the area, it is not considered to be a significant problem.

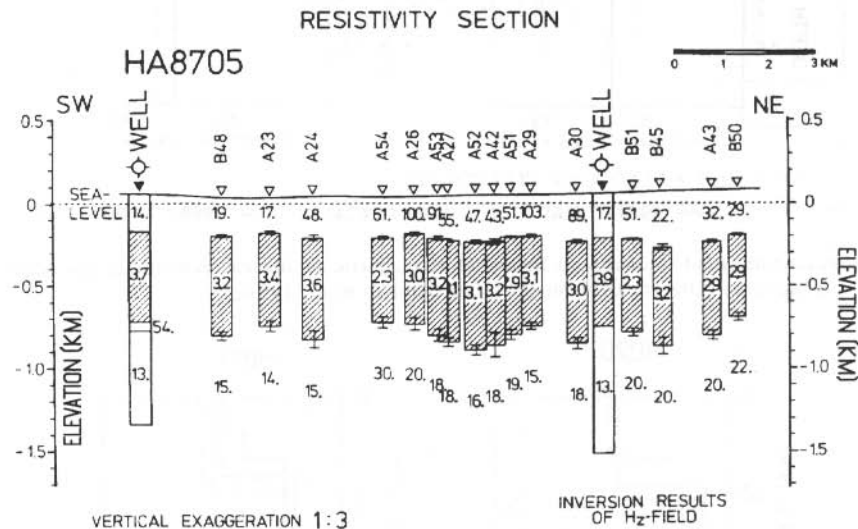


Fig. 7.9: Interpreted resistivity cross section through well nos. 1 and 2 of figure 7.1 (after Stephan et al, 1991).

The large amount of field data requires that the data are first evaluated for consistency of the interpretation. Only when consistency is proven, can general structures within the area be interpreted. One way of showing the consistency is the presentation of the field data in form of contour maps. Figure 7.12 (top) shows a contour map of the resistivity of the conductive unit. Although the inversions were all carried out independently and individually, their resistivity varies little throughout the survey area. The dashed contour lines show the range where the data density was not high enough. This tells us that the interpretation is very consistent throughout the area. No special anomalies exist. To interpret the structure within the survey area, the depth to the *near top of the Carboniferous* was contoured (Near top because in the south-western part of the area it is not clear whether the resistivity contrast is at the top of the Carboniferous).

ous or at the top of the Zechstein);(see figure 7.12). The contour lines are 50 to 70 m deeper (approximately 5 to 8 % of total depth) than expected from the well log but

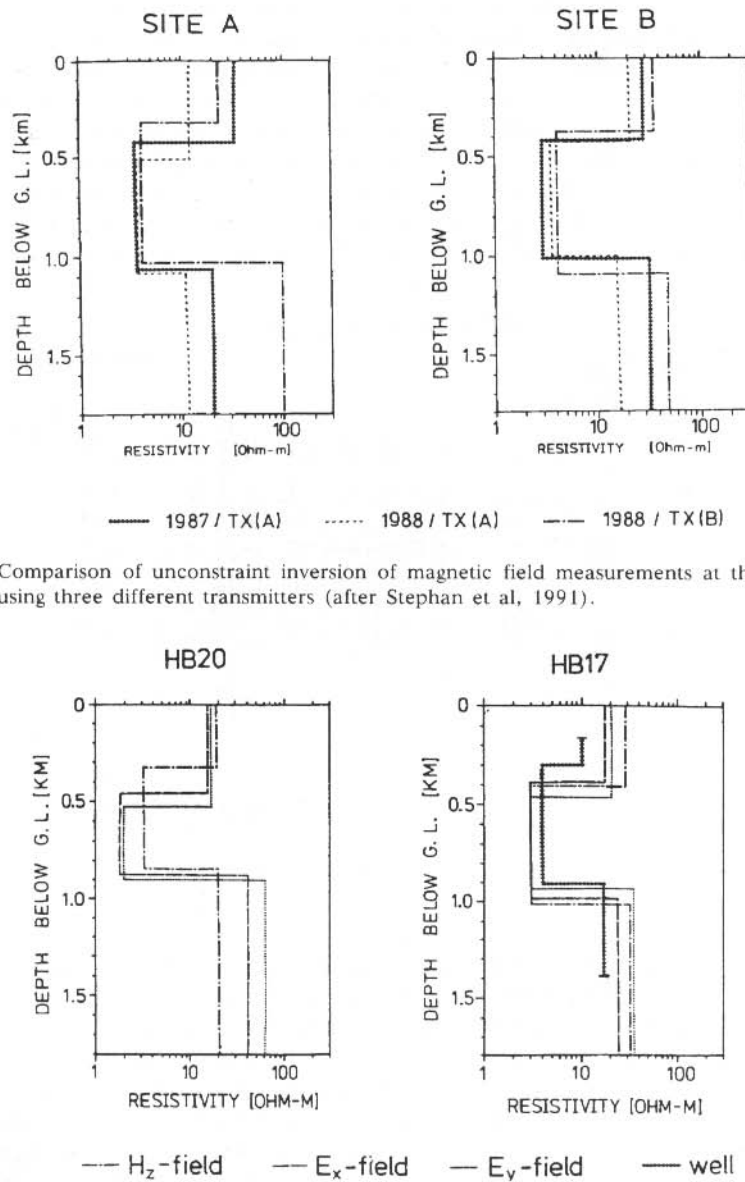


Fig.7.10: Comparison of unconstrained inversion of magnetic field measurements at the same sites using three different transmitters (after Stephan et al, 1991).

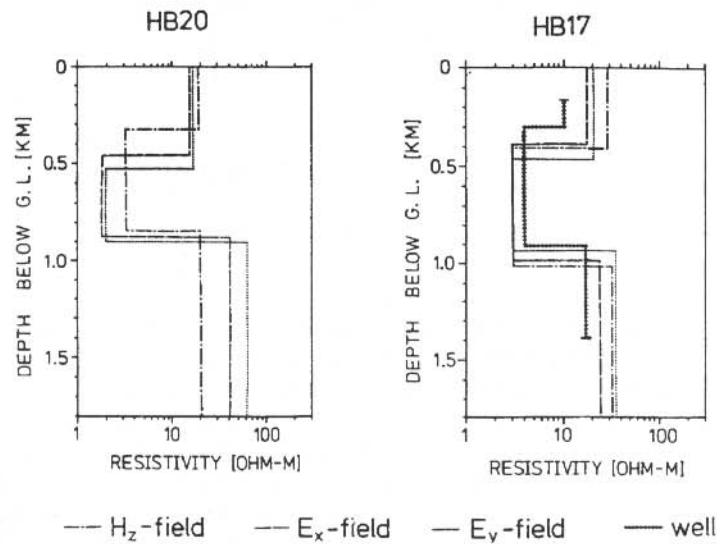


Fig. 7.11: Comparison of inversion of the electric and magnetic field measurements at two sites (after Stephan et al, 1991).

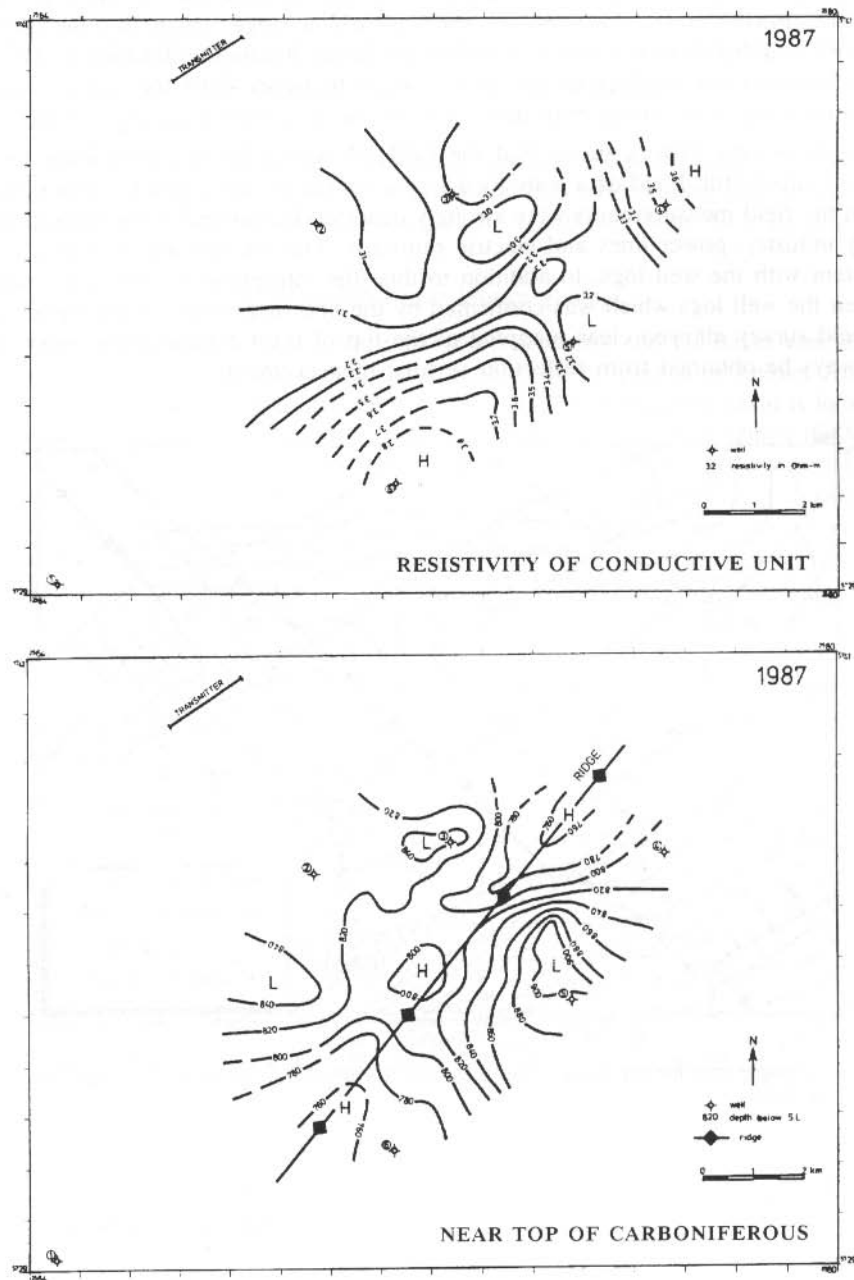


Fig. 7.12: Resistivity contour map of the second conductive layer (top) and contour map showing the near top of Carboniferous (after Stephan et al, 1991).

structurally the results are in accordance with the information obtained from the boreholes. Furthermore, the contours show clearly a ridge which lies between the boreholes and therefore is not indicated directly by the borehole information. This was checked against the geology of the survey area. In figure 7.13 this ridge could be confirmed using a structural map derived from the well known geology of the area.

The above case history shows that the LOTEM survey North of the Ruhr District was very successful. Field data with good signal-to-noise ratio could be obtained even though the field measurements were strongly distorted by cultural noise caused by the nearby industry, power lines and electric railroads. The interpretation yielded results consistent with the well logs. In addition to this, the interpretation showed a ridge in between the well logs which was confirmed by the known geology of the survey area. The field survey allowed clear mapping of the top of the Carboniferous which could not always be obtained from reflection seismic measurements.

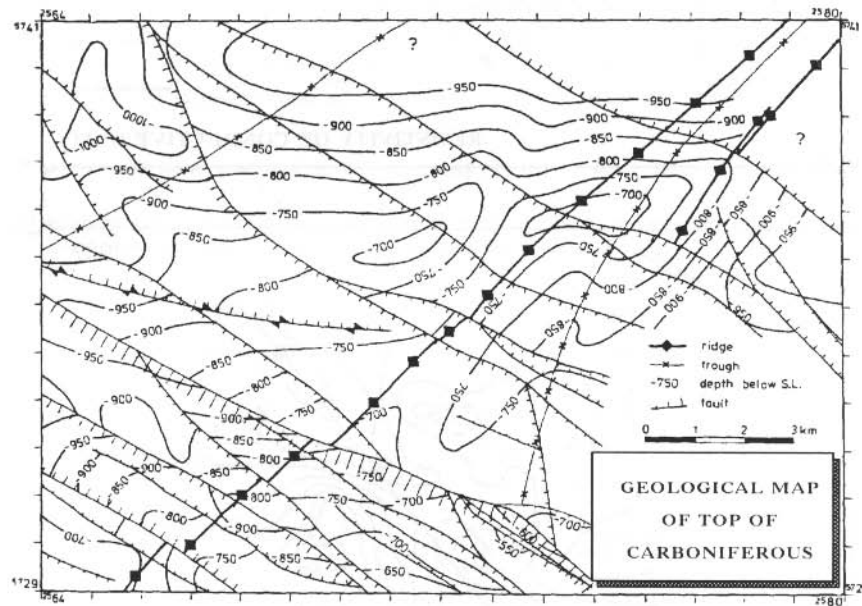


Fig. 7.13: Geologic map for the survey area including the structural interpretation (after Stephan et al, 1991).

GEOLOGICAL CALIBRATION OF THE TECHNIQUE IN THE DENVER-JULESBURG BASIN, USA

An important test with a new technique is to conduct measurements with the instruments over known geology. In the second half of 1981, a test survey was conducted by Group Seven Inc. in the Denver-Julesburg Basin (DJ Basin) with the following objective:

- Calibration of the LOTEM method over known geology.

In order to compare several different receiver systems, the DJ Basin was selected because a great deal of the geology and geoelectric properties is known from the analysis of numerous well logs (Harthill, 1968). This oil-producing basin is located in the north-eastern part of Colorado, USA. The Colorado School of Mines (CSM) test area is shown in figure 7.14. It is approximately 19 kilometers wide and 280 kilometers long. The topography of the area is relatively flat and only minor distortions due to cultural noise (power lines) exist. Within the CSM test area are a number of oil producing fields. Harthill (1968) analyzed several thousand well logs to derive the geoelectric-geologic cross section shown in figure 7.15. The good knowledge of the geoelectric and geologic parameters make this area appropriate for geophysical test measurements.

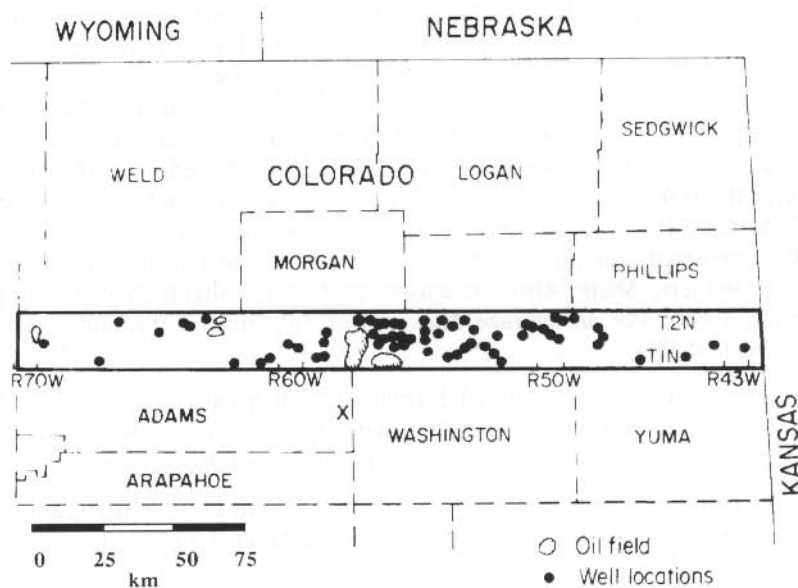


Fig. 7.14: Location map of the Colorado School of Mines test area (heavy border) (after Harthill, 1968).

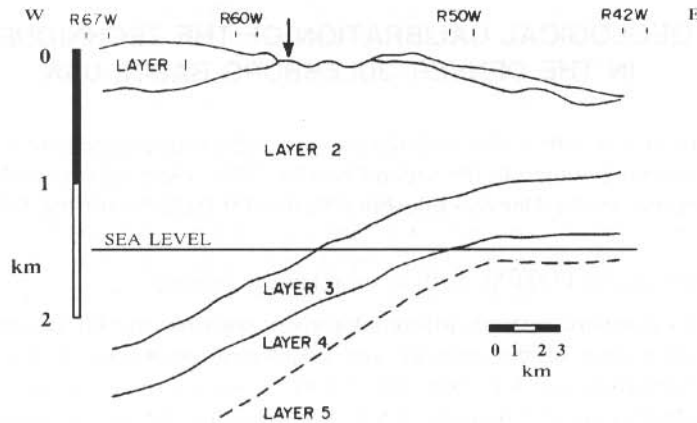


Fig. 7.15: Generalized geoelectric-geologic cross section for the CSM test area (after Harthill, 1968).

The first geologic unit (layer 1) varies through the CSM test area in thickness and resistivity because it consists of a number different geologic formations (Foxhills, Laramie, Denver, Ogallala, Arapaho). Because this layer makes up the weathering layer, the test site was moved 15 kilometers south of the CSM test area (see X in figure 7.14). The test station was located on a crop out of Pierre Shale. The Pierre Shale (layer 2) is geoelectrically fairly homogeneous and has low coefficients of anisotropy (compare figure 1.10). The thickness of the Pierre Shale becomes slightly smaller above the structural high to the east; its resistivity is approximately $3 \Omega\text{m}$. This particular unit has also been of interest for other geophysical test measurements (White et al, 1983; Schneider et al, 1982). The third layer consists of a mixture of sandstones, shales and limestones, and is again electrically uniform (Harthill, 1968). In this layer the Dakota sandstone is highly petroliferous and contains several oil fields in the CSM test area. The thickness of this layer is approximately 400 meters. The longitudinal resistivity for this particular unit is not as constant through the CSM test area as for the Pierre Shale. Also, the anisotropy factor is slightly higher (compare fig. 1.10 for range 58). For an average thickness of 400 meters, the unit's resistivity is approximately $60 \Omega\text{m}$.

The fourth layer consists again of formations which vary in resistivity. However, macroscopically this unit makes up a 300 meter thick layer with high resistivity. The units involved are mainly of Pennsylvanian, Permian and Jurassic ages.

The fifth layer is the precambrian basement consisting of granites and gneisses. Their resistivity is greater than $500 \Omega\text{m}$. Combining layer 4 and 5, one obtains a high resistive unit.

Resulting from this analysis the basic geologic model for the CSM test area is:

Pierre Shale	$\rho_1 = 3 \text{ } \Omega\text{m}$	$H_1 = 1600 \text{ m}$
Sandstones	$\rho_2 = 6 \text{ } \Omega\text{m}$	$H_2 = 1600 \text{ m}$
Electrical basement	$\rho_3 = 500 \text{ } \Omega\text{m}$	

The field system consisted of three of Group Seven's receiver systems. All of the systems used SQUID magnetometers as receivers. All SQUIDS were different models of different age. One of the biggest problems with the receiver systems was the instability of the superconducting magnetometers and lengthy system calibrations had to be done with all systems to obtain comparable results. The apparent resistivity curves for three different receiver systems are shown in figure 7.16. Even after careful system calibrations the system responses of the three different systems are sufficiently different that deconvolution could not restore the signals to become close to each other earlier than 300 milliseconds. Also, at later times, high frequency noise can be seen. However, it is remarkable that in the intermediate time range the apparent resistivity curves for all three systems are almost identical. Thus the data points before 300 milliseconds were eliminated and at later times smoothed yielding a reliable estimate for the sounding at the test station and eliminating the noise of the RF amplifiers of the SQUIDS. As transmitter, a 1.5 kilometer grounded dipole was used at 15 kilometers distance north of the receiver site.

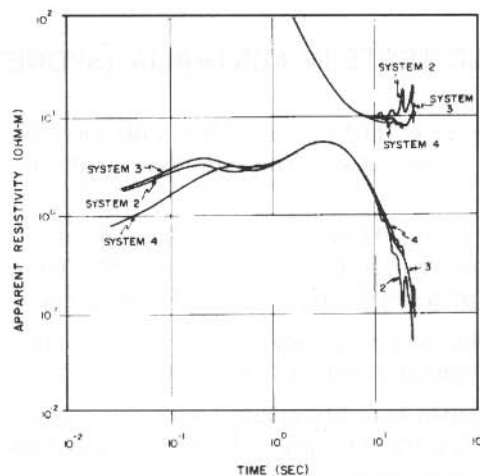


Fig. 7.16: Apparent resistivity curves for the LOTEM measurements over the CSM test area (after Strack, 1985).

The deconvolved smoothed apparent resistivity curves were then compared with the synthetic curves for the geoelectric model published by Harthill (1968). The result of this comparison is displayed in figure 7.17. The match between the field data (dots) and the synthetic curve (solid line) is quite good and thus the geologic calibration of

the systems was successful. From these test measurements further improvements in the data handling procedures and instruments were then derived.

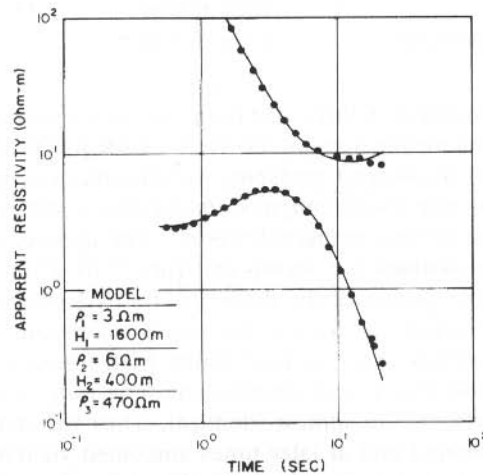


Fig. 7.17: LOTEM field data (dots) and theoretical curves (solid line) for the generalized geoelectric model in figure 7.15 (after Strack, 1985).

FIRST FIELD TESTS IN AUSTRALIA (SYDNEY BASIN)

During 1983 a prototype LOTEM system (DEMS III) was built at Macquarie University and tested in the Sydney Basin. The objectives of the test measurements were twofold:

- Demonstration that the LOTEM method can be applied in difficult areas such as the densely populated Sydney Basin near Sydney. Also the resistivity structure was to be determined for a depth range of 1 to 4 kilometers.
- Demonstration of the simple operation of the entire field system, including data processing, giving special attention to the cost.

The research was funded by a Macquarie University research grant supporting the collaboration between CSIRO, Macquarie University and BHP. A summary of the measurements can be found in Strack (1984).

The measurements were conducted during two days during October, 1983, in an area located about 20 kilometers north-west of Sydney. The Sydney Basin is approximately 380 kilometers long with a total continental area of 36,000 squarekilometres and lies along the east coast of New South Wales (see figure 7.18). The Sydney Basin is divided into five areas: the Southern Area, the Western Area, the Central Area, the Northern Area, and the North-Western Area. In all areas coal is/has been produced.

The individual areas are further subdivided into sub-basins. Hydrocarbons have been found in the Sydney Basin but not in commercial quantities. The test area was selected due to its closeness and accessibility with respect to Sydney and the fact that a topographic map showed the area as open for the receiver sites, and transmitter setup seemed possible in the creeks. When the measurements were being conducted, only a limited number of clearings could be found which explains the distribution of the receiver sites shown in figure 7.19.

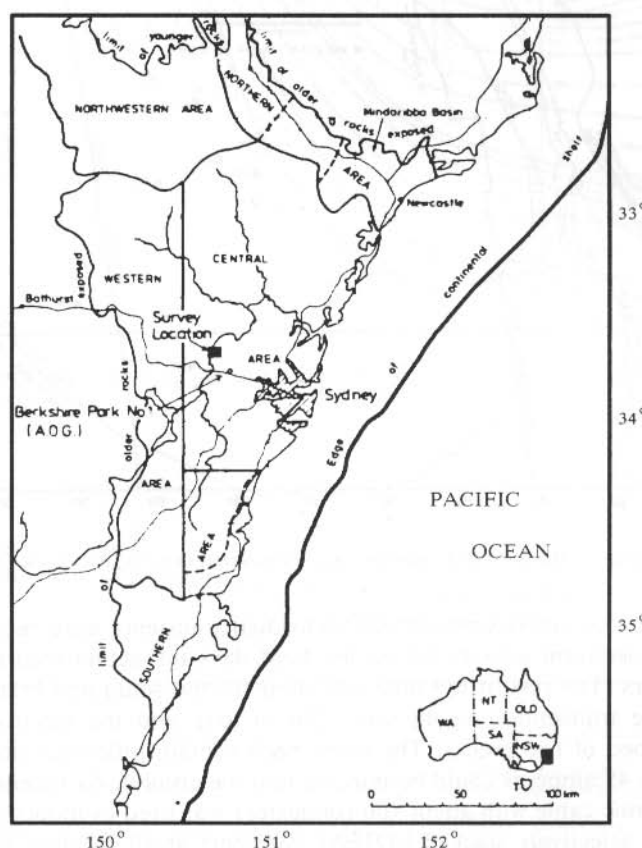


Fig.7.18: Generalized geographic location map of the LOTEM survey area in the Sydney Basin (after Strack, 1984).

The geology of the Sydney Basin consists of a complex mixture of deltaic and marine sediments which results potentially in mainly stratigraphic hydrocarbon traps. This makes the interpretation of geophysical data more complicated because detailed borehole control is required. A more detailed description of the geology of the Sydney Basin can be found in Mayne et al (1974). Figure 7.20 shows a simplified geological cross-section in north-south direction through the Sydney Basin. The arrow marks the

approximate location of the survey area. At this location the strata are horizontally layered (conformably) to a depth of about 3 kilometers, and resistivity contrasts due to lithology are expected. From this section an approximate inversion starting model was postulated. A newer east-west section is shown in figure 7.21 (Mayne et al, 1974), which gives a better overview of the lithology of the Sydney Basin. The exact depth of the Sydney Basin is yet not known.

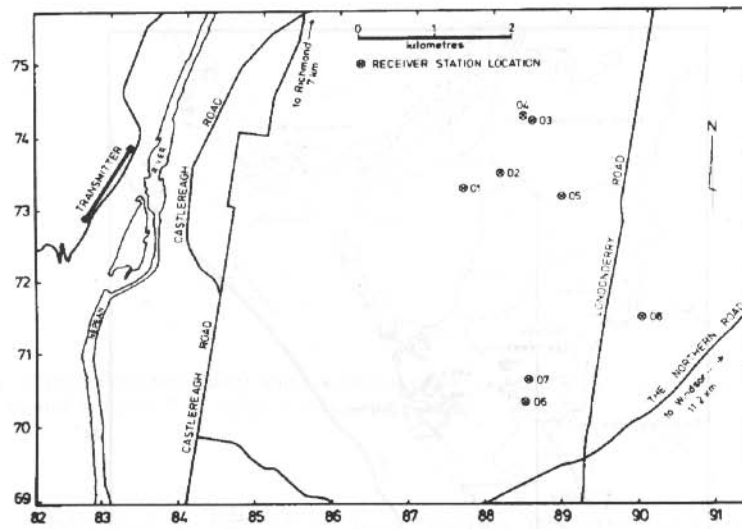


Fig. 7.19: Survey plan of the LOTEM receiver and transmitter sites (after Strack, 1984).

At 8 receiver sites approximately 320 individual transients were recorded. Due to the strong thunderstorm activity during the field days the actual recording time was less than 8 hours. The rest of the time was used for the setup and breakdown of the transmitter. The transmitter dipole was 1200 m long and the electrodes were implanted in the bed of two creeks. The creek beds contain little mud and thus only a current of up to 45 amperes could be injected into the ground. As receiver, a standard 200 m long seismic cable with about 100 conductors was used as induction coil. Figure 7.22 shows the selectively stacked LOTEM transients at all receiver sites. The data become increasingly noisy going towards station 8 because of thunderstorm activity and thus the electromagnetic noise was increasing with time. No data processing was done prestack, which could be part of the reason why the stack of station 8 is so noisy. After stacking the data were filtered, smoothed and the system response deconvolved. An example of the resulting apparent resistivity curves is shown in figure 7.23. The apparent resistivity curve shows already three distinctive layers at early times (compare flexure in figure 7.23).

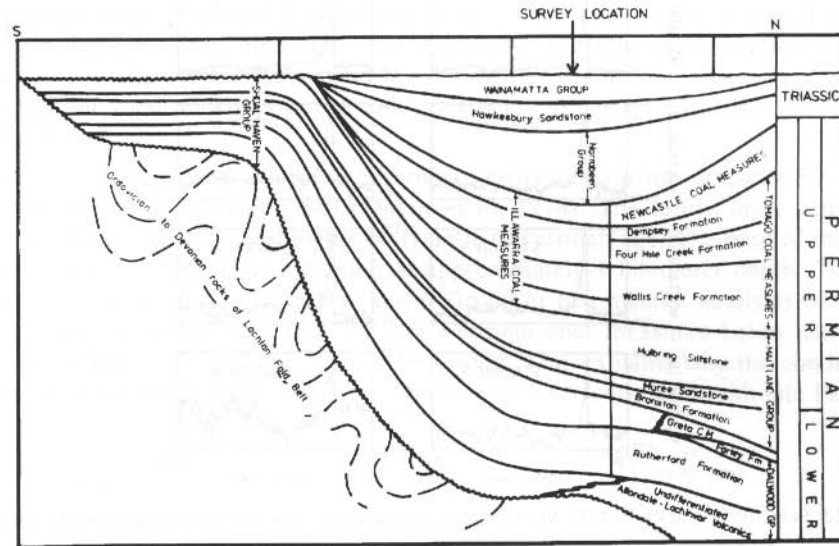


Fig. 7.20: Simplified general geological north-south cross section of the Sydney Basin (after Strack, 1984).

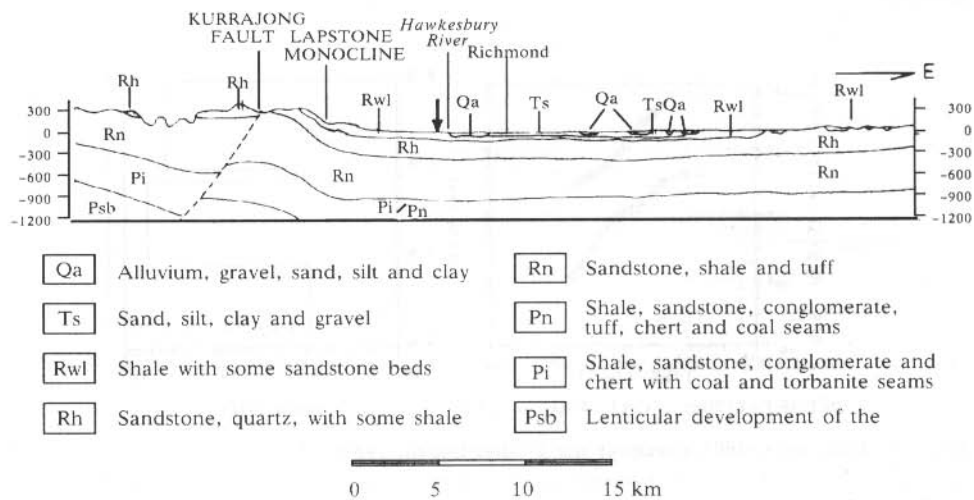


Fig. 7.21: Simplified shallow geologic west-east cross section of the Sydney Basin (after Strack, 1985).

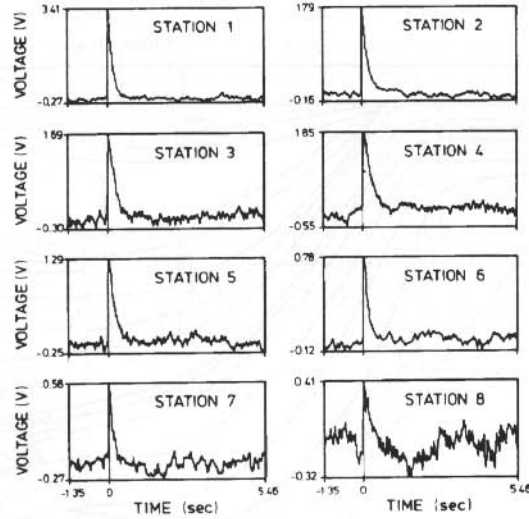


Fig. 7.22: Selectively stacked LOTEM transients of the eight receiver sites (after Strack, 1984).

The known geology required a three-layer starting model. After inversion tests it was found that the inversion required an additional fourth conductive layer which could not be explained initially. Later on this conductive layer was explained by the geology.

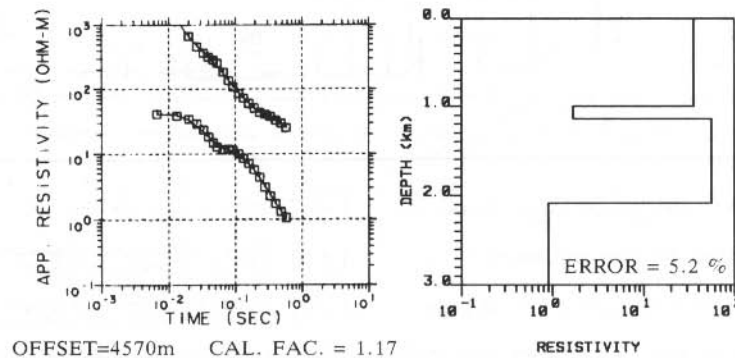


Fig.7.23: Inversion result for receiver site 1 (after Strack, 1985).

The first layer in the starting model consists of a mixture of sandstones, shales, conglomerates and tuffs, the second of a sequence of sandstones, clay shales, tuffs, oil shales and coals. In general one would expect the resistivity of this layer to be the same as the resistivity of the first layer. However, the inversion clearly required this layer to be more conductive. Later on, the analysis of the well completion report showed that the clays in this layer are responsible for the high conductivity of it. The

third layer consisted again of sandstones and shales with a slightly higher resistivity than the first layer. The only information on the fourth layer is that it probably correlates with the Greta coal measures. The geoelectric parameters of the first layer are well resolved, whereas for the second layer only the conductance is resolved. For the third layer the total thickness to the conductor below is resolved, but the resistivity of the third layer not.

Figure 7.24 shows the interpreted geologic cross-section in comparison with the results from the BMR bulletin 149 (Mayne et al, 1974). The fourth layer consists of approximately 1 kilometer sediments of Triassic to Permian age. The base of this layer lies (from the LOTEM measurements) at approximately 1 kilometer depth. The seismic results give the base of the Narrabeen Group at 850 meters. Analysis of several well completion reports says that the late Permian coal measures below start quite sandy at the base of the of the Narrabeen Group. This explains why the conductivity contrast is below the seismic reflector. The second layer correlates with late Permian

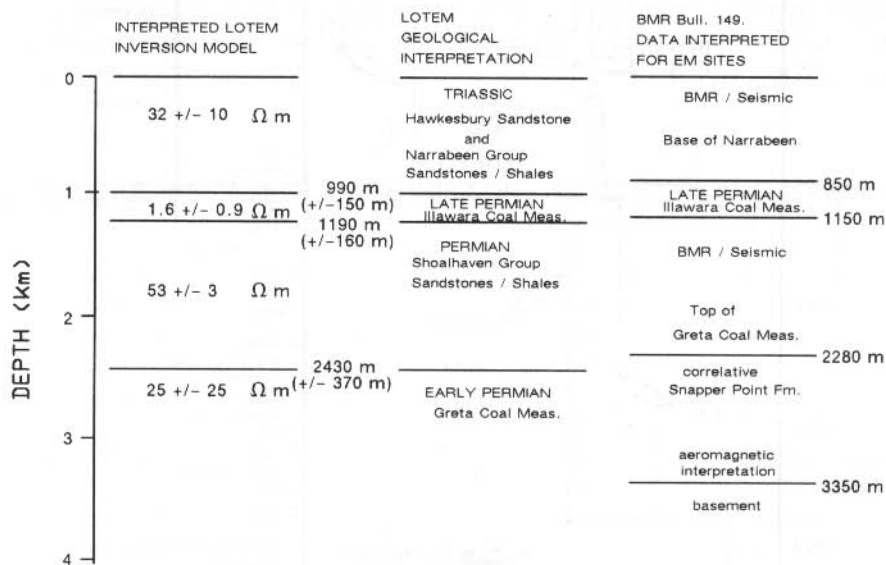


Fig.7.24: Interpreted geological section in comparison with the results from BMR bulletin 149 (after Strack, 1984).

Illawarra coal measures which are in general more resistive. This layer, however, is seen by the LOTEM method as very conductive because of the clay beds within it. The base of the coal measures is in the LOTEM interpretation at approximately 1200 m with 1150 m from the seismic interpretation. The correlation of this horizon is probably caused by abrupt facies changes between the late Permian coal measures and the Shoalhaven Group below. The third layer is a 1200 meter thick unit of resistive marine sequences interpreted to be of the Permian Shoalhaven Group. The average geoelectric boundary at 2430 meters depth is thought to correlate with the seismic pick

at the top of the Greta coal measures and the correlative Snapper point formation at 2280 meters. The discrepancy in the interpretation between the LOTEM and the seismic could either be caused by the LOTEM or the seismic which is based on unmigrated data.

Figure 7.25 shows a comparison of the LOTEM interpretation with the interpretation of audio magnetotelluric data, SIROTEM data and UTEM data. The results of two well logs within the vicinity of the area are also shown. Unfortunately, the wells are too far away from the survey area thus only a qualitative correlation can be done. The Kurrajong Heights (not shown) well shows a very good conductor around 1 kilometer

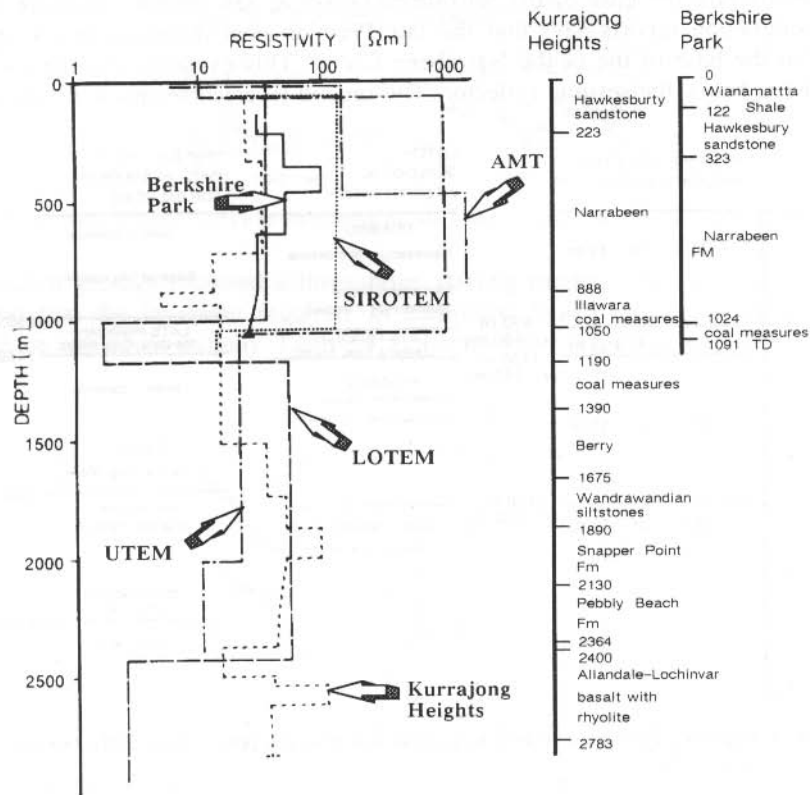


Fig. 7.25: Comparison of inversion results with other geophysical techniques and well log data (modified after Vozoff et al, 1984).

depth. The other well, the Berkshire Park, only goes to approximately 1100 meters depth and does not penetrate this conductive unit. However, this well also shows a decreased in resistivity around 1 kilometer depth. The audio magnetotelluric (AMT) measurements do not penetrate deeper than 500 meters due to the noise in the area. The SIROTEM data shows also a very strong resistivity change towards more conduc-

tive units at approximately the same depth as the LOTEM. However, the resistivities of the SIROTEM measurements are approximately three times larger than the LOTEM measurements. This can either be attributed to the different coupling of the transmitter (the LOTEM uses an earthed dipole, whereas the SIROTEM system uses an induction loop) or systematic differences in the interpretation procedures between both systems. The UTEM results are higher in the upper kilometer as are these of the LOTEM and SIROTEM but very closely approach the SIROTEM resistivity values around 1 kilometer depth. In general the LOTEM measurements average the resistivity of the two wells in the upper kilometer nicely. The LOTEM resistivity seems to be fairly close to the average resistivity for the well log. Since inductive source systems do not resolve resistors as well as galvanic source systems (see chapter 8), the derivation in the resistivity of the SIROTEM and UTEM data from the LOTEM data and well log is acceptable.

The above case history demonstrates that the LOTEM technique could be successfully applied to new exploration problems with a fairly simple prototype system. The data interpretation was done quite rapidly and the interpretation results are comparable with the additional geophysical information available from the survey area.

3-D INTERPRETATION CASE HISTORY MÜNSTERLAND BASIN, FRG

During 1987, a field survey was carried out in the Münsterland Basin near the 5 km deep borehole Münsterland 1. The objective of the survey was to calibrate the method in an area of known geology. Some parts of the survey area show anomalous transients which indicate a 3-D structure. Here, focus is given on the interpretation of these anomalous transients as described by Hördt et al (1991).

Figure 7.26 shows the distribution of the LOTEM stations in the survey area. Magnetotellurics (MT) and Controlled Source Audio-frequency Magnetotellurics (CSAMT) data were recorded in this area at an earlier date by other research groups. They were used for comparison with the results of the LOTEM survey and for 1-D joint inversion with the LOTEM data (Hördt et al, 1991). The LOTEM stations lie along two profiles, which cross near the location of the borehole Münsterland 1. The shaded area denotes the region where 3-D effects were observed in the data. The creeks are related to the geology and are shown in figure 7.26 for orientation.

Figure 7.27 shows the results of 1-D inversions along the profile ML8701, using a second order Marquardt algorithm (Jupp and Vozoff, 1975). To improve the consistency along the profile, the final model of one station serves as the initial model for the next, starting from the western end. The section shows a consistent three-layer model in the western part of the area, but is different in the eastern part (the shaded area in figure 7.25). Stations A03, A07 and A06 require a first layer which is more resistive and thicker than on the rest of the profile.

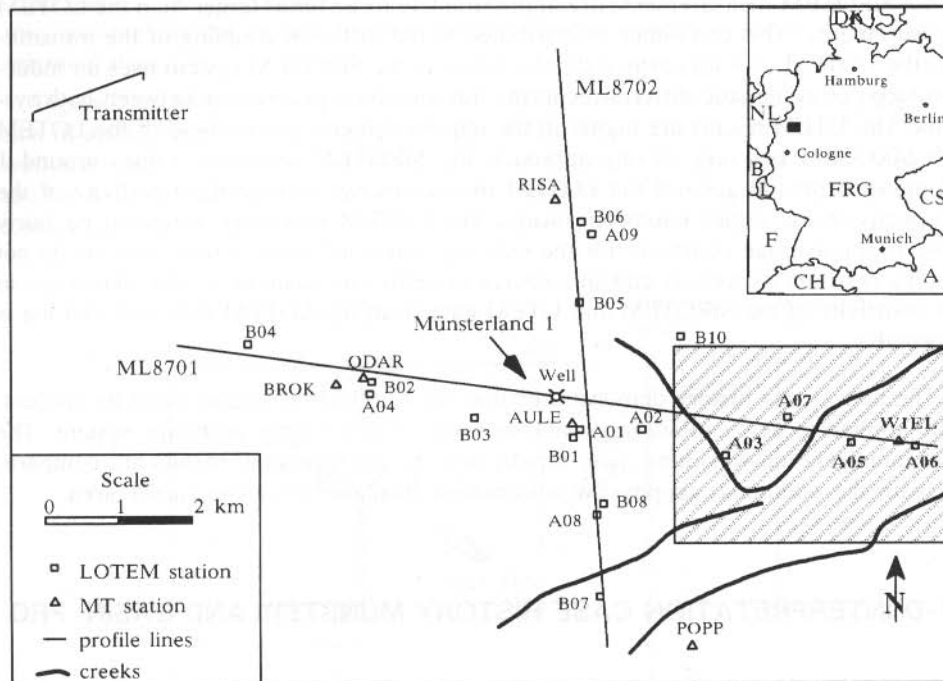


Fig. 7.26: Basemap showing the LOTEM and MT stations in the Münsterland survey area. The shaded area denotes the 3-D region. The creeks are indicated for orientation.

Also displayed in figure 7.27 are six selected data sets. (The field data still contain the system response and look different from synthetic 1-D data at early times. For numerical stability the forward modeling curves are convolved with the measured system response of the corresponding data set, rather than carrying out the deconvolution.) Stations B03 and A01 belong to the consistent part of the profile and show the typical curve shape for this survey area. Stations A03, A07 and A06 have a larger amplitude at early times. A satisfactory fit could be obtained with 1-D inversion, but in fact the large early-time amplitude is a 3-D effect. Station A05 includes a sign reversal in the measured voltage curve which cannot occur over a layered half-space (Newman, 1989). Thus, this station cannot be interpreted using 1-D inversion and clearly indicates a 3-D structure.

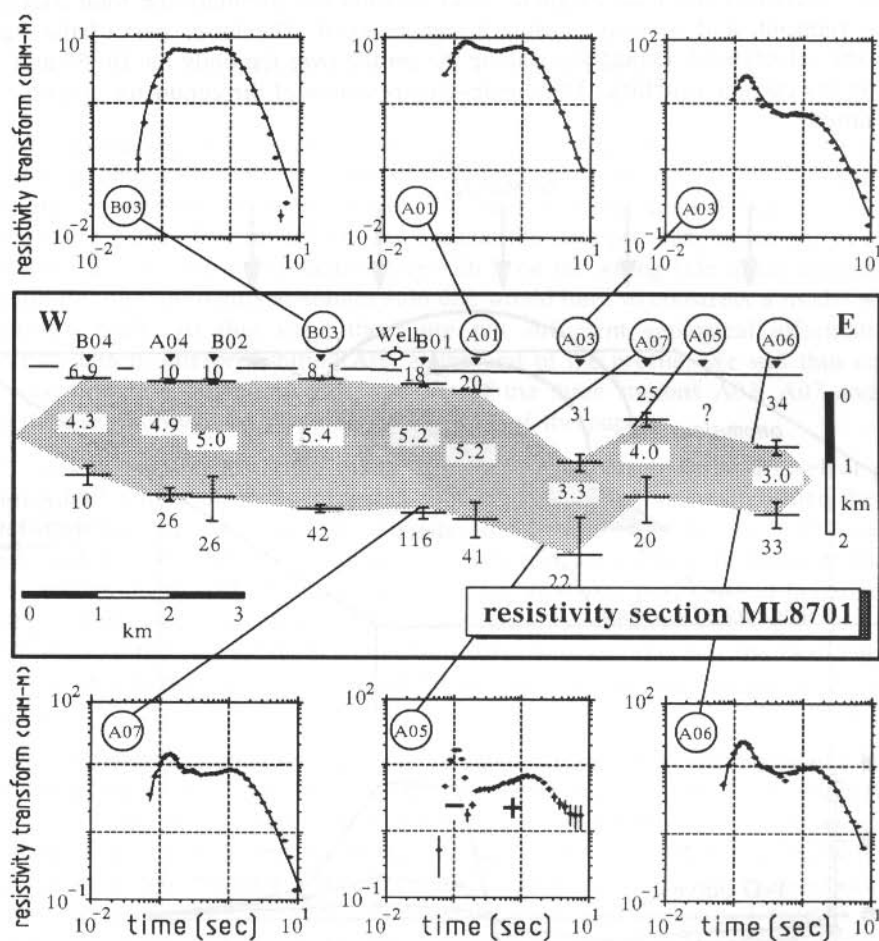


Fig. 7.27: Inversion results along profile ML8701 with the data sets around the 3-D anomaly. The squares correspond to the measured, the solid lines to the calculated data. Data sets B03 and A01 show layered behavior, the other data sets show 3-D effects. Station A05 includes a sign reversal on a linear scale. On the logarithmic scale in the figure the absolute values are shown. The positive and negative data for site A05 are indicated by "+" and "-".

Newman (1989) explains that a near-surface conductor causes a sign reversal if the station is on the side away from the transmitter. On the side towards the transmitter the curve is shifted to higher amplitudes at early times. This effect can be observed in the model responses, used for comparison of the 3-D programs (compare chapter 4). A sketch of a simplified physical explanation is presented in figure 7.28. After the transmitter current is switched, the induced currents in the earth are channelled through the conductive body. This causes a local anomalous current and associated anomalous magnetic field. At the receiver sites towards the transmitter this anomalous

magnetic increases the total magnetic field; beyond the anomaly the total magnetic field is reduced, and possibly causing a sign reversal. The lower part of the figure shows the calculated 3-D responses along the profile over the body for 10, 50 and 100 ms after the current switching. The dipole-type response of the conductor is visible for early times.

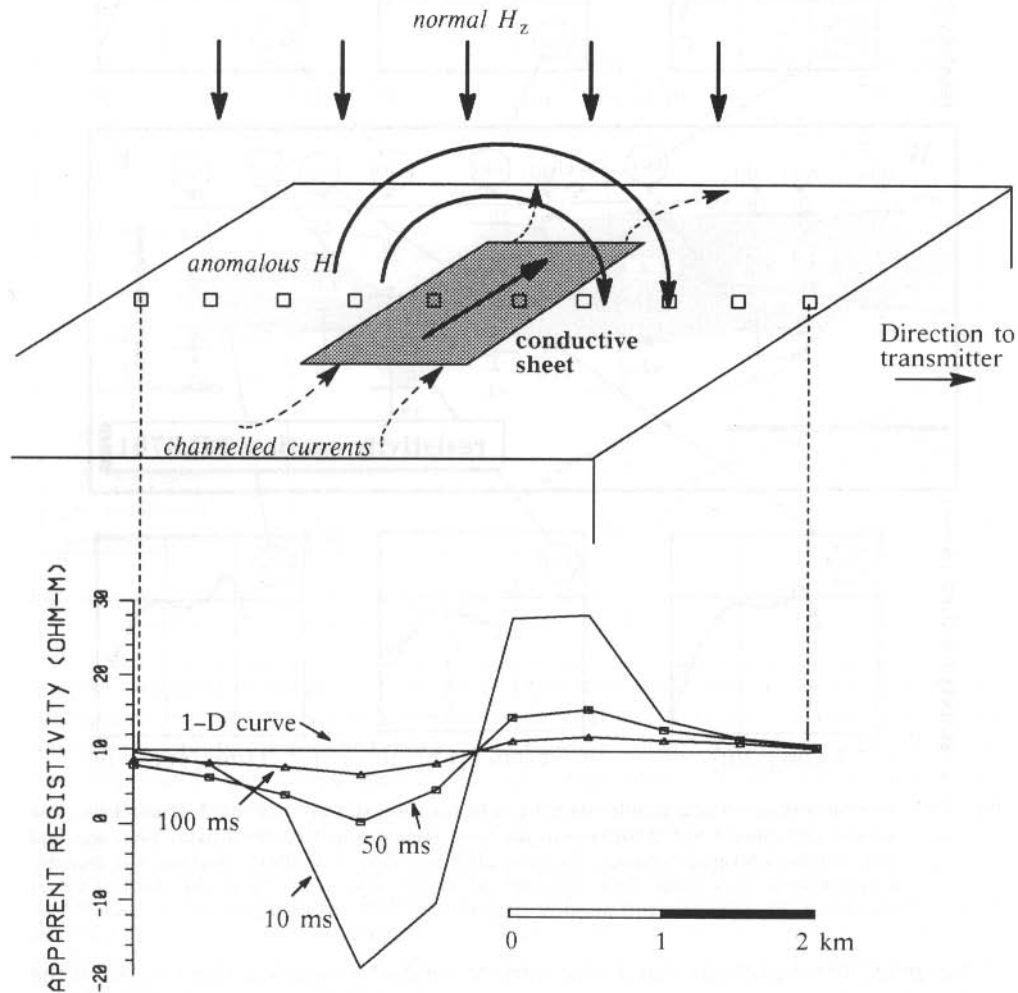


Fig. 7.28: Physical explanation of the 3-D effects observed in the field data. The upper part of the figure schematically shows the behaviour of currents and magnetic fields when the 1-D structure is disturbed by a local conductive body. The squares are the receiver locations on the surface. The lower part shows the apparent resistivity for different times along the profile over the body in comparison with the 1-D response.

Results of Thin-Sheet Modeling

After explaining the observed 3-D response, we apply the 3-D forward modeling routines to obtain a quantitative interpretation. First, we select a conductive body with one edge somewhere between stations A07 and A03 and another between A07 and A05 (figure 7.29). This model will not explain the data set A06, which shows similar behaviour as A03 and A07, because site A06 is on the wrong side of the anomaly. To explain the measurements at station A06 one would have to construct a model with an additional body. At this stage there are not sufficient geological information or LOTEM data to interpret station A06 at the end of the profile. We will thus concentrate on finding a quantitative explanation of the three stations A03, A07 and A05. The data set A06 will be discussed at the end of the paper.

Even with the above starting model it is still a cumbersome trial-and-error procedure to find a thin-sheet model which fits the data. Thus, we incorporated the thin-sheet modeling into an inversion routine, using an algorithm for the 1-D inversions (Jupp and Vozoff, 1975). The variable parameters are the conductance of the thin sheet and its depth. All other parameters, such as strike, position and horizontal extensions of the sheet are fixed. The underlying 1-D earth is also kept fixed at the parameters of the nearest non-3-D station A01. This incorporates the reasonable assumption that in the 3-D area the layering does not change, but is disturbed by a local structure.

Some forward modeling was necessary to find a reasonable starting model. For the first model runs, the 3-D effect on the calculated data was not large enough. The reversal occurred at very early times and was not comparable with the large effect in the data of station A05. We found that we had to use an elongated sheet with strike approximately SW-NE and with increased conductance. Different models which appeared promising after the forward modeling were used as starting models for the inversions. Figure 7.29 shows the best-fitting thin-sheet model, with the corresponding data fits illustrated in figure 7.30. Considering the simplicity of the model, the fits are extremely good. Note also that the early-time amplitudes of station A03 and A07 are well-matched. This was a difficult task because the 3-D effect at station A03 is larger than at station A07, although site A07 is closer to the expected position of the anomalous structure. For the model in figure 7.29 station A07 is so close to the midpoint of the sheet that the 3-D effect is weaker than at station A03. Figure 7.28 illustrates how the 3-D effect becomes smaller when approaching the midpoint of the anomaly, because the scattered magnetic field becomes predominantly horizontal.

The drawback of the model in figure 7.29 lies in the shallow depth of the thin-sheet and its high conductance. This was a common feature of all inversion results. The inversion always moved the sheet towards the surface and increased the conductance, suggesting a man-made conductor – such as railroad tracks or power lines – as cause of the anomaly (Sternberg, 1979). Since these do not exist in this area, we assume that

the shallow depth and the high conductance are an effect of the thin-sheet modeling. The true conductivity structure is probably much more complicated than a thin sheet, and the conductive anomaly could extend vertically rather than horizontally. Thus, we cannot expect to determine the correct depth to the anomalous zone. We can conclude from the thin-sheet modeling that we can fit the data with a conductive anomaly between station A03, A07, and A05, and that the strike is approximately SW-NE. With this information we refine our model further using another 3-D program.

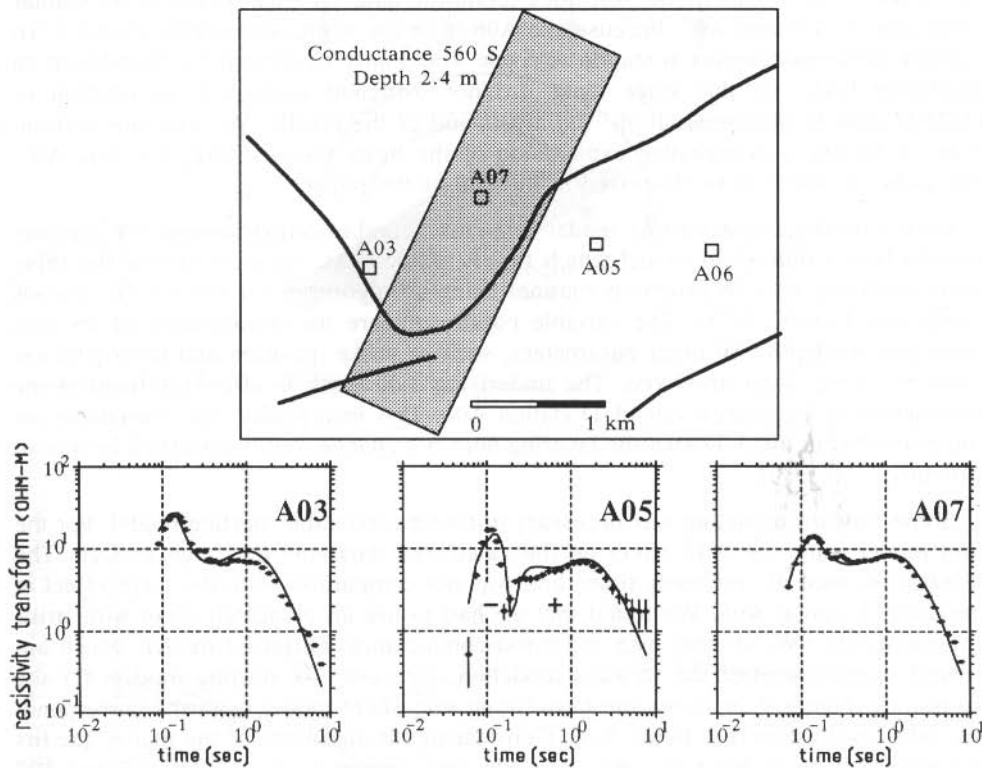


Fig. 7.29: The "best fit" thin-sheet inversion model (plan view). The map corresponds to the shaded area in figure 7.26.

Results of Integral Equation Modeling

After the thin-sheet modeling we must incorporate the geology as a priori information to reduce the number of possible models. The survey area lies within a large sedimentary basin with the upper 1500 m consisting of Cretaceous North Sea Basin deposits. Geoelectrically, the area is horizontally layered. There are no indications of large conductivity anomalies in the upper few hundred metres (Jödicke, 1990). The

only reasonable explanation of the anomaly is deep brine, which is very conductive and could move to the surface along faults or weak zones.

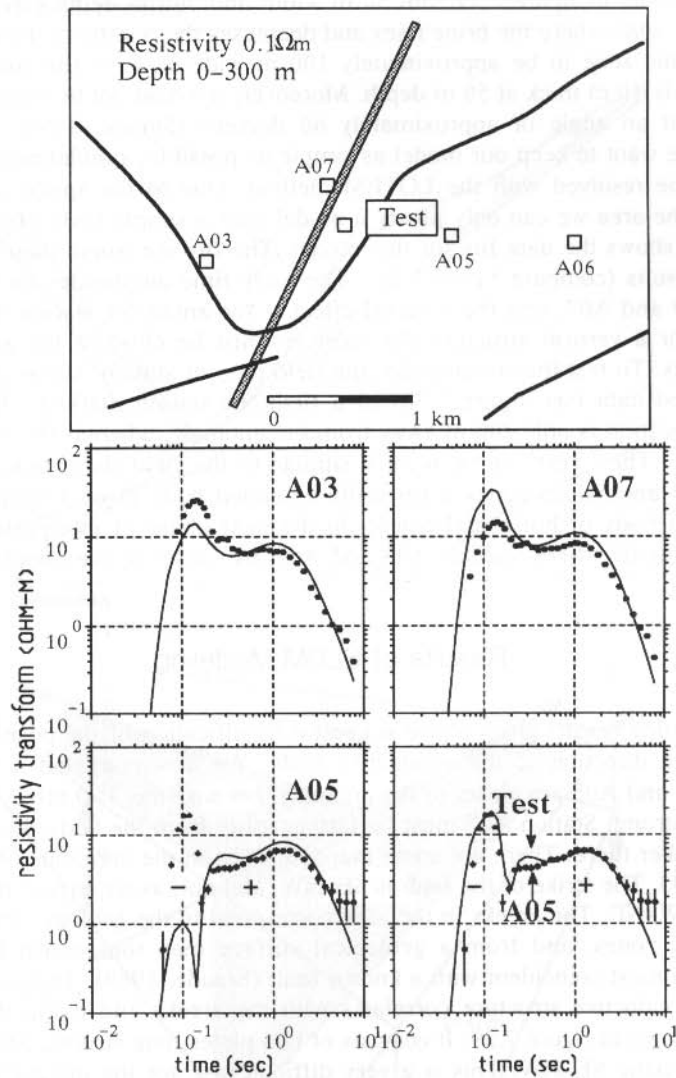


Fig. 7.30: The 3-D model (plan view) used for the simulation with the IE program. The midpoint and the strike of the conductive body are the same as for the thin-sheet model in figure 7.29. The body extends from the surface down to 300 m depth. Data fit for the model configuration is displayed at the bottom. The squares correspond to the measured data, the solid line is the calculated curve. The bottom shows a comparison of data set A05 with the calculated curve of location "Test". It gives a better fit than the calculated curve at the location of site A05.

■ We constructed a model based on the best fit of the thin-sheet inversion, but considering the possible mechanism for the resistivity decrease. A plan view of the model is shown in figure 7.30. The strike of the anomalous structure is the same as for the thin-sheet model in figure 7.29 with 50 m width and 300 m depth extent. This simulates a shear zone where the brine rises and decreases the resistivity. From the geology we expect this zone to be approximately 100 m wide close to the surface and only approximately 10 m thick at 50 m depth. Moreover, it would not be vertical, but rather would dip at an angle of approximately 60 degrees (Staude, 1990, pers. comm.). However, we want to keep our model as simple as possible, simulating only structures which can be resolved with the LOTEM method. Due to the sparse distribution of stations in the area we can only justify a model with a simple body of vertical extent. Figure 7.30 shows the data fits for this model. The fits are worse than the thin-sheet modeling results (compare figure 7.29). The early time amplitudes do not match for stations A03 and A07, and the reversal effect is too small for station A05. This suggests that for a vertical structure the receiver must be close to the anomaly to get strong effects. To test this assumption, the field data of station A05 is compared with the calculated data (see figure 7.30) of a fictitious station marked "Test" in figure 7.30. This location is only 200 m away from the anomaly, whereas the A05 location is 900 m away. The "Test" curve is very similar to the field data, indicating that for near-surface anomalous zones a vertically extended body gives a spatially narrower effect than a body of horizontal extent. In the next phase of interpretation we must construct a model where stations A03 and A05 are closer to the anomalous body.

Results of SLDM Modeling

The modeling results given above suggest a modification of the position and possibly the strike direction of the conductive body. We now construct a model, where stations A03 and A05 are closer to the anomaly, because the 3-D effect in the respective data is strong. Station A07 must be farther away from the body, because the 3-D effect is weaker there. There are some mapped faults in the area; one of them crosses at station A03. The strike of the fault is SE-NW, and not, as we expect from the above modeling, SW-NE. The creeks in the area correspond to the geology. They flow along former weak zones, and from a geological surface map the branch flowing in SE direction is almost coincident with a known fault (Staude, 1989). The resultant model, where the conductive structure correlates with the creeks and mapped faults at the surface is shown in figure 7.29. It consists of two plates, one striking SW-NE, and the other one striking SE-NW. This is a very difficult task for the integral equation program, but it is a reasonable model for the SLDM program, which has been designed for large structures like this.

■ The results of the forward modeling are shown in figure 7.32. The data fit is very good for stations A03 and A05. Note that now the early time part of A03 is fit nicely by the modeled curve. The fit is not perfect for station A07. One could improve the model further to reduce the deviation for A07. This requires additional model runs

where we modify our model step by step. Initial testing has shown that the main conclusions do not change substantially in this process.

The SLDM model

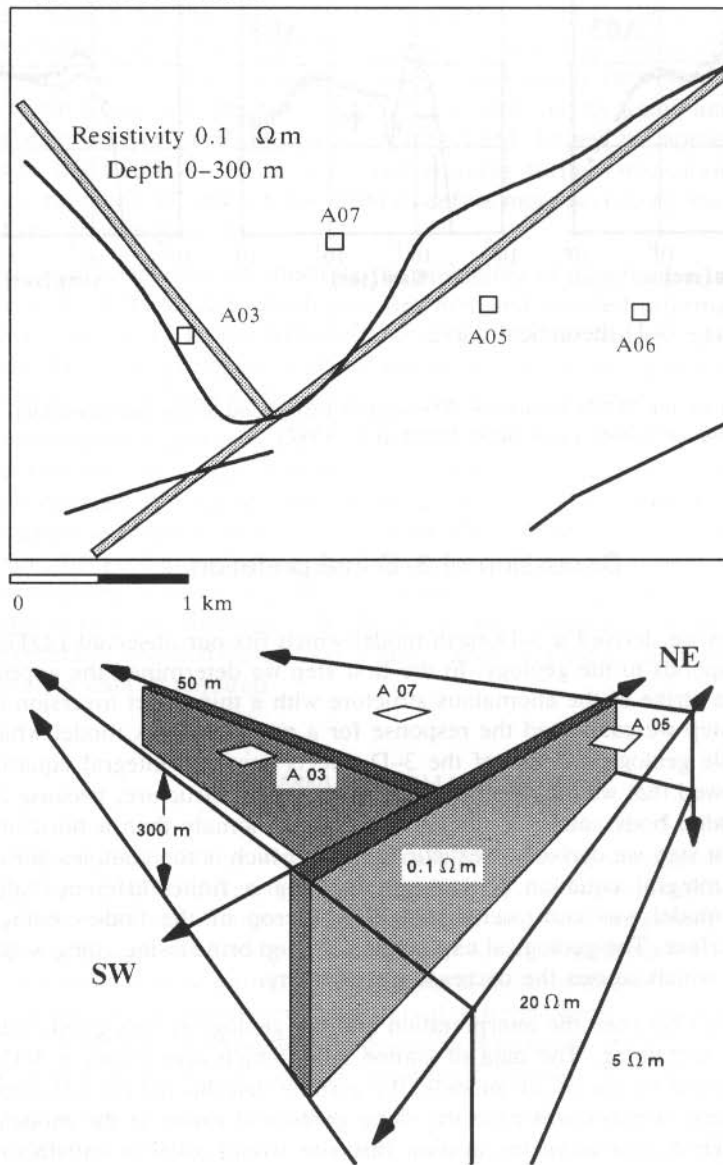


Fig. 7.31: Top: The 3-D model (plan view) used for the simulation with the SLDM program. Bottom: Schematic 3-D sketch of the 3-D SLDM model (after Hördt et al, 1992).

Data fit for the SLDM model

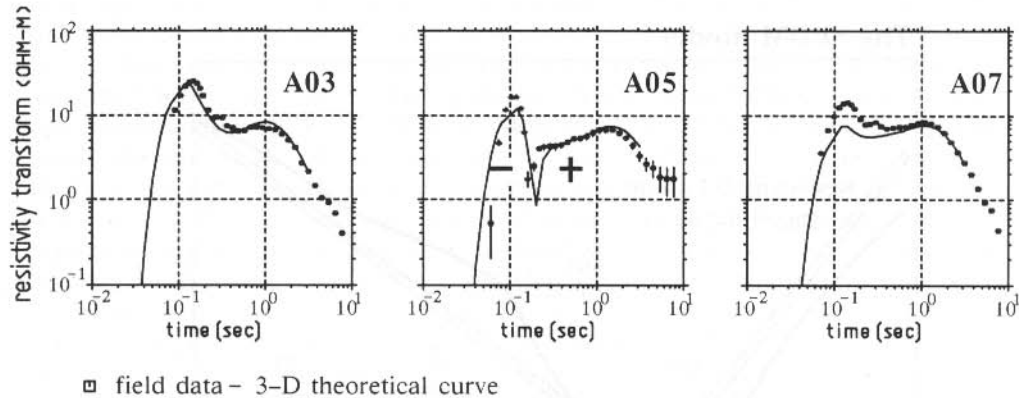


Fig. 7.32: Data fit for the SLDM simulation. The squares correspond to the measured data, the solid line is the calculated curve (after Hördt et al, 1992).

Discussion of 3-D Interpretation

In three steps we derived a 3-D earth model which fits our observed LOTEM data and also corresponds to the geology. In the first step we determined the approximate position and the strike of the anomalous structure with a thin-sheet inversion routine. In the second step we calculated the response for a more complex model which integrates a possible geological cause of the 3-D effects using an integral equation program. This showed that we had to modify the strike of the structure, because the now vertically extended body causes a spatially narrower anomaly than a horizontal thin sheet. In the last step we derived a realistic model – which is too complex for calculation with the integral equation program – applying a finite-difference algorithm (SLDM). The model was constructed with the outcrop of the bodies being below creeks at the surface. The geological explanation is deep brine rising along weak zones (Staude, 1989) which causes the decrease in resistivity.

The correlation between the interpretation and the geology is very good, with some open questions remaining. The data of station A06, which also shows a 3-D effect, cannot be explained by any of our models. We assume that this data is influenced by a different structure, which could have the same geological cause as the modeled one. Additional LOTEM measurements around this site would allow a satisfactory 3-D interpretation. Supplementary geophysical information in this area exists in form of MT and CSAMT measurements. The MT data at site "WIEL" (see figure 7.26) does not show any 3-D effect in the depth range of the LOTEM measurements (Hördt et al,

1991). Additional MT data and data from different geophysical measurements are either not available, or not directly comparable.

In the computations for the final model we used a resistivity of $0.1 \Omega\text{m}$, which is very low even for high salinity brine. Calculations with different resistivities and larger structures suggest that the resistivity of the structure could be higher, but not above $1 \Omega\text{m}$. An explanation of the low resistivity could be salty clay, which in addition to the decrease in resistivity may cause an induced polarization (IP) effect. IP effects on TEM data have been investigated by Flis et al, (1989) and by Smith and West (1989), who explained sign reversals in coincident loop TEM. To test the applicability of their theories to the LOTEM data in this area requires further measurements, such as geoelectric mapping, IP and shallow TEM to define more accurately the physical properties of the anomalous zone.

As our main conclusion we illustrate the possibility of quantitative interpretation of 3-D effects in LOTEM data which provides new and detailed information about the conductivity structure. In the Münsterland area, it is difficult to give a conclusive judgement about the geological truth of the model due to the sparse station density, but it is an excellent basis to design more detailed investigations.

Our interpretation approach can be applied in different areas, where the observed 3-D effect shows also a sign reversal at one receiver site together with an early time amplitude increase at other stations. In these cases we recommend the use of a thin-sheet program to obtain a first fit to the data. The second and third step will depend on the specific geologic situation, but the sequential use of simple and then more complex modeling routines may be reasonable in any case. Our procedure will not necessarily work if the observed 3-D effects are more complex than those shown here (i.e. the reversals are distributed over a large area). For these cases more experience with real field data is required.

SUMMARY CHAPTER 7

This chapter demonstrates with several case histories the successful application of the LOTEM method on different continents. For all case histories different hardware systems, processing and interpretation procedures and field crews were used. In Germany the objective of the survey was to obtain additional information between closely spaced wells in an area of extremely high cultural noise level and to interpret complex geology. In the United States several different systems were calibrated under known geology. In Australia a newly built field system was tested in an electromagnetically noisy environment under difficult field conditions (weather and accessibility).

In all cases the results are better than the expectations were before the survey. In the Ruhr Area survey the structure mapped with the LOTEM surveys matches with the known structure which is derived from numerous mines within the area. In Colorado the results from the three field systems turned out to be comparable although several data points had to be eliminated at the beginning because of irregularities in the sys-

tem response. During the field tests in Australia the LOTEM system confirmed that it could achieve a depth investigation of 1 to 2 kilometers and define geologic interfaces which were confirmed by other geophysical data and well logs.

Finally, three different 3-D numerical modeling routines are used to interpret LOTEM data from the Münsterland area, FRG. First, a thin-sheet algorithm gives the approximate strike direction of the structure. The second, an integral equation program, is used to explain the effect of the anomaly and its vertical extent. Last, a more realistic geological model is calculated using a finite difference algorithm. The combination of all three routines yields an interpretation strategy for complex structures.

PROBLEMS CHAPTER 7

1. Would we resolve the top of Carboniferous (Haltern case history) if directly above is a 100 m layer of Zechstein? Use the forward modeling program MODALL and high resistivities for the Zechstein.
2. How can you 'see' from the display of the inversion results and the importances the parameters are not highly correlated?
3. Calculate some representative curves for the DJ Basin case history including the weathering layer. What do you conclude from that?
4. Why do the deconvolved curves for the different receivers in the DJ Basin case history do not match?
5. Calculate comparative LOTEM synthetic curves for all the different models derived from the EM measurements for the Sydney Basin case history. Explain the differences and show which curves could also explain the LOTEM data.
6. Which is the range of applicability for the different 3-D programs used to interpret the Münsterland 3-D data?

KMS Technologies – KJT Enterprises Inc.
6420 Richmond Ave., Suite 610
Houston, Texas, 77057, USA
Tel: 713.532.8144

Please visit us
<http://www.kmstechnologies.com>

This material is not longer covered by copyright. The copyright was released by Elsevier to Dr. Strack on November 5th, 2007.

The author explicitly authorizes unrestricted use of this material as long as proper reference is given.

KMS Technologies – KJT Enterprises Inc.

An EMGS/rxt-company

Chapter 8 Case Histories : Resolving Resistive Layers with LOTEM

extract from

Strack, K.-M., 1992, reprinted 1999
***Exploration with deep transient
electromagnetic:*** Elsevier, 373 pp.

This material is not longer cover by copyright. The copyright was released by Elsevier to Dr. Strack on November 5th, 2007.

The author explicit authorizes unrestricted use of this material as long as proper reference is given.

Chapter 8

Case Histories: Resolving Resistive Layers with LOTEM

One of the most difficult tasks for electromagnetic geophysicists is the development of new applications of EM techniques. In the exploration environment the physics of EM methods are often either not clearly understood or the capabilities are incompletely evaluated. Some of the newer applications of the LOTEM technique are demonstrated in this chapter. Although mostly simple one- or two-channel field systems have been used to date, the results show a very promising potential for newer applications. The first two case histories cover the resolution of resistive layers using the LOTEM technique. The information presented here is based on a paper by Strack et al (1989). The first successful field tests of applying LOTEM with electric field measurements were pioneered by Vozoff in Australia and subsequently the work was continued in FRG. Following, a case history from China is shown, where the use of the technique was demonstrated to a structure involving carbonates.

In areas of basalt cover, crystalline overthrusting or surface carbonates (Berkman et al, 1983; Andrieux and Wightman, 1984; Prieto et al, 1985; Stanley et al, 1985) electromagnetic methods have been successful, because they respond to different physical properties than seismics. However, since electromagnetic methods do not have the intrinsic resolution of reflection seismics, it is very important to utilize the available resolution of EM to the fullest. The next step, beyond passive EM methods such as magnetotellurics (MT), is the use of a controlled source method such as transient EM which might offer higher resolution.

Here the case histories follow the work of Eadie (1981) and Verma and Mallick (1979). The first is an exploration problem from an oil field in Europe where a resistive layer had to be defined in an oil-producing environment. In the second case history, LOTEM was applied in Australia to define porous regions in a carbonate within a sedimentary sequence. In both cases interpretation was assisted by inversion using models incorporating prior information such as well logs, reflection seismics and/or geology.

EXTENSION OF THE PHYSICAL CONCEPT TO RESISTIVE LAYERS

In chapter 2, the basic physical background of the LOTEM method were discussed and the smoke ring concept was introduced. Now, let us compare the effect of conductive and resistive layers embedded in a medium resistive host. To visualize the current flow in the subsurface, figure A.7.6 (appendix 7, color figures) shows contours of current densities for a conductive (left, $1 \Omega\text{m}$) and a resistive (right, $400 \Omega\text{m}$) layer in a half-space of intermediate resistivity ($20 \Omega\text{m}$). The individual frames are snapshots in time starting with 0.01 seconds at the top to 1 second for the bottom frames. The difference between the left and right sides lies in the current densities within the second layer. For the conductive case (left column) the currents remain relatively longer within the conductive layer. For the resistive case there are no induction currents visible in the resistive layer. A secondary contribution to the electric fields is due to a charge accumulation at the horizontal interfaces for the resistive layer resulting from vertical current flow. In the conductive layer case most of the energy is transmitted through the second layer by currents. For the resistive case the magnetic field carries the currents through the layer.

All inductive electromagnetic sources – such as used with MT and large loop EM methods – can only induce horizontal induction current flow in the subsurface (Verma and Mallick, 1979; Boerner, 1992). The galvanic part of the grounded electrical dipole causes a vertical component of the electric field (Nekut and Spies, 1989). This component generates electrical charges at the horizontal layer boundaries. The frames in figure A.7.7 are horizontal sections at the top of the second layer for different times. They can be pictured as a horizontal time slices through a vertical smoke ring. These time slices show the distribution of the charge density for the resistive (right column) and for the conductive (left column) case of figure A.7.6. The charges are positive (yellow and red colours) when the electric field points from a conductor towards a resistor. They are negative (green and blue colours) when the electric field points towards a conductor. The polarity of these charges depends on a) the transmitter polarity and b) the jump in the electric field which is needed in order to satisfy the continuity of the normal current density component. The charges have opposite signs on either side of the transmitter. They also have opposite signs according to whether the bed is resistive or conductive (compare left with right column). The latter means that the charges are sensitive to the resistivity contrast at the layer boundary. Any measurable effect of the charge accumulation should therefore be a good indicator of the embedded layer resistivity. Initially, the lateral moveout in both cases is the same. Then the charge build-up moves out faster for the resistive case. The bottom two frames show that the uniformity of the charge distribution increases with time, but proceeds faster in the resistive case. The charge distribution on the resistive layer is also stronger for all times. However, the electric charges at the second layer remain longer at the interface for the resistive case. As a

result, conductive targets can be found measuring the effect of the induction currents (figure A.7.6) and resistive targets by measuring the effect of the charges at the resistive layer interface (figure A.7.7). In both cases, when the conductive or resistive layer becomes too thick or its resistivity too extreme, it will act as a screening layer masking the section below.

One can simplify the explanation by describing the measurements of electric and magnetic fields as a combination of time focussing electromagnetic soundings with DC-resistivity soundings. This means through the grounded dipole transmitter and the electric field sensors one carries out a dipole-dipole sounding with the time and the volume focussing effect of the temporal diffusion of the induction current. In this one has more depth resolution (due to smaller volumes of integration) because of the transient phenomenon.

The two test surveys were done with different sets of hardware. In Europe we used DEMS IV (Digital Electromagnetic System, IVth generation) – the system described in chapter 5. In Australia a Zonge GDP 12 receiver (with a special LOTEM preamplifier) and transmitter (25 kVA), especially modified for the survey, were used. In both systems the magnetometers consisted of large multiturn loops with effective areas of the order of 200 000 squaremeters laid flat on the surface. Transmitter dipoles were wires 1–1.5 km long, earthed at each end. The electric fields were measured between grounded copper-copper sulphate non-polarizing electrodes 100 m apart. In both systems, the transmitter injected commutated currents with periods of seconds to minutes.

In the Zonge equipment, a current of 30 Amperes was maintained, and both E and H signals were recorded (with or without stacking) in the two-channel receiver. The incoming signal traces could be observed in real time on a portable oscilloscope. The DEMS IV receiver also allows online quality control and storage of individual transients. The DEMS IV transmitter injects currents of the order of a hundred Amperes provided by a high power switch/rectifier which uses all three phases of an 80 kVA motor generator. Transmitter switching and receiver sampling in both systems were synchronized by precision quartz oscillator clocks. Preamplifiers/filters located near the sensor units sent signals in the millivolt-to-volt range to the main amplifier/filter units and from there to the digital data acquisition systems.

EUROPEAN CASE HISTORY

A test survey was carried out in Europe with the objective of mapping geologic structure in an area of known geology over an oil field. In this, as in many other areas, the zone of interest was electrically resistive. On the basis of earlier suggestions by Eadie (1981), verified in Australia, electric field measurements were used in addition to the magnetic fields for better resolution of resistive features.

Figure 8.1 shows a survey plan of the test profile over an oil field. The sites shown on the map are only a small part of a larger survey. The receiver locations were

occupied twice, from two different transmitters, one located in the northeast and in the southwest, respectively. This was done primarily to see whether structural complications might lead to different interpretations for the data from the different transmitters. Currents of 50 and 150 Amperes were used at the different transmitters. Both transmitters gave comparable results as indicated by the two inversion results at station -2 shown in figure 8.2. The slight differences can be attributed to the smaller signal-to-noise ratios and the shorter recording time (higher sampling rate) for transmitter A measurements. Thus, for this survey we assumed the validity of one-dimensional inversion.

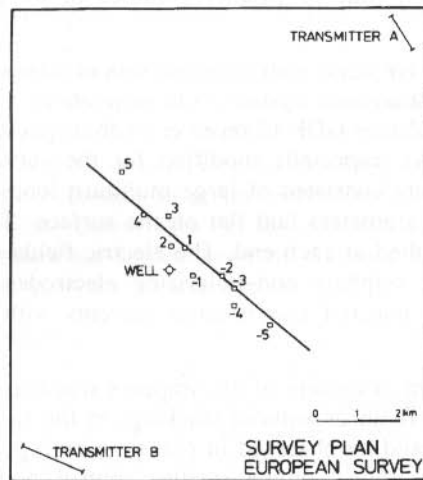


Fig. 8.1: Transmitter and receiver survey plan (partial) of the European test. Station numbers start with 0 at the well, going positive in the western and negative in the eastern direction (after Strack et al, 1989b).

Since the survey area is over an oil-producing field some pipelines and wells existed. In order to evaluate whether these distort the signal by either induced polarization or current channeling near the transmitter, routine walkaway tests are done (receiver locations not shown here). This means that the receiver is moved along the equator of the transmitter. Because for the LOTEM system used for this survey the system response was about 100 ms long, early time pipeline effects would be attenuated. Only if they are very strong they would show as reversals on the walkaway test (compare chapter 4). For this survey area the walkaway test did not show any anomalous behavior which is mainly because pipeline response in this area lies in a frequency range which is filtered out by the analog filters (which are required due to the strong cultural noise). Furthermore, the receivers were kept at least 50 meters away from the pipelines and 200 meters from pumping wells in order to avoid excessive electromagnetic noise in the measurements.

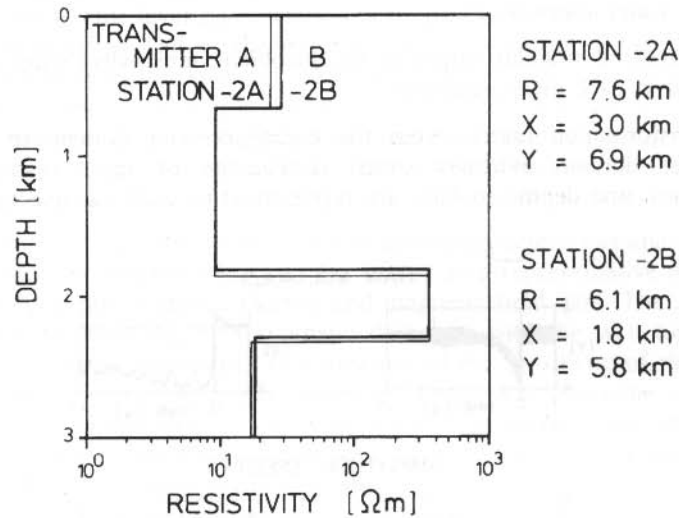


Fig. 8.2: Comparison of inversion results at station -2 for two different transmitter locations displayed on a log-linear scale (after Strack et al, 1989b).

Examples of the magnetic and electric field transients and their respective processing steps for station 4 on this profile are shown on figure 8.3. The upper two frames show a raw transient for the magnetic (left) and the electric field (right). Below, their amplitude spectra are displayed. These spectra are used only for quality control and to define accurately the noise frequencies for each individual transient. These noise frequencies are then removed using recursive filters which retain true amplitudes (third pair of frames). Finally, the individual transients (routinely 50) are selectively stacked, rejecting the sporadic noise (Strack et al, 1989). The resulting stacked transients are shown at the bottom. After this processing the raw voltages are converted to true magnetic and electric fields. The magnetic fields are then corrected for first order transmitter overprint (Zonge et al, 1986) using the calibration factor described in chapter 3. The data are then converted to the logarithmic domain and resampled for data reduction. The reduced data are input into the inversion routines (Strack, 1984). At this stage we use a parametric inversion described by Jupp and Vozoff (1975), Vozoff and Jupp (1975) and Raiche et al (1985), which also outputs error statistics and a detailed resolution analysis of the individual model parameters. Some of the transients (less than 10%) were too strongly distorted by cultural noise to be interpreted.

For the starting model required for the inversion was derived from the well log. This was reduced to a sequence of models having various numbers of layers in order to obtain the simplest model which would explain the observed transients. The inversion outputs for the useable magnetic fields at each receiver position are shown in figure 8.4. The statistics output of the inversion program contains three different

pieces of information which show the model resolution (Raiche et al, 1985) (compare also chapter 4 and appendix 3):

- The normalized singular values of the Jacobian (sensitivity) matrix indicate the *confidence* in each eigenparameter.
- The transformation matrix from the eigenparameter domain to the physical parameter domain indicates which *combination* of layer resistivities, layer thicknesses, and depths-to-base are represented by each eigenvector.

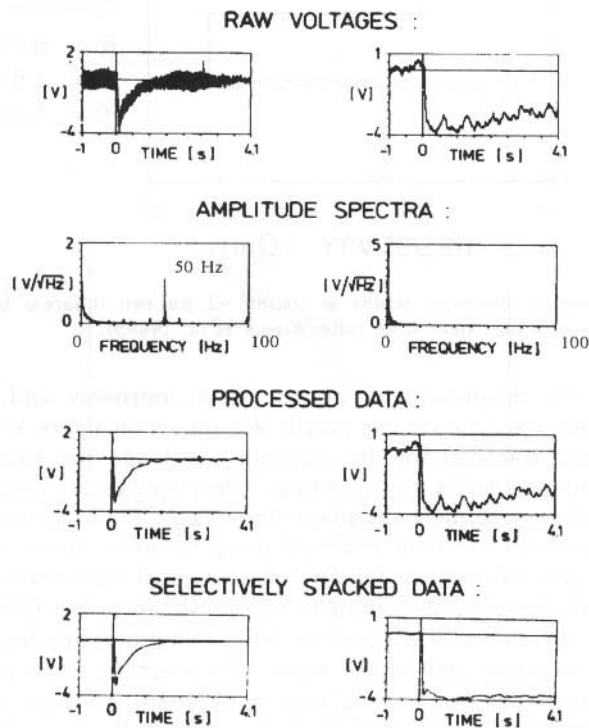


Fig. 8.3: Intermediate results from the data processing at one station of the test profile in figure 8.1. The magnetic response (time derivative of the magnetic field) is shown on the left column and the electric field signal on the right (after Strack et al, 1989b).

- The damping factors for the original parameters are measures of the *importance* of each resistivity, thickness or depth-to-base in the fit of the calculated curve. Resistivities of the upper two layers and their respective thicknesses were well resolved. Their importance are above 80% and they are contained in the eigenvectors with confidences above 70%. The resistivity of the resistive layer (hatched) was poorly resolved. Its importance was below 1%, and it was not contained in the eigenvector with the highest confidence.

Figure 8.5 shows a profile with the usable electric field inversion results. The electric field resolves the layer parameters (resistivities and thicknesses) of the top two layers, but not quite as well as the magnetic field (importances between 50% and 80%). However, both the thickness of the resistive third layer, and its resistivity were better resolved by the electric field data with importances between 10% and 30% as compared to less than 1% for the magnetic field data. The consistency in the third layer of the magnetic field inversions across the profile is only because the third layer is input as starting model.

This difference in sensitivity to the resistive layer parameters was analyzed with the Jacobian matrix. The blocked resistivity log served as a representative model for the survey area to generate synthetic electric and magnetic field data. The Jacobian was then calculated by inverting both synthetic data sets with the well log as starting model. Each column of this matrix is a measure of the sensitivity of the data set to variations in the corresponding earth parameter. Figure 8.6 shows the sensitivities to variations of the parameters of the intermediate (resistive) layer and has little sensitivity to thickness changes of this unit. The magnetic field appears almost insensitive to changes in the resistivity of the resistive layer whereas the electric field shows strong effects for both resistivity and thickness variations.

The above results show that LOTEM measurements can be made successfully in the electrically noisy environment of industrialized Western Europe. The resistive layer parameters could be resolved over a producing oil field. The initial objective of the survey to match the well log was successfully achieved. Furthermore, the resistivity of the resistive unit could be determined, a task previously not possible with surface geophysical methods.

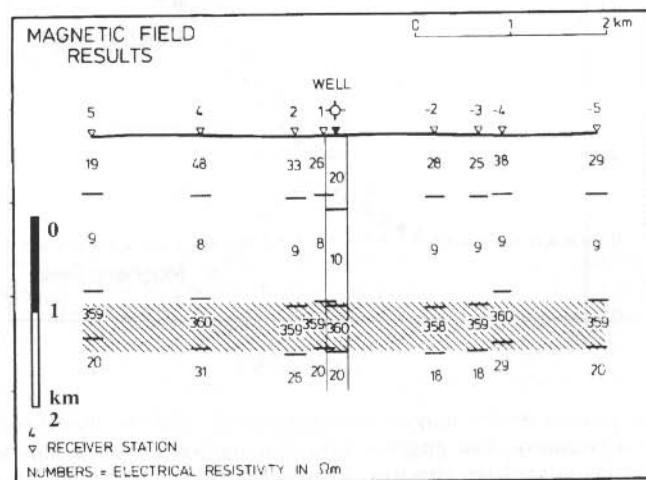


Fig. 8.4: Inversion results based on the magnetic response data using both transmitters. The depth to the top of the resistive region (shaded) is resolved but not its resistivity or thickness (after Strack et al, 1989b).

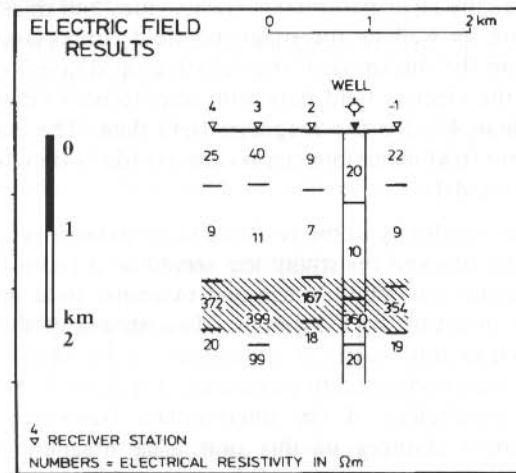


Fig. 8.5: Inversion results based on the electric field data using both transmitters. The depth to the top of the resistive region (shaded) is resolved, as is its resistivity (after Strack et al, 1989b).

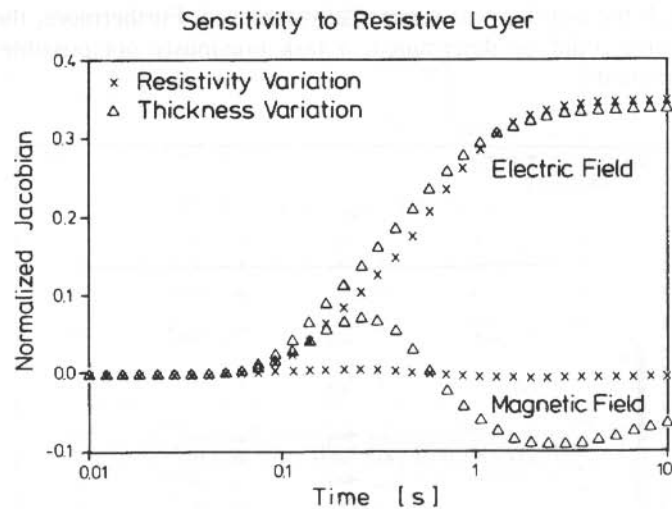


Fig. 8.6: Resolution analysis for the resistive layer parameters using the normalized Jacobian as a measure of sensitivity. The magnetic field (bottom two curves) is almost insensitive to changes in the target layer resistivity, whereas the electric field (top two curves) is very sensitive to both thickness and resistivity variations (after Strack et al, 1989b).

CANNING BASIN, AUSTRALIA, CASE HISTORY

In evaluating LOTEM in Australia, the capabilities of the method for resolving variations in resistive strata was of particular interest in the Canning Basin (figure 8.7). Minor production is obtained from porous zones within the very extensive Windjana / Nullara limestone of Devonian-Famenian age (figure 8.8). The limestone is easily mapped by reflection seismic surveys, as is shown below. The major exploration difficulty has been in locating zones of adequate porosity.

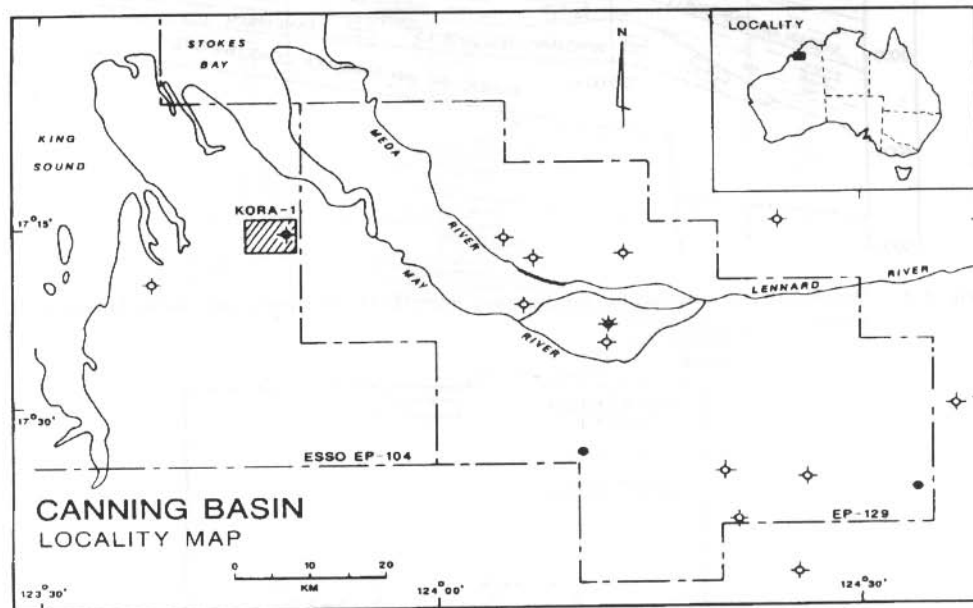


Fig. 8.7: Basemap of the Australian survey (after Strack et al, 1989b).

For evaluation purposes a region was selected where high quality seismic sections and good well logs were available. Kora-1 (figures 8.7 – 8.13, 8.15) had already been completed and West Kora (figure 8.9) was being drilled in mid-1985 when the LOTEM survey was undertaken. Both holes showed poor porosity. A geological section through Kora-1 is shown in figure 8.8. As the well bottomed in the Napier formation, lithology and structure below drilling depth are conjectural.

Figure 8.9 shows the LOTEM survey plan. LOTEM measurements were conducted using a current of 30 Amperes through approximately 1.5 km long grounded wire dipoles. Both electric and magnetic field measurements were made on line 4 from transmitter 2. The area was electrically relatively quiet, which resulted in clean field data.

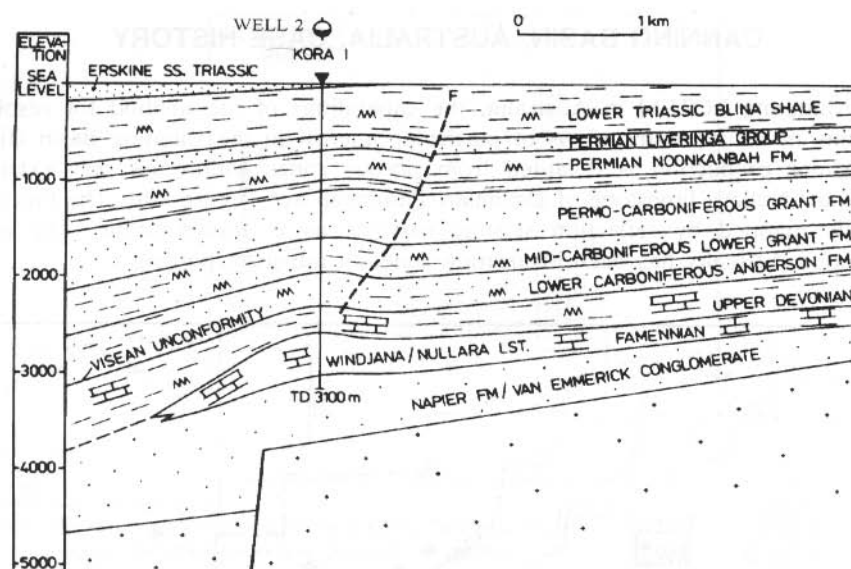


Fig. 8.8: Geological cross section for the Canning Basin LOTEM survey area (after Strack et al, 1989b).

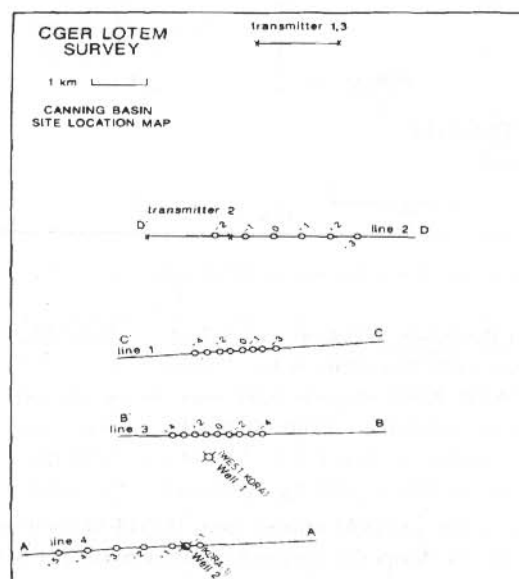


Fig. 8.9: Canning Basin LOTEM survey plan (after Strack et al, 1989b).

Assuming that the seismic data accurately represented depth variations along the line, LOTEM data were inverted starting at the well Kora-1 (figure 8.10) to investigate resistivity variations within the various units. The good quality of the seismic results shown figure 8.11 and the blocked well log from figure 8.10 motivated the use of a 9

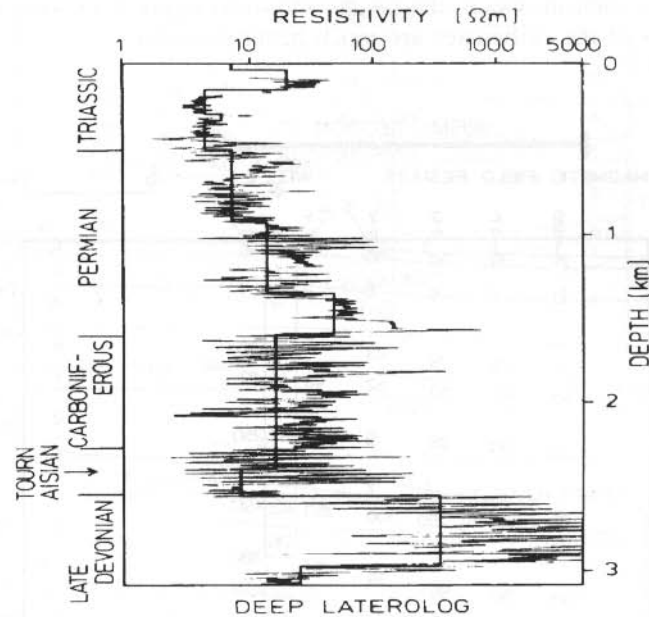


Fig. 8.10: Well log with blocked model (heavy line) for the well Kora-1 in figure 8.9 (after Strack et al, 1989b).

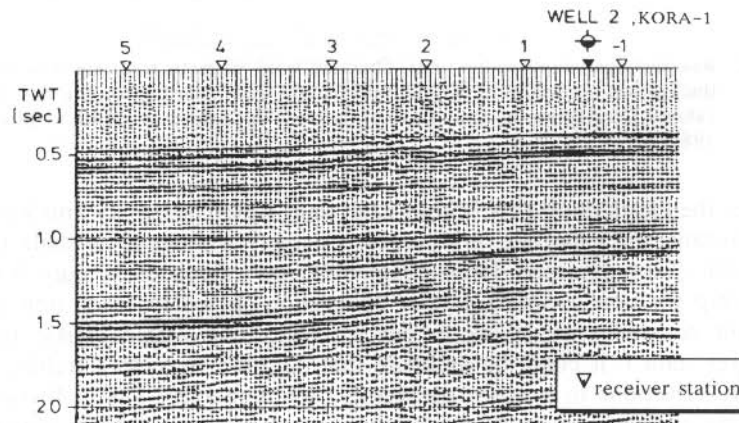


Fig. 8.11: Seismic section for line 4 which was used to fix the geologic structure for the inversion (after Strack et al, 1989b).

or 10 layer model, which would have otherwise been unthinkable. The layer thicknesses were kept fixed in inversion on the basis of seismic mapping. Figure 8.12 shows interpreted resistivity variations based on the magnetic component data only. The values shown for the resistive carbonate (unit i) were poorly resolved by the inversion when only magnetic data were used. However, when the electric field data were added for joint inversion, the results shown in figure 8.13 were obtained. Now the resistivities of the carbonates are much better resolved.

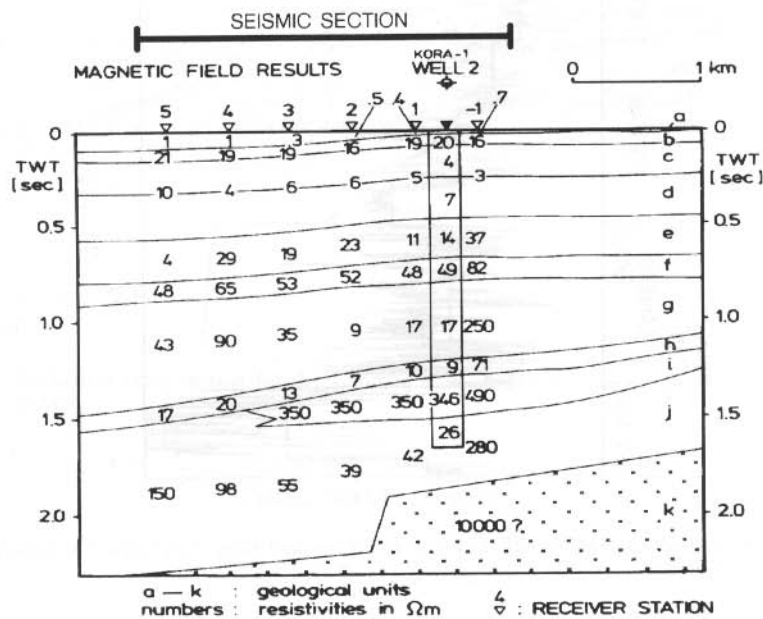


Fig. 8.12: Resistivity variations within units, obtained from magnetic transient data by fixing all layer thicknesses according to seismic information and inverting for the best fitting resistivity values. Confidence in Unit i values is poor because it is resistive (after Strack et al, 1989b).

Under the assumption that, within each unit, water resistivity and water saturation were constant, the expected variation of resistivity with sand-to-shale ratio for each clastic unit (Schlumberger, 1987, chapter 2) was calculated. Figure 8.14 shows the relationship for unit e. Using similar calibration curves for each unit allowed us to transform resistivity variations to percent sandstone within clastic units. For the carbonates, unit i, it could be assumed that Archie's formula (Archie, 1942) relates resistivity variations to porosity variations (Schlumberger, 1987). Figure 8.15 shows the results of transforming the resistivity section of figure 8.13 to percent sandstone ratios. The variations within unit i are seen to be small, indicating a uniformly low porosity.

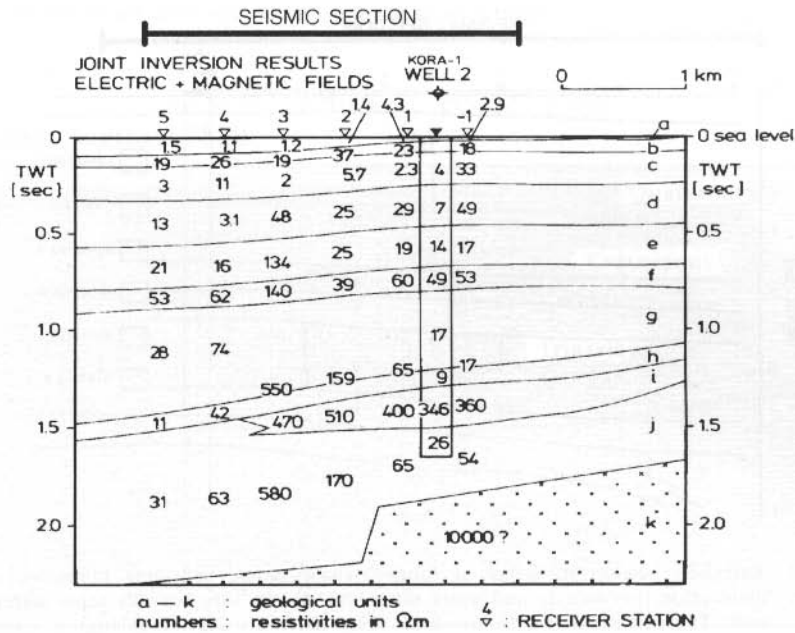


Fig. 8.13: Resistivity variations within units. They were obtained from magnetic and electric transient data by fixing all layer thicknesses according to seismic information and inverting for the best fitting resistivity values using joint inversion. The statistical confidence in the resistive unit i is much greater than in figure 8.12 (after Strack et al, 1989b).

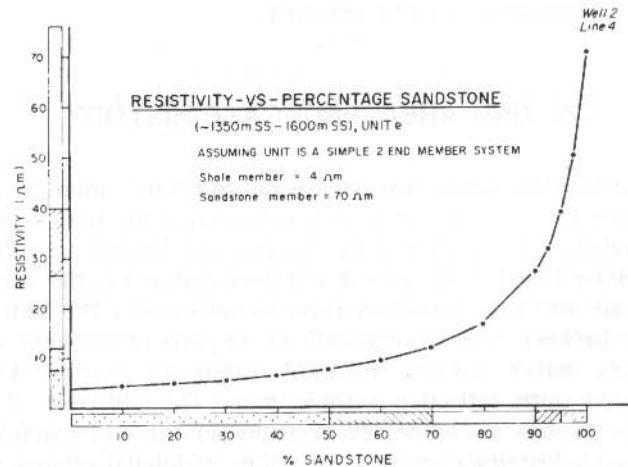


Fig.8.14: Resistivity versus percentage sandstone for unit e. The relationship is derived from the well log and used to convert the interpreted resistivity values to sand-to-shale ratios (after Strack et al, 1989b).

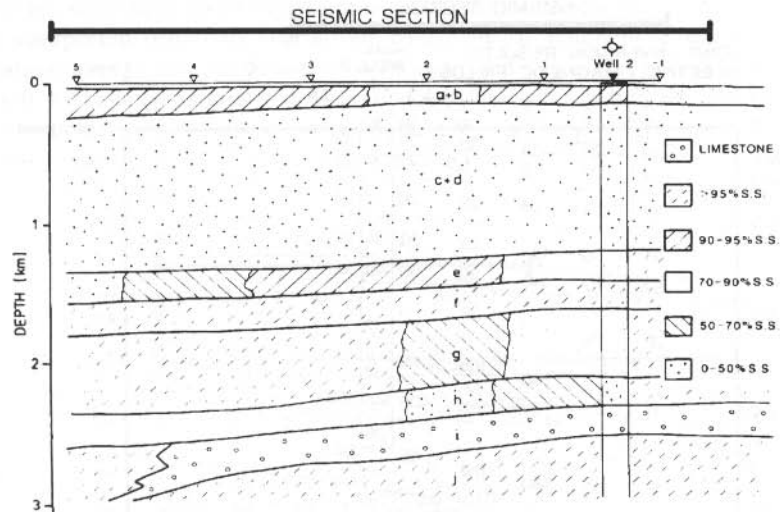


Fig.8.15: Resistivity section in terms of sand-to-shale ratios, reflecting porosities under the assumption that salinity and water saturation do not vary laterally same within a clastic unit. The percentage sandstone values were derived using the calibration curve and the scales along the axis from figure 8.14 (after Strack et al, 1989b).

This example demonstrated the benefits of jointly inverting electric and magnetic transients as well as the successful use of seismic data to achieve higher resolution in the EM data. It also shows that with high quality data and integrated interpretation, a porosity map of the subsurface can be obtained.

TAI XING AREA, PRC, CASE HISTORY

During 1988, a LOTEM survey was carried out in China within the German TEM Pilot-Demonstration Project. The survey area is located in the Jiangsu province which is tectonically located at the junction of the Yangtze and Huabei paraplatforms. Many oil and gas shows are found in the area. From the Cambrian to the Triassic, the area underwent orogenic and transgressional-regressional cycles. The sediments have a total thickness of between 3000 m and 9000 m. In parts of the area, the sediments include carbonates and/or volcanic material within the section. Both can give significant problems with reflection seismic data. The objective of the LOTEM demonstration survey was to define the structure of the carbonates/volcanics and possibly to investigate the strata below it. Very little additional geological information was available before the survey was carried out. The geophysical information consisted of a seismic section, one interpretation map (top of Triassic) and a well log. Although the seismic data shown in figure 8.18 are not very good, they clearly show

three reflectors as marked in the figure. On the left side of the section, the data quality become poor and one would expect a structured depression.

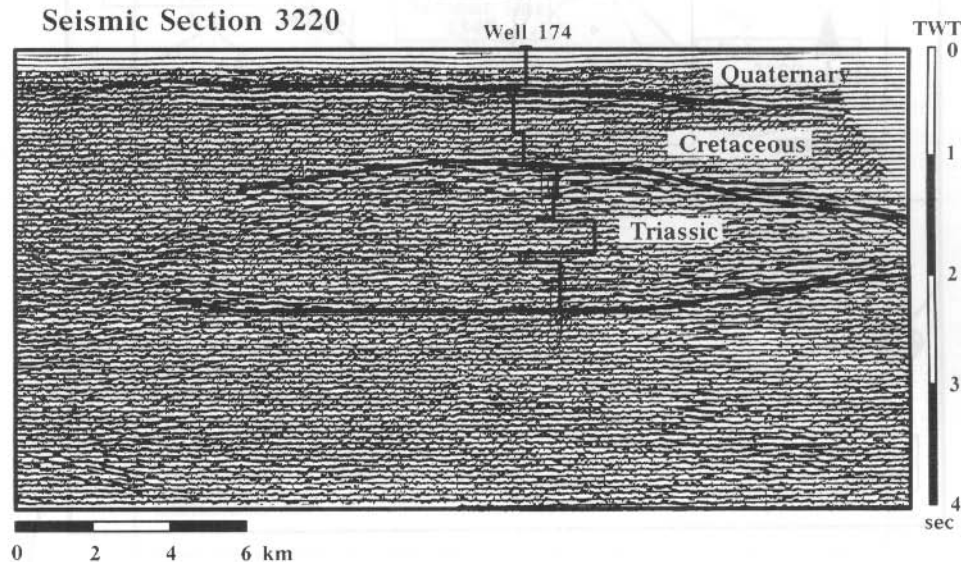


Fig. 8.18: Seismic section for line 3220 with three interpreted reflectors.

From this section and other (not available) data a contour map showing the top of Triassic was derived and is given in figure 8.19. The objective was to map the top of the Triassic, Permian and Carboniferous carbonates and possibly structures within and below the carbonates. The overall goal of the project was to demonstrate the LOTEM technique in this environment in comparison with other methods. From the geology and the seismic section the lowest reflector in figure 8.16 is thought to be the top of Devonian.

The LOTEM survey was designed to measure one profile as close as possible to seismic line 3220, the coordinates of which are not exactly known. The survey plan and the approximate location of the seismic lines are shown in figure 8.18. In addition to the profile parallel to the seismic line, a walkaway test from the transmitter was carried out. This was done because only one transmitter was used in the survey area and the effect of possible transmitter overprints had to be checked. Also displayed in figure are the power lines in the survey area. The density of the power lines and the variable power line frequency might make magnetotelluric measurements very difficult. It appears that only a controlled source technique could overcome this problem.

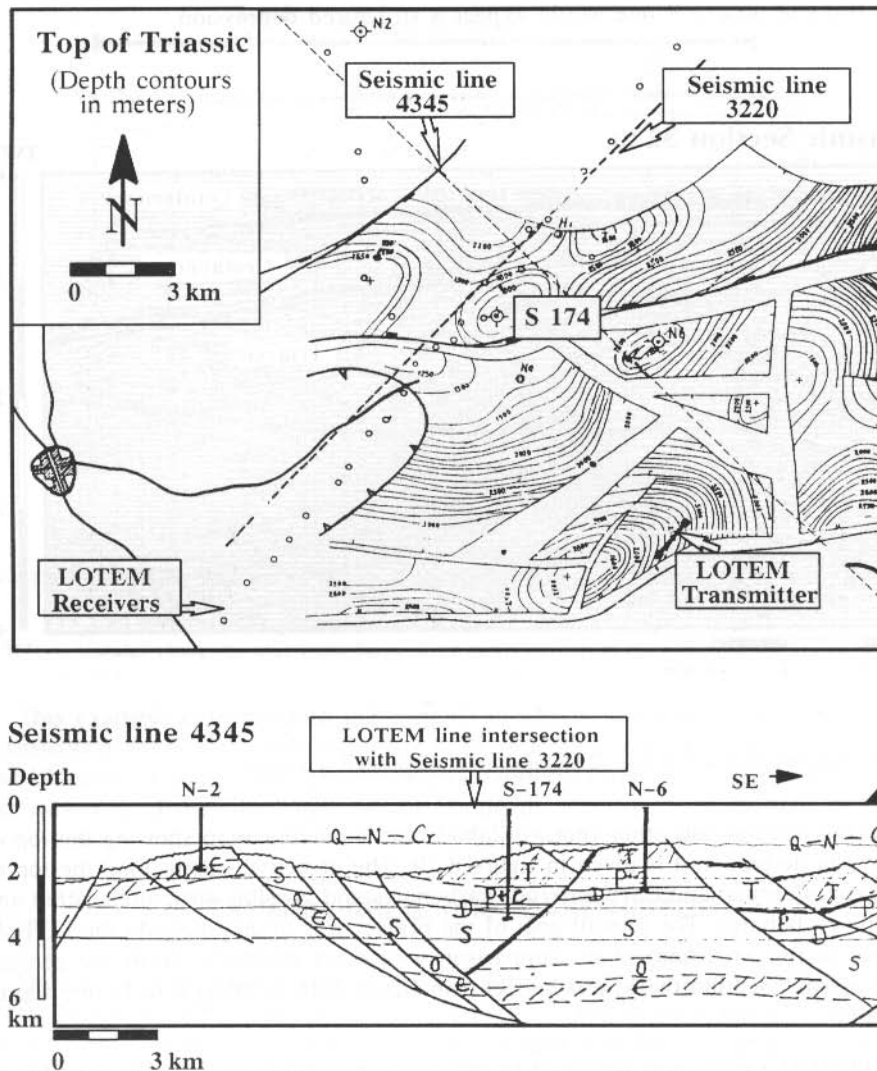


Fig. 8.17: Contour map derived from seismic information of the top of the Triassic. The south-western part of the seismic line 3220 shows a depression. At the bottom a geological section along a perpendicular seismic line is shown.

From the well log information different, blocked logs were derived and are shown in figure 8.19. The solid line represents a well log which was blocked based on the lithology only. Significant features in this log are the rise in resistivity for the Triassic and Permian limestones. The dashed line in the figure represents a blocked well log after forward modeling for the LOTEM method. Now, only three layers can be

distinguished. One layer boundaries just below the Cretaceous siltstones and the others is at the top of the Triassic limestone. The Permian limestone could not be distinguished according to forward modeling.

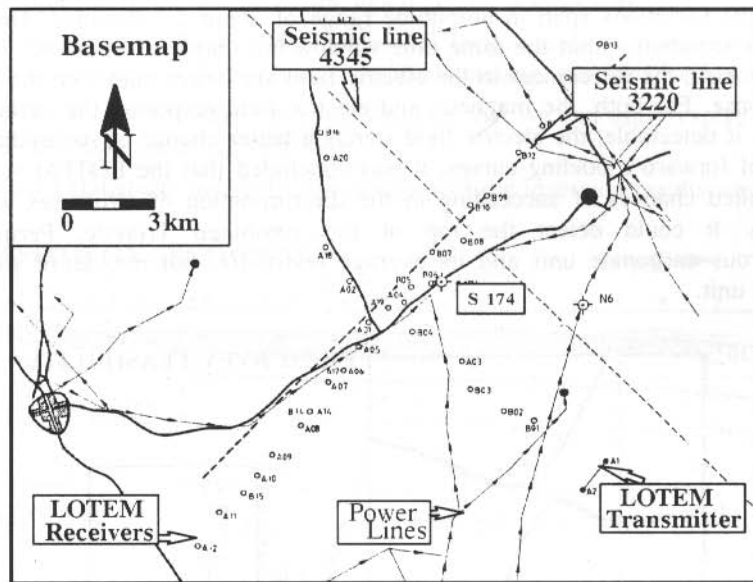


Fig. 8.18: Survey plan of the LOTEM survey near Tai Xing, PRC.

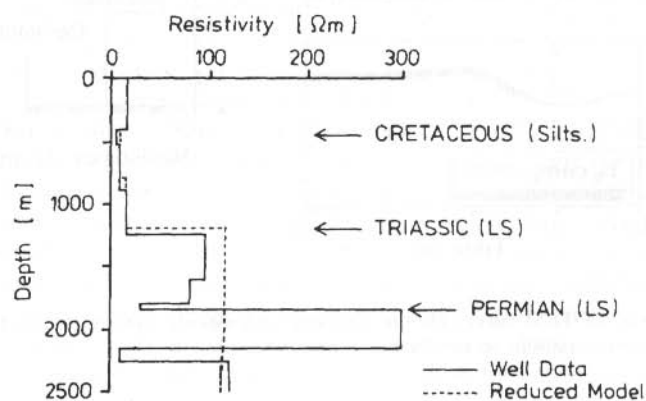


Fig. 8.19: Two reduced induction logs. The blocked one represents the blocked preserving the lithology and the dashed one considers LOTEM layer resolution.

The results from the forward modeling caused by the parameter variations for the electric and magnetic field components are shown in figure 8.20. Here, the resistivity

of the Permian carbonates was varied. The changes simulate variations in porosity in the limestone. The magnetic field derivative is displayed as early and late time apparent resistivity curves, while the electric field is displayed as voltage measured at the receiver. The magnetic field response shows variations from 0.1 seconds to 10 seconds. The variations span in amplitude range of about 2.5 decades. The electric field shows variation within the same time window but only over about 0.5 decade of amplitude. Also, the differences in the electric field are larger than with the magnetic field response. For both, the magnetic and electric field response, the variations are small and, if detectable, the electric field stands a better chance of succeeding. From this type of forward modeling curves, it was concluded that the LOTEM survey had only a limited chances of succeeding in the discrimination of structures within the carbonates. It could detect the top of the combined Triassic, Permian and Carboniferous carbonate unit and its average resistivity, but not detail within and below this unit.

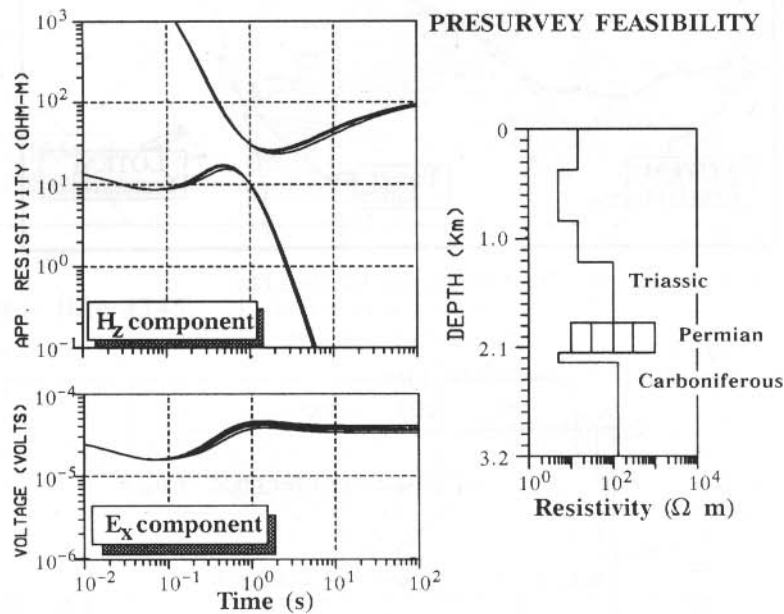


Fig. 8.20: Synthetic LOTEM curves for the magnetic and electric field responses for porosity (thus resistivity) variations in the Permian limestone.

The field data were processed in the field using standard procedures as described in previous chapters. The data were then interpreted using a one-dimensional layered earth inversion program. The results were plotted as a resistivity section and are displayed in figure 8.21. On top of the inversions two of the three seismic reflectors are superimposed. For the depth conversions an average velocity of 2.5 km/s was used (more detailed velocities were not available). The match between the seismic

reflectors and the layered inversion results in figure 8.21 is remarkable. To judge the reliability of this fit we must consider the following:

- The field data were processed in the field which means that no fine tuning of the processing for the optimum signal-to-noise ratio was done.
- The depth conversion of the low quality seismic data was done using only an average seismic velocity because detailed stacking velocities were not available.
- The presurvey forward modeling suggests that we can only resolve the top of the carbonates average resistivity.
- Detailed statistical and resolution analysis of the inversion results was not done.

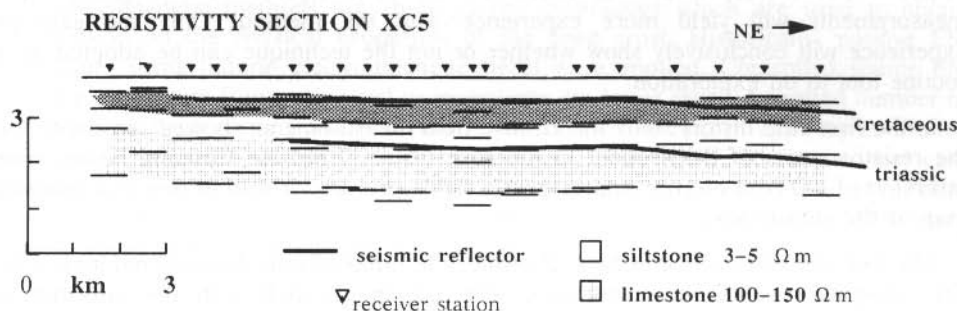


Fig. 8.21: Resistivity section derived from one-dimensional inversions for the LOTEM profile. Superimposed are the seismic reflectors.

In light of the above factors, one would not trust the the results displayed in figure 8.21. When inspecting the inversion statistics, it becomes clear that none of the parameters (layer resistivities and thicknesses) below the Triassic limestone top are resolved. The inversion simply maintained the starting model which was derived from the well log. This presents a serious problem with these data, because it means that the layered earth model assumption had reached its limits. Thus the field data were reinspected and other ways of displaying data were considered. In this case we used the source or current imaging technique described in chapter 2 was used. Figure A.7.8 (appendix 7) displays the result of the current imaging with the seismic section superimposed to it. One can clearly see the depression in the LOTEM current image which is consistent with the depression in the seismic data. Further, the top of the carbonates is clearly visible as start of the resistive unit. There are also variations visible in the blue image which represents data within the carbonates. However, to confirm that these variations are real one would need additional information such as well logs and/or better seismic data.

The case history near Tai Xing clearly shows that the LOTEM technique has a higher potential than we are hereto able to interpret. When considering that the LOTEM image section is constructed with about 30 records while the seismic section uses several thousand traces, the interpretation results are very good.

SUMMARY CHAPTER 8

Most surface controlled source (inductive) and natural source electromagnetic methods are strongly biased towards the more conductive parts of the geoelectric section. The case histories show that LOTEM can be successfully applied in exploration of hydrocarbon reservoirs where the task is to define variations in the resistive part of the geoelectric section. In examples from Europe and Australia LOTEM provided specific information for the section with an accuracy previously not possible. An increased use of LOTEM with both electric and magnetic field measurements will yield more experience with the method. Only the gain in experience will conclusively show whether or not the technique can be adopted as a routine tool to oil exploration.

In the first case history, only the electric field measurements showed sensitivity for the resistive parts of the section. In the case history from the Canning Basin, joint inversion of LOTEM electric and magnetic fields provided a way to derive a porosity map of the subsurface.

The last case history from China illustrates the limits of one-dimensional inversion. The inversion results were unreliable although they match with the information available from seismic. A different technique using directly the field data had to be used. The current or source imaging technique proved to be the most reliable one. In addition to confirming the *a priori* information trends can already be recognized in the source imaging. This indicates that the LOTEM method has a higher resolving capability as hereto used.

PROBLEMS CHAPTER 8

1. What is the difference between the use of the magnetic field and the electric field components?
2. How do you confirm that one-dimensional interpretation is applicable and gives valid results?
3. How can you see from figure 8.4 that the inversion do not resolve the resistivity of the third layer?
4. How was the sand-to-shale ratio map (figure 8.15) derived for unit i?
5. Which electromagnetic techniques do you consider applicable in the Tai Xing area? Please elaborate.
6. How can you see that the interpretation in figure 8.21 is unreliable?

KMS Technologies – KJT Enterprises Inc.
6420 Richmond Ave., Suite 610
Houston, Texas, 77057, USA
Tel: 713.532.8144

Please visit us
<http://www.kmstechnologies.com>

This material is not longer covered by copyright. The copyright was released by Elsevier to Dr. Strack on November 5th, 2007.

The author explicitly authorizes unrestricted use of this material as long as proper reference is given.

KMS Technologies – KJT Enterprises Inc.

An EMGS/rxt-company

Chapter 9 Case Histories : Deep Crustal Applications

extract from

Strack, K.-M., 1992, reprinted 1999
***Exploration with deep transient
electromagnetic:*** Elsevier, 373 pp.

This material is not longer cover by copyright. The copyright was released by Elsevier to Dr. Strack on November 5th, 2007.

The author explicit authorizes unrestricted use of this material as long as proper reference is given.

Chapter 9

Case Histories: Deep Crustal Applications

Electromagnetic methods are some of few techniques which are used to obtain information on the physical properties of the deep crust. Historically, passive EM techniques using natural electromagnetic fields were applied. Controlled source EM techniques are less frequently used to investigate the lower crust. A limited number of surveys have been carried out. A review of the state-of-the art in applying controlled source EM to crustal studies is given by Boerner (1992). Here, some historical case histories are selected which are important when considering the application of LOTEM to deep crustal studies. Following are more recent case histories of LOTEM deep crustal applications from Europe, Africa and China.

HISTORICAL CASE HISTORIES

A significant amount of deep crustal applications of LOTEM has been done in the Soviet Union where the technique originated. In particular the use of MHD generators has been of great interest there (Velikov et al, 1986). Since the information reaching the Western world from the USSR concerning other LOTEM measurements for deep crustal work is very sparse, only a small number of selected "western" case histories illustrate the framework needed to carry out LOTEM soundings around the world.

One of the first observations of deep crustal transients was done in Southern Africa during ultra long line DC-resistivity soundings (Van Zijl, 1969; Van Zijl et al, 1970; Van Zijl et al, 1975; Blohm et al, 1977). Especially impressive were the recordings from the Cabora Bassa power line. A short example of the large amount of strip chart records found in the archives of the CSIR is shown in figure 9.1. S. Joubert who was doing the technical support at that time still remembered the details leading to the additional labeling of the figure. The transients in the record were contaminating the wanted DC-signal. In figure 9.1 several of these transients can be seen as double peaks. These double peaks are caused by the transmitter switching. The polarity change is done with an off-time before the switches turn on the other polarity. At the beginning of the record the initial adjustment with respect to timing and recording can be seen in the more sporadic behavior. The important part for the use of the data as DC-resistivity data was the time between switching since the unwanted transient should have decayed completely before the DC-resistivity value could be read. This resulted in a tremendous amount of data processing which had to be done. All strip

charts had to be digitized and the data fed into a computer. The transients were used as timing markers only. One entire record is displayed in figure 9.2. The individual transients are now barely visible and the record had to be split into small windows

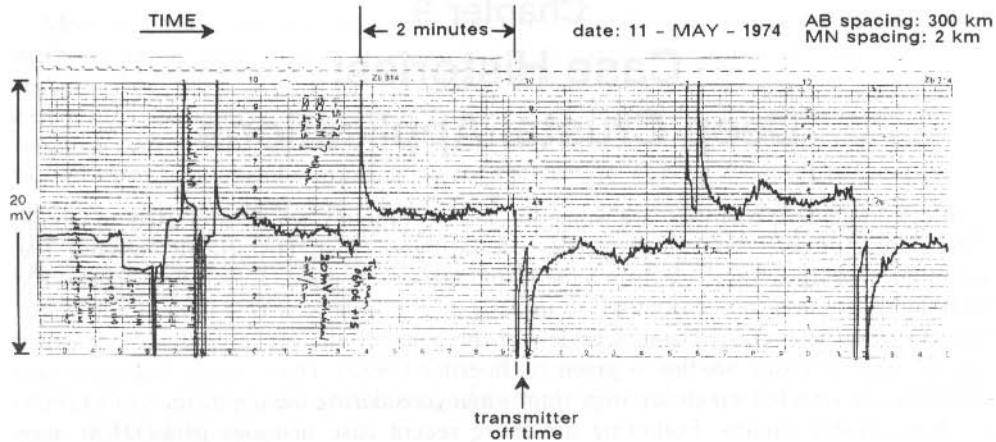


Fig. 9.1: Reproduction of an original strip chart record from the Cabora Bassa line ultra deep resistivity measurement. The information leading to the labeling of the figure was supplied by S. Joubert (pers. comm.).

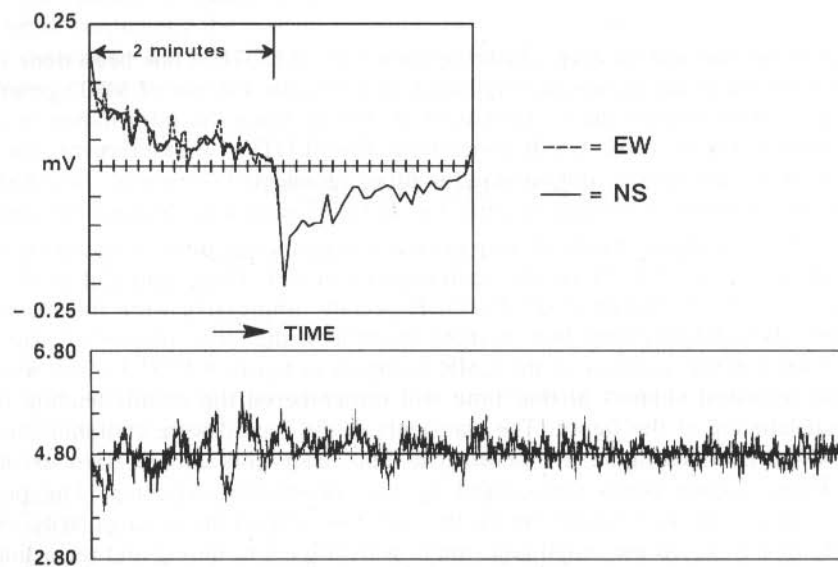


Fig. 9.2: Example of a processing display of the Cabora Bassa DC-resistivity measurements. The bottom shows the complete time series after digitization. The top left frame displays the resulting stack after picking windows out of the time series and stacking them (courtesy S. Joubert, CSIR).

which were stacked. The stack is displayed on the upper left of figure 9.2. The windows were shifted so they would yield a clean transient after stack. From this stack the very last part was used to read the DC-resistivity response value. Although, at that time the interpretation of the data as transients were not carried out, the basic motivation was laid for the integration of transient electromagnetics into the research objectives of the CSIR.

The first megasource transient EM survey was carried out by Sternberg (Sternberg and Clay, 1977; Sternberg, 1979) over the Southern extension of the Canadian Shield. The megasource consisted of approximately 22 km long dipoles with about 70 Amperes of excitation current giving a source moment of 1,540,000 Am. Sternberg integrated DC-resistivity measurements with transient sounding to derive a model satisfying both techniques. Figures 9.3 and 9.4 show some representative data sets for

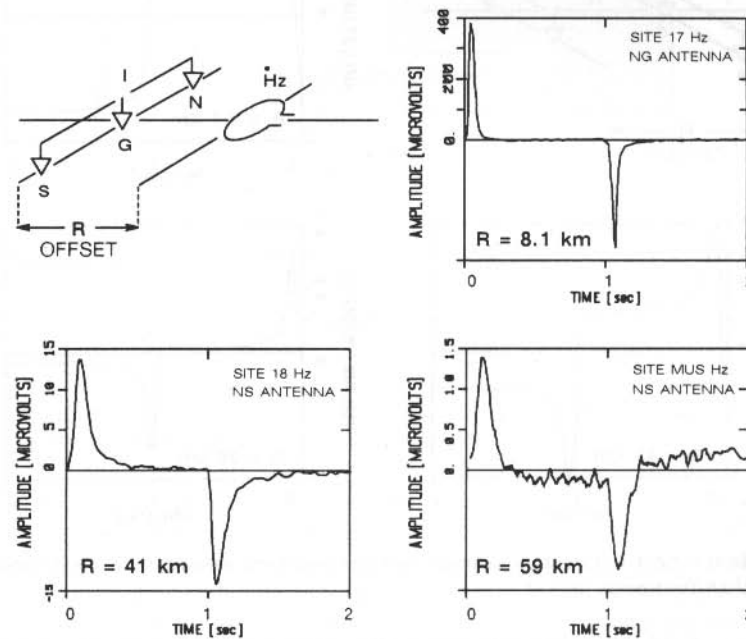


Fig. 9.3: Magnetic field transients measured over the Southern extension of the Canadian Shield (after Sternberg, 1979).

the magnetic and electric field receivers. The signals look very much like the signals measured nowadays; they become wider for larger offsets with decreasing absolute amplitude. The electric field transient in figure 9.4 also exhibits different characteristics for increasing offset. For the very long offset of 59 km the electric field measurement could even be mistaken for magnetic field transients. Sternberg interpreted the magnetic field transient at site MUS (see figure 9.3) as containing a reversal. He interprets it as being caused by the conductors in the Flambeau anomaly, which is a logical explanation of this type of 3-D effect (Newman, 1989; Hördt et al,

1992). In order to obtain a realistic estimate of the candidate models, Sternberg interpreted the data using Monte Carlo inversion. The range of possible models is displayed in figure 9.5. The bounds for the second layer (resistor) and the third layer (conductor) would probably be smaller using joint inversion routines incorporating DC-resistivity, LOTEM electric and LOTEM magnetic field measurements. Nevertheless, Sternberg's work is probably the most important early deep TEM research because he already includes three important approaches of today's state-of-the-art LOTEM systems, namely:

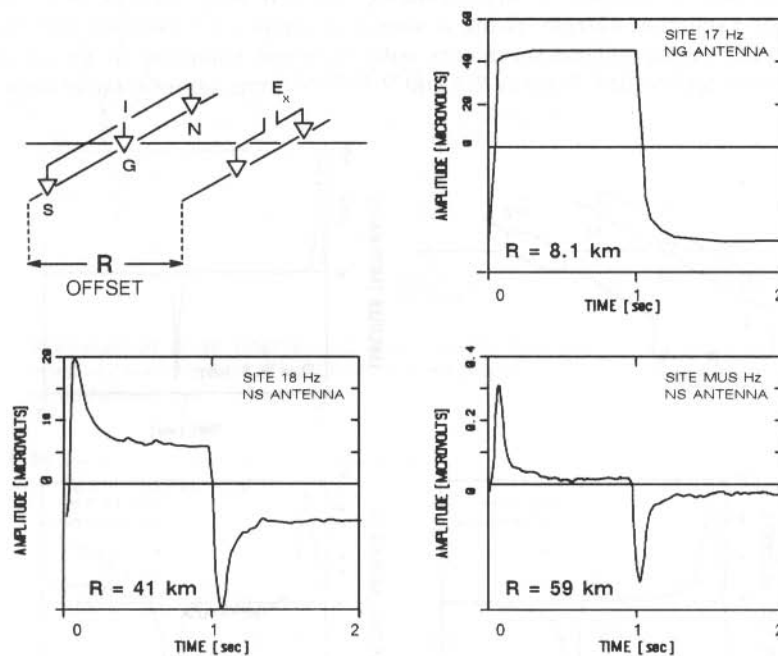


Fig. 9.4: Electric field transients measured over the Southern extension of the Canadian Shield (after Sternberg, 1979).

- Electric field measurements which allows the interpretation of resistive parts of the section.
- Inversion methods yield a class of models and thus confidence limits.
- Integrating different methods (TEM, DC-resistivity) to obtain a more unbiased interpretation.
- Qualitative explanation of 3-D effects (reversals).

More recently, Keller et al (1984) published case histories on using megasource TEM for deep geothermal and hydrocarbon applications (investigation depth greater than 3 km). Their megasource consisted of a short wire (about 1–2 km) but large currents (about 2000 A peak-to-peak). This type of source has the disadvantage of

difficulties in controlling the current switching (because of the high currents) resulting in sometimes unpredictable effects in deconvolution of the system response. The first case history in their paper has early and late time apparent resistivities which are either sometimes far apart or almost crossing. From the discussion on the calibration

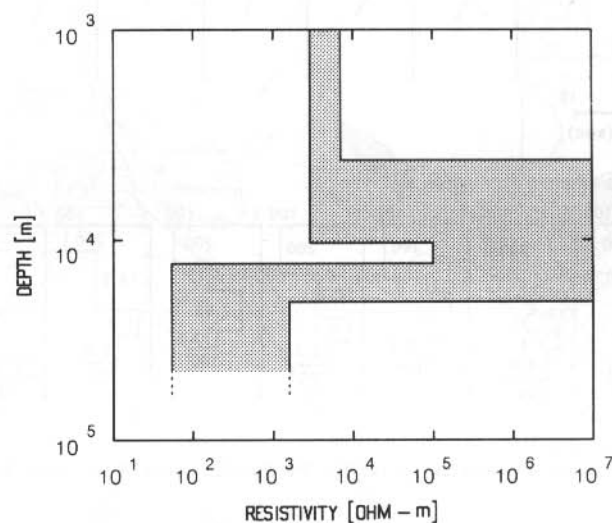


Fig. 9.5: Interpreted model range for the explanation of the transient soundings over the southern extension of the Canadian Shield the (after Sternberg, 1979).

factor earlier in this book and the paper by Newman (1989), we know that these effects can be caused by transmitter overprints which can be treated as static shifts. The consistency in their interpretation of the data lies in the inversion program they used. This routine automatically left the calibration factor floating during inversion thus compensating for the effect of static shift. Figure 9.6 shows another example of their interpretations for a different profile. The top of the figure displays the early and late time resistivities. Note that some of the early time curves have narrow bumps which are particularly strong at stations 431, 461, and 459. These bumps are symptomatic of deconvolution effects and they can usually not be matched with a layered earth model. The paper by Keller et al (1984) illustrates the large effort one has to undertake to carry out deep LOTEM surveys and obtain many data sets over a large area.

In the following, the developments of the German deep transient EM systems and the application to deep crustal problems are described in historical order, starting with a very initial test done for the German deep drilling project and ending with the first demonstrations for earthquake prediction in China.

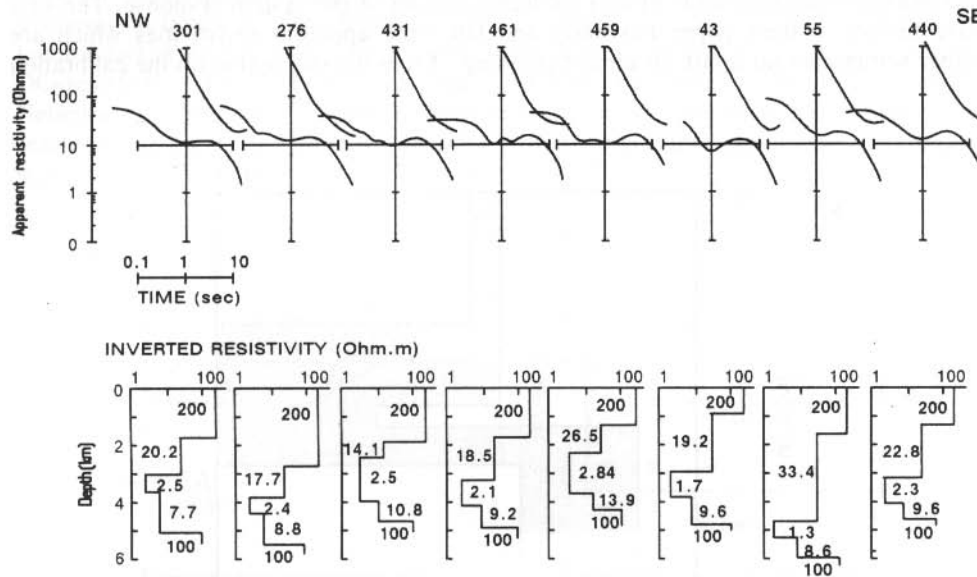


Fig. 9.6: Example of an interpreted profile for the Pacific North-West (after Keller et al, 1984).

The first LOTEM measurements for deep crustal applications in the Oberpfalz caused the request for additional measurements in the Black Forest, which was an alternative site for the deep drilling project. To confirm the results obtained in the Black Forest, a calibration survey was carried out near the Urach Geothermal Area, where a conductor was known in the upper crust. A map of the LOTEM sites within the framework of the seismic reflection lines is shown in figure 9.7.

THE FIRST DEMONSTRATION FOR DEEP CRUSTAL APPLICATIONS IN FRG

During the site selection process for the German deep drilling location, test measurements were done in the Oberpfalz area, which is now the drilling site. The main question to be answered with the LOTEM survey was:

- Is there a crustal conductor below 10 km? If yes, what would be the depth range?

A crustal conductor was seen in magnetotelluric measurements, but the depth was only approximate. When the survey started, the behavior of the LOTEM method to such a resistive target (resistivities larger than 1000 Ωm) was completely unknown. Very little experience existed to set up a powerful transmitter in resistive terrain and

on frozen ground. As a result maximum current of only 60 Amperes (peak-to-peak) could be injected into the ground. Within a total survey time of one week only 22 receiver sites could be occupied. They were scattered around the area with 11 stations being aligned along a profile.

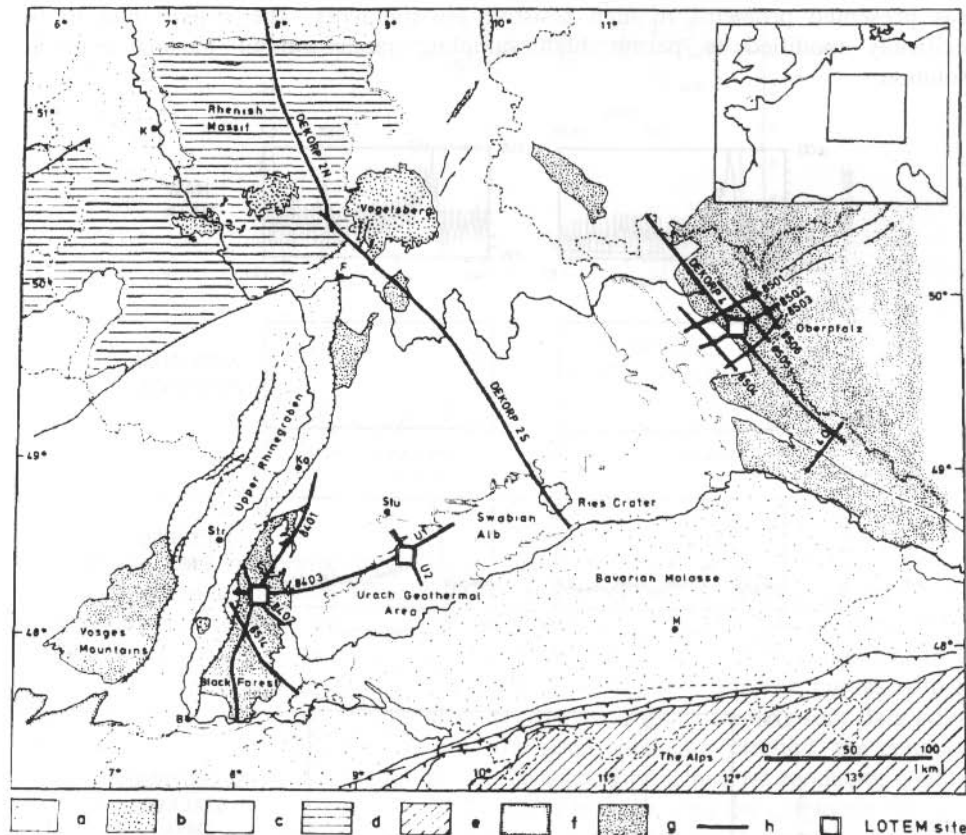


Fig. 9.7.: Regional geologic map of Southern Germany with LOTEM and deep reflection seismic survey locations. geologic key: a: Tertiary and Quaternary basin and graben fill; b: Tertiary volcanic rocks; c: Permian to Triassic sediments; d: Devonian (Rhenish Shield); e: Alpine orogen; f: Jurassic sediments (Swabian Alb); g: crystalline Hercynian basement. Map notation: K – Köln, F – Frankfurt, M – Munich, Str – Strasbourg, Ka – Karlsruhe, B – Basel, Stu – Stuttgart. A basemap of the LOTEM survey areas (squares) is shown in figures 9.12 and 9.21 (after Strack et al, 1990).

A typical representative processing sequence of the 1986 survey is shown in figure 9.8. The top row shows two typical individual records. The transient signal is clearly visible in the records. The data is still contaminated by predominantly periodic cultural noise. Below the raw records are the amplitude responses obtained after

Fourier transforming the raw data. They exhibit a significant amount of power line noise starting with the base frequency of $16 \frac{2}{3}$ Hz and higher harmonics thereof. Using the true amplitude filters discussed in chapter 3 the filtered record in the third row of figure 9.8 was obtained. Finally, the data was selectively stacked yielding the bottom smooth transient. Note that the transient signal is only about one second long; in 1986 the digital data acquisition system designed for exploration in sedimentary areas presented problems in high resistive environments. The system had to be specifically modified to permit high sampling rates without losing dynamic resolution.

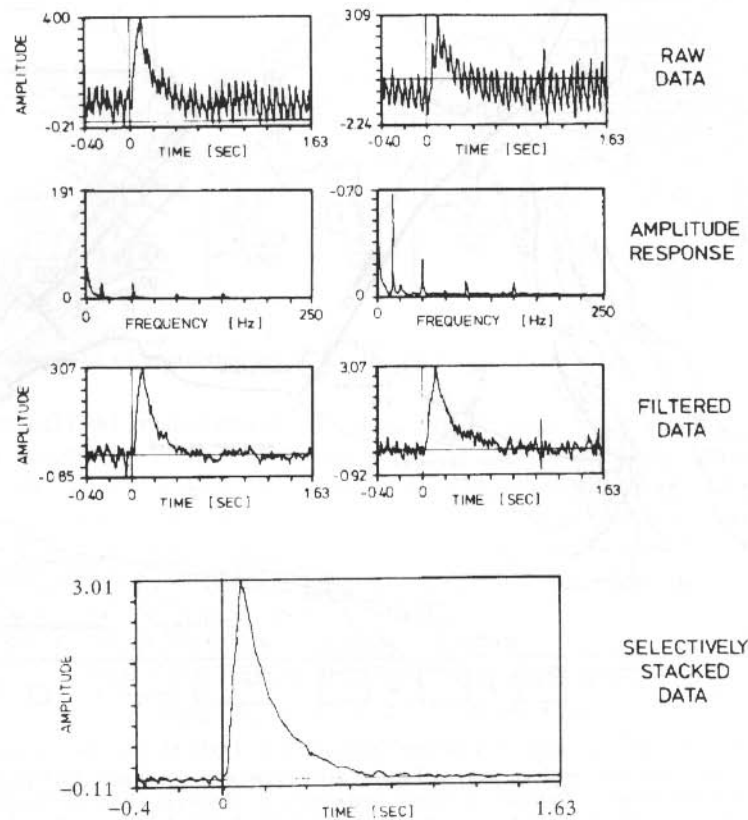


Fig. 9.8: Representative data set for the 1986 LOTEM survey in the Oberpfalz area, Germany. The different displays show the different processing steps.

After carrying out a significant amount of prestack processing, the data were interpreted using one-dimensional layered earth inversion. The inversion with layered models proved to be more difficult than usual. After a large number of forward model calculations, only one starting model could be found which gave a consistent interpretation along the measured profile shown in figure 9.9. The inversion result was

highly unstable and it was apparent that a conductor existed at about 10 km depth, but it was not clear whether or not this conductor was resolved or not. The error bounds were very small, yet the feeling of poor confidence in the interpretation never left the interpreter because enough experience in this environment and 3-D modeling did not exist at that time.

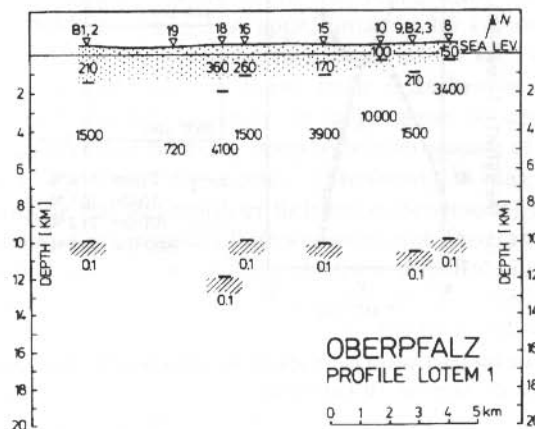


Fig. 9.9: Interpreted resistivity cross section for the LOTEM survey near the location of the German continental drill hole.

Although the interpreter may argue differently, the data clearly required the conductor when using 1-D inversion. To reinforce this type of interpretation two different tests were done. First, a conductor resistivity test: in this, the resistivity of the last layer was changed successively from being conductive to being identical to the resistive layer above. The results are displayed in figure 9.10. The curves with the conductor not being present deviate from the data for approximately four data points. This suggests that the data does require the good conductor. Second, the conductor thickness test: this test gives the interpreter an idea of how thin the conductor could be and still honor the data. From figure 9.11 it can be seen that the conductor has to be at least 250 m thick, otherwise the curve would deviate too much from the data. Also, at this minimum thickness, a fitting error minimum is observed.

The measurement and the interpretation demonstrated that when using 1-D inversion, one must include a crustal conductor in the Oberpfalz area below crystalline rock at approximately 10 km depth. After drilling of the pilot hole, we know that the geology is very complicated and further 3-D modeling should be applied. This is confirmed by the large number of reversals in the survey area, indicating the multi-dimensionality directly in the data. A more complex 3-D survey with well over 100 stations was carried out in the area but the interpretation is still under way.

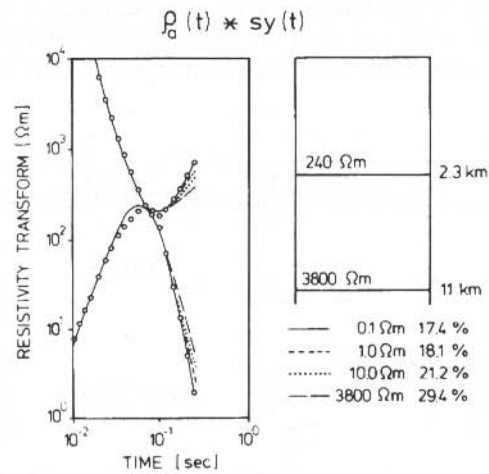


Fig. 9.10: Resistivity test for the Oberpfalz model (Oberpfalz site 15), illustrating that the data require a conductive last layer in 10 km depth.

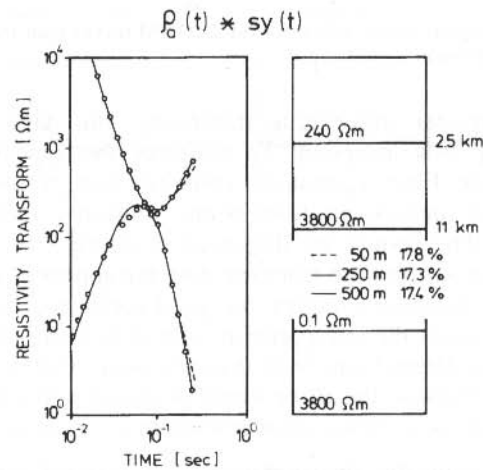


Fig. 9.11: Minimum conductor thickness test for the 1986 LOTEM data (Oberpfalz site 15), showing that the data requires a minimum thickness of the conductor being 250 m.

BLACK FOREST SURVEY

During July 1986, a LOTEM survey was conducted in the Black Forest area near Haslach (see figure 9.12) in conjunction with site investigations for the German deep

drilling project. The objective of the survey was to define the resistivity distribution in the upper 10 km of the earth's crust. The survey was a direct result of the successful mapping of the conductor in the Oberpfalz.

Existing geophysical data includes reflection and refraction seismic, and magnetotelluric measurements. From wide-angle and near-vertical seismic surveys, the upper crust to approximately 14 km depth was found to be relatively transparent except for a bright spot which appears at approximately 9.5 km depth in the seismic section in figure 9.13. Below a rather constant depth of 14 km, a highly reflective, seismically laminated zone defines the lower crust (Lüschen et al, 1987). This is typical for the Hercynian crustal structure in large areas of central, western and northwestern Europe as revealed by many deep reflection studies of the BIRPS (British Institutions Refection Profiling Syndicate) (Matthews, 1986), ECORS (Etude Continentale et Oceanique par Reflexion et Refraction Seismique) (Cazes et al, 1986) and DEKORP (Deutsches Kontinentales Reflektionsseismik Programm) (Bortfeld et al, 1985) groups. Refraction seismic measurements show a distinct low-velocity channel starting at approximately 7 km depth (Lüschen et al, 1987). Magnetotelluric measurements yield a lower crustal conductor of 650 Siemens below 12 km depth, but no definite interpretation of the upper 12 km could be obtained (Tezkan, 1988). This is attributed to the strong cultural noise in the area, which was so strong that the audio magnetotelluric data did not yield a reliable interpretation in the upper section (Wilhelm et al, 1990).

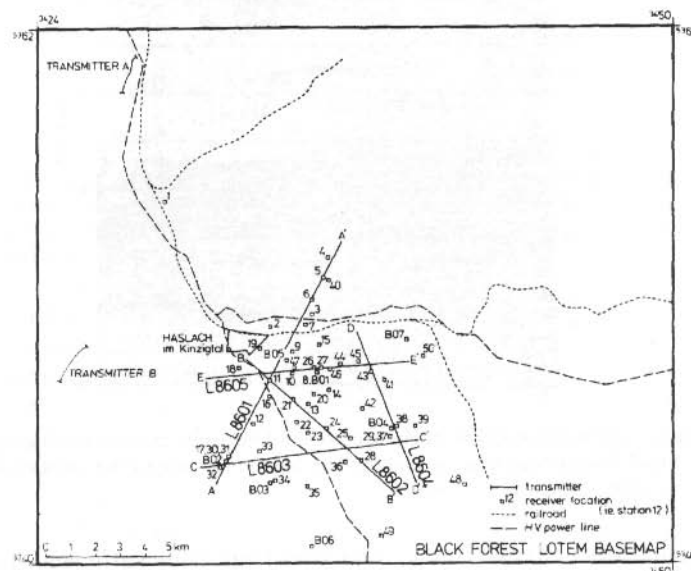


Fig. 9.12: Basemap for the Black Forest survey (after Strack et al, 1990).

The LOTEM survey was designed to achieve a high station density and data redundancy for improved interpretation since severe cultural noise problems were anticipated. Due to the difficult topography only two transmitter locations were possible: one of them to the north of the survey area (TRANSMITTER A) and one to the west (TRANSMITTER B in figure 9.12). LOTEM soundings were carried out at approximately 60 stations during 2 weeks of field work. Because of strong railroad and power line noise, the data were recorded with 16 2/3 Hz analog notch filters; otherwise no useful signal would have been received. This restricts the signal information to below the frequency range of the notch filter (0–13 Hz), because higher frequencies of the transient are severely distorted by harmonics. Since the measurable signal length in time increases with increasing source-to-receiver distance, offsets of 8 to 13 km were chosen so that the signal would be in a time window unaffected by the analog filters. Given this offset range, the system response (including transmitter and receiver analog filter effects) and the resistivity distribution at the subsurface yield a minimum depth of investigation which may vary at each station due to changes in the above factors (Spies, 1989).

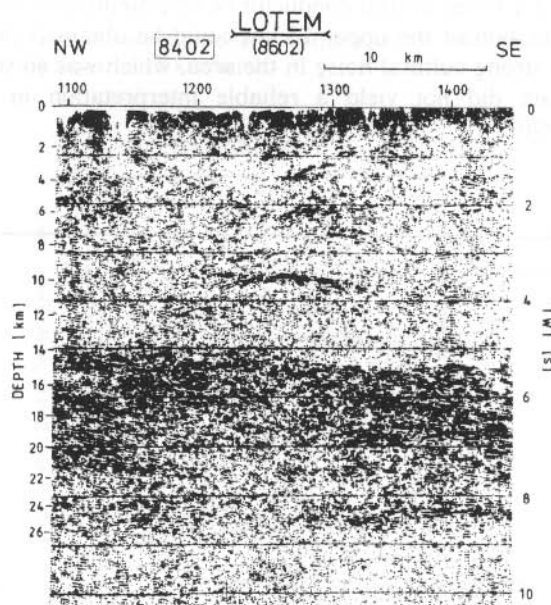


Fig. 9.13: Seismic section showing the bright spot at 9.5 km depth and the laminated lower crust of the Black Forest beginning at 14 km. The bar on top marks the location of the LOTEM survey (after Strack et al, 1990).

The raw data are extremely noisy and transients with sufficient signal-to-noise ratios were obtained with extensive prestack filtering, and with a selective stack tuned for the noise characteristics at each station (Strack et al, 1989). Figure 9.14 shows a representative example of the data processing sequence for the Black Forest survey.

The top frames display two consecutive recordings in time at one receiver site. The individual transients are strongly contaminated by cultural noise. Below are the respective amplitude responses used for quality control and to determine which noise frequencies to filter out. The third set of frames shows these individual transients after applying a true amplitude, digital recursive filter to remove the periodic $16\frac{2}{3}$ Hz noise. The bottom frame in figure 9.14 is the selectively stacked transient after filter, resulting from all data measured at this particular receiver site.

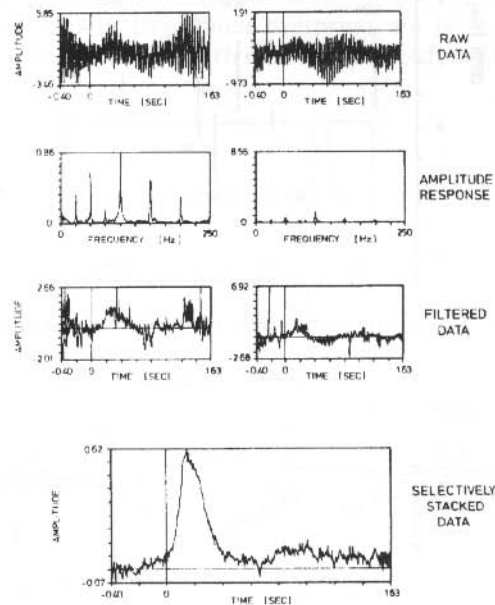


Fig. 9.14: Data processing sequence from the Black Forest survey (site 12). Two consecutive recordings versus time at one receiver site show slightly different noise characteristics. The filtered data from all recordings (250 transients) at this site were then selectively stacked to yield the bottom transient (after Strack et al, 1990).

The standard deviations derived from the selective stack are used as weights in the inversion. No *a priori* information was used. The one-dimensional inversion results were then assembled into resistivity versus depth sections, one of which is shown in figure 9.15. A distinct resistivity contrast exists across the profile at a depth of 7 to 9 km, where the deepest layer (with resistivities from 10 to 80 Ωm) is more conductive than the upper layer of 150 to 800 Ωm resistivity. The error bars in depth describe a 68 percent confidence value for the depth to the base of a layer. The increased error bar size with depth is primarily due to decreasing signal-to-noise ratios with increasing time.

Figure 9.16 gives the inversion results for the NW-SE profile 8602 and the NE-SW profile 8601. A dip in the conductor to the NW is visible. Also a deep conductor is visible to the NE. This conductor could be the one the MT measurements define.

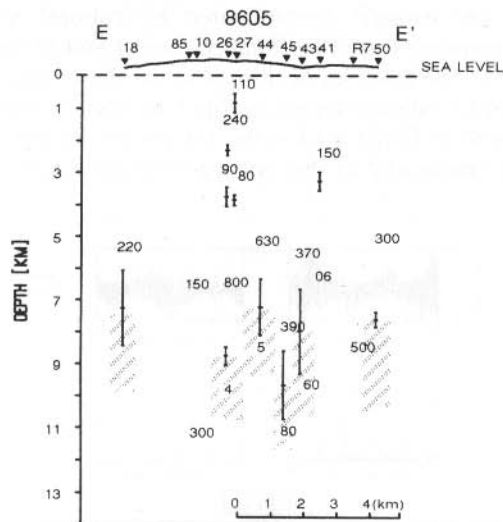


Fig.9.15: Interpreted E-W resistivity profile 8605 (E-E' 9.12) (after Strack et al. 1990).

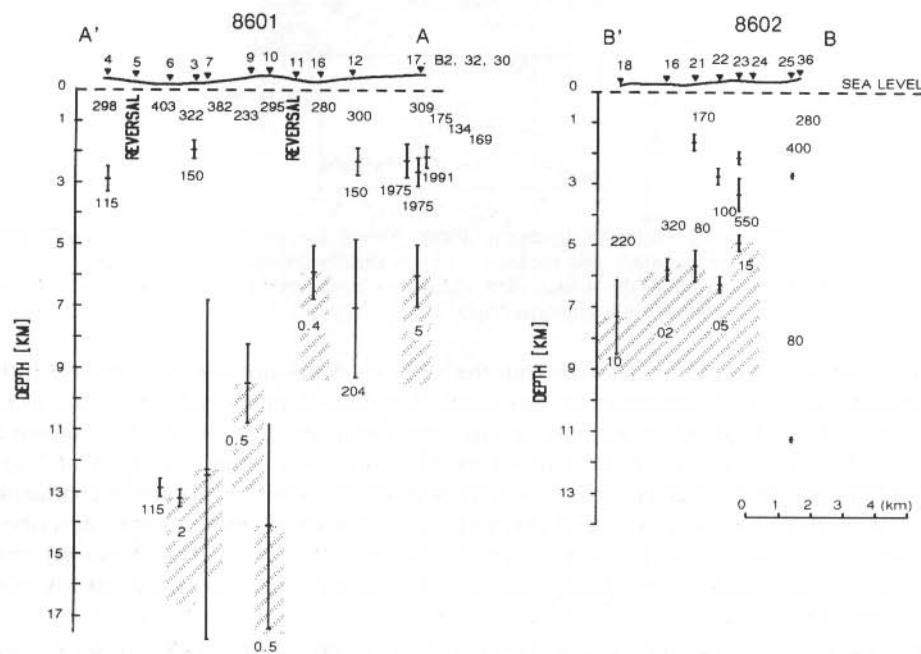


Fig.9.16: Interpreted resistivity sections 8601 and 8602 derived from 1-D inversions. Note the apparent dip of the conductor to the NW. The error bars are the 68% confidence limit.

The dip could also be confirmed in other stations. The question whether this is a multi-dimensional effect or real geology arises. Using two transmitters to immediately illuminate the same area with very similar interpretation results support the hypothesis that the cause of the dipping conductor is geological.

Figure 9.17 shows a representative comparison of 1-D inversion results from different transmitters, with the receiver sites 200 m apart. Station 27 was measured from transmitter A in the north, and station 46 from transmitter B in the west. Due to logistical reasons (cows and electrical fences) the same site could not be reoccupied. Two transmitters were used to illuminate the survey area from different directions. If multi-dimensional structures or transmitter overprints are present, the interpretation at sites close to each other would be different using one-dimensional models.

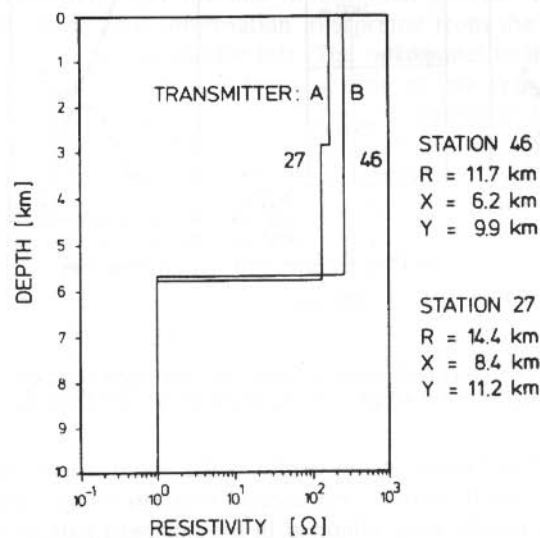


Fig. 9.17: Representative comparison of independent 1-D inversions for closely spaced stations with two different transmitter locations (after Strack et al, 1990).

The inversion model from station 27 consists of a three-layer model where the upper two layers have approximately the same resistivity of 150 Ω m and the top of the conductive layer is at 5.8 km depth. The inversion result from station 46 is a two-layer model with a slightly higher resistivity of 360 Ω m and a depth to the top of the conductor of 5.7 km. The consistency in depth to the top of the conductor confirms the one-dimensional interpretation for this area. It is also consistent with the seismic interpretation of the area which indicates plane layering and a zone boundary from 6 to 8 km depth (Lüschen et al, 1987). The difference in first layer resistivities of the two stations is partly because the response of the shallow layers lies largely in the high frequencies, which are distorted by the 16 2/3 Hz analog notch filter.

Figure 9.18 shows similar tests for the resistivity of the conductor and its minimum thickness as carried out for the Oberpfalz survey. The resistivity test (left frame in

figure 9.18) simulates the existence of a resistor, a half-space with the same resistivity as the second layer, and a conductor. Only the synthetic curves with the conductor present match the field data in an acceptable way. This means that a conductive unit exists at depth. Yet unclear is its thickness. Since the MT measurements did not observe this conductor, its thickness was gradually reduced until the synthetic curves would no longer match the field data. the result is shown on the right side of the figure. It can be seen that the match becomes worse when the conductor thickness is smaller than 500 m.

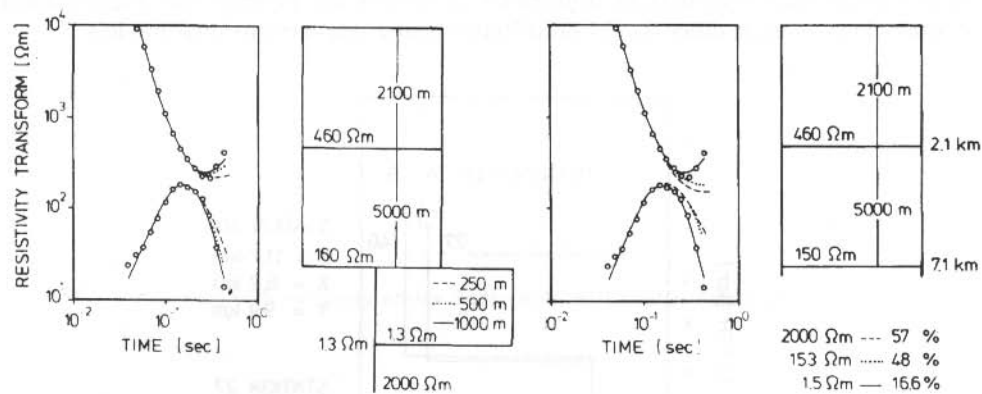


Fig. 9.18: Resistivity test (left) and minimum thickness test (right) carried out for the evaluation of the existence of the conductor in the Black Forest LOTEM data.

The statistical distribution of the depth to the conductor is shown in figure 9.19. Two maxima are clearly visible, one around 6–8 km depth and one around 14 km depth. The deeper results were obtained in the northern part of the survey area. The deep conductor could be the same as the shallow, but it seems more likely that the shallow conductor is of different nature. It is conductive enough to be detected by LOTEM in the southern part but its conductance is too low to be detected by MT. In the northern part, this conductor either has a decreased conductance or disappears. The lower conductor coincides with the conductor found in the MT measurements. Since the area was strongly contaminated by noise, it was not possible to detect this lower conductor at greater depth in presence of the shallow one in the southern part of the survey area. The first conductor is shielding the second one, because the signal from the conductor below disappears in the noise. This explanation seems to be the more reasonable one because it does not contradict Tezkan's (1988) explanation.

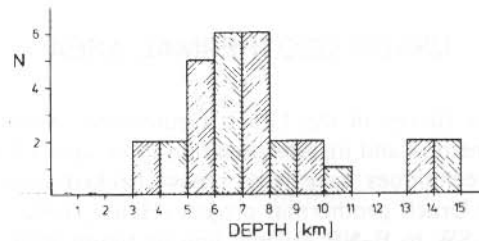


Fig. 9.19: Histogram of the depth to last conductor from all inversions to the Black Forest data.

Figure 9.20 is a comparison of the one-dimensional LOTEM interpretation with seismic survey results. Structural information interpreted from the reflection seismic sections is shown schematically at the far left. The next panel to the right shows the seismic p-wave velocity model which exhibits a zone of low velocity from approximately 6 to 14 kilometers, situated directly above the laminated lower crust. In the same depth range the ratio of compressional-to-shear-wave velocity also shows a distinct minimum, with a Poisson ratio decrease of 0.25 to 0.22 (Lüschen et al, 1987). On the far right of the figure are the interpreted resistivities from the LOTEM survey, with an integrated MT result because the base of the 10 ohm-m zone could not be resolved by the LOTEM measurements. From the LOTEM results, two layer boundaries are defined: one at approximately 3 km depth, and the second between 6 and 8 km which correlates well with the onset of the low-velocity zone. Its transition to the high conductivity zone revealed by magnetotellurics can not be explained conclusively and only the deep conductor at about 14 km depth indicates that there must be some sort of transition.

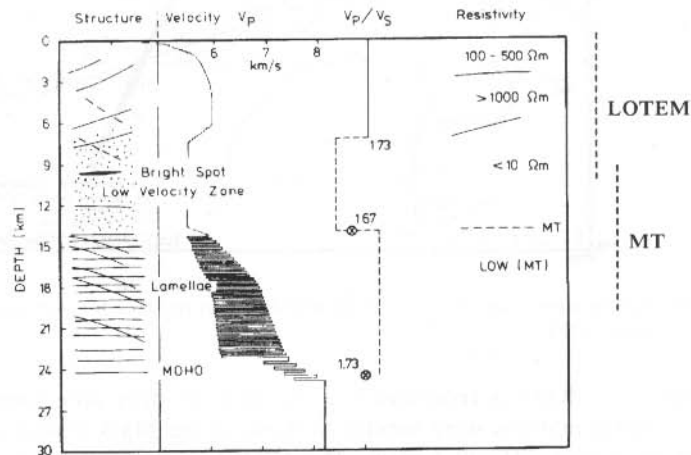


Fig. 9.20: A comparison of reflection profile data, velocities from seismic modeling of wide angle data, and EM depth soundings (after Lüschen et al, 1987).

compared with only 40 A in the Black Forest. The data were the processed in the same manner as those in figure 9.14.

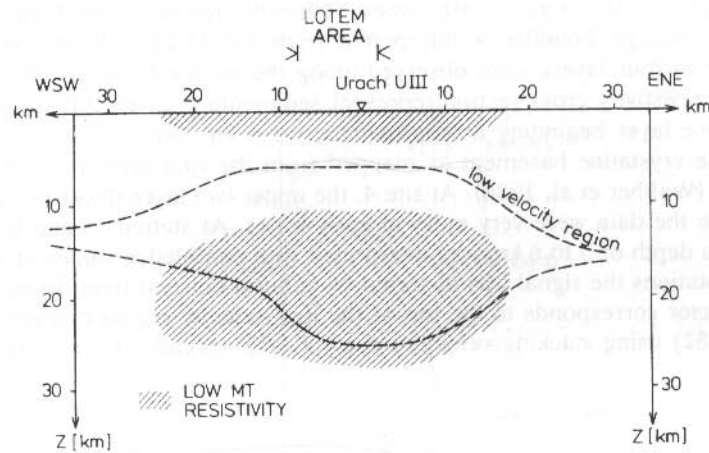


Fig. 9.22: Existing geophysical information (seismic and magnetotellurics) for the Urach Geothermal Area (after Berkthold et al., 1982) with a low velocity region. The LOTEM survey covered 7 km directly over the region.

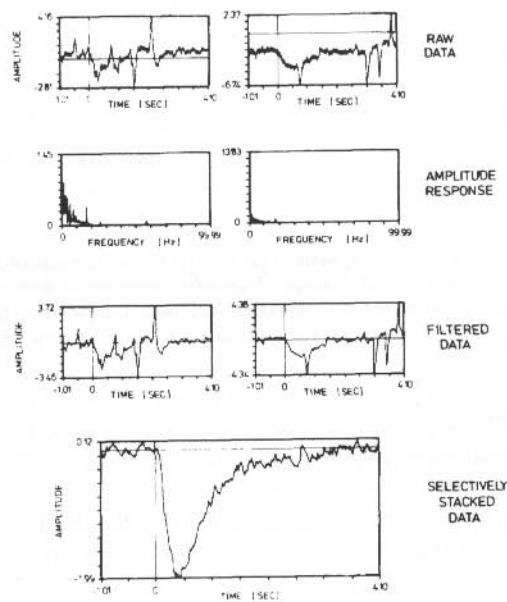


Fig. 9.23: Data processing sequence for the Urach survey (site 6). The polarity of the signal is selected by the first transmitter pulse and all consecutive signals are adjusted to it. The data processing follows that of figure 9.14 (after Strack et al., 1990).

Figure 9.24 shows a resistivity versus depth section for one of the two profiles measured. The data at the sites 1, 2, and 8 could not be used because of excessive noise in the data. No *a priori* information were used for the interpretation except for station 4 which was distorted at early times. Hence the top two layer boundaries were fixed at the geologic boundaries interpreted from the U III well log (Wohlenberg, 1982). Three to four layers were observed along the profile UL8601. The upper two layers in the resistivity cross section represent sedimentary cover. All stations show a highly resistive layer beginning at approximately 1.6 km depth. This corresponds to the top of the crystalline basement as mapped from the first arrivals of multifold reflection data (Walther et al, 1986). At site 4, the upper two layer thicknesses were kept fixed because the data were very noisy at early times. At stations 6 and 9, a conductive layer at a depth of 5 to 6 km was interpreted with confidence values of 95 percent. At all other stations the signal was distorted by cultural noise at later times. The depth of the conductor corresponds to the top of the low-velocity region mapped by Bartelsen et al (1982) using stacking velocities from a long-spread reflection survey.

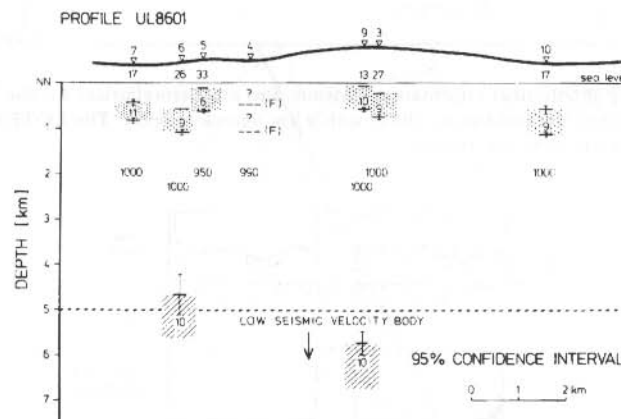


Fig. 9.24: Interpreted LOTEM resistivity depth section from one-dimensional inversions along traverse UL8601. Mesozoic and younger Paleozoic sediments from 0 to 1600 m are above resistive crystalline basement (gneisses). The crosshatching and shading of corresponding resistivity units is used to aid geologic correlation (after Strack et al, 1990).

Figure 9.25 shows a comparison to 3500 m depth of the resistivity well log from U III with a 1-D LOTEM inversion result from receiver station 10 which is 400 meters from the well. The resistivities from the upper kilometer were obtained from an induction log (Wohlenberg, 1982). The LOTEM inversion result (dashed line) correlates fairly well with the log resistivities to the final drilling depth of 3334 meters, although the LOTEM data do not resolve the resistivity difference in the high resistive unit below 1700 m depth.

To confirm the existence of the conductor at 5 km depth, synthetic apparent resistivity curves were calculated and convolved with the system response. The result of the convolution, a resistivity transform, is then directly compared with the field data which

still contain the influence of the system response. Figure 9.26 shows the field data and the synthetic curves for earth's models with and without the conductor. Without the conductor (curves B) the data do not fit with the model for over half a decade in time. The difference between the theoretical curves indicates that the conductive layer of $10 \Omega\text{m}$ resistivity at 6.1 km depth is necessary to interpret the data.

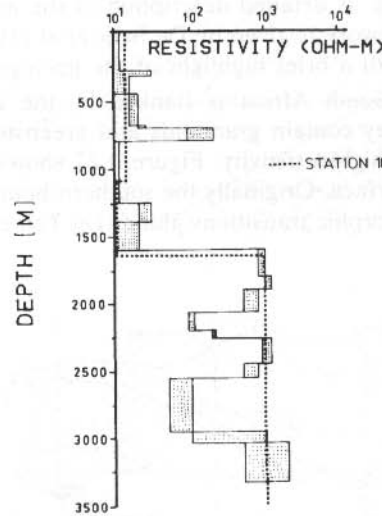


Fig. 9.25.: Comparison of inversion result and induction log at the Urach geothermal well site. The shaded part marks the confidence bounds. LOTEM station 10 is 400 m from well U III apart (after Strack et al, 1990) and its interpretation given by the dashed line.

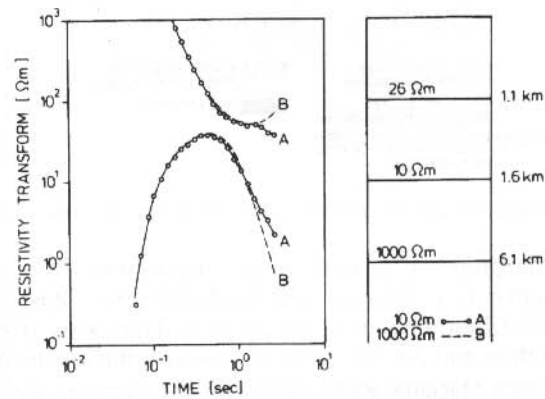


Fig. 9.26: Last layer resistivity test for Urach LOTEM station 6. The upper and lower curves represent early and late time resistivity transform curves for the respective models on the right. The circles represent the observed data and the solid/dashed lines the synthetic curves derived from the model on the right (after Strack et al, 1990).

TEST SURVEY OVER THE KAAPVAAL CRATON, R.S.A.

During 1987, a test survey with the LOTEM method was carried out over the Kaapvaal craton in South Africa. A detailed description of the interpretation and its place within the geological framework is given by De Beer et al (1991). Here, a summary of the geophysical aspects with a brief highlight of the geology is given.

The Limpopo Belt in South Africa is flanked by the Zimbabwe and Kaapvaal cratons. At the surface they contain granitoids and greenstones of low metamorphic grade. The cratons are of high resistivity. Figure 9.27 shows a rough overview of the resistivity as seen at the surface. Originally the southern boundary of the Limpopo was defined in terms of metamorphic transitions alone (Du Toit et al, 1983; Mason, 1973),

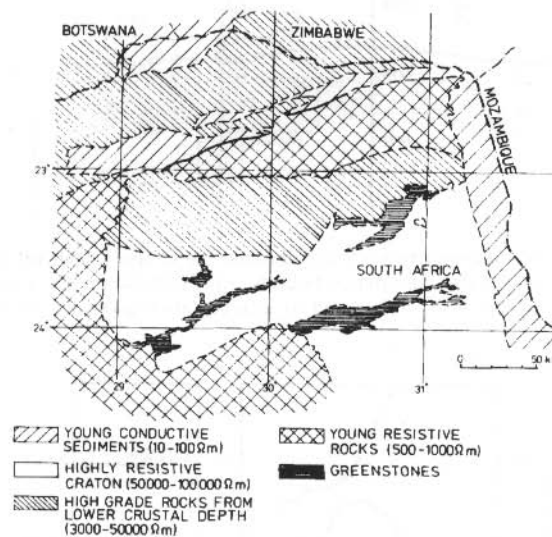


Fig. 9.27: General geologic features around the Kaapvaal craton in terms of their resistivities.

but more recently the proposed tectonic model incorporated the aspect of a steeply southward-dipping crust (e.g. Coward and Fairhead, 1980; Baston and Keys, 1981; Baston, 1983). A significant amount of geophysical data exists (De Beer et al, 1991) and was used by De Beer and Stettler (1988) to confirm the results of Van Zijl (1977a, 1978). For the Southern Marginal Zone (SMZ) of the Limpopo Belt it was found that the highly resistive, low-grade rocks dip northward underneath the moderately resistive, high-grade SMZ. The objective of the LOTEM survey was to determine the behavior of the conductive zone observed near the base of the cratonic crust when the transition from low-grade Kaapvaal craton to the high grade SMZ is crossed. A base-

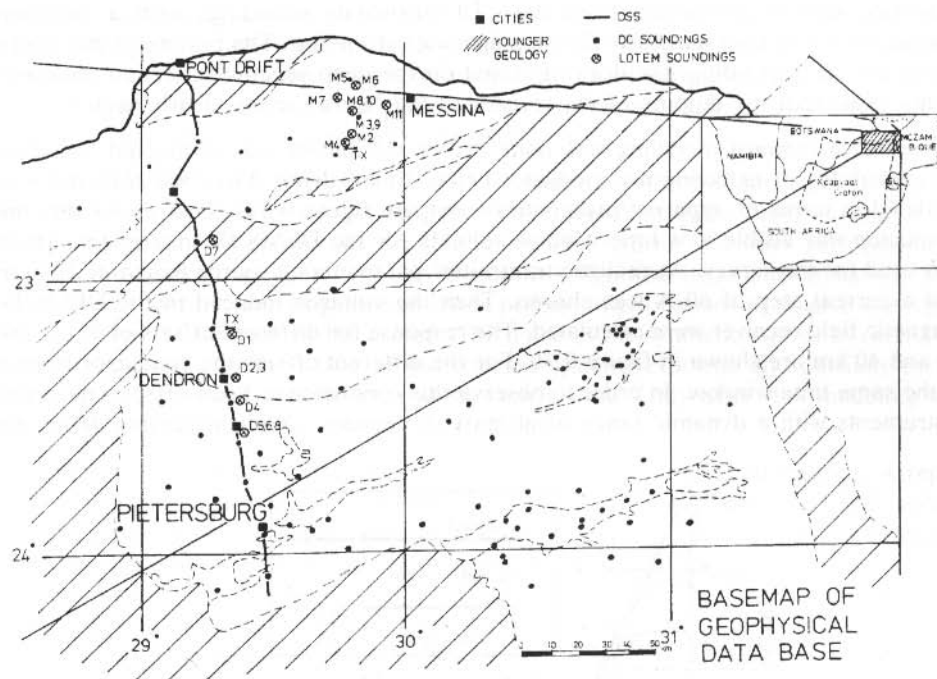


Fig. 9.28: Basemap of the LOTEM survey including the most important deep DC-resistivity soundings.

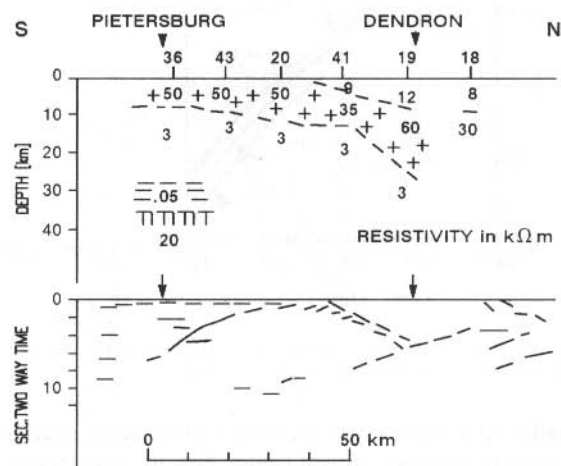


Fig. 9.29: Top: Geoelectric section from Pietersburg to north of Dendron along the seismic reflection profile. Resistivity values are $k\Omega m$. Bottom: Line drawing of the seismic reflection pattern in the Pietersburg-Dendron section of the profile (after De Beer et al, 1991).

map with the geophysical data base is shown in figure 9.28. Figure 9.29 shows the resistivity section interpreted from deep DC-resistivity soundings with a common spacing of 30–40 km (some are 1200 km spacing) at the top. The bottom of the figure shows the corresponding line drawing based on the deep seismic reflection measurements. Note that the dipping of the resistor to the North can be clearly seen.

Extensive forward modeling was done before the survey was conducted to assess the probability of detecting the conductor below 20 km depth. First, the response was modeled in terms of apparent resistivities (compare figure 9.30). This shows that the conductor was visible at a time window suitable for the DEMS IV instrument, which was used for the survey. As realistic transmitter parameters a source length of 2000 m and a current step of 60 A was chosen. Then the voltages induced in the DEMS IV magnetic field receiver were calculated. The response for different offsets of 5, 10, 20, 30 and 40 km are shown in figure 9.30. For the different offsets the conductor is seen at the same time window. In order to observe this conductor at 5 km offset, one needs instruments with a dynamic range of at least 6 decades. With increasing offset the

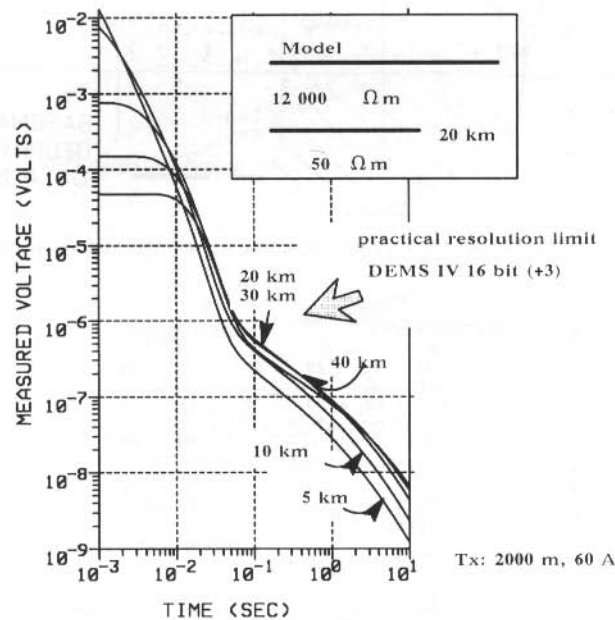


Fig. 9.30: Voltage responses for different transmitter to receiver offset using an average model for the conductor near the base of the Kaapvaal craton.

signal becomes smaller at earlier times but not significantly smaller at the time window around 100 msec which is the central time when the conductor is seen. In fact, at this time the response of the conductor increases for larger offset by about a factor of two. There is an optimum offset when the signal is largest around 20 to 30 km. The key question is whether the DEMS IV system can resolve these changes. Apart from

the instrument resolution limit around $20 \mu\text{V}$, one must consider the prestack processing and stacking which allows us to resolve signals below the instrument resolution limit. Although, in favorable condition we have been able to resolve signals 1000 times smaller than the resolution limit, one must be conservative and give the resolution limit as $1 \mu\text{V}$. This meant for the South African survey that a large offset in combination with high amplifier gains had to be used.

One important — but usually omitted — factor for the forward modeling is the system response, which strongly influences the signal at early times. Using a real measured system response, the forward curves of figure 9.30 were redisplayed as predicted measured voltages. The curves exhibit a significantly smaller dynamic range than in 9.29 and one can now expect (after proper amplification) to resolve the top of the conductor at the base of the craton. The noise in the synthetic curves at early time is partially caused by the shape of the selected system response, and partially by the fact that a few sample points exist at this early time. Only after this modeling was done and evaluated, was the survey carried out.

A large number of single records were collected at the individual stations. A representative example is shown in figure 9.30. At the stations DE04 and DE05 several thousand stacks were acquired with the maximum of 3800 stacks at DE05 during two days of recording time. This effort was necessary to reduce the noise most efficiently. The transients were all corrected for DC-level drifts and then stacked using an extended median stacking technique. Only minor filtering, using a time-variant Hanning window was done poststack. The stacked but not yet smoothed signal is shown at the bottom of figure 9.30. This stacked transient was then transformed to apparent resistivities and input into a Marquardt type inversion, yielding layered earth models.

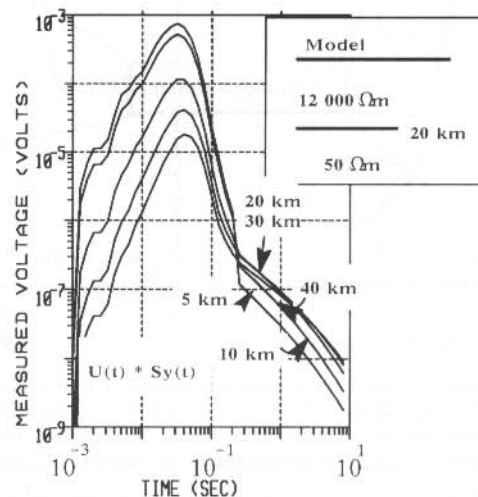


Fig. 9.31: Response resulting after convolving the data of figure 9.30 with a measured system response taking filters and transmitter waveform into account.

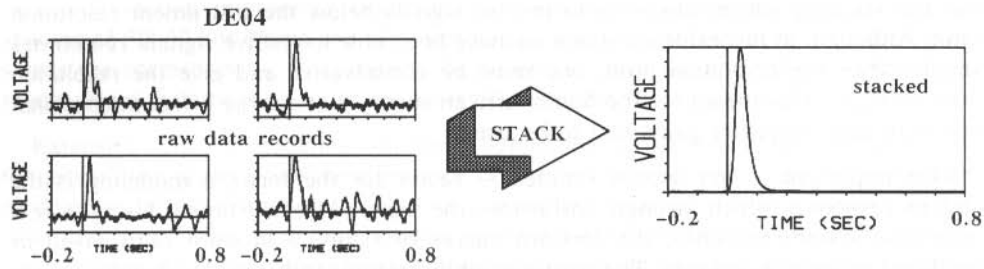


Fig. 9.32: Representative data set from the LOTEM survey. The left four frames show four single records. The right frame displays the result after removing the DC-level from all the records and stacking the data using an extended median stacking technique.

Figure 9.33 shows the results of inversion for stations DE04 and DE05 for offsets of 30 and 40 km, respectively. The points represent the data. The error bars derived from the selective stacking are smaller than the plotting symbol. The theoretical curve for the inversion result is drawn through the data points. Superimposed on the figure are the calculated curves for a half-space without the conductor (dashed line).

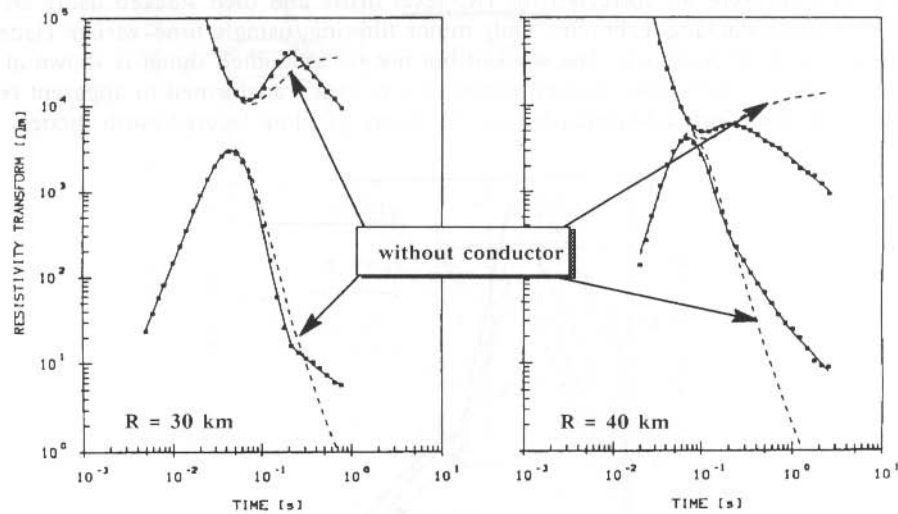


Fig. 9.33: Early and late time apparent resistivities for stations DE04 and DE05 (see figure 9.28). The field data are represented by the points and the theoretical curve for the inversion results by the solid line through the data points. The dashed line represent a half-space response when the conductor is absent (after De Beer et al, 1991).

For both data sets the existence of the conductor and its depth bounds is most often the key question. In order to determine these bounds many responses are calculated for different resistivity and depth values of the conductive layer. The χ^2 fit with the

data is displayed in figure 9.34. The 7% error ellipse encloses all possible models with fitting errors smaller than 7%. This type of analysis resulted in the models and their variation (dashed lines) shown in figure 9.35 and shows that depth is fairly well resolved (20.5 ± 2.5 km) but that the resistivity is more poorly resolved (22.5 ± 20 Ωm).

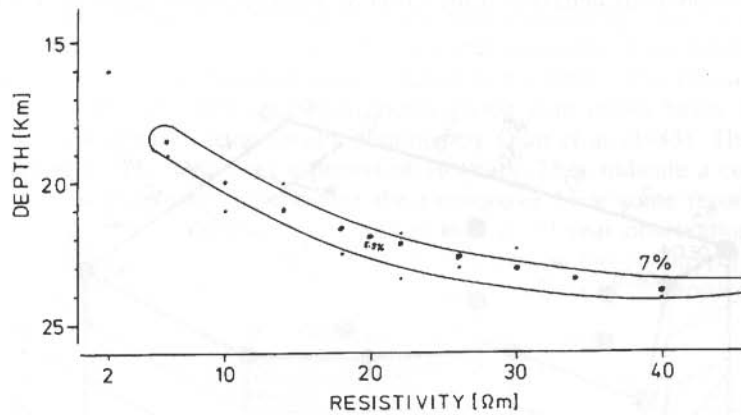


Fig. 9.34: Error ellipse for an χ^2 fit better than 7% for different resistivities and depths of the conductor.

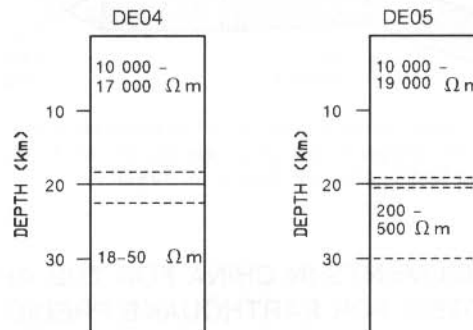


Fig. 9.35: The earth models interpreted for LOTEM sounding data for DE05 and DE04 as shown in figure 9.33 (after De Beer et al, 1991).

The difference in depth to the conductor for the two stations on either sides of the SMZ – craton boundary is very interesting (see figure 9.35). DE04, in the SMZ indicates a lower conductive layer at a depth of 21 to 24 km. The resistivity of this conductor ranges from 18 to 50 Ωm . For site DE05 on the craton, this conductor could not be satisfactorily interpreted as a single layer. A moderately conductive zone of 200 – 250 Ωm was modeled at a depth of 20 km, overlying the lower portion of 30 – 120

Ωm which start at approximately 30 km depth. As can be seen in figure 9.36, the depth to the lower crustal conductor ties in well with the DC-resistivity sounding recalls on the craton further to the south.

The combination of DC-resistivity and LOTEM shows that the idea of a steeply southward-dipping crustal margin between the SMZ of the Limpopo Belt and the Kaapvaal craton to the south is incorrect. If this would be the case one would have clearly seen anomalous behavior in the LOTEM interpretation caused by a 3-D effect.

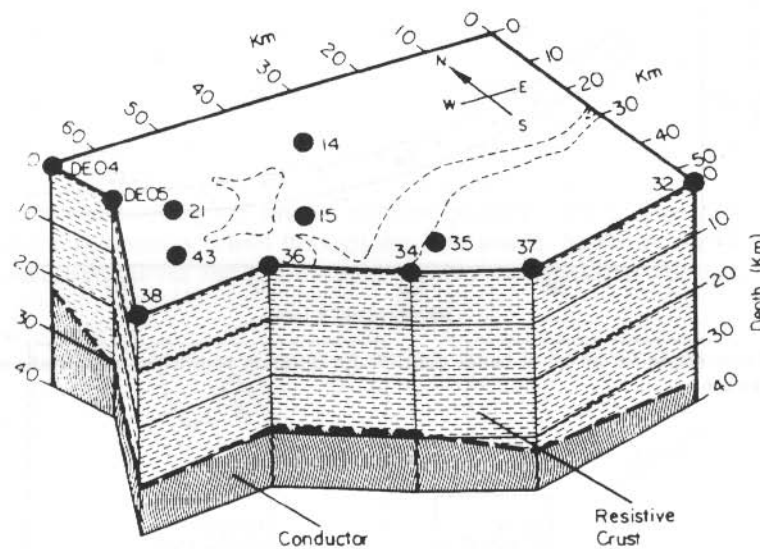


Fig. 9.36: The depth to the deep crustal conductor in the Kaapvaal craton and SMZ as determined by ultra-deep Schlumberger soundings at sites 32, 37, 34, 36 and 38 and LOTEM soundings at DE05 and DE04 (after De Beer et al, 1991).

TEST MEASUREMENTS IN CHINA FOR THE APPLICATION OF LOTEM FOR EARTHQUAKE PREDICTION

During 1988, LOTEM measurements were carried out near the Tangshan area in China, where a large earthquake on 28th of July 1976, killed over 200 000 people. Under the assumption that resistivity changes can be used for earthquake prediction, the objectives of the survey were defined as:

- Demonstration of the repeatability of LOTEM measurements within a period of several weeks.
- Demonstration of the depth investigation range of the LOTEM technique.
- Demonstration of the cost effectiveness.

Ωm which start at approximately 30 km depth. As can be seen in figure 9.36, the depth to the lower crustal conductor ties in well with the DC-resistivity sounding recalls on the craton further to the south.

The combination of DC-resistivity and LOTEM shows that the idea of a steeply southward-dipping crustal margin between the SMZ of the Limpopo Belt and the Kaapvaal craton to the south is incorrect. If this would be the case one would have clearly seen anomalous behavior in the LOTEM interpretation caused by a 3-D effect.

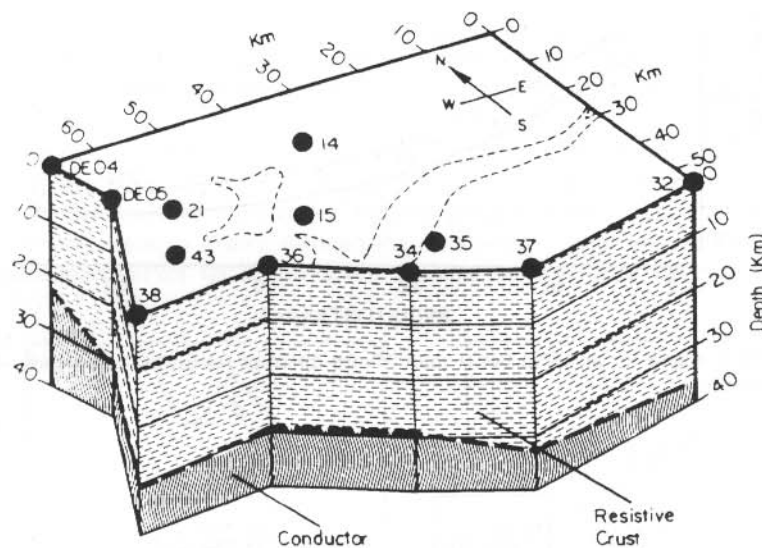


Fig. 9.36: The depth to the deep crustal conductor in the Kaapvaal craton and SMZ as determined by ultra-deep Schlumberger soundings at sites 32, 37, 34, 36 and 38 and LOTEM soundings at DE05 and DE04 (after De Beer et al, 1991).

TEST MEASUREMENTS IN CHINA FOR THE APPLICATION OF LOTEM FOR EARTHQUAKE PREDICTION

During 1988, LOTEM measurements were carried out near the Tangshan area in China, where a large earthquake on 28th of July 1976, killed over 200 000 people. Under the assumption that resistivity changes can be used for earthquake prediction, the objectives of the survey were defined as:

- Demonstration of the repeatability of LOTEM measurements within a period of several weeks.
- Demonstration of the depth investigation range of the LOTEM technique.
- Demonstration of the cost effectiveness.

Data Base of the Tangshan Area

Before the LOTEM survey started, very little was known to us about the electrical subsurface structure Tangshan area except that electrical resistivity measurement had been used successfully for earthquake prediction. Usually, Wenner arrays with electrode spacing of 1–3 km were used for the measurement. This yielded a depth of investigation of several hundred meters (Qian et al, 1983). The measurements were carried out with well calibrated instruments giving data errors below 0.5 %. Figure 9.37 gives a summary of the results obtained by Qian et al (1983). The curves show the variation in resistivity over a period of 10 years. They indicate a continuous drop in resistivity starting 2–3 years before the earthquake. For some recording sites this drop in resistivity had been the only feature over a 13 year observation period. The Tangshan earthquake is the only strong earthquake in the vicinity of the area and occurred in the immediate neighborhood of the minimum of the apparent resistivity.

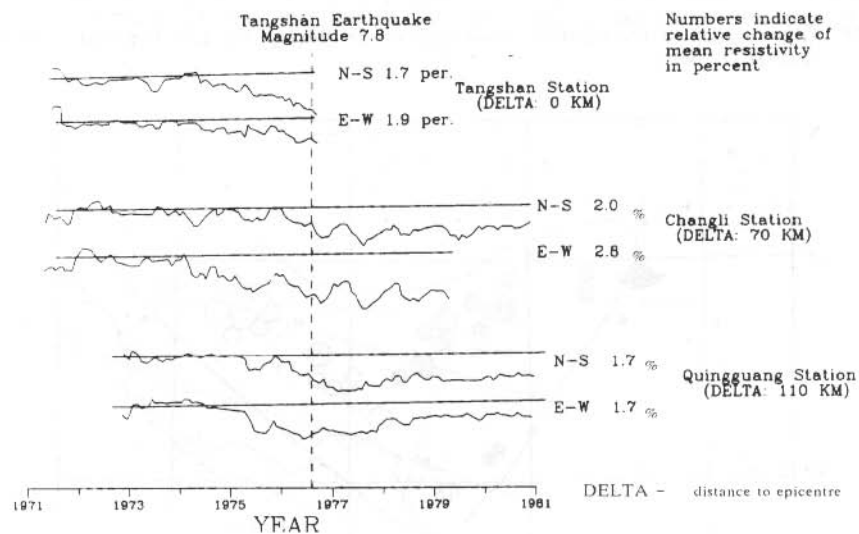


Fig. 9.37: Percentage change of the mean monthly resistivity measured by Wenner arrays in the Tangshan area (after Qian et al, 1983).

Figure 9.38 shows the contour lines of the resistivity anomalies. The Tangshan area lies clearly in the center of the anomaly. Qian et al (1990) gives an explanation of the precursor as being triggered by tidal forces. Their explanation is new compared to the classical concept of rock failure being the cause of the resistivity anomaly. Figure 9.39

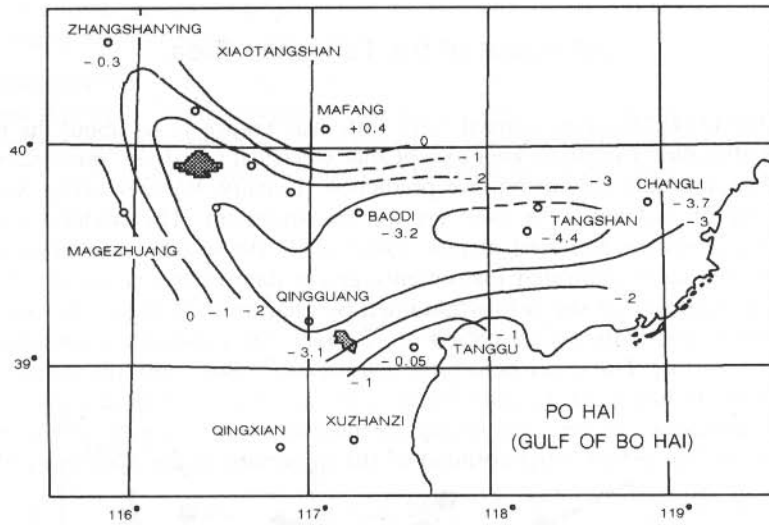


Fig. 9.38: Contour map of the resistivity anomalies in the Beijing-Tianjin-Tangshan area (after Qian et al, 1979).

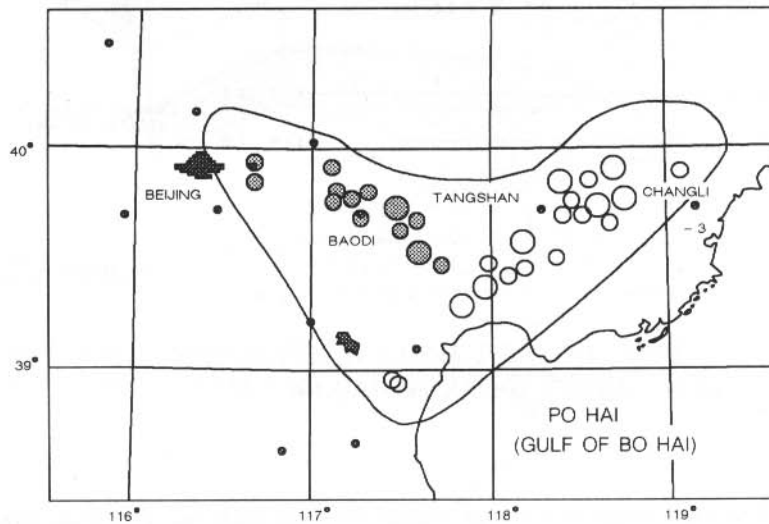


Fig. 9.39: Distribution of earthquakes with magnitudes above 4 after the Tangshan earthquake. Open circles represent aftershocks while the closed ones are earthquakes appearing to be unrelated to the aftershocks (after Qian et al, 1979).

shows a map of earthquakes after the Tangshan area. The earthquakes with magnitudes higher than 4 are shown. The aftershocks line up along one zone, whereas an-

were acquired at each site with three parallel profiles and one walkaway test on a profile. The walkaway profile was used to verify that one transmitter location was sufficient for the area.

A sample transient for the area is displayed in figure 9.41. The transient displayed is from the set of noisy transients. From this transient it can be seen that the signal is lost when the noise prevails resulting in a limited depth of investigation. Only ten percent of the data was as noisy as the data of site 15 in figure 9.41. At the control site transient were recorded at the beginning and at the end of the survey. In figure 9.42 the stacked signals at the control site are superimposed on each other. These transients are fairly smooth and show much better signal-to-noise ratios than the one in figure 9.41. The transients at the control site are also normalized for receiver gain, equivalent loop area, and transmitter moment which gives voltages in the femtovolt range.

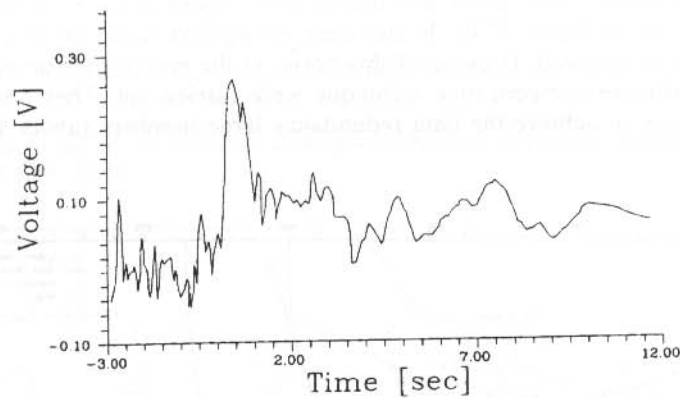


Fig. 9.41: Representative stacked transient (FB15) for the survey in the Tangshan area, PRC.

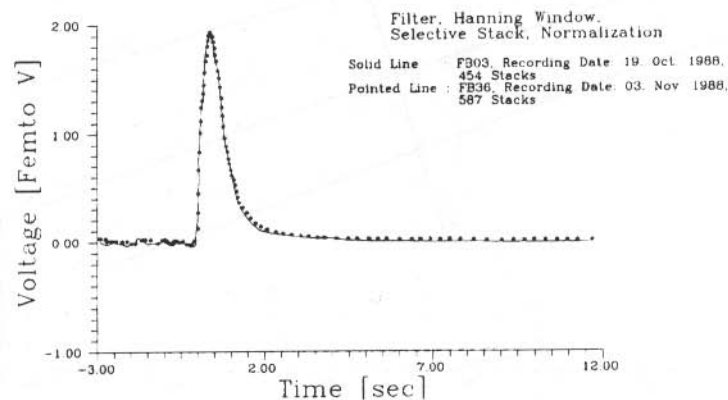


Fig. 9.42: Selectively stacked transients at the control site in the Tangshan area, PRC.

The objective of the measurements at the control site was to demonstrate the repeatability of the technique. Both measurements were carried out 14 days apart under different noise conditions. In figure 9.42 the difference in the stacked data is negligible. A better way to estimate the difference between the curves is to carry out inversions of these data sets. The results are shown in figure 9.43.

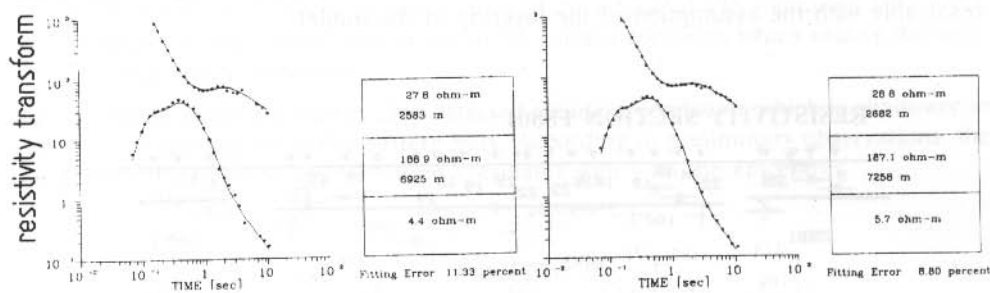


Fig 9.43: Inversion results for the measurements at the control site in the Tangshan area, PRC.

Discussion of the Results

Results of the repeated measurements (figure 9.43) clearly show a conductor at a depth of about 9.5 and 9.8 km. The upper conductive layer is sedimentary and about 2.5 km thick at the control site. The second, more resistive layer is interpreted as crystalline rock. The nature of the conductor below is not very clear. Qian and Peterson carried out MT measurements about 100 km away from the LOTEM site. They observed a similar resistivity structure, with the resistivity of the last layer being poorly constrained in their measurements. This can similarly be attributed to the strong cultural noise in the area, which made the interpretation of the data very difficult.

Figure 9.44 shows two resistivity sections for one of the profiles outlined on figure 9.40. The top of the figure displays the inversion results as they are output from the inversion program. The error bars in depth give the depth uncertainty. The inversion statistics clearly indicated that for the first layer only the inverse conductance was resolved. This means we can keep the conductance at the sites fixed, determine an average resistivity from the inversion results and adjust the thickness. This procedure is in this case also geologically reasonable because one can not expect strong lateral resistivity variations in this area. This procedure which we termed conductance referencing was applied across the profile and the bottom of the figure resulted. The boundary to the second layer has now become significantly smoother than in the top display where the heavy lines mark the interpreted layer boundary. The jagged inter-

face with the third layer is not significantly smoothed by this procedure because it is mainly focused on the part of the data where the model parameters are correlated. The depth to the conductor in the eastern part of the profile is notably different from the western part where the conductive layer begins at a depth of approximately 6 km. The parallel profiles show very similar results, a deepening conductor in the east and a shallow one in the west. One possibility is that a local structure is superimposed on the survey area upon the regional structure. The transition from the shallow conductor to the deeper one could be associated with a fault or somewhat smoother which is not resolvable with the assumption of the layering of the model.

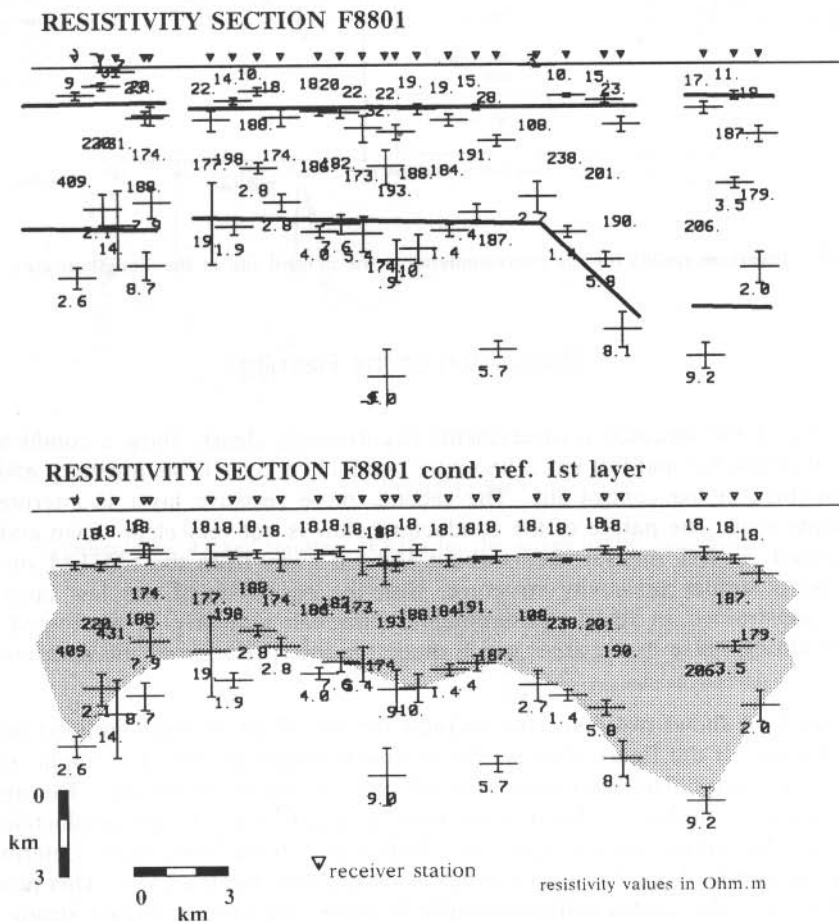


Fig. 9.44: Resistivity depth sections for profile F8801. The top section displays the results as they are given by the inversion. The bottom section shows the same results after adjusting for the fact that the inversion resolved only the first layer conductance and not the individual layer parameters (conductance referencing).

The main conclusion from the measurements were that the goals were reached namely:

- The technique yields highly repeatable measurements in this area (for a second repeat site the crew could not find the site for reoccupation).
- The depth of investigation in this area lies between 6 to 9 km and is far greater than the depth of investigation of DC-resistivity technique which are routinely used in the area.
- Within a total of three weeks of survey time a total of 115 soundings (over 1300 single records) were carried out at 74 surface locations which makes the technique very competitive.

Besides these goals, the survey also detected clearly a conductor which is shallower in the western and deeper in the eastern part. According to preliminary observations, the fault from the LOTEM interpretation correlates well with the epicentres.

DISCUSSION

The above surveys in the USA, Europe, South Africa and China show that the LOTEM sounding method contributed significant information to geophysical investigations of the earth's crust.

The results from the North American measurement clearly demonstrated the capability of the technique. However, in all cases very powerful transmitters were used. Since the operation of very powerful transmitters is very expensive and can be a safety hazard, the German surveys used smaller transmitters with a source moment of about one tenth of the North American tests. In the Oberpfalz the results gave a picture which is consistent, but the interpretation is questionable because of the possible multi-dimensional effect. The final answer to this question will be obtained sometime in the future, as the continental deep drilling project progresses.

In the Black Forest a low velocity channel in the lower crust coincides with a low resistivity zone. In the Urach Geothermal Area the top of a low-velocity anomalous region correlates with a low resistivity zone in the LOTEM interpretation. Consistent results were obtained to a depth of approximately 8 km under noisy electromagnetic field conditions. For both surveys the interpretation is confirmed by other geophysical information.

Interesting geologic and petrologic correlations are demonstrated for the Black Forest. The low-velocity zone in the lower part of the upper crust correlates with 1) a seismically transparent zone, 2) a zone of decreased Poisson's ratio, and 3) a zone of low electrical resistivity. The decreased Poisson's ratio is a very attractive indicator for pore fluids, since the P-wave velocity is more sensitive to fluids than the S-wave velocity (Helbig and Mesdag, 1982; Ensley, 1984). Low electrical resistivity can be produced by aqueous fluids with high ionic content such as saline water (Shankland and Ander, 1983; Haak and Hutton, 1986; Gough, 1986) and by unmetamorphosed

sedimentary rocks, graphite, hydrated minerals and metallic sulphides. A purely compositional influence of the lithology, such as an increased ratio of quartz/ feldspar content could explain the decreased Poisson's ratio (Kern, 1982) but would not account for the low resistivity. Our favored explanation of this correlation is the existence of fluid filled pores or cracks which could be the result of recent lower crust dehydration processes (Fuchs et al, 1987; Lüschen et al, 1987).

In the Urach area similar type of correlation between P-wave velocity and resistivity is observed in the upper 5 to 7 km crystalline crust. The low resistivity supports the concept of hydrothermal alteration of the crystalline rocks or postvolcanic gas exhalations from great depth (Berkthold et al, 1982). In both cases the conductor is associated with an area of high geothermal gradient.

In the survey in South Africa the LOTEM results clearly correlated with the DC-resistivity sounding in the area. It clearly indicated that the idea of a steeply southward-dipping of the Limpopo Belt is incorrect. The LOTEM and DC-resistivity results are in very good agreement with seismic (De Beer et al, 1991). In South Africa neither saline fluids nor graphite film can be ruled out conclusively as explanation for the lower crust conductor.

In China the LOTEM measurements provided a good statistical basis for the interpretation of the upper crust resistivity. Considering how noisy the area is (Qian and Peterson, 1991), this is very important. The deep geoelectric model in the area provided a basis for the determination of the extreme models for the MT measurements in the area. In the survey area itself a more localized conductivity anomaly consistent throughout the area exists. This is judged by the statistics of the individual inversion which clearly indicate the conductor at depth. The change from the lower to the deeper crustal conductor could be smooth or as localized fault. Only more detailed measurements can answer this question.

These studies motivate further investigation with LOTEM and MT using a more advanced approach to data acquisition and interpretation, such as extensive stacking, noise compensation techniques and MT/LOTEM joint inversion, for a more complete integration of geophysical information on the earth's near crust.

SUMMARY CHAPTER 9

Controlled source electromagnetic techniques are not very often used for deep crustal application. Some of the early work in the western hemisphere included deep DC-resistivity measurement in southern Africa and megasource transient EM measurement in the USA. The records from the deep DC-resistivity measurement showed transients when the transmitter polarity was changed. The transient signals were only used as timing marker and were not quantitatively interpreted. The work in the USA used large source moments to achieve sufficient investigation depth. Some of the early work already indicated most of the phenomena known today about transient soundings.

In Europe, the LOTEM method was initially only tested with small transmitters for deep crustal applications, although experience from the USA suggested that small moment (low power) transmitters were insufficient for such an investigation depth. The first test in the Oberpfalz area, site of the German deep continental drilling project, required a conductive layer at 10 km depth to yield a consistent interpretation. However, the interpretation was not very stable. The subsequent measurement in the Black Forest area shows very consistent results using two transmitters. Here, a low seismic velocity zone could be clearly correlated with a zone of low resistivity. Further confirmation of this relationship was obtained when carrying out measurements in the Urach Geothermal Area where also a low-velocity zone had also been found.

In South Africa, the objective of the LOTEM survey was to define the nature of the transition zone between the Southern Marginal Zone of the Limpopo Belt and the Kaapvaal craton. The LOTEM results clearly show that the conductor at 20 to 30 km depth continues through the transition zone. These results are in agreement with deep DC-resistivity measurements in the area.

In China, LOTEM test measurements were carried out in the Tangshan area, site of the devastating earthquake of 1976. The measurements illustrated that over a period of several weeks repeatable measurements can be obtained with the technique. In addition to this objective, the survey results indicated that a lower crustal conductor exists in the survey area.

PROBLEMS CHAPTER 9

1. Draw the transmitter current waveform for the analog recordings displayed in figure 9.1.
2. Find in the magnetic field transients in figure 9.3 the reversals and explain it qualitatively.
3. How can you see that the results could be unstable for the Oberpfalz data?
4. What are the major factors backing the stability of the Black Forest interpretation?
5. Why could a low dynamic range system (such as DEMS IV) resolve the conductor in the Kaapvaal craton case history?
6. Explain why and how LOTEM could be used for earthquake prediction.

KMS Technologies – KJT Enterprises Inc.
6420 Richmond Ave., Suite 610
Houston, Texas, 77057, USA
Tel: 713.532.8144

Please visit us
<http://www.kmstechnologies.com>

This material is not longer covered by copyright. The copyright was released by Elsevier to Dr. Strack on November 5th, 2007.

The author explicitly authorizes unrestricted use of this material as long as proper reference is given.